ARISTOTLE UNIVERSITY OF THESSALONIKI
SCHOOL OF GEOLOGY
LABORATORY OF ENGINEERING GEOLOGY AND HYDROGEOLOGY

**MAISURADZE A. LEVAN**
**Graduated Geologist**

# ENGINEERING GEOLOGICAL AND GEOTECHNICAL INVESTIGATION OF LANDSLIDE IN REGION OF ZVARE, CENTRAL GEORGIA, ALONGSIDE TO NEW RAILWAY LINE

**MASTER DIPLOMA THESIS**

THESSALONIKI
2017

ΑΡΙΣΤΟΤΕΛΕΙΟ ΠΑΝΕΠΙΣΤΗΜΕΙΟ ΘΕΣΣΑΛΟΝΙΚΗΣ
ΤΜΗΜΑ ΓΕΩΛΟΓΙΑΣ
ΕΡΓΑΣΤΗΡΙΟ ΤΕΧΝΙΚΗΣ ΓΕΩΛΟΓΙΑΣ ΚΑΙ ΥΔΡΟΓΕΩΛΟΓΙΑΣ

ΛΕΒΑΝ Α. ΜΑΪΣΟΥΡΑΤΖΕ
Πτυχιούχος Γεωλόγος

# ΤΕΧΝΙΚΟΓΕΩΛΟΓΙΚΗ ΚΑΙ ΓΕΩΤΕΧΝΙΚΗ ΔΙΕΡΕΥΝΗΣΗ ΚΑΤΟΛΙΣΘΗΣΗΣ ΣΤΗΝ ΠΕΡΙΟΧΗ ZVARE ΤΗΣ ΚΕΝΤΡΙΚΗΣ ΓΕΩΡΓΙΑΣ, ΚΑΤΑ ΜΗΚΟΣ ΤΟΥ ΝΕΟΥ ΣΙΔΗΡΟΔΡΟΜΙΚΟΥ ΔΙΚΤΥΟΥ

ΜΕΤΑΠΤΥΧΙΑΚΗ ΔΙΠΛΩΜΑΤΙΚΗ ΕΡΓΑΣΙΑ

ΘΕΣΣΑΛΟΝΙΚΗ
2017

Levan A. Maisuradze
Graduated Geologist

# ENGINEERING GEOLOGICAL AND GEOTECHNICAL INVESTIGATION OF LANDSLIDE IN REGION OF ZVARE, CENTRAL GEORGIA, ALONGSIDE TO NEW RAILWAY LINE

Submitted to the School of Geology in the context of Postgraduate studies
«Applied and Environmental Geology»
Department of Geology

Date of Oral Examination: 20/12/2017

**Examination Committee:**
Assistant Professor, Vasilios P. Marinos, Supervisor
Professor, Theodoros Chatzigogos, Member of the Examination Committee
Professor, Vasilios Christaras, Member of the Examination Committee
**Advising Committee:**
Assistant Professor, Vasilios P. Marinos, Supervisor
Professor, Vasilios Christaras, Member of the Advising Committee
Dr, Makedon Thomas, Member of the Advising Committee

Αριθμός Παραρτήματος Επιστημονικής επετηρίδας Τμήματος Γεωλογίας N°

# ΤΕΧΝΙΚΟΓΕΩΛΟΓΙΚΗ ΚΑΙ ΓΕΩΤΕΧΝΙΚΗ ΔΙΕΡΕΥΝΗΣΗ ΚΑΤΟΛΙΣΘΗΣΗΣ ΣΤΗΝ ΠΕΡΙΟΧΗ ZVARE ΤΗΣ ΚΕΝΤΡΙΚΗΣ ΓΕΩΡΓΙΑΣ, ΚΑΤΑ ΜΗΚΟΣ ΤΟΥ ΝΕΟΥ ΣΙΔΗΡΟΔΡΟΜΙΚΟΥ ΔΙΚΤΥΟΥ

“Nature, to be commanded, must be obeyed”
Francis Bacon

To my Mother,

# Table of Contents

**Abstract**..........16
**Περίληψη**..........17
**Acknowledgments**..........18
**Chapter 1 Introduction**..........19
1.1 General..........19
1.2 Study Area..........20
1.3 The Aim of the Study..........22
1.4 Methods of Study..........22
1.4.1 Field Work..........22
1.4.2 Desk Work..........22
1.5 Provided Data..........23
**Chapter 2 Theoretical Approach**..........24
2.1 General..........24
2.2 Landslides..........25
2.2.1 General..........25
2.2.2 Landslide Types..........26
2.2.2.1 Slope Failures on rock Formations..........27
2.2.2.2 Slope Failures on Soil Formations..........28
2.3 The incident of the failure..........32
**Chapter 3 Geological & Engineering Geological Surface Investigation**..........34
3.1 General..........34
3.2 Geomorphological Approach..........36
3.2.1 Small Scale Approach..........36
3.2.2 Large scale Approach..........39
3.3 Approach by aerial photographs and satellite imagery...........43
3.4 Geological Approach..........44
3.4.1 Regional Geology..........44
3.4.2 Seismicity..........46
3.4.3 Rainfall..........46
3.4.4 Large Scale Geological Approach..........48
3.4.5 Map Units..........52
3.4.5.1 Landslide Mass..........52
3.4.5.2 Fill Material..........53
3.4.5.3 Alluvium..........53
3.4.5.4 Colluvium..........53
3.4.5.5 Basaltic Andesite..........53
3.4.5.6 Calcareous Sandstone..........54
3.4.6 Structural features..........55
3.4.6.1 Faults..........55
3.4.6.2 Bedding..........57
3.4.6.3 Joints..........58
3.4.7 Mapping of cracks..........59
3.4.8 Hydrogeological Regime..........61
3.5 Conclusions..........62
**Chapter 4 Geological & Engineering Geological Subsurface Investigation**..........63
4.1 General..........63

4.2 Drilling Method ......................................................64
4.3 Core Logging Parameters ......................................................66
4.3.1 Total Core Recovery ......................................................66
4.3.2 Solid Core Recovery ......................................................66
4.3.3 Rock Quality Designation ......................................................66
4.4 Boreholes ......................................................68
4.4.1 Borehole: BDZ_22_01A ......................................................68
4.4.2 Borehole: BDZ_22_02 ......................................................71
4.4.3 Borehole: BDZ_22_03A ......................................................73
4.4.4 Borehole: BDZ_22_05 ......................................................75
4.4.5 Borehole: BDZ_22_06A ......................................................77
4.4.6 Borehole: BDZ_22_07 ......................................................80
4.4.7 Borehole: BDZ_22_08 ......................................................81
4.5 Conclusions ......................................................84
**Chapter 5 Geotechnical Monitoring** ......................................................88
5.1 General ......................................................88
5.2 Inclinometers ......................................................89
5.2.1 General ......................................................89
5.2.2 Boreholes ......................................................91
5.2.2.1 Borehole: BDZ_22_01A ......................................................92
5.2.2.2 Borehole: BDZ_22_03A ......................................................95
5.2.2.4 Borehole: BDZ_22_06A ......................................................99
5.2.2.5 Borehole: BDZ_22_08 ......................................................102
5.2.3 Conclusions ......................................................104
5.3 Water Pressure and Water Table ......................................................106
5.3.1 General ......................................................106
5.3.2 Installation ......................................................107
5.3.3 Provided data ......................................................107
5.4 Monitoring Points ......................................................110
5.4.1 General ......................................................110
5.4.2 Unit A ......................................................113
5.4.4 Unit C ......................................................117
5.4.4.1 Subunit C1 ......................................................117
5.4.4.2 Subunit C3 ......................................................118
5.4.4.3 Subunit C4 ......................................................118
5.5 Conclusions ......................................................119
**Chapter 6 Geological & Engineering Geological Model** ......................................................120
6.1 General ......................................................120
6.2 Analysis of Two-Dimensional Sections ......................................................122
6.2.1 Cross Sections ......................................................122
6.2.1.1 Section AA’ ......................................................122
6.2.1.2 Section BB’ ......................................................122
6.2.1.4 Section FF’ ......................................................124
6.2.1.5 Section GG’ ......................................................124
6.2.2 Long Sections ......................................................126
6.2.2.1 Section DD’ ......................................................126
6.2.2.2 Section EE’ ......................................................126

6.3 Conclusions ....................................................................................................128
**Chapter 7 Geotechnical Investigation** ......................................................................129
7.1 General.............................................................................................................129
7.2 Estimated design parameters of rock mass.........................................................130
7.2.1 Estimation of Shear Strength from GSI...........................................................130
7.2.2 Estimation of Shear Strength from RMR .........................................................131
7.3 Estimated design parameters for the Landslide Material ...................................134
7.3.1 General..........................................................................................................134
7.3.2 Back Analysis Procedure ...............................................................................136
7.3.3 Estimation of design Shear strength................................................................138
7.4 Conclusions ........................................................................................................142
**Chapter 8 Suggestions**..................................................................................................143
8.1 General...............................................................................................................143
8.2 First Scenario........................................................................................................146
8.3 Second Scenario...................................................................................................148
8.4 Conclusions .........................................................................................................150
**Chapter 9 Conclusions**..................................................................................................151
**References** ........................................................................................................................153
**Appendix**...........................................................................................................................156

## Table of Figures & Tables

Figure 1. Georgia, Caucasus (Google Earth). .......... 20
Figure 2. The railroad network of Georgia, Caucasus (From Wikipedia). .......... 20
Figure 3. The complete railroad alignment from Khashuri to Zestaphoni (from railway.ge). .......... 21
Figure 4. The area of railway construction from Khashuri to Zestafoni (Google Earth) .......... 21
Table 1. The characterization of a landslide based on the velocity of its occurrence (From Hungr O., et al 2014). .......... 25
Figure 5. The geometry and the characteristic features of landslides, demonstrated at a rotational landslide (From Highland, L.M., and Bobrowsky, P., 2008). .......... 26
Figure 6. Types of landslides, Toppling (left) and Rockfall (right) (From Highland, L.M., and Bobrowsky, P., 2008) .......... 27
Figure 7. Types of landslides, Rock wedge (left) and Rock slide (right) (Modified, Highland, L.M., and Bobrowsky, P., 2008). .......... 27
Figure 8. Types of landslides, Translational Slide (a) and Lateral Spreads (b) (From Highland, L.M., and Bobrowsky, P., 2008). .......... 29
Figure 9. Types of flows. (a) Debris flow, (b) slow earth slow (creep), (c) debris avalanche, (d) earth flow. (Highland, L.M., and Bobrowsky, P., 2008) .......... 30
Figure 10. The Topographical map, with depicted the excavation, the presented outline section and Trial pit. Contour interval 2m (provided by contractor). .......... 31
Figure 11. Logging from Trial Pit, located at the toe of the landslide, from the preexisting geological and geotechnical investigation (provided by Contractor). .......... 32
Figure 12. The Excavation outline development with time (Provided by the contractor). .......... 33
Figure 13. Regional (large scale) topographical map of study area. Red square represents the study area, red circles old landslides and green dashed lines, lineation related to geological contacts or faults (Modified, U.S.G.S.). .......... 36
Figure 14. Aspect map, which presents the orientation of slopes regional (large scale) of study area. In black square, the study area. .......... 37
Figure 15. Map of slope inclination in wider of study area territory. The black square represents the study area. .......... 38
Figure 16. Large-Scaled topographical map of close study area. The grey line represents the limits of landslide. The green circles indicate flat areas NE than landslide which needs to be investigated, and red circles indicate sizable landslides northern, effecting the alignment. .......... 39
Figure 17. Large-Scaled map, demonstrating the orientation of the slopes. The grey line represents the limits of landslide. The black line in the north represents back tilt activity on another than this study's' landslide. .......... 40
Figure 18. Slope Steepness map. The grey line represents the limits of landslide. The black circles indicate flat areas NE of the major landslide which needs to be investigated and blue circles indicate sizable landslides northern than the study are. .......... 41
Figure 19. Google Earth image of close study area, before the implemented excavation. .......... 42
Figure 20. Landslide borders and tectonic faults depicted by UAV after the implemented excavation (Provided by Contractor). .......... 43

Figure 21. Geological Map, zoomed from the geological map of Georgia 1:500.000 (Gudjabidze G.E., Gamkrelidze I.P., 2003) ....44
Figure 22. The distribution of seismicity expressed by PGA (Seismic Code of Georgia) ....45
Figure 23. Borjomi Fault (Philip H., et al., 1989) ....45
Figure 24. Annual precipitation level at Georgia (Bondyrev I., et al., 2016) ....46
Figure 25. Northern Landslide Limits (a) The bedding of sandstone in which the mass slips, (b) very altered bedrock shown in the slope, (c) the major difference on color on landslide mass and bedrock material, (d) 3-4m formed slope in the middle of north slope ....48
Figure 26. Southern slope, (a) slickensides on soil and rock formation, (b) slickensides on soil type formation, (c) steep 4-5m high slope, (d) the presence of bedrock in the south slope. ....49
Figure 27. The presence of Alteration on the bedrock, (a) The bedrock owns colors in shade of purple and becomes friable, (b) high concentration of sulfur in the bedrock. ....50
Figure 28. Landslide Mass, (a) presence of boulder within the mass, (b)&(d) The complete heterogeneity observed in landslide mass, with angular fragment on clayey material, (d) the border on northwestern part of the landslide and clean differences with the surrounding material ....52
Figure 29. Basaltic Andesite ....53
Figure 30. Calcareous Sandstone, (a) Marly intercalations, (b) Moderately weathered Sandstone, (c) lenses of chert within sandstone, (d) Slightly weathered dark grey sandstone. ....54
Figure 31. Presence of grey clayey material as lenses into the bedrock, Sandstone. .55
Figure 32. The tectonic contact between sandstone and basaltic andesite. Northern fault. ....56
Figure 33. The geological reverse fault southern of close study area. ....56
Figure 34. Projection of bedding measurement of close study area into Schmitt diagram (Equal Area/Lower Hemisphere) ....57
Figure 35. Projection of total joint sets of close study area into Schmitt diagram (Equal Area/Lower Hemisphere) ....58
Figure 36. Landslide divided into categories regarding behavior type and surface ruptures. ....59
Figure 37. Aerial Images by UAV depicts the toe of the slide, and surface of ruptures, Provided by the Contractor. ....59
Figure 38. The Surface ruptures on the landslide, (a) Ruptures on the first unit on the head of the landslide, (b) radial surface ruptures on the end of the main body towards C1 Subcategory, (c) radial ruptures on the main body of the landslide, (d) Ruptures on C4 subcategory. ....60
Figure 39. The springs in the toe of the Landslide ....61
Table 2. Implemented exploratory geotechnical boreholes with the corresponding coordinates on UTM (Zone 38) projection system, altitude and depth in meters. ....63
Figure 40. Example of TCR, SCR, RQD indexes measurements (Price D.G. & de Freitas M.H., 2009) ....67
Figure 41. Picture of Landslide from the opposite slope, with greed dashed line, the boundary of landslide and with red circles, the executed ant evaluable boreholes. .68

Figure 42. RQD and SCR indexes versus depth, for Borehole: BDZ_22_01A ..............69
Figure 43. GSI and RMR indexes versus depth, for Borehole: BDZ_22_01A ..............70
Figure 44. RQD and SCR indexes versus depth, for Borehole: BDZ_22_02. ................71
Figure 45. GSI and RMR indexes versus depth, for Borehole: BDZ_22_02 ................72
Figure 46. RQD and SCR indexes versus depth, for Borehole: BDZ_22_03A ..............73
Figure 47. GSI and RMR indexes versus depth, for Borehole: BDZ_22_03A ..............74
Figure 48. RQD and SCR indexes versus depth, for Borehole: BDZ_22_05 ................75
Figure 49. GSI and RMR indexes versus depth, for Borehole: BDZ_22_05 ................76
Figure 50. RQD and SCR indexes versus depth, for Borehole: BDZ_22_03A ..............77
Figure 51. GSI and RMR indexes versus depth, for Borehole: BDZ_22_06A ..............78
Figure 52. RQD and SCR indexes versus depth, for Borehole: BDZ_22_07 ................80
Figure 53. GSI and RMR indexes versus depth, for Borehole: BDZ_22_07 ................81
Figure 54. RQD and SCR indexes versus depth, for Borehole: BDZ_22_08 ................82
Figure 55. GSI and RMR indexes versus depth, for Borehole: BDZ_22_08 ................83
Figure 56. The product of drilling, characterized as unstable landslide material. ......84
Figure 57. The product of drilling, characterized as stable bedrock, calcareous sandstone. At (c) can be observed the lenses of clay into bedrock. ..........................85
Figure 58. The product of drilling, characterized as stable stiff clayey geomaterial...86
Table 3. The depth of the sliding zone in each borehole............................................86
Figure 59. Size distribution curve, for the questionable origin, sands. ......................87
Figure 60. The product of drilling, characterized as stable sandy geomaterial..........87
Figure 61. Principles of inclinometer configuration of inclinometer equipments (Stark D.T., & Choi H., 2008)..........................................................................................90
Table 4. The Structural Characteristics of used Inclinometer (rst.com) .....................91
Figure 62. Incremental Displacement for Borehole: BDZ_22_01A.............................93
Figure 63. Cumulative Displacement for Borehole: BDZ_22_01A .............................93
Figure 64. Vector Displacement for Borehole: BDZ_22_01A ....................................94
Figure 65. Rate of Movement for Borehole: BDZ_22_01A ........................................94
Figure 66. Incremental Displacement for Borehole: BDZ_22_03A.............................95
Figure 67. Cumulative Displacement for Borehole: BDZ_22_03A .............................96
Figure 68. Vector Displacement for Borehole: BDZ_22_03A ....................................96
Figure 69. Rate of Movement for Borehole: BDZ_22_03A ........................................97
Figure 70. Incremental Displacement for Borehole: BDZ_22_05 ..............................97
Figure 71. Cumulative Displacement for Borehole: BDZ_22_05 ...............................98
Figure 72. Vector Displacement for Borehole: BDZ_22_05 .......................................98
Figure 73. Rate of Movement for Borehole: BDZ_22_05 ..........................................99
Figure 74. Incremental Displacement for Borehole: BDZ_22_06A...........................100
Figure 75. Cumulative Displacement for Borehole: BDZ_22_06A ...........................100
Figure 76. Vector Displacement for Borehole: BDZ_22_06A ..................................101
Figure 77. Rate of Movement for Borehole: BDZ_22_06A ......................................101
Figure 78.Incremental Displacement for Borehole: BDZ_22_08 .............................102
Figure 79. Cumulative Displacement for Borehole: BDZ_22_08 .............................102
Figure 80. Vector Displacement for Borehole: BDZ_22_08 .....................................103
Figure 81. Rate of Movement for Borehole: BDZ_22_08 ........................................104
Table 5. Information about the timeline of processes concerning inclinometers. ...104
Table 6. Information provided by inclinometers regarding the magnitude, the rate and the direction of the movement. ................................................................105

Figure 82. Sketch of the piezometer installation in borehole BDZ_22_02. ...............106
Table 7. Boreholes and depth of piezometer installation. .......................................107
Figure 83. Piezometrical map of the under-study landslide territory. ......................107
Table 8. The depth of the water table regarding the altitude of boreholes and the altitude of water table within the boreholes. .........................................................108
Figure 84. Fluctuation of water Table at borehole BDZ_22_07. ..............................108
Figure 85. Fluctuation of water Table at borehole BDZ_22_02. ..............................109
Figure 86. Map of lateral movements corresponding to the direction of movements and surface ruptures of landslide. ............................................................................110
Figure 87. Map of vertical movements corresponding to the direction of movements and surface ruptures of landslide. ............................................................................111
Table 9. Calculated direction of movement by the monitoring points. ....................112
Figure 88. Lateral Displacement versus time for the Unit A, the head of the Landslide. ..............................................................................................................................113
Figure 89. Vertical Displacement versus time for the Unit A, the head of the Landslide. ..............................................................................................................113
Figure 90. Lateral rate of movement versus time for the unit A, the head of the landslide. ...............................................................................................................113
Figure 91. Vertical rate of movement versus time for the unit A, the head of the landslide. ...............................................................................................................114
Figure 92. Lateral displacement versus time for the unit b, the main body of the Landslide. ..............................................................................................................114
Figure 93. Vertical displacement versus time for the unit b, the main body of the landslide. ...............................................................................................................115
Figure 94. Lateral rate of movement versus time for the unit A, the main body of the landslide. ...............................................................................................................116
Figure 95. Vertical rate of movement versus time for the unit B, the main body of the landslide. ...............................................................................................................116
Figure 96. Lateral displacement versus time for the unit A, the toe of the landslide. ..............................................................................................................................117
Figure 97. Vertical displacements versus time for the Unit A, the toe of the landslide. ..............................................................................................................................117
Figure 98. Lateral rate of movement versus time for the unit C, the toe of the landslide. ...............................................................................................................118
Figure 99. Vertical rate of movement versus time for the unit C, the toe of the landslide. ...............................................................................................................118
Figure 100. Geological & Engineering Geological Cross Section AA'. ........................121
Figure 101. Geological & Engineering Geological Cross Section BB'. ........................121
Figure 102. Geological & Engineering Geological Cross Section CC'. ........................123
Figure 103. Geological & Engineering Geological Cross Section FF'. .........................125
Figure 104. Geological & Engineering Geological Cross Section GG'. .......................125
Figure 105. Geological & Engineering Geological Long Section EE'. ..........................127
Figure 106. Geological & Engineering Geological Long Section DD'. .........................127
Figure 107. Distribution of estimated by drill cores GSI index (Conservative). .........130
Table 10. Mechanical and Physical Properties of Sandstone ..................................131
Figure 108. Distribution of estimated by drill cores RMR index (conservative). .......131
Figure 109. GSI chart (Hoek E., Marinos P., 2000). .................................................132

Figure 110. RMR Chart (Beniewski T.Z., 1989)........................................................133
Figure 111. The procedure of stability analysis. ......................................................135
Table 11. Friction angle and safety factor regarding the surface of rupture(B) derived by instrumentation, unit weights and water tables. ..............................................136
Figure 112. The Back analysis for the established engineering geological model for shear strength regarding the landslide mass with unit weight 17kN/$m^3$ and saturated unit weight 20kn/$m^3$, and shear strength expressed only by friction angle ϕ=10,25° ..........................................................................................................................137
Table 13. Physical and mechanical properties of engineering geological units (* The calculated shear strength is estimates for the surface of the rupture, the shear zone). ..........................................................................................................................139
Figure 113. Conceptual Engineering Geological Model Regarding the South Border of the Landslide ..........................................................................................................140
Figure 114. Conceptual Engineering Geological Model Regarding the North Border of the Landslide ..........................................................................................................141
Figure 115. The concept, the Mohr cycles moving to the right, avoiding the failure envelope, for the counter measures. ....................................................................143
Figure 116. Model of the Berm and the excavation, according to the second scenario. ..........................................................................................................................145
Figure 117. Model of the Berm, according to the first scenario. ............................145
Figure 118. The stability response of the model of the first scenario for the surface A, (a) for high water level and no seismic event, (b) low water level and seismic event. ..........................................................................................................................146
Figure 119. The stability response of the model of the first scenario for the circle surfaces on the berm, (a) for high water level and seismic event, (b) low water level and no seismic event. ..........................................................................................147
Table 14. Different cases for the model of scenario 1............................................148
Figure 120. The stability response of the model of the second scenario for the circle surfaces on the berm. ..........................................................................................148
Figure 121. The stability response of the model of the second scenario for the surface A. ..........................................................................................................................149
Figure 122. The stability response of the model of the second scenario for the surface A. ..........................................................................................................................149
Figure 123. Core Logging of borehole BDZ_22_01A (1/3) .......................................157
Figure 124. Core Logging of borehole BDZ_22_01A (2/3) .......................................157
Figure 125. Core Logging of borehole BDZ_22_01A (3/3) .......................................157
Figure 126. Core Logging of borehole BDZ_22_02 (1/3) .........................................157
Figure 127. Core Logging of borehole BDZ_22_02 (2/3) .........................................157
Figure 128. Core Logging of borehole BDZ_22_02 (3/3) .........................................157
Figure 129. Core Logging of borehole BDZ_22_03A (1/3) .......................................157
Figure 130. Core Logging of borehole BDZ_22_03A (2/3) .......................................157
Figure 131. Core Logging of borehole BDZ_22_03A (3/3) .......................................157
Figure 132. Core Logging of borehole BDZ_22_05 (1/3) .........................................157
Figure 133. Core Logging of borehole BDZ_22_05 (2/3) .........................................157
Figure 134. Core Logging of borehole BDZ_22_05 (3/3) .........................................157
Figure 135. Core Logging of borehole BDZ_22_06A (1/3) .......................................157
Figure 136. Core Logging of borehole BDZ_22_06A (2/3) .......................................157

Figure 137. Core Logging of borehole BDZ_22_06A (3/3) ........................................157
Figure 138. Core Logging of borehole BDZ_22_07 (1/3) ..........................................157
Figure 139. Core Logging of borehole BDZ_22_07 (2/3) ..........................................157
Figure 140. Core Logging of borehole BDZ_22_07 (3/3) ..........................................157
Figure 141. Core Logging of borehole BDZ_22_08 (1/4) ..........................................157
Figure 142. Core Logging of borehole BDZ_22_08 (2/4) ..........................................157
Figure 143. Core Logging of borehole BDZ_22_08 (3/4) ..........................................157
Figure 144. Core Logging of borehole BDZ_22_08 (4/4) ..........................................157
Figure 145. Core Logging of borehole BDZ_22_09 (1/2) ..........................................157
Figure 146. Core Logging of borehole BDZ_22_09 (2/2) ..........................................157
Figure 147. Core Logging of borehole BDZ_22_10 (1/2) ..........................................157
Figure 148. Core Logging of borehole BDZ_22_10 (2/2). .........................................157
Figure 149. Core Logging of borehole BDZ_22_11 ..................................................157
Figure 150. Coring samples photographs from borehole BDZ_22_01A (0-24m). .....157
Figure 151. Coring samples photographs from borehole BDZ_22_01A (24-47m). ...157
Figure 152. Coring samples photographs from borehole BDZ_22_02 (0-24m). .......157
Figure 153. Coring samples photographs from borehole BDZ_22_02 (24-46m). .....157
Figure 154. Coring samples photographs from borehole BDZ_22_03A (0-24m). .....157
Figure 155. Coring samples photographs from borehole BDZ_22_03A (24-47m). ...157
Figure 156. Coring samples photographs from borehole BDZ_22_05 (0-24m). .......157
Figure 157. Coring samples photographs from borehole BDZ_22_05 (24-46m). .....157
Figure 158. Coring samples photographs from borehole BDZ_22_06A (0-24m). .....157
Figure 159. Coring samples photographs from borehole BDZ_22_06A (24-40.8m). 157
Figure 160. Coring samples photographs from borehole BDZ_22_07 (0-24m). .......157
Figure 161. Coring samples photographs from borehole BDZ_22_06A (24-44.30m). ..............................................................................................................157
Figure 162. Coring samples photographs from borehole BDZ_22_08 (0-24m). .......157
Figure 163. Coring samples photographs from borehole BDZ_22_06A (24-48m). ...157
Figure 164. Coring samples photographs from boreholes BDZ_22_09, BDZ_22_10, BDZ_22_11. ..........................................................................................157
Figure 165. Geological & Engineering Geological Map of southern of village Zvare Region, Imereti, Central Georgia. ...............................................................157

# Abstract

Within the context of Postgraduate studies, the current dissertation regarding slope instability at the wider area of Zvare village, of Imereti region, central Georgia, central Caucasus, adjacent to railroad alignment, was carried out. The present dissertation is relied on both field and desk work. The field work was focused at geological and engineering geological mapping, supervision of geotechnical exploratory boreholes, and measurements regarding geotechnical monitoring. Beside the implementation of the current thesis, the most worth mentioning desk work concludes the completion of drill core loggings, geological and engineering geological map, analysis of data regarding geotechnical monitoring and stability analyses, in order to provide feasible solutions regarding the problems, provided by the activation of massif landslide in the region.

The landslide, of approximately 400m length and 230m wide, was activated at 13/05/2017 at the underlying region, due to excavations, which were carried out at the toe of old stabilized landslide, for the construction of railroad line. The underlying landslide, although constitutes a complex system of minor landslides, generally is classified as a rotational landslide. Recorded displacements approach 16m in lateral direction and 7m in vertical, respectively. The maximum depth of shearing due to boring and instrumentation, is estimated at depth of 40m, which through to back analysis shown shear strength of shear surface, expressed as Mohr Coulomb shear parameters, cohesion c=0 and friction angle ϕ=10°.

The underlying activation, provides several geotechnical and social related problems. The underlying issues are focused at the relocation of the alignment which is located at the toe of the slide, the maintenance of the secure passing of river, which now passes from the toe of the slide, which is located at the right bank of the river. In addition, the maintenance of the road which is located at the left bank of the river, and the springs of natural carbonated water, which are also located at the left bank of the river is considered essential. So, in this case the construction of berm, at the toe of the landslide is recommended, taking though into consideration, the maintenance of the underlying features.

# Περίληψη

Στα πλαίσια των μεταπτυχιακών σπουδών, εκπονήθηκε η παρούσα διατριβή, σχετικά με αστάθεια πρανούς στην ευρύτερη περιοχή του οικισμού Ζβάρε, του Ιμερέτι, της κεντρικής Γεωργίας, κατά μήκος της χάραξης υπό κατασκευής σιδηροδρομικής γραμμής. Η παρούσα διατριβή στηρίχθηκε εξίσου σε εργασίες γραφείου και υπαίθρου. Οι εργασίες υπαίθρου ήταν επικεντρωμένες στη γεωλογική και τεχνικογεωλογική χαρτογράφηση, επίβλεψη γεωτεχνικών ερευνητικών γεωτρήσεων και μετρήσεων σχετικών με γεωτεχνική ενόργανη παρακολούθηση. Εκτός από τη συγγραφή της παρούσας διατριβής, η κυριότερες εκ τελεσθέντες εργασίες γραφείου θεωρούνται η συγγραφή και σύνταξη των δελτίων των ερευνητικών γεωτρήσεων, του γεωλογικού και τεχνικογεωλογικού χάρτη της περιοχής, ανάλυση των διαθέσιμων στοιχείων σχετικών με την ενόργανη γεωτεχνική παρακολούθηση και ανάλυση ευστάθειας, με απώτερο σκοπό, να προαχθούν εφικτές λύσεις, σχετικά με τα προβλήματα που παρουσιάζονται από την ενεργοποίηση της κατολίσθησης στη περιοχή.

Η κατολίσθηση, μήκους και πλάτους, περίπου 400μ και 230μ αντίστοιχα, ενεργοποιήθηκε στις 13/05/2017, στη παραπάνω περιοχή, εξαιτίας εκσκαφών που έλαβαν χώρα στο πόδι παλιάς σταθεροποιημένης κατολίσθησης, στα πλαίσια της κατασκευής σιδηροδρομικής γραμμής. Η παραπάνω κατολίσθηση, αν και αποτελείται από ένα σύστημα μικρότερων κατολισθήσεων, γενικά ταξινομείται ως περιστροφική κατολίσθηση. Η αναγραφόμενες μετακινήσεις προσεγγίζουν τα 16μ και 7μ οριζόντιας και κατακόρυφης διεύθυνσης αντίστοιχα. Το μέγιστο βάθος της διάτμησης, εκτιμάται στα 40μ, βασιζόμενοι στις γεωτρήσεις αλλά και την ενόργανη γεωτεχνική παρακολούθηση. Η επιφάνεια της διάτμησης, μέσω ανάστροφης ανάλυσης, υποδεικνύει διατμητική αντοχή εκφρασμένη από τις παραμέτρους διατμητικής αντοχής του κριτηρίου Mohr Coulomb, συνοχή $c=0$ και γωνία εσωτερικής τριβής $\varphi=10°$.

Η παραπάνω ενεργοποίηση της κατολίσθησης σχετίζεται με τη πρόκληση τόσο προβλημάτων γεωτεχνικής φύσεως, όσο και προβλημάτων σχετικά με την τοπική κοινωνία. Τα προβλήματα αυτά επικεντρώνονται, στην επαναχάραξη της σιδηροδρομικής γραμμής, η οποία στη παρούσα κατάσταση, περνά από το πόδι της κατολίσθησης, η διασφάλιση του ασφαλούς περάσματος του ποταμού, το οποίο στη παρούσα κατάσταση περνά από το πόδι της κατολίσθησης, η οποία βρίσκεται στο δεξί αντέρεισμα της όχθης του ποταμού. Επιπλέον, η διατήρηση της ύπαρξης τόσο του δρόμου που περνά από το αριστερό αντέρεισμα της παραπάνω όχθης, όσο και των πηγών φυσικού ανθρακικού νερού που επίσης εντοπίζονται στο αριστερό αντέρεισμα, κρίνεται ζωτικής σημασίας. Έτσι λοιπόν, προτείνεται η κατασκευή αντίβαρου, στο πόδι της κατολίσθησης, λαμβάνοντας ωστόσο υπόψιν τη διατήρηση των προαναφερθέντων στοιχείων.

# Acknowledgments

Due to implementation of the current thesis I would like to express my gratitude to the Chief Manager of ILF branch in Georgia, Steve Moran, who allowed this dissertation to be carried out, and contributed to my accommodation, due to fieldwork, in Georgia.

I would also like to thank the employees from the China Railway 23rd Bureau and the ILF, branch in Georgia, whose cooperation due to completion of the current thesis proved vital as the staff in Aristotle University of Thessaloniki.

In addition, I am also grateful for the cooperation with Mr. Nikolaos Kazilis, M.Sc. geologist of ILF, branch in Georgia, whose professionalism, and attributing of the knowledge at the specific sector constitutes great example for me, and his guidance, modifications and instructions during the completion of the current thesis proved essential.

Nevertheless, I would also like to thank Mr. Vasilios Marinos, Assistant Professor at Aristotle University of Thessaloniki, supervision of the current dissertation, for his guidance and the cutting-edge notions and ideas, regarding the development of the dissertation.

In addition, I would also like to thank the members of the examining and the advising committee.

# Chapter 1 Introduction

## 1.1 General

Within the context of postgraduate studies in applied and environmental geology with sector of specialization engineering geology, at School of Geology of Aristotle University of Thessaloniki, the present dissertation was carried out.

The underlying dissertation focuses on the study of slope failure during railway construction in central Georgia, Caucasus. More precisely, in the present study, the evaluation regarding the formed landslide and its characteristics will occur, with purpose, to point out the risks engaged with the further development of the landslide and to provide feasible solutions for its stabilization.

The present dissertation was carried out within approximately four months. More precisely, although the subject of the dissertation was known, it begun with the arrival of the author at the site of construction, considering that the provided data about the failure and its characteristics were restricted earlier. Forty days, from 20th of August to 1st of October, were spent at the site, in which the exploratory geotechnical program was implemented. From 1st of October until the present time, the analysis regarding the collected data and the writing regarding this thesis were carried out.

The studied slope failure represents a part of construction, which is widely known as Georgian Railway Modernization Project, implemented by Georgian Railway. The contractor in this case is the company: China Railway 23rd Bureau. The supervision and technical support due to current project is provided by ILF consulting engineers, branch in Georgia, with whom the major cooperation have taken place.

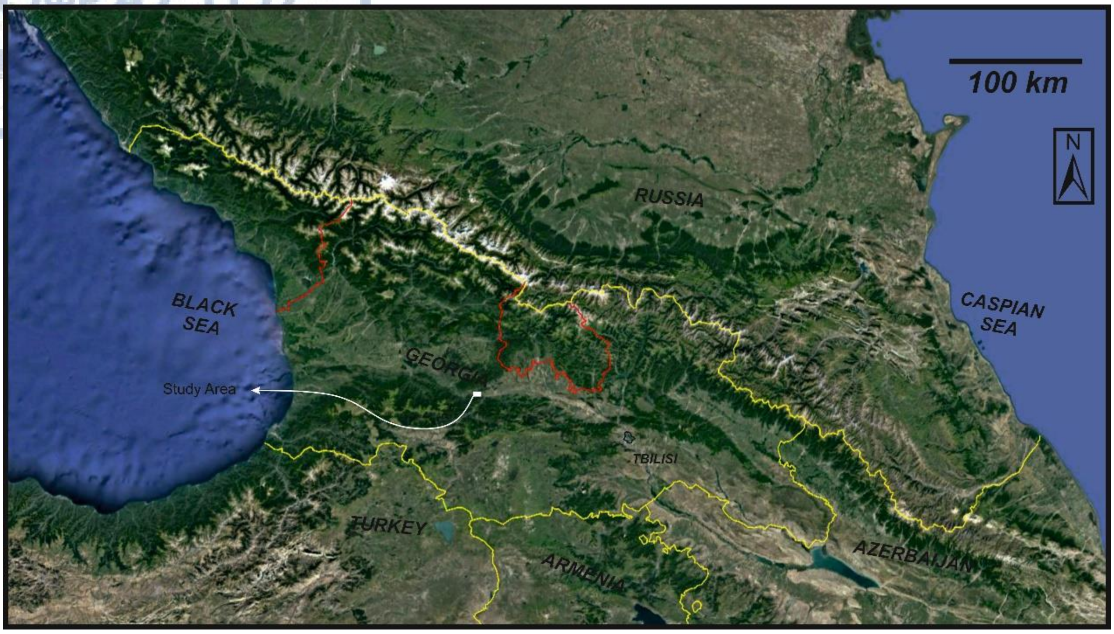

*Figure 1. Georgia, Caucasus (Google Earth).*

## 1.2 Study Area

Georgia is a country of Caucasus located at the borders of Europe and Asia. Georgia borders with Turkey and Armenia in the south, with Azerbaijan to the south east and Russia to the north. In addition, it shares borders with two autonomous territories of South Osetia and Abhkazia in north. The population of the country reaches four million people, and approximately 25% of the total population lives in Tbilisi, the capital of the Georgia. Other great cities of Georgia are Batumi, Gori and Kutaisi *(From Wikipedia).*

Geomorphologically, Georgia is located between two major mountain chains, the Great Caucasus in the north and the Lesser Caucasus in south, which are estimated as the highest mountains in the Europe. The biggest rivers in Georgia are considered Rioni, Alazani, Mtkvari and Enguri, which are generally oriented parallelly to the mountain chains *(From Wikipedia).*

The study area is located in Central Georgia, at the region of Imereti which capital is the city of Kutaisi. More precisely, the location is situated in the border of Shida Kartli and Imereti regions, and geomorphologically the area can be described as a mountainous territory. The construction of the railway begins from the city of Khashuri, major city of Shida Kartli region, to the city of Zestafoni, major city of Imereti region.

*Figure 2. The railroad network of Georgia, Caucasus (From Wikipedia).*

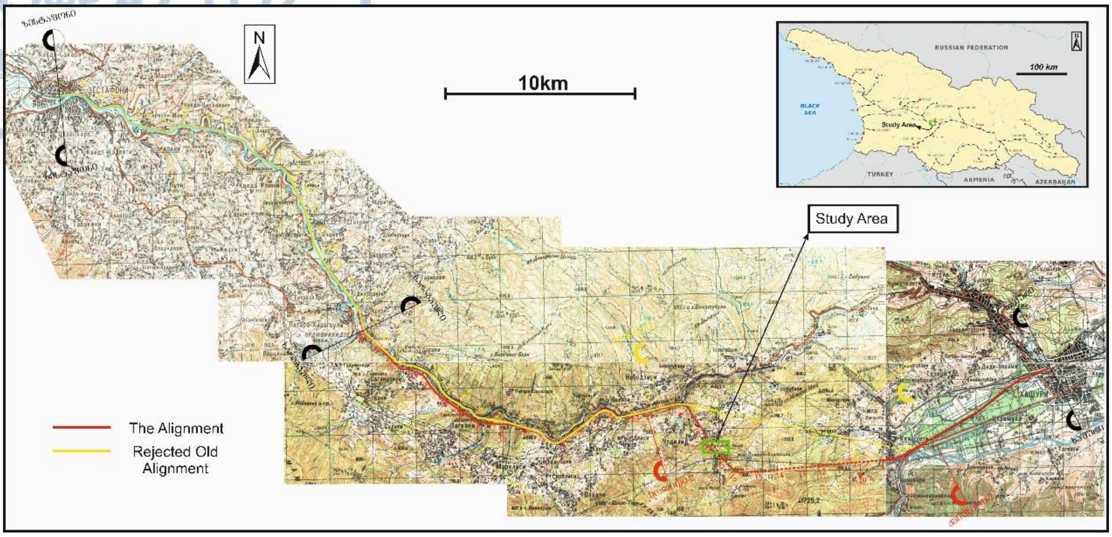

*Figure 3. The complete railroad alignment from Khashuri to Zestaphoni (from railway.ge).*

The construction of the railway is implemented within the context of railway modernization project, which is focused on the optimizing of the present conditions of railway. The aim of this project is to improve the current conditions in the Georgian Railways, concerning the quality of the railway mainline which runs from Tbilisi to western regions of Georgia, Batumi and Poti, the main ports of the country in Black Sea. The railway network includes a 40-kilometre mountainous gorge region in Central Georgia, in which the current study is taking place. The main purpose of the modernization project is to improve the average speeds from 55km/h to 80km/h, which corresponds at reducing of maximum gradient from 2,9% to 1,75%.

The underlying project is generally divided into two major categories. The first category contains the construction of new railroad, of approximately 20km from Khashuri to Moliti, and the reconstruction of the current railroad from Kharagauli to Zestafoni which is estimated 23km long. The section between Moliti and Kharagauili will remain approximately the same. The project of the modernization of Georgian railways includes the construction of single truck and double truck tunnels, bridges, culverts, subgrades, retaining walls, station and substations *(from railway.ge).*

*Figure 4. The area of railway construction from Khashuri to Zestafoni (Google Earth)*

## 1.3 The Aim of the Study

The aim of the present dissertation focuses at the complete evaluation of the stability regarding the slope failure. The complete evaluation includes the detailed study of the phenomenon of formed landslide, the recognition of risks involved from the underlying phenomenon, and finally to provide feasible solutions regarding to the stabilization of the slide.

More precisely, the detailed study of the landslide includes geological and engineering geological mapping at a scale of 1:1.000, exploratory boreholes, geotechnical monitoring, by which the detailed engineering geological model is acquired. The understanding of the engaged risks from the further, and in general, activation of the slide, is taking place. Finally, the suggestion of feasible counter measures regarding the stabilization of the formed landslide is to be occurred. Furthermore, the present thesis focuses on providing another case study regarding slope failure during construction, with more engineering and less environmental, approach.

## 1.4 Methods of Study

### 1.4.1 Field Work

During the implementation of the current thesis forty days were spent in the field in order to select all the valuable data regarding geological, engineering geological and geotechnical properties of features related directly and indirectly, with the stability assessment of the failed slope. Features which are related indirectly to the stability assessment, are composed by general data regarding adjusting to the close study area territory.

More precisely the fieldwork focuses at the supervising of the geotechnical exploratory boreholes and the completion, at the outset, of daily reports and finally the core loggings for ten exploratory boreholes. In addition, measurements related to the geotechnical monitoring, such as inclinometer and piezometer measurements, were also carried out. However, the most critical activity implemented at the field was the geological and engineering geological mapping which provides fundamental information for the geological and engineering geological characteristics of the area, related though to the construction.

### 1.4.2 Desk Work

The desk work was focused initially in the completion of drill logging data, and the geological and engineering geological map, at a scale of 1:1.000. Thence, the processing of raw data regarding the monitoring measurements took place, in order to product tables, diagrams and figures which are necessary in order to draw reliable conclusions related to the failure evaluation. Furthermore, the completion of engineering geological cross sections which followed, not only interpret and evaluate the current geological and engineering geological features, but also is to be used in the stability analysis which will follow. The estimation of mechanical parameter of the engaged geomaterial was followed by suggestions regarding the solution related to the instability.

During desk work several computer programs were used for the analysis of provided information, and they are referenced below.

- AutoCad
- Microsoft Office (Word, Excel, Power Point),
- Arc GIS of ESRI,
- Corel Draw,
- Matlab of Mathworks,
- Slide of RocScience and
- RocData of RocScience.

## 1.5 Provided Data

The information in which this dissertation is based, are categorized into three major categories. The first category is constituted mostly by information provided by the contractor. The second category contains data selected in the field by the author, and the third category contains bibliographical sources.

The first category contains:

- Topographical Map at a scale of 1:1.000.
- Surface monitoring data, regarding approximately 60 monitoring points.
- Aerial photographs UAV origin.

The second category is constituted by:

- Geological & Engineering Geological map at a scale of 1:1.000.
- Drill core loggings from ten exploratory boreholes.
- Raw Data regarding geotechnical instrumentation (inclinometers & piezometers).
- Field and core Photographs.

# Chapter 2 Theoretical Approach

## 2.1 General

At the present chapter, the theoretical approach of landslides will be presented. More precisely the classification of the landslides, regarding engineering point of view and also the mechanism of failure will be implemented. Furthermore, the analysis of mechanism of landslide, as the triggering factor is to be occurred. It is essential, before the current study be developed to present or define, important features regarding landslides. To be more accurate, the geometry of landslides, the segments and the features involved, is to be presented at following chapters.

In addition, in this chapter the presentation of the failure, considered essential. To be more accurate, in the end of the current chapter the major failure will be presented, accompanied with the triggering factor which drove to the incident. Furthermore, key factors regarding the preexisting geotechnical investigation will be also referred. The limited organization of engineering geological and geotechnical exploration programs, are considered the source of the problem, with great impact on the results regarding the construction.

## 2.2 Landslides

### 2.2.1 General

Down slope mass movements under the effect of gravity, are generally characterized as landslides. The term 'mass', involves soil, rock, organic material and also a combination among them. Contrary, the term movement involves falling, sliding or even flowing. Furthermore, landform formed by landslides can also be characterized as landslide (*Bell F.G., 2007; Highland, L.M., and Bobrowsky, P., 2008*). The landslides occur at slopes, which are formed by the surface excavation. The surface excavation can be occurred, by both natural (e.g. river erosion, coastal erosion etc.) or man-made (e.g. excavation for roads, railways, mining etc.) processes. Whether the formed slope is too steep, or the strength of the excavated material is gradually reduced, from the exceeding of the ground's strength, landslides are formed *(Price D.G. & de Freitas M.H., 2009*). Usually, slip surfaces are formed separating the failed material from the stable material, but the lack of the underlying surface is not rare, considering that landslide types such as falls, toppling and flows do not present such clear surfaces (*Bell F.G., 2007*).

In general, landslides are formed, because the ground is impelled by disturbing forces, usually composed by gravitational and hydrostatic forces, which are exceed the resisting forces, composed by materials' strength and also gravitational forces. The stability of the slope is depended on the slope angle, the shear strength of the material or the slip surface, the orientation of slip surface or any other discontinuity, the weight of the potential to fail material and the groundwater regime (*Price D.G. & de Freitas M.H., 2009; Bell F.G., 2007*). Considering that the stability is depended at the materials' or slip surfaces' shear strength, which is expressed by cohesion (c) and the friction angle (ϕ), the angle of slope (ω), the area of the sliding surface (A) and the weight of the sliding material (W), in simple scenario, the stability is expressed by the factor of safety (FS) which can be calculated by *(Price D.G. & de Freitas M.H., 2009*):

$$FS = \frac{\mathrm{cA} + (\mathrm{W}\cos\omega)tan\varphi}{Wsin\omega}$$

Safety occurs whether the FS is greater than unit.

The occurrence of landslides is taking place with a range of velocity. More precisely, there are landslides which are developed rapidly, and other landslides which are developed extremely slow. Most common rapidly developed landslides are considered rock falls, and contrary, very slow to extremely slow, developed landslides are considered soil creeps. However, it does not mean that other types of landslide cannot be developed rapidly or very slow. The knowledge of the landslides' velocity is considered vital in order to evaluate the risk regarding human life, properties, machinery, environmental effects and more, downslope.

| Description | Velocity (mm/sec) |
|---|---|
| Very Slow | $5x10^{-5}$ to $5x10^{-7}$ |
| Slow | $5x10^{-3}$ to $5x10^{-5}$ |
| Moderate | $5x10^{-1}$ to $5x10^{-3}$ |
| Rabid | $5x10^{1}$ to $5x10^{-1}$ |
| Very Rapid | $5x10^{1}$ to $5x10^{3}$ |
| Extremely Rapid | $> 5x10^{3}$ |

*Table 1. The characterization of a landslide based on the velocity of its occurrence (From Hungr O., et al 2014).*

Landslides usually are divided into several segments in order to be acquired better, or understand better the mechanism of failure. So, the describing of features existing at the landslide is considered vital. Several definitions regarding the geometry the dimensions and the existing features have been proposed. However, the most dominant appears to be

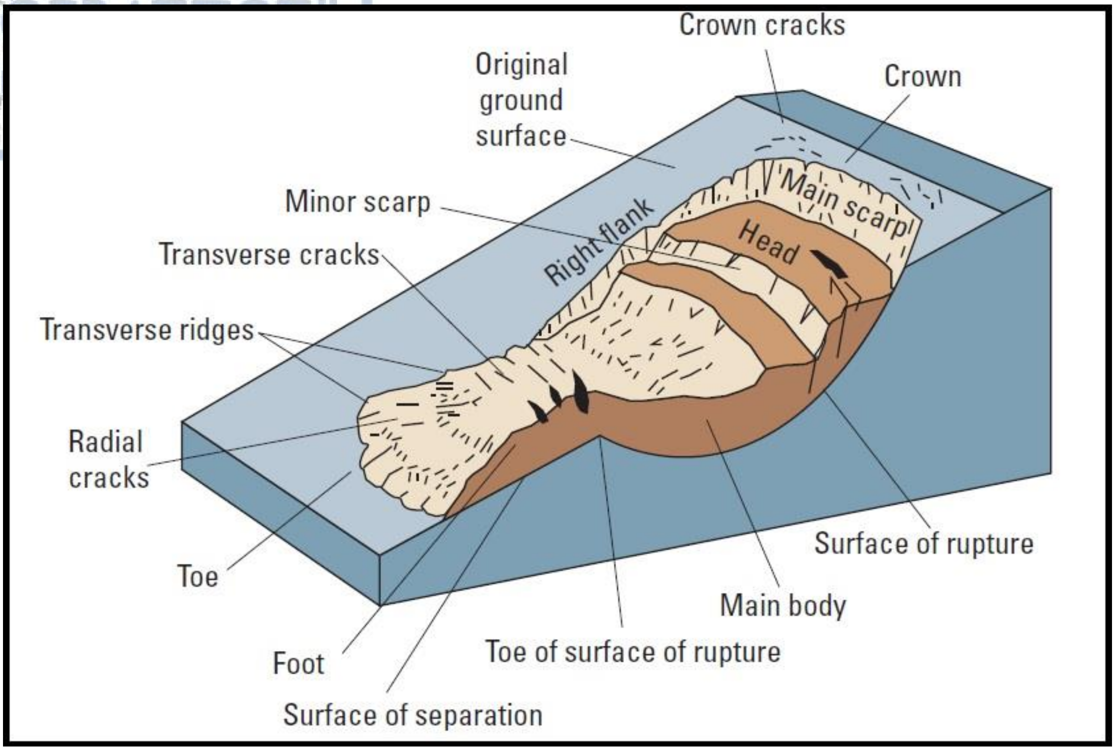

*Figure 5. The geometry and the characteristic features of landslides, demonstrated at a rotational landslide (From Highland, L.M., and Bobrowsky, P., 2008).*

proposed by *Varnes D.J., 1978 (From Cornforth, D.H., 2005; Cruden D.M., Varnes D.J., 1996).* The general terms regarding the landslides' geometry and features appear at *figure 5.* Beside those, the length of the landslide is considered the horizontal distance from the main scarp to the toe of the landslide. The width is considered the widest distance across the slope in which the landslide is formed and the depth of the landslide is considered the maximum depth of the sliding surface *(From Cornforth, D.H., 2005).*

### 2.2.2 Landslide Types

Many classifications for the landslides are existed, and they are mostly depended on the approach, which for example can be environmental approach or engineering approach. For engineering purposes, landslides are categorized into two major categories, which are the ground which is failed for the first time, and the reactivated slides. On site, the underlying cases are likely to appear as three types (*Price D.G. & de Freitas M.H., 2009)*:

- Downslope ground movements, as activated or reactivated, caused by natural agencies, such as river erosion and extensive weathering.
- Reactivated downslope mass movements, caused by man-made activities, such as excavation at the toe of the landslide, overloading the head of the slope or change the groundwater regime.
- First time failures, during and after excavations, as a result of failed design.

The underlying classification focus mostly on the reason of landslide occurring. Other classifications regarding the pattern of the failure, the pattern of triggering factor and more also occur. One of the most widely accepted classification is the landslide classification proposed by Varnes *(From Cruden D.M., Varnes D.J., 1996).*

It should be noted that the failures which occur on rock type material are different regarding the failures involved at soil type material, which are also referred as earth failures. The failures which are occurred at rock type of material are characterized by anisotropy in the movement, considering the orientation and the condition of discontinuities such as bedding, joints and faults, have a crucial impact on the pattern of failure, in contrast to the failures on earth type material which usually are behave as homogenous material *(Bell F.G., 2007).*

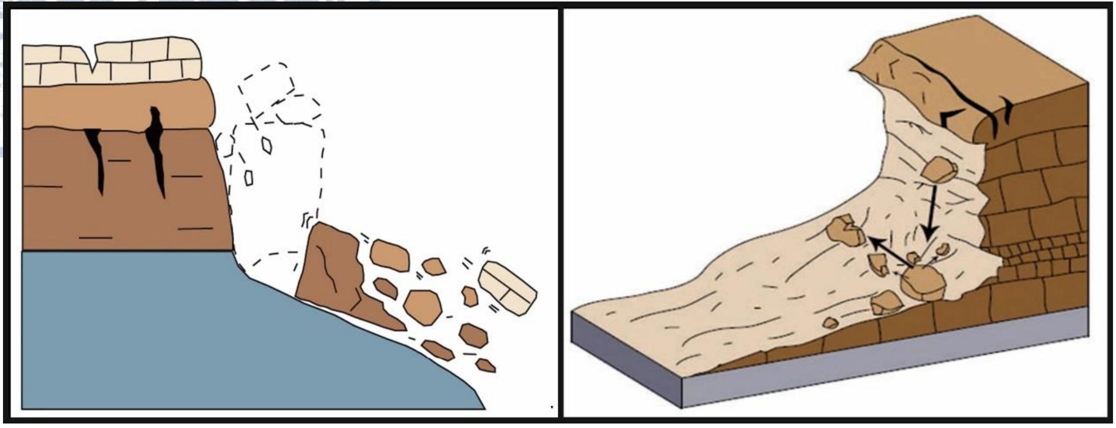

*Figure 6. Types of landslides, Toppling (left) and Rockfall (right) (From Highland, L.M., and Bobrowsky, P., 2008)*

### 2.2.2.1 Slope Failures on rock Formations

So, considering the underlying data, slope failures at rock type of material are categorized in:

- Rock falls,
- Topplings,
- Rock slides,
- Wedges,
- Rotational Slides.

Rockfalls *(figure 6, right),* are usually take place in steep slopes. The magnitude of fallen rock blocks ranges from gravel size to boulders with a diameter of several meters. The velocity of the landslide phenomenon in this case is considered as extremely rapid. This type of failure is usually developed at rocky banks of rivers, sea shores or even by man-made excavated slopes. It can be triggered by rainfall, earthquake or other intense shaking, weathering regarding freeze thaw cycle and else.

Topplings *(figure 6, left),* are usually developed rapidly at rocky slopes controlled by structural elements of rock mass, such as discontinuities. More precisely in this case the orientation of discontinuities, which is composed either by joints or bedding or even faults, is critical. The underlying discontinuities should be dipping opposite to the slope dipping with dip angles, greater than 60-70°. Topplings are usually triggered by differential weathering, development of pore water pressures within the discontinuity, shaking provided by earthquake or another source and more.

Rock slides *(figure 6, right),* usually are developed rapidly at rocky slopes controlled by structural elements of rock mass, usually the bedding. In this case, the slope and the major structural-critical element have the same orientation but the dip angle of the slope should be

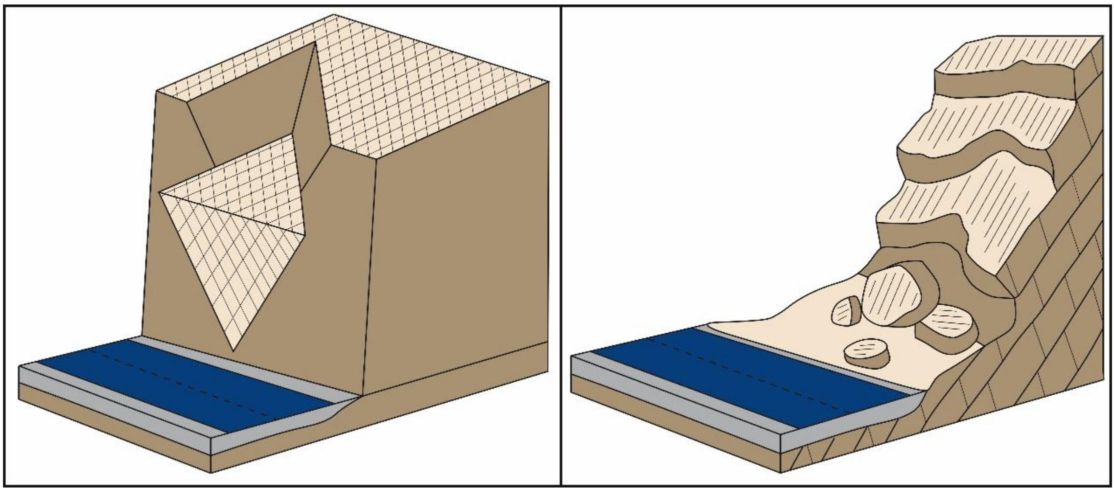

*Figure 7. Types of landslides, Rock wedge (left) and Rock slide (right)*
*(Modified, Highland, L.M., and Bobrowsky, P., 2008).*

greater than the dip angle of the major structural element (e.g.bedding). Such failures are common during the construction of roads or railways, so usually are triggered by man-made excavation. However, this kind of landslides could also occur at river banks or sea shores and more. In addition, the weathering through the discontinuity is also crucial factor, which reduces the shear strength from on the surface of discontinuity. Common triggering factors are also considered the shaking by earthquake or other source, intensive rainfall with increase of pore water pressure at the surface of discontinuity or another *(Highland, L.M., and Bobrowsky, P., 2008).*

Rock wedges *(figure 7, left),* are very similar with the rock slides as a landslide pattern, however the slip is taking place at the section of two discontinuities. The strike of the section should be oriented parallelly to the dip direction of the slope, and the dip angle of the slope should be greater than the dip angle of the section.

Rotational slides *(figure 5),* although are usually observed at soils, they are taken place at rock type formations, whether the strength of the rock mass is deeply reduced by geodynamic or surface processes.

#### 2.2.2.2 Slope Failures on Soil Formations

In contrast, slope failures at soil type of material are categorized as slides and flows. The major slides which occur on soil type material are:

- Rotational slides,
- Translational slides,
- Topplings,
- Lateral spreads.

Rotational landslides *(figure 5),* are the most common types of slides occurring mostly at soils. At rotational landslides, the major scarp appears to be curved upwards, and have the characteristic spoon shape. In addition, this kind of slope failures are called rotational, because they appear rotational movement. This movement occurs regarding rotation axis which is perpendicular to the length of landslide and is placed approximately at 3/5 from the scarp. So, in this type of failures, sizable vertical movements are taking place. More precisely, at the head of the landslide settlements occur, in contrast to the toe of the slide where uplift can be observed. The uplift at toe is characterized as back tilt, because beyond the uplift rotation occurs, resulted a low angle slope with dipping contrary to the morphology. The surface of failure which depth is 0.1-0.3 of width, appears to be curved too. To be more accurate the surface could be circular, usually at homogenous geomaterial, or non-circular curve whether the material is heterogenous. The magnitude of shearing at the surface of the rupture is considerable different than the shearing at the material within the landslide mass. So, the internal deformation above the surface of the rupture is limited *(Highland, L.M., and Bobrowsky, P., 2008; Knappett J.A., & Craig, R.F., 2012;*)

Rotational landslides occur at slopes with dipping angle ranging among 20°- 40°, and they are developed from very slow to rapid. In order to approach better the pattern of the failure, it is essential to divide individually each landslide into three major segments or parts. The head of the landslide, in which the maximum settlements and lateral displacements occur, is composed by minor cracks with similar geometry to the scarp of the landslide. The main body of a typical rotational landslide is located approximately to the middle of the failure. The magnitude of lateral displacements are comparable to the head of the landslide, however, the vertical displacements usually are restricted compared to the head of the slide. The last segment of a rotational landslide is the toe of the landslide, in which the characteristic back tilt is observed.

Rotational landslides occur in a vast of material from rock formations, coarse of fine grained soils, and even fills. It can be triggered by intensive rainfall, shaking, excavation at the toe, change in groundwater regime and more. Those types of slides occurring at

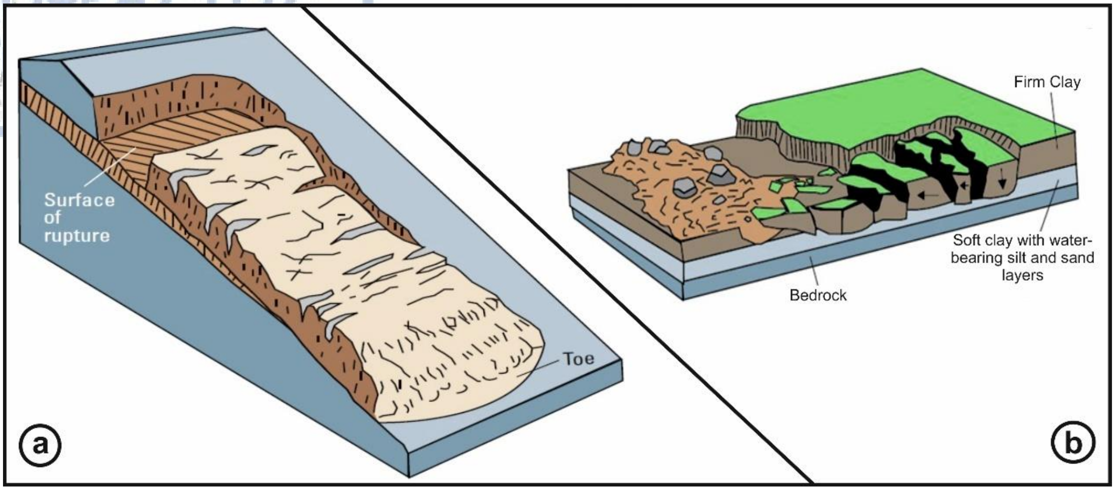

*Figure 8. Types of landslides, Translational Slide (a) and Lateral Spreads (b)*
*(From* Highland, L.M., and Bobrowsky, P., 2008*).*

mountainous territories, combined with intense rainfall, can easily developed into flows, such debris and earth flows.

Translational landslides *(figure 8, a),* appear to be similar with rock slides, however in this case the failed material is composed by soil. Translational landslides are also common, and they usually occur between the residual soil, and the bedrock, with a slightly curved or planar surface of rupture, which is considered the underlying geological contact. In contrast to the rotational landslides, where usually there is a considerable rotational movement and then the development of the phenomenon decrease, at translational landslides the phenomenon carries on, whether the surface of rupture is inclined, or until the phenomenon stops by geomorphological issues. Generally, the translational landslides are considered shallow landslides and regarding their velocity, at the outset they can developed slowly but usually they gradually accelerate with a result to be developed extremely rapid. As, in rotational slides, translational slides can be easily developed into debris or other type of flow. Regarding the triggering factors, the translational landslides can be easily triggered by rainfall, earthquake, excavation in the toe, similarly to the rotational slides. In addition, translational landslides are similar, whether the soil is characterized permafrost, during thaw period *(Highland, L.M., and Bobrowsky, P., 2008).*

Toppling at soils occur similarly with the toppling at rocky materials. However, now the discontinuity usually appears to be a tension crack, which is vertical, and usually the stratum below the failed material is very susceptible to weathering and erosion. The environments in which toppling at soil type of material are developed, are the coastal territories, in which the erosion, by waves, at formed cliffs, is intense, and cliffs are becoming steeper and steeper, with a result that the soil material regardless how compacted it is, cannot support itself. So, vertical, or slightly inclined towards the cliff, tension cracks are created and toppling occurs. These types of failures, as it is described, are triggered by intensive erosion to the toe, but the intense rainfall and seismic shaking will also have crucial impact at the stability of the slope *(Highland, L.M., and Bobrowsky, P., 2008)*

Lateral spreads *(figure 8, b),* occur usually at a specific geological pattern. The pattern involves the existence of stiff or firm, 1-5m thick, layer of clay overburden to loose sandy material. The exceeding pore water pressure developed by dynamic or static source, liquefies the layer of sandy material with a result, lateral and vertical movement of the overburden clay. In order to lateral movement be developed, the layers or the morphology should be at least slightly inclined. In addition, lateral movements are developed very slow to moderate speed. Considering the mechanism of the phenomenon, they are common in regions with active seismicity. So, the triggering factor could be considered the liquefaction provided by seismic shaking. Furthermore, static liquefaction is developed without seismic triggering, which means that lateral spreads are likely to happen in regions without seismicity. The only criterium in this case is that the ratio of pore water pressure in the liquefiable layer to the effective stress in the same layer should be greater than unit (*Kramer, S.V., 1996; Highland, L.M., and Bobrowsky, P., 2008)*

The earth flows are subdivided into:

- Debris flows,
- Lahars,
- Debris avalanches,
- Earthflows and,
- Slow Earthflow (Creep).

Debris flows *(figure 9, a),* which are also known as mudflows, are commonly observed at mountainous territories with high precipitation levels, or sustain snow melting periods. It can be described by mass, composed by water, rock fragments, soil, organic matter and also tree trunks or other vegetation, flows downslope. It is likely that other types of landslides combined by availability of water, such as intense rainfall or snow melting, developed into debris flows with catastrophic results downslope.

Lahars, are considered debris flows, developed with significant speed. However, they are composed by the output of volcanic eruptions and the content temperature is considered significantly greater regarding debris flows. When the volcanic eruption accumulates, most commonly tuffs, at the slopes of the volcano, the slopes are becoming steeper and steeper, resulting landslides. Considering that due to volcanic eruptions, the close area suffers earthquakes, and during eruption tuffs which are not considered completely solid are deposited into unstable slopes, lahar is produced. Furthermore, intense rainfalls have vital impact on unsaturated material such as tuffs, considering that the additional shear strength of unsaturated soils, contributed by matric or total soil suction, due to rainfall is lost *(Fredlund D.G., et al 2012)*, and flows are produced.

Debris avalanches *(figure 9, c),* are characterized by their magnitude and are developed extremely rapidly. These failures usually occur at territories with unstable ground and are commonly triggered by intense rainfalls or massif and rapid snow melting. Debris avalanches can be easily developed into debris flows or lahars.

Earthflows *(figure 9, d),* generally can be rapidly developed, whether the shear strength of the failed material is suddenly gone. This type of behavior is ordinary at Loess formations,

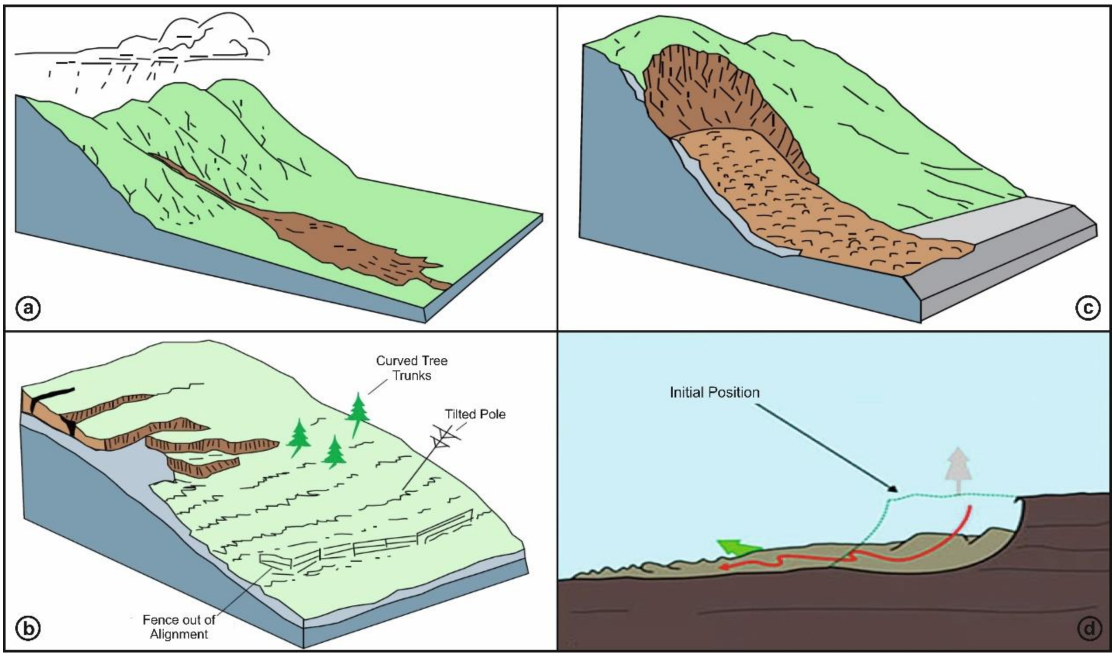

*Figure 9. Types of flows. (a) Debris flow, (b) slow earth slow (creep), (c) debris avalanche, (d) earth flow.* (Highland, L.M., and Bobrowsky, P., 2008)

which are collapse under the impact of moisture. In this type of soils, in unsaturated conditions, the shear strength is expressed by the equation, modification to Mohr-Coulomb criterium, proposed by *Fredlund D.G., et al., 2012*, in which the shear strength of soil is contributed by matric or total soil suction, and is lost whether the saturation is acquired.

Slow earthflows *(figure 9, b),* which are usually referred as soil creeps are considered very to extremely slow downslope movements of soil. Soil creep is divided into three major categories. The first category involves seasonal movements of soil depended on a period of intensive rainfall or snow melting, and period of drought. The second category involves continuous movement on the slope, with the same velocity, which means that the shear strength of the material is continuously exceeded, but in restricted magnitude, by the shear deformation. The third category is associated with gradual acceleration of the movement, until other type of failure is triggered. The earth creep is considered common phenomenon worldwide. It occurs generally at gentle slopes, in which constructions could be observed, and being damaged. The triggering factor depends at the creep category, but generally the poor drainage of rainfall and snow melting, the destabilizing constructions and the weathering, restricted shear strength of the soil, contribute to the development of the phenomenon *(Highland, L.M., and Bobrowsky, P., 2008).*

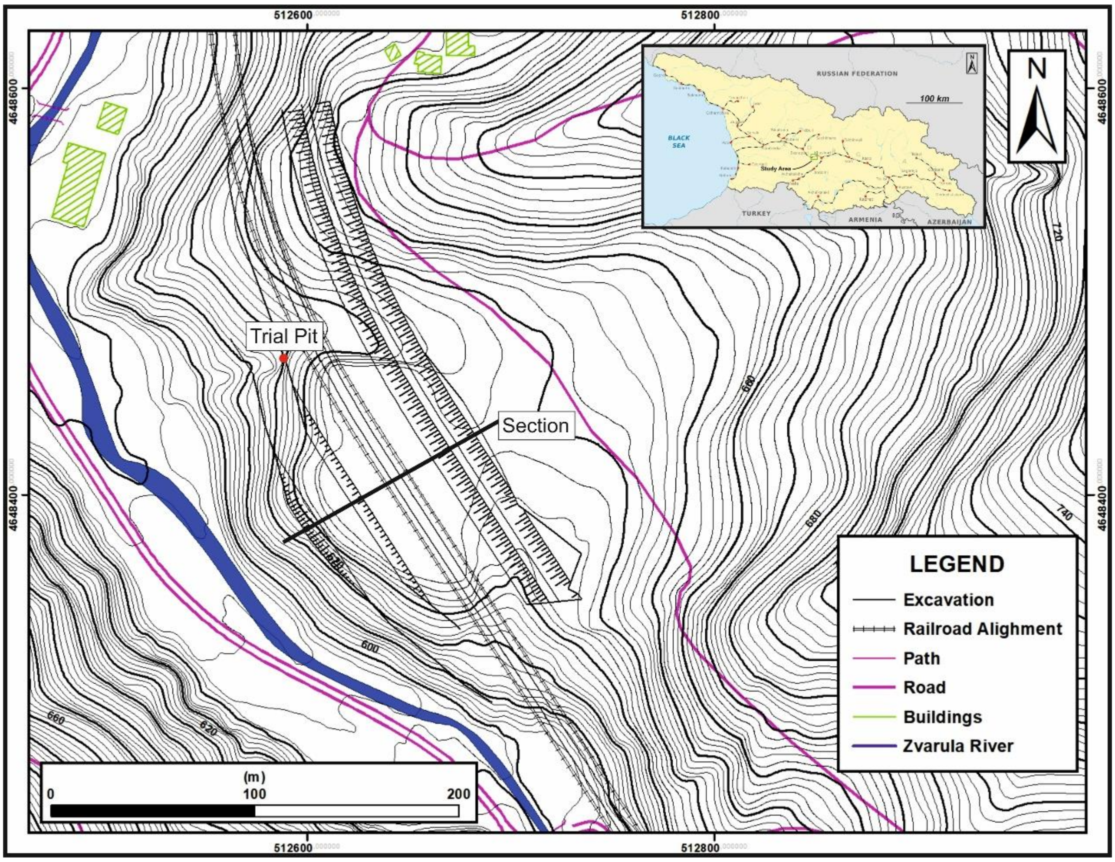

*Figure 10. The Topographical map, with depicted the excavation, the presented outline section and Trial pit. Contour interval 2m (provided by contractor).*

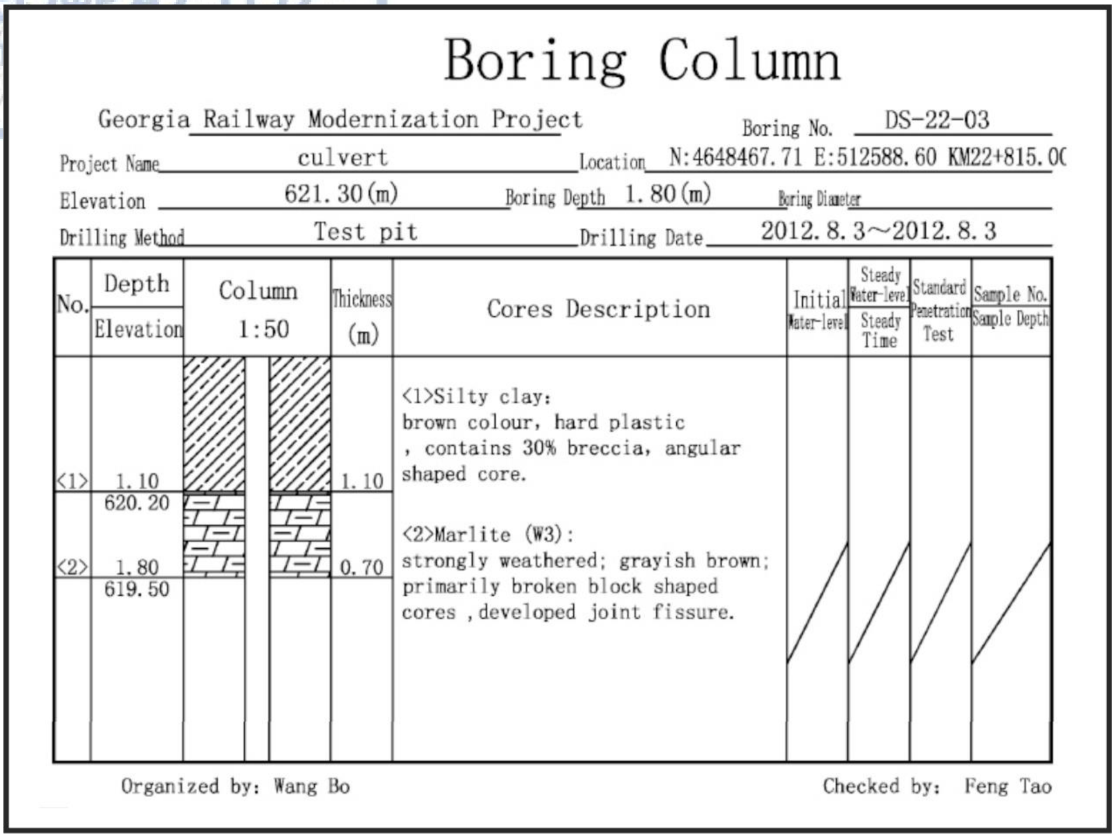

# Boring Column

Georgia Railway Modernization Project Boring No. DS-22-03
Project Name culvert Location N:4648467.71 E:512588.60 KM22+815.0
Elevation 621.30(m) Boring Depth 1.80(m) Boring Diameter
Drilling Method Test pit Drilling Date 2012.8.3～2012.8.3

| No. | Depth<br>Elevation | Column 1:50 | Thickness (m) | Cores Description | Initial Water-level | Steady Water-level<br>Steady Time | Standard Penetration Test | Sample No.<br>Sample Depth |
|---|---|---|---|---|---|---|---|---|
| <1> | 1.10<br>620.20 | ▨ | 1.10 | <1>Silty clay: brown colour, hard plastic , contains 30% breccia, angular shaped core. | | | | |
| <2> | 1.80<br>619.50 | | 0.70 | <2>Marlite (W3): strongly weathered; grayish brown; primarily broken block shaped cores ,developed joint fissure. | | | | |

Organized by: Wang Bo Checked by: Feng Tao

Figure 11. Logging from Trial Pit, located at the toe of the landslide, from the preexisting geological and geotechnical investigation (provided by Contractor).

## 2.3 The incident of the failure

In the close study area during subgrade excavations, slope failure occurred. The excavation, which serves two purposes, is described well at *figure 12,* and its spatial distribution can be observed at *figure 10.* The first purpose is the obvious one, considering that the alignment of the railroad is planned to cross the specific subgrade as it is illustrated at *figure 12*. The second purpose, focuses at the creation of relatively flat area in which other works regarding the construction can be occurred. Considering that in such mountainous territory, the flat areas in which those type of works could take place are restricted.

Although there was clear geomorphological indication about preexisted landslide at close study area *(figure 10),* and will be discussed in detail in next chapters, the preexisted geological and geotechnical investigations drive to the failure. First of all, the close study territory was approached with one shallow trial pit in 2012 *(figure 11).* Secondly, the trial pit reached rock type formation at depth of 1.10m, continued up to 1.80m and stopped. In addition, the trial pit was located 40m to 290° from the committed and evaluated by this study, borehole BDZ_22_05, at the north-right flank of the existing landslide. Not only the choice of trial pit in this case was incorrect but also the location in which it was located. The location was incorrect because in such cases the investigation should be carried out at the center of the study feature, in order for the sample taken, be more representable. Furthermore, considered that the material in such cases is completely heterogenous, the 70cm thick excavated rock is easily interpreted as a boulder. So, the implementation of one trial pit is barely considered as an investigation regarding the nature of studying material. So, in this case, at the outset engineering geological mapping should have been carried out, which would indicate the presence and the magnitude of the old stabilized landslide, and then geotechnical investigation should have followed by the implementation of geotechnical exploratory boreholes to approach the depth of the old landslide, and more precisely the shearing zone.

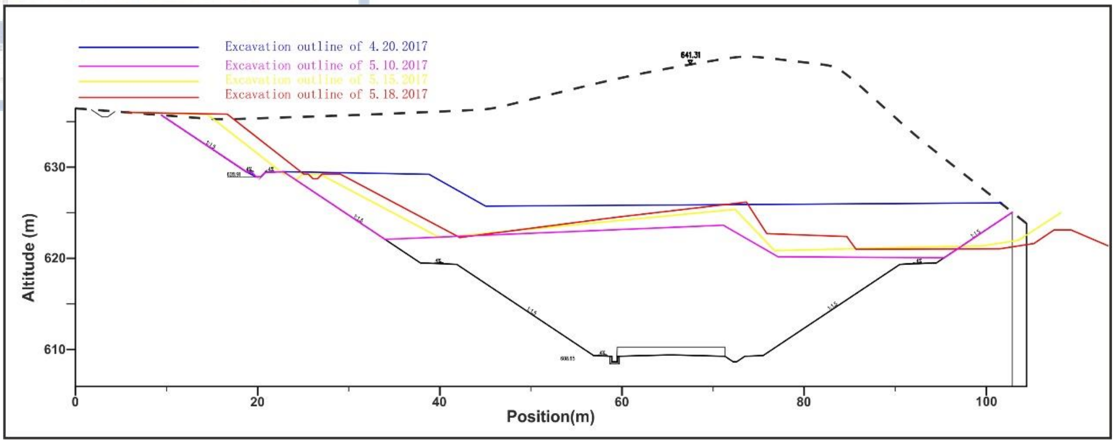

*Figure 12. The Excavation outline development with time (Provided by the contractor).*

Of course, after the recognition of the old stabilized landslide, boulders with varying diameters should be expected during drilling.

Although warnings regarding the old stabilized landslide were depicted, by the engineers of the supervisors, the excavation was implemented anyway. At the outset of the excavation process, at 20/04/2017, excavation until approximately the first bench occurred, as it is illustrated at *figure 12*. After the completion of this excavation failure did not observe and the excavation continued until 10/05/2017. The excavation stopped at 13/05/2017 when the major failure occurred. The failure was observed immediately, considered that displacements and the velocity of the displacement approach 1-2m per day.

Considering that during failure no seismic event observed, and the meteorological events were stable from 20/4/2017 to 13/10/2017, the triggering factor of the landslide is concluded the excavation. More precisely taking account the geometry of the formation, the triggering factor of the landslide in this case was the excavation at the toe of the old landslide.

# Chapter 3 Geological & Engineering Geological Surface Investigation

## 3.1 General

The surface investigation on site of construction, is mainly composed by geological and engineering geological mapping. The approach of the close study area of construction, by surface mapping, is one of the most important investigation tools. Subsurface investigation, through the implementation of exploratory boreholes, trial pits, geotechnical instrumentation related to the monitoring, are considered also important investigation tools. The purpose of geological and engineering geological mapping is firstly to understand the engineering geological and geotechnical conditions at the site of construction. Secondly, more detailed investigation should be carried out and finally the geological and the engineering geological map of large scale, shall be produced, in which all the characteristic features with impact on the construction, should be depicted.

It is fair to point out that the geological mapping is partly different process than the engineering geological mapping. The performance of engineering geological mapping must occur on large scale, in order to approach in detail, the features which have significant impact on the construction. The scale of engineering geological mapping begins from 1:2.000, and approaches scales of 1:500 and 1:200. Most of such maps are conducted at scale of 1:1.000. In contrast, geological mapping, is implemented at small scales, which begin from scale of 1:100.000 and high resolution geological maps are committed at scales of 1:10.000 to 1:5.000. In addition, geological maps are implemented in context of understanding the processes of geological evolution, regarding geodynamic and surface processes, which occurred at certain location. The major difference in geological and in engineering geological maps is the purpose of the mapping, which for engineering geological mapping is more specific. So, in engineering geological mapping, only the features which have an impact on the construction should be mapped in detail *(Price D.G. & de Freitas M.H., 2009).*

The result of engineering geological maps, is the knowledge of spatial distribution of features, which are considered as map units, and their characteristics, considering lithology and composition, structure, tectonic disintegration, weathering, even the strength and much more. So, lines which represent the boundaries between map units are also presented, as well as lines which represent geological faults.

Furthermore, the mapping of structural elements such as joints, bedding or foliation should be carried out. There are plenty of ways to illustrate those elements such as lines like faults or curves, structural diagrams or specific symbols which are indicate the strike, the dip direction, and labeled dip angle of the structural element. The lines and curves are rarely used at engineering geological maps in contrast to the structural diagrams and the specific symbols. Structural diagrams are used whether more than single set of joints occur, in order to avoid confusions, but in general the symbol indicating the strike and the dip direction has satisfying results.

All the underlying data, are collaborated in order to accurate engineering geological model be created for the site of construction. In addition, it is possible to export two, or even three-dimensional models, taking into account only the result of mapping. More accurate models though, are exported by combination of surface, subsurface investigation and geotechnical monitoring.

In the current study, engineering geological mapping occurred on area of approximately 0,4km$^2$ (770 x 490m). The mapping took place at a scale of 1:1.000, and it was focused, not only in failed geomaterial, but also to the adjacent formations with impact on the construction. The geological and engineering geological mapping in this study, was approached by three different points of view, which in total resulted the final engineering geological map *(Appendix, figure 165).* The study area was approached at the outset, in small scale, and then in large scale. To be more accurate, the approach begun by observing geomorphological features at small and thence large scaled topographical maps. It continued by selecting vital information by aerial photographs and satellite imagery. Finally, the study area was approached geologically at small scale initially and thence in large scale respectively.

The geomorphological and the approach by aerial photographs and satellite imagery, will provide vital elements, which would be taken into consideration in geological approach, which will result, the engineering geological map.

The features which will be taking into consideration from the underlying processes will be:

- Map units, which indicate groups of geological formations with same characteristics on the constructions' site.
- Structural features, which are the geological faults, bedding, joints etc.
- Surface ruptures (cracks) strongly on the site of constructions.
- Hydrogeological regime, at close study area.

## 3.2 Geomorphological Approach

At the current study, the close study area was approached, at the outset in small scale in order to detect mega-structures in the referenced and adjacent territories, which impacts directly and indirectly at the site of construction. Thence, the study zoomed up on the close study area, and large scale geomorphological study at the site of construction, conducted.

### 3.2.1 Small Scale Approach

In the very early stage of mapping, the analysis of small-scale geomorphology was carried out. The underlying analysis occurred on topographical map, produced by digital elevation model (DEM) of U.S.G.C., with contour interval of 5m *(figure 13).* In this map, it is possible to produce crude observations related to the general orientation of ridges and basins. It is also possible to correlate, in crude of course level, this type of observations with geological processes which generally formed the current morphology.

The detailed observation of topographical map of *figure 13,* provides general information, related to the geodynamic evolution of the wider area. Generally, lineation with strike ENE-SSW is observed. This crude observation is confirmed by the map of *figure 14*, which represents the orientation of slopes. To be more accurate, in the study area, there is a major river, called Zvaroula, with orientation NNW-SSE, and runs to NNW where joints another major river which has an orientation of ENE-SSW, the same with the major lineation represented in the topographical map. Although Zvaroula river is oriented perpendicular to the main lineation observed on the topographical map, there are a dozen of other cases of streams which run to the zvaroula and they are oriented according to the main observed lineation. Those lineations indicate structural data, related to the geodynamic evolution of the wider area. More precisely, it is likely for those elements to be geological contacts or even geological faults in which river and streams now run.

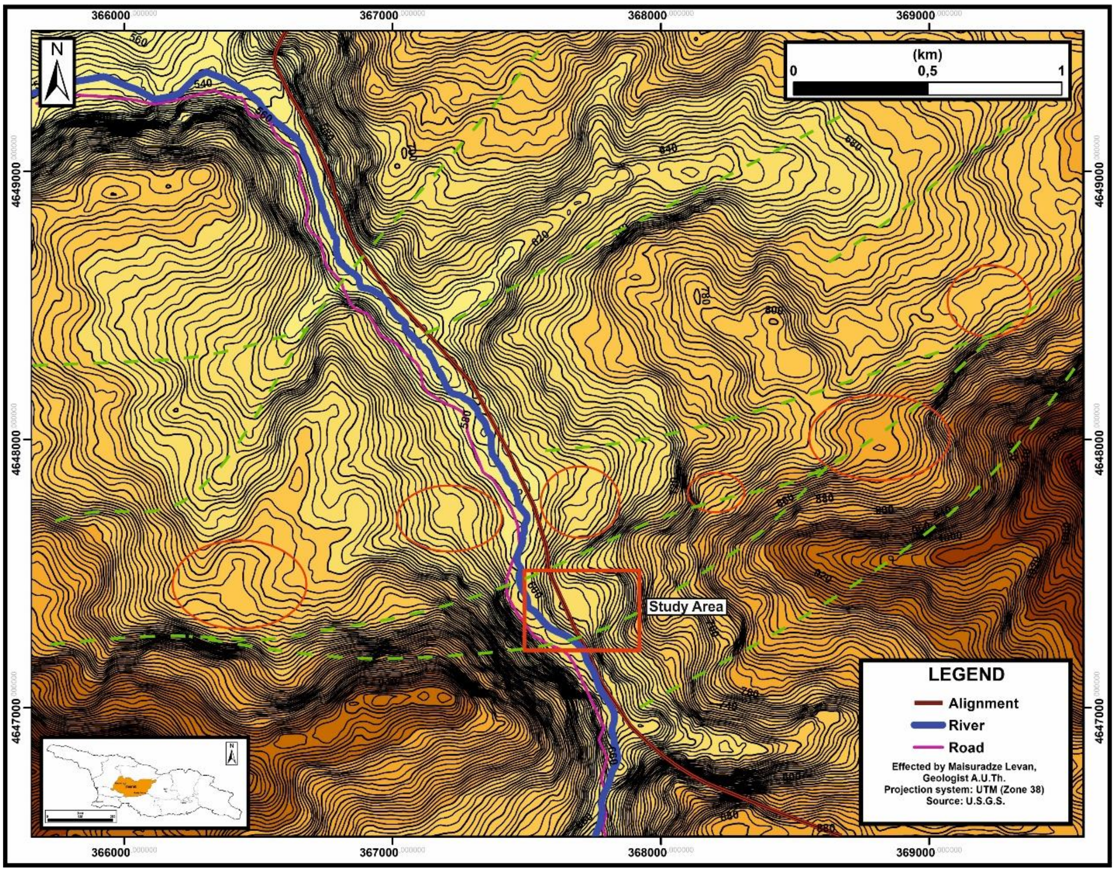

*Figure 13. Regional (large scale) topographical map of study area. Red square represents the study area, red circles old landslides and green dashed lines, lineation related to geological contacts or faults (Modified, U.S.G.S.).*

Furthermore, a change in the morphology, from mountainous to more flat area, occurs from south to north, and considering that the morphology of the northern area, which becomes mountainous again, there is a formation of basin in the middle with ENE-SSW direction. The presence of the basin, can be explained by two major assumption. The first assumption includes geodynamic activity, and more precisely conjugated normal faults with the underlying orientation. The second assumption includes less geodynamics and more surface processes. According to the second assumption, the geological formation in the basin is more favorable to erosion than the formation northern and southern of the basin. So, this basin was created by the erosion, of susceptible to it formation which is located between other formations, lesser susceptible to erosion.

To conclude about the geodynamic evolution of the wider study area, the existence of major structural elements, such as geological contacts or geological faults, with strike of ENE-SSW is observed.

Beside the structures which are related with geodynamic evolution, in the map of *figure 13*, the presence of landforms related to landslides occur too. So, a sequence of abnormalities and irregularities in the form of contour curves occur along of wide area in which the morphology changes. More precisely, those irregularities appear to occur in area where the morphology transforms form mountainous terrain to more flat terrain. This change of morphology occurs alongside to relatively straight line which indicates a change in geological structures, and possibly constitutes geological contact or even fault. The underlying abnormalities in the form of the contours in mountainous territories, indicate the presence of landslides. To be more accurate, those kinds of abnormalities pinpoint landslides, which happened to the past, and now they are temporarily stabilized.

The process of landslide generally creates steep scarp upslope and wide flat area downslope. Sometimes, the wide area downslope presents an inclination contrary to the

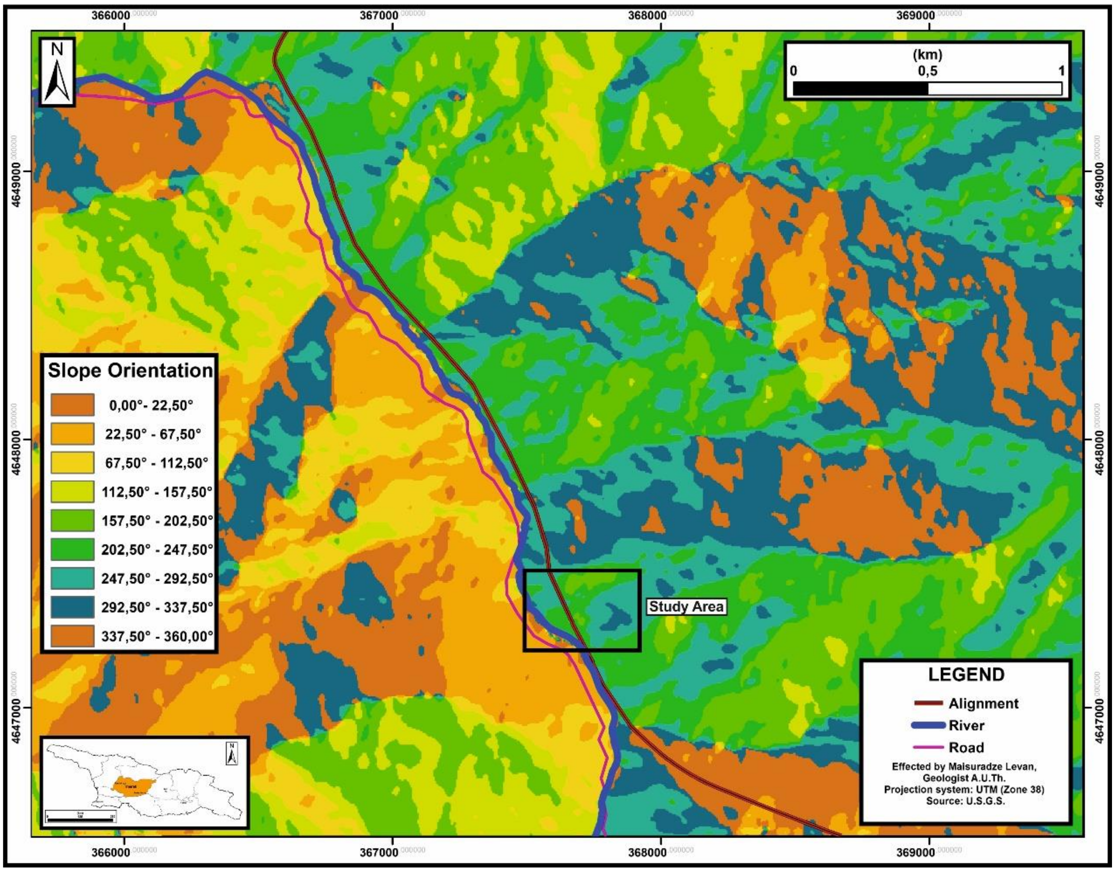

*Figure 14. Aspect map, which presents the orientation of slopes regional (large scale) of study area. In black square, the study area.*

morphology. The underlying process creates the referenced abnormalities in the contour lines.

Beside the morphological approach by crude observation of topographical maps there are other techniques, according to which the recognition of flat areas, and consequently the detection of old, stabilized, landslides, is possible. Taking into account, maps which represent the terrain steepness *(figure 15; figure 18),* the presence of landslides in various territories, is more detectable. More precisely, the existence of flat areas among steep territories indicates most likely old landslides. This happens because firstly, the landslides occur in territories in which the slopes are steep and secondly the existence of flat areas among steep slopes is not ordinary. It is worth to mention that riverbed territories, which are flat by definition, should not be taken into consideration.

In the wide study area, although there is a presence of several cases in which old now stabilized landslides appear, three of them are relatively close to the alignment of the railroad. This is concluded by observation of both, topographical *(figure13)* and slope steepness map *(figure 15)*, in which abnormalities on the contours are observed, as well as suspicious flat areas. So, the statement of existence of three major, incidents of old slides related to the position of the alignment is noticeable and unquestionable.

It is worth to mention that the accuracy of the underlying maps *(figure 13,14,15)*, considering not only the alignment but also other structural data, is limited. The purpose of studying those maps though, is to understand the concept of geological regime, considering geodynamic evolution and surface processes which are responsible for forming the study area as it is now.

Furthermore, considering that the current study, begun after the major incident of failure, and the underlying data present the morphology before failure occur, the existence of the ancient landslide, which was reactivated during the construction, was detectable. In addition, the landslide was detectable on small scale map with restricted accuracy, which means that the dimensions of the old landslide are sizeable.

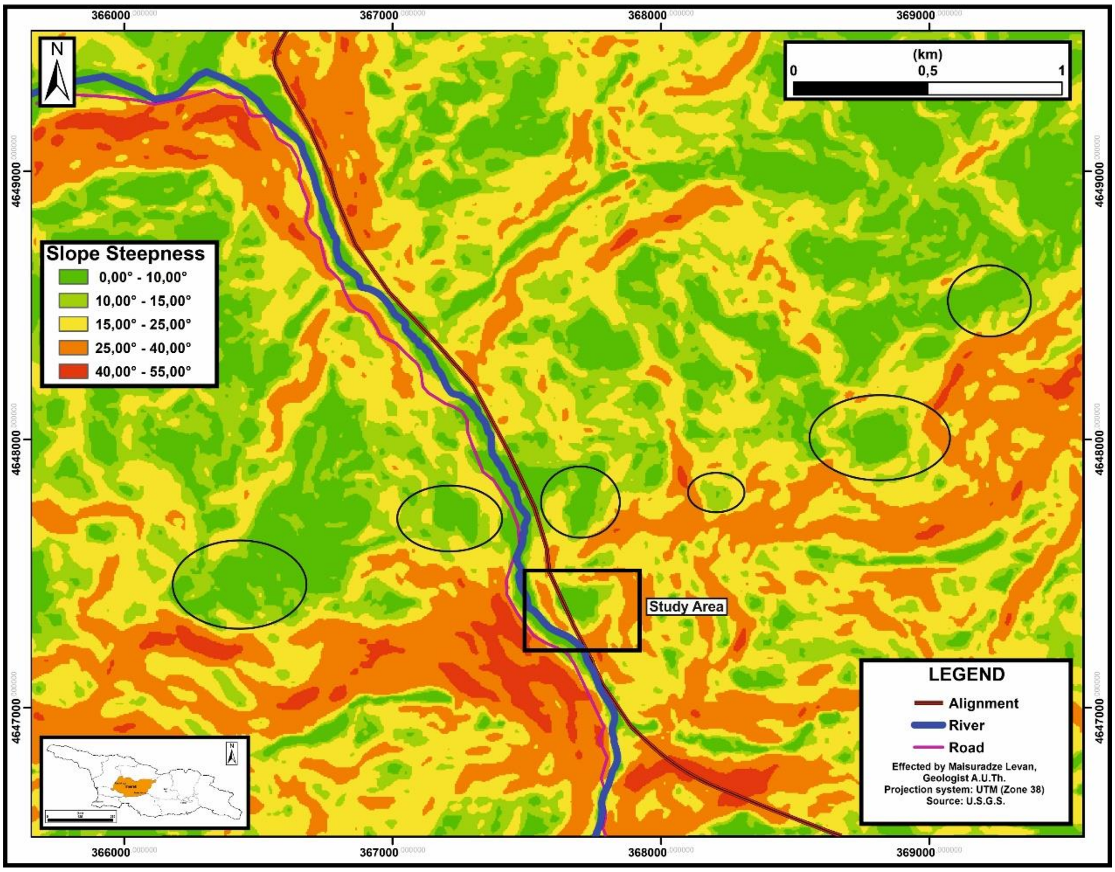

*Figure 15. Map of slope inclination in wider of study area territory. The black square represents the study area.*

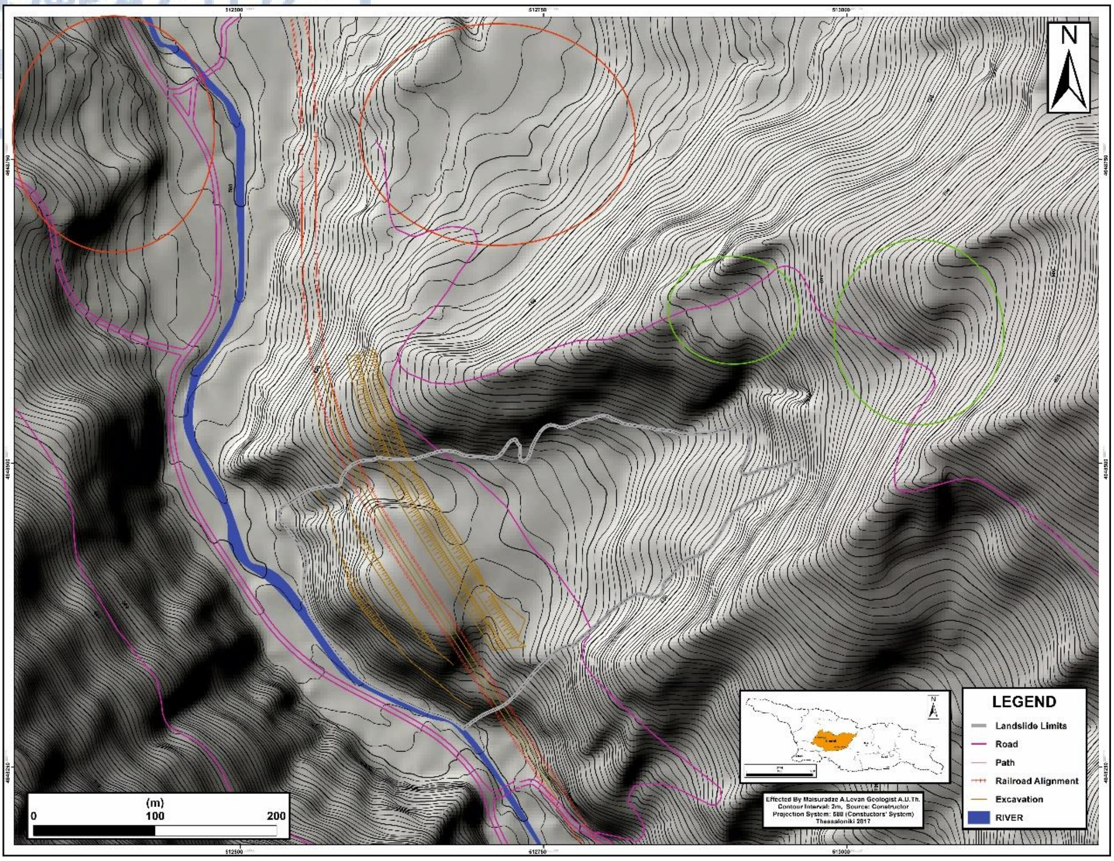

Effected By Maisuradze A.Levan Geologist A.U.Th.
Contour Interval: 2m, Source: Constructor
Projection System: 580 (Constuctors' System)
Thessaloniki 2017

*Figure 16. Large-Scaled topographical map of close study area. The grey line represents the limits of landslide. The green circles indicate flat areas NE than landslide which needs to be investigated, and red circles indicate sizable landslides northern, effecting the alignment.*

### 3.2.2 Large scale Approach

Similarly, to the study of small scale topographical map, study of large scale topographical map *(figure 16)* is considered vital, and should be implemented, before visit in the area has paid. Firstly, the accurate topographical maps of one area, is valuable in order to understand accurately the morphology of it. Secondly, the accurate morphology indicates important geological structures considering not only surface processes, such as erosion and landslides, but also geodynamic evolution, such as geological faults and contacts.

To begin with the surface processes, in the close study area, Zvaroula river, which runs from SSE to NNW, with noticeable curve towards WSW is observed. To the left of the river there is an area presented by steep slopes, without abnormalities and irregulates in contours, which generally means, based only at the morphology, that there is not any noticeable case of landslide in this slope. In contrast, at the right of the river slope, the position in which the underlying curve of the river occurs. Closely to the river the slope is steep, but it is becoming very flat in relatively close distance from the river. The flat underlying territory, which dimensions based only on the flat area illustrated at *figure 18*, with inclination less than 10 degrees, are approximately 350m length, perpendicular to the river, and 250m wide, presents the major interest of the current study. In map of *figure 17*, in which the orientation of slopes is demonstrated, can be noticed that the SW of the flat area shows inclination towards NE, contrary to the morphology. That is a characteristic feature of rotational landslides, in which the toe of landslide presents tilting with inclination towards the scarp of the slide. This is the major explanation for the difference in orientation which is observed in the toe of this old landslide. This feature could be taking into account in order to detect the direction of the movement which in this case is concluded generally as NE to SW.

The drainage system on the study area seems to divide the major slide, recognized previously, into three major categories in the toe. The first unit seems to be located at the middle of the slide and it is mainly composed by the back-tilt area. It seems that this area is less favorable to erosion, which forces the surface drainage to the sides, which are more favorable. This indicates the remaining two categories, northern and southern that referenced area, in which surface drainage of the old landslide occurs.

Northeastern of the studied landslide, in slope steepness map of *figure 18*, relatively flat areas can be observed. More precisely there are two areas with slope inclination from 5 - 20 degrees. Abnormalities and irregularities in the form of contours are also presented in those territories, but compared with the same abnormalities in contours presented in the major reactivated landslide, their magnitude is restricted. Either way, these territories should be investigated in detail during geological mapping, in order to detect if those territories appear to be old stabilized landslides too or not.

Worth mentioning are two other cases in which sizable landslides seem to be occurred. Both cases are northern to the study area, and they are in both sides of river Zvaroula. Their dimensions are also remarkable, and their presence were also detectable by small scale observation. To begin with the case of the right side of the river, and only by the observation of topographical map, the irregularities on the form of contours seem to be intense. In addition, on slope orientation map *(figure 17),* although the morphology seems to be inclined to northwest there is a territory where the inclination appears to be against morphology. This phenomenon is explained above, and it is related to the back-tilt action on the toe of landslides. Also, considering the forms on the contours, curves seem to occur towards NW. Taking into account the presented information, the old landslide seems to occur on SE to NW direction. Of course, on slope inclination maps there is a wide flat area surrounding by steeper cliffs, which confirms the underlying assessment, about the presence of old landslide. The dimensions of this unit seem to be less than 300m length, however in needs further

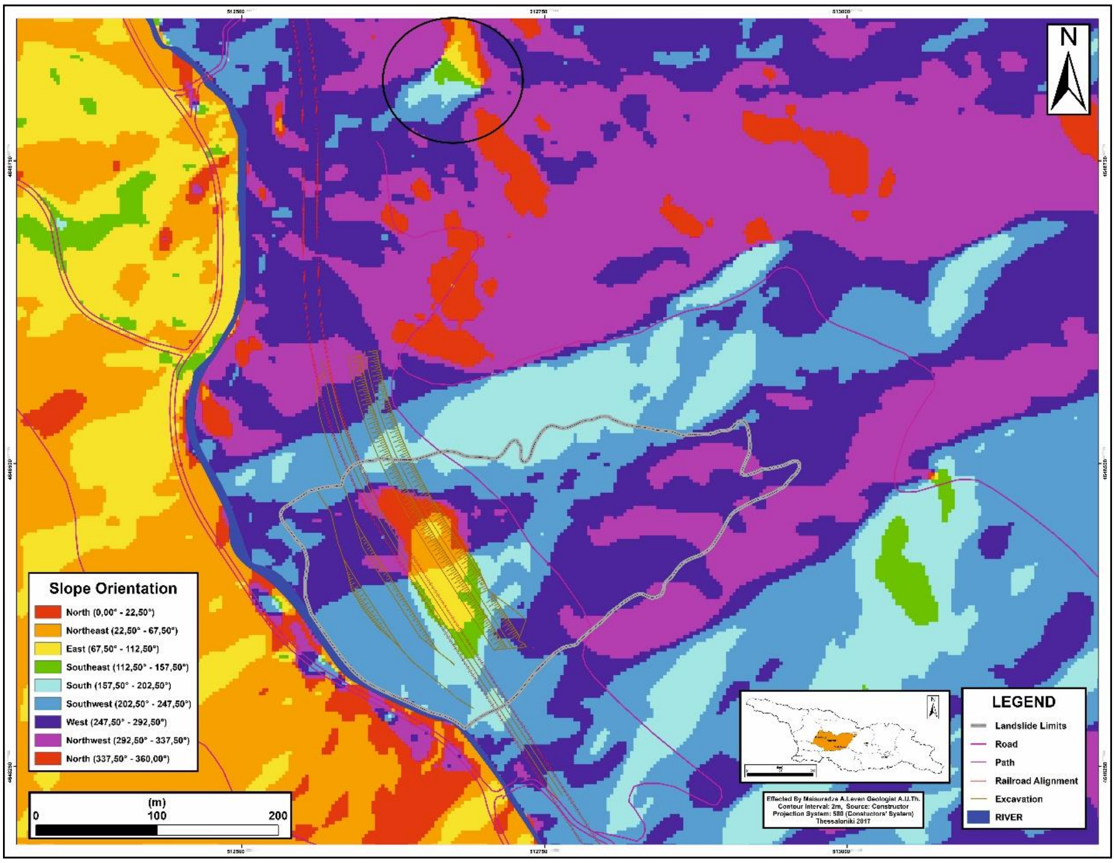

*Figure 17. Large-Scaled map, demonstrating the orientation of the slopes. The grey line represents the limits of landslide. The black line in the north represents back tilt activity on another than this study's' landslide.*

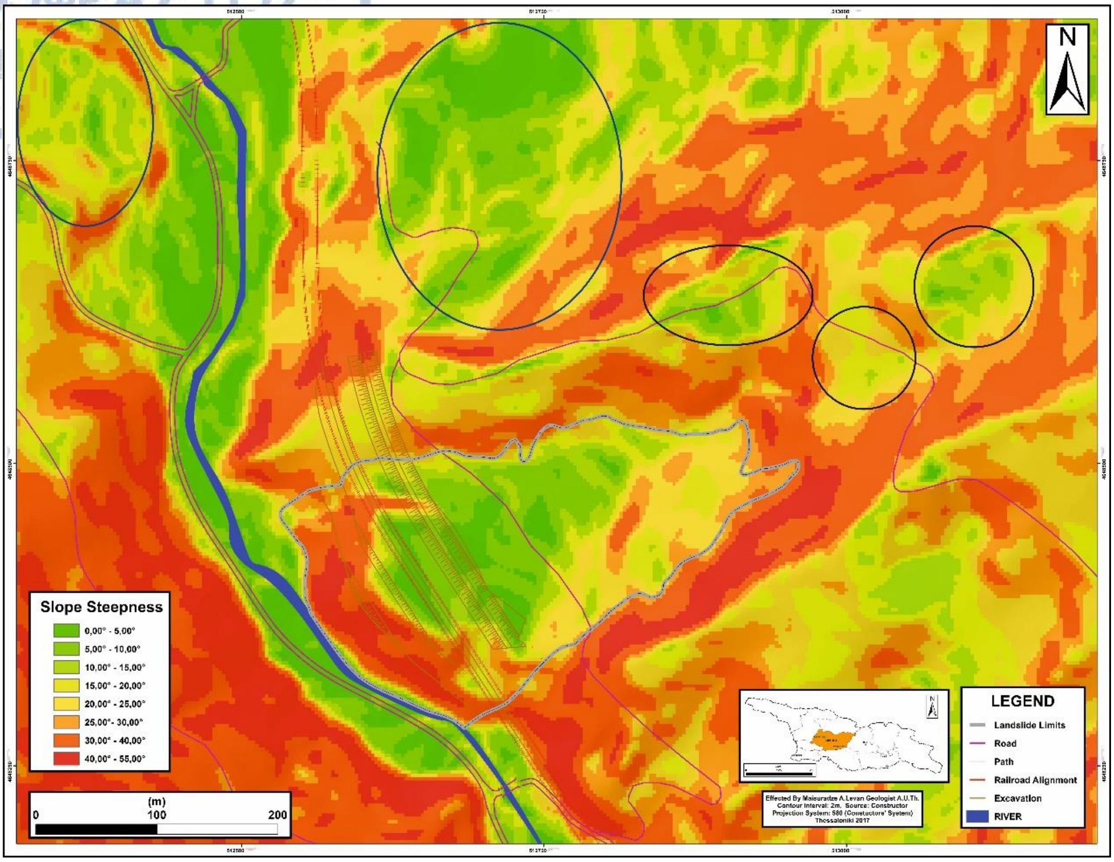

*Figure 18. Slope Steepness map. The grey line represents the limits of landslide. The black circles indicate flat areas NE of the major landslide which needs to be investigated and blue circles indicate sizable landslides northern than the study are.*

investigation. The case of old stabilized landslide, in the left bank of river, has also remarkable dimensions. Although, in this case the presence of back-tilt area is not clear, other characteristics such as irregularities in contour forms seems to be lucid. Those features allow to draw conclusions about the direction of movement, which is considered to SSE, such as the curves in contour lines. Although, both cases are important because their position is relatively near to the alignment, the current study focuses on the assessment of landslide which were presented firstly, southern than these two cases. So, accurate studies related to these cases should be carried out, but other information about them would not be presented in this study.

In the large-scale topographical map of *figure 16*, considering only geodynamic evolution, lineation on direction of ENE-WSW is observed mainly in two cases. Such lineation, taking account the same type of observation which occur on small-scale maps, characterizes regionally the study area, so its presence on the restricted area of study, was expectable. These features are located northern and southern of the reactivated landslide.

Considering the case of lineation northern to the landslide, it is worth to mention that from the slide to the lineation the terrain is considered rough and it also presents a characteristic morphology type referenced as front range faults. Northern than the lineation the rough territory is becoming smoother. So, the lineation is considered a border between rough and smooth morphology. Furthermore, this feature appears to create relatively straight line in *figure 17*, which demonstrates the orientation of slopes. From the topographical map, the presence of ridge in the underlying territory, is clear but, the geometry of the ridge appears to be relatively straight, and in this case, it could be considered suspicious. The underlying information should be considered valuable in geological evaluation, and attention should be paid in geological mapping, regarding this lineation.

Considering the case of the southern than landslide lineation, it has approximately the same characteristics. There is also a transition from rough terrain to smoother, and the formation of front range faults also occurs. This feature of lineation, seems to affect the morphology of left to the river slope, by making it gentler. Like previously, this element should be considered and investigated during geological mapping more accurately.

To conclude, from investigation carried out considering only the morphology of close study area, before visit has paid in the area, there are clear indication of rotational old landslide, which was reactivated. Also, there is a presence of two features, which probably are related to geodynamic processes and they should be investigated om detailed during geological mapping. In addition, northeastern of the major detected landslide, flat areas appear to occur, which origin should be also investigated, during geological mapping. In the end, mechanism of the landslide should be investigated, considering the categorization which is carried out previously.

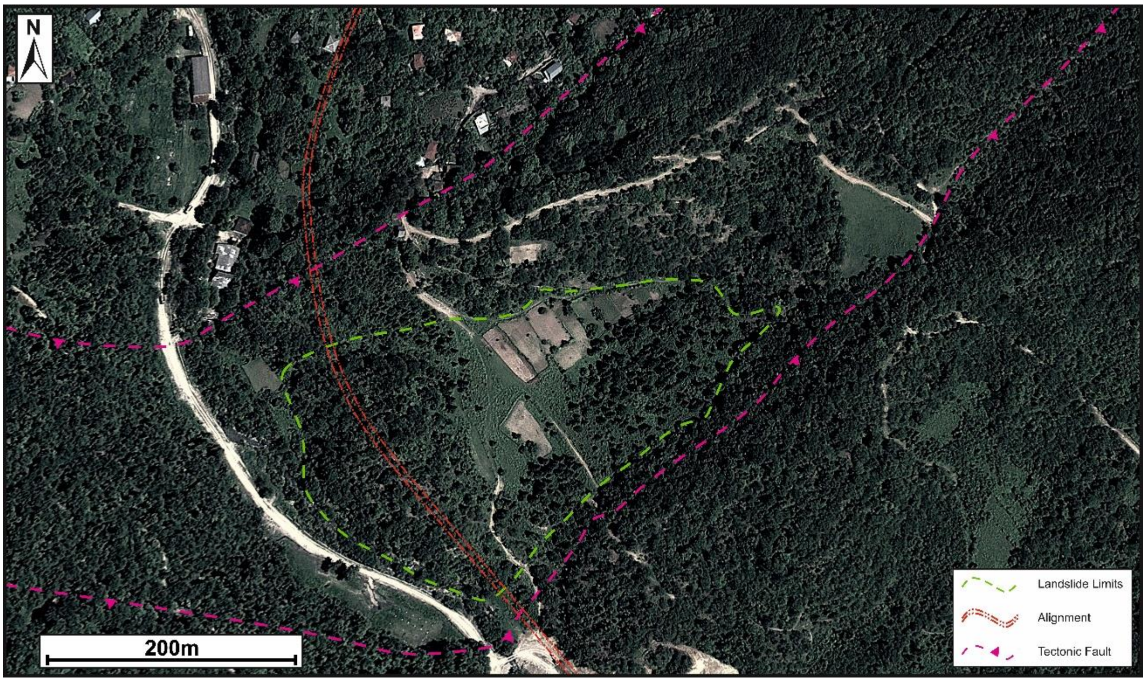

*Figure 19. Google Earth image of close study area, before the implemented excavation.*

*Figure 20. Landslide borders and tectonic faults depicted by UAV after the implemented excavation (Provided by Contractor).*

### 3.3 Approach by aerial photographs and satellite imagery.

The importance of aerial photographs and satellite imagery in geological and engineering geological mapping is widely accepted (*Price D.G. & de Freitas M.H., 2009*). In this case, aerial photographs (by google earth), which represents the area before the failure, were studied in order to approach the fundamental geological structures of the territory. Furthermore, during mapping images by UAV, were also provided. Those images are extremely useful for the mapping of landslide limits and surface ruptures, as well as other geological structures in close study and adjacent territories.

In aerial photograph of *figure 19*, the close study area is represented. The image was taken in 2012, however the limits of old and now reactivated landslide is satisfactorily detectable. Furthermore, in the aerial photograph, cultivating fields are shown only on the main body of the old landslide. This fact justifies clearly that in this area, the material is completely different than its surrounding.

Apart from the limits of the landslide, in *figure 19,* significant observations regarding geodynamic processes are possible to be detected. As the topography indicate previously, northern and southern of landslide, two major features occur. Those features indicated differentiation in the vegetations in narrow zone. Usually, this kind of features occur where there is a presence of tectonic faults. So, the presence of tectonic faults northern and southern of active landslide, is considered more than possible and field observation should confirmed their existence. The same observations are made in the images provided by UAV on *figure 20.*

Regarding the limits of the landslide, at *figure 20*, the actual limits of landslide are shown, considering that this image has been taken after the rupture. More precisely, the underlying image, has taken, approximately a month after the main rupture, which is considered enough time in order for the scarp to form a steep slope of significant height. The occurred excavation is also shown on the underlying image, which represents the triggering factor of the landslide.

## 3.4 Geological Approach

### 3.4.1 Regional Geology

The study of regional geology, in geological studies is considered essential, and the given information is the base of the geological study of close area. In the map of *figure 21*, which is zoomed by the geological map at a scale of 1:500.000 *(Gudjabidze G.E., Gamkrelidze I.P., 2003)*, the regional geology of study area is shown. The dominance of sedimentary formations of Mesozoic and Cenozoic era, is clear in the region. There is no existence of metamorphic formations, however the presence of igneous rocks, intruded in the sedimentary formations is referenced.

To be more accurate, the sedimentary process in the region, starts at middle Jurassic, with deposition of clastic sediments, and continues up to the middle Neogene, with molassic type sediments. Although the process starts with the sedimentation of clastic sediments, in Early Cretaceous the facies of sedimentation changes into carbonate facies. The type of sedimentation changes gradually in Upper Cretaceous, where the clastic type sedimentation continues.

The Cenozoic era begins with carbonate facies sedimentation in Paleocene-Eocene, and it changes during middle Eocene into clastic facies, with dominance deposition of conglomerates. Sediments of Oligocene age, are not observed, which means that there is a discontinuance in the sedimentation in upper Paleogene. The process of sedimentation continues at Miocene with molassic type sediments.

Concerning geodynamic processes, it seems that the underlying sedimentation took place, generally into compression stress field, with different rates of compression. The orogeny phases which are developed in the area, are the Late Cimmeridian and Austrian phases during Mesozoic era, and Alpine phase, which is expressed by overthrusting of Arabian plate towards northeast during Cenozoic era *(Gamkrelidze I.P., 1986).*

The age of geodynamic processes which effects the regional though, but larger than continent-scale area of study, seems to be occurred in Cenozoic era. Those processes are expressed by folding and thrusting of older than Eocene formations. From the map of *figure 21,* ductile deformation seems to be occur in Paleogene, which is responsible for the folding of co-aged and older formations. The sedimentation stops in the Oligocene and continues to the Miocene with molassic sediments. That means that the compression continued until the middle Miocene in which molassic type sediments were deposited at syncline type basins. Post orogeny processes are expressed in this region by brittle deformation. This deformation

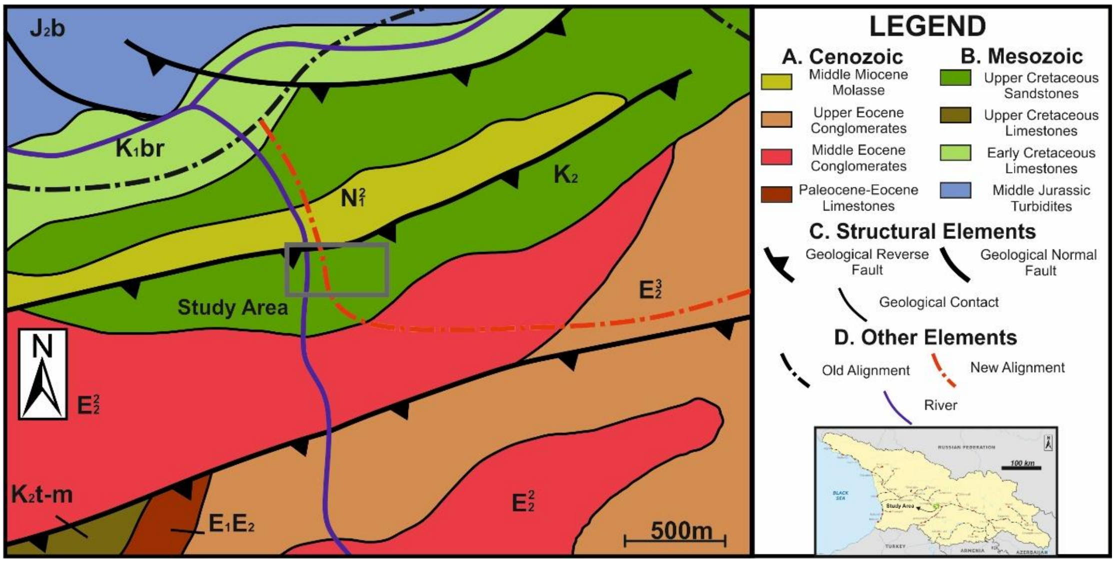

*Figure 21. Geological Map, zoomed from the geological map of Georgia 1:500.000 (Gudjabidze G.E., Gamkrelidze I.P., 2003)*

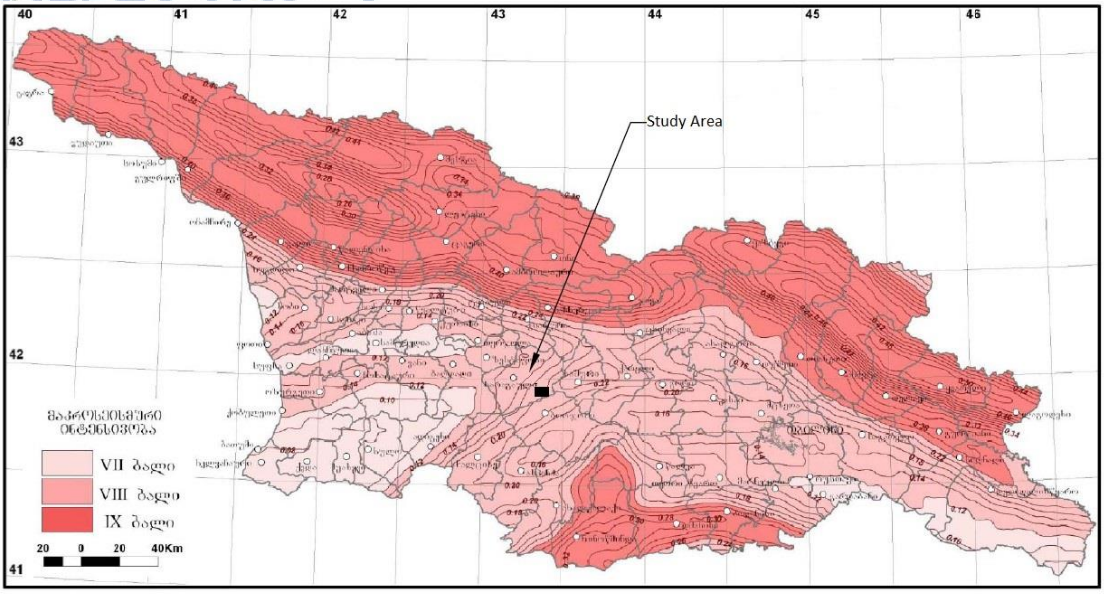

Figure 22. The distribution of seismicity expressed by PGA (Seismic Code of Georgia)

affects the molassic sediments which age is presented as middle Miocene. That means that the post orogenetic compression continues until upper Miocene-Pliocene age. So, the age of reverse faults and thrusts at the area is considered younger than upper Miocene-Pliocene age. Furthermore, volcanic processes seem to occur continuously, from the Cretaceous to Oligocene, expressed by intermediate and felsic intrusive rocks and tuffs.

According to *Phillip H., et all 1989.,* the active stress field in the area, continues in the present as compression, with a direction NNW-SSE *(figure 23).* At the underlying stress field, reverse faults and thrusts, with strike perpendicular to the compressive stress vector are

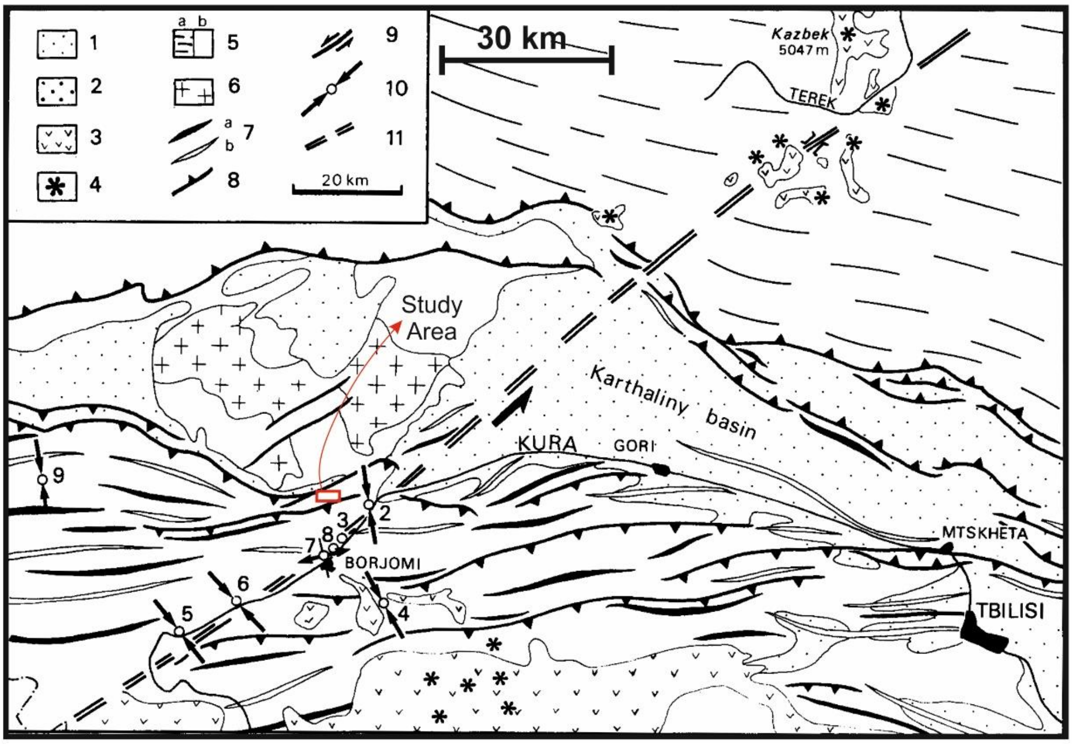

Neotectonics of the Borjomi region. *1* = Neogenic to Quaternary; *2* = Thrust Nappe, Cretaceous to Quaternary; *3* = Neogene to Quaternary volcanoes; *4* = recent volcanoes; *5a* = strongly deformed Jurassic; *5b* = weakly deformed Jurassic; *6* = crystalline basement; *7* = folds (*a*–anticline, *b*–syncline); *8* = thrusts, *9* = strike-slip; *10* = principal stress axis; *11* = Borjomi–Kazbeg left-lateral strike-slip.

Figure 23. Borjomi Fault (Philip H., et al., 1989)

considered active, as strike slip faults with similar strike. In general, this type of deformation indicates late orogenic processes, and could also characterized as transpressional type of deformation.

To conclude, the information which were produced from the study of regional geology, regarding the close study area, is the type of geological formations, which occur on site of construction, and the origin and orientation of deformation which occurred on the underlying formations. So, the formations in close study areas seems to be cretaceous clastic sediments, and more precisely sandstones. Furthermore, considering the regional geology, intrusive rocks of intermediate composition, can be found into sandstones. Finally, the strike of brittle features regarding geodynamic evolution of area, is generally shown as ENE-SSW.

### 3.4.2 Seismicity

Generally, Georgia is considered seismic actively country with several catastrophic recorded earthquakes in 20th century, such as Racha earthquake at 1991 of magnitude Mw=7.0 *(from Tan, O., Taymaz, T., 2006)*. The underlying seismicity is the product of collision among Eurasian and Arabian tectonic plates. The underlying collision is expressed with strike slip and thrust faults, which ruptures are expressed by the earthquakes.

One of the most well studied faults in the region is the Borjomi – Kazbeg fault, which is characterized as left lateral strike slip fault and corresponds to compression with orientation NNW-SSE *(Philip H., et al., 1989)*. The underlying fault is located in a distance of approximately 10 km from the close study area, and should be taken into consideration. Although there is a clear presence of thrust and reverse faults in the area which correspond in the same stress field, their activity produces earthquakes of limited magnitude (Mw<5), with no surface ruptures. So, even if the displacements produced from the ruptures in the surfaces of the faults, do not effect significantly the construction, and in general the construction of the railroad, near field effects, from the underlying earthquakes should be studied in detail. Of course, considering that the close study area, belongs at the near field of the Borjomi – Kazbeg fault, the results of possible activation of the underlying faults should also be examined.

According to the Seismic Code of Georgia, the general ground earthquake acceleration in the close study area is approximately equal to PGA=0,2g. This value will be taken into consideration for the present study, however greater accelerations are also expected.

### 3.4.3 Rainfall

Georgia in general are divided into two major categories regarding the rainfall. East Georgia is characterized by low magnitude of annual precipitation, below 600mm at south east basins and 1200mm at mountainous territories Great Caucasus of north east Georgia. In

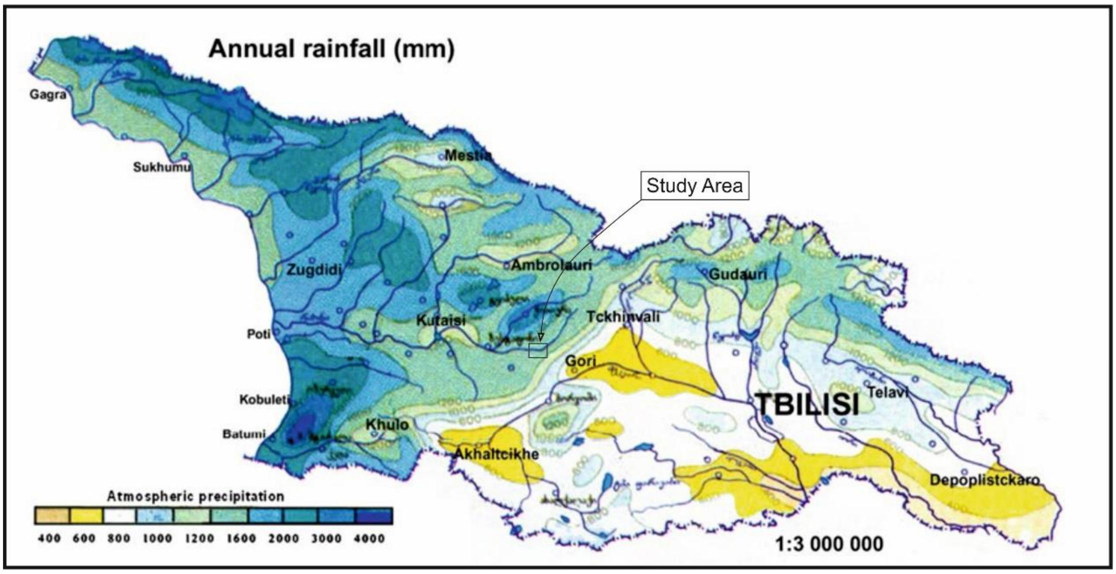

*Figure 24. Annual precipitation level at Georgia (Bondyrev I., et al., 2016)*

the contrary the precipitation levels in western Georgia appears to be relatively greater than in east. In western Georgia, the annual precipitation is generally greater than 1000mm. This can be explained as a result of the location of the great Caucasus, which is a natural barrier and stops the humid winds produced at black sea, resulted intense rainfall at the wider territory. Most emphasized example is the region of Adjara in southwest Georgia, which although it is not considered as a mountainous area, the precipitation is greater than 4000mm per year.

In the study area which is located at central Georgia the precipitation, according to the *figure 24*, ranges between 1200-1600mm per year, which is considered sizable value. The rainfall, and generally the precipitation, has a vital impact at landslides. Considered that in the study area, as it referenced, a lot of landslide phenomenon are observed, the major triggering factor, beside the triggering factors related to human activity, could consider the rainfall and in general, the precipitation.

### 3.4.4 Large Scale Geological Approach

The large scale geological approach contains mostly the procedure of geological mapping, in which all the underlying information, regarding geomorphology both in large and small scale, observations from aerial photographs and satellite imagery and of course, regional geology will be taken into account, and in cooperation with the information provided by the geological and engineering geological mapping, the final product, which is the understanding of the engineering geological model, expressed by engineering geological map, will be produced in the end of this chapter.

The mapping of the area started with the mapping of the limits of active landslide. Considering that the landslide activated, slopes-boundaries northern and southern of the slide with dipping angle 50-60° and 70-80°, and height 3-6 and 4-8m respectively, was formed. Although, investigation concerning tension cracks beyond the major scarp, in adjacent area, was committed, none of them was detected. The landslide appears to have 400m length, from the major scarp to the toe, and be 230m wide. Taking into account that the ratio between the depth to the wideness in soil material when rotational landslides occur, is 0,1-0,3 the depth of the landslide can be estimated *(Highland, L.M., and Bobrowsky, P., 2008).* That means that only by surface mapping the depth of the slide ranges between 23-69m. It is also worth to mention that the limits of the landslide, as they are mapped in the field present correlation with the limits which were drawn on the slope steepness map of *figure 18*. Whether the limits of landslide were clearly determined, the mapping of surfaces ruptures on the landslide occur. Also, any presence of spring on the landslide material were also recorded.

The northern border of the landslide, is detected on the bedrock. More precisely the clayey material of landslide, mainly slips on the bedding of bedrock *(figure 25, a).* Exception constitutes the northwestern part of the slide, in which the landslide is just in contact with the bedrock, which is in poor geotechnical condition, considering that joints filled with grey clayey

*Figure 25. Northern Landslide Limits (a) The bedding of sandstone in which the mass slips, (b) very altered bedrock shown in the slope, (c) the major difference on color on landslide mass and bedrock material, (d) 3-4m formed slope in the middle of north slope*

*Figure 26. Southern slope, (a) slickensides on soil and rock formation, (b) slickensides on soil type formation, (c) steep 4-5m high slope, (d) the presence of bedrock in the south slope.*

material, and in some cases 1-2m thick clayey intercalations. Furthermore, the bedrock appears to be exclusively altered *(figure 25;27).* In this position, the formed slope, by the failure is no higher than 3-4m, and the bedding appears dipping towards south with dipping angle less than the angle of slope. So, in this position, failure of the bedrock towards the mass of landslide (southern) is expected, and small failure is noticeable in this position.

Completely different situation occurs in the opposite, southern slope, in which the presence of bedrock is kindly restricted. The failure on the southern slope occurs on the same material, produced by landslide in the past, but the thickness of this material on the slope seems to be restricted. In some cases, in which bedrock appears, it becomes clear that the thickness of the colluvium material on the slope is restricted *(figure 26).* In the same cases concerning the bedrock, its dipping direction is opposite to the formed slope, but there are joints with dipping towards the formed slope. The dip angle of those joints is high, and usually greater than the slope angle. So, generally can be estimated that as appears at *figure 26, d,* the landslide slips, in the southern border, on joint surfaces. The bedrock appears only at the southwestern and in southeastern side of the southern border, with a lack in presence of approximately 200m-250m in the middle of south border. At the south border, whether the bedrock appears, it seems to be at good geotechnical conditions, and its alteration seems to be restricted *(figure 26).*

Beside the under-failure material, the morphology indicated as previously mentioned, several cases which needs further investigation. So, investigation was conducted northeastern of the landslide, to clarify the conditions and the origin of material by which flat area northeastern than the active landslide, are composed. The committed investigation showed that those flat areas are composed by rocky formation, and more precisely sandstone. Although the geotechnical quality of rock mass in those positions seems to be restricted, the bedrock on these positions appears to have clear pictures of structure, regarding the bedding and other discontinuities such as joints. So probably the underlying frat areas correspond to the excavation related to the paths, which are located on those positions.

Furthermore, the morphology, the observation of aerial photographs and satellite imagery and of course, the study of regional geology, provide information related to the orientation and the position of geological faults. So, the exact detection and the origin of those features followed.

The definition of map units, is probably the most important process during mapping. Generally, the mapping is related to the detecting of map unit's borders, and it cannot be committed if the map units are not defined clearly. Although the process of defining the map units is crucial in order to continue the process of mapping, it cannot be committed in the beginning of the process. Map units are individual groups of materials with distinctive characteristics. The complete knowledge of those characteristics cannot be defined in previous stage. Also, it cannot be defined in the beginning of mapping stage, so time needs to be spent in order to obtain all those distinctive characteristics of materials in order for the geologist or engineering geologist, to be in position to classify those materials into map units.

The nature of those materials should be related to the construction. This manly should occur for two major reasons. The first reason is that complicated engineering geological maps, with a vast of information, mostly unrelated to the construction, creates difficulties related to the reading and the interpolation, from other specialties, such as engineers, who in the end, ignore the results of mapping. The second reason is related to the time consuming, both by the mapper and the one who interpolates-reads, the final map. So, the construction has important influence on the underlying division, as the scale does. As soon as the classification on map units occur, the mapping of their borders will follow. The obtaining of those distinctive characteristics of each map unit, is important, and that why the recording of those characteristics could be also occur, after the characterization of map units complementary. This happens because those characteristics are defining the material's, which map unit is composed, properties.

During mapping structural elements, such as the orientation of bedding and other discontinuities such as joints and faults were also recorded, in referenced positions on the map. Furthermore, elements related to hydrogeological conditions is vital and the recording of those ones were conducted too.

It is also worth mentioning that in the close study region, there is a presence of hydrothermal activity, expressed by springs which produce naturally carbonated mineral water. The natural carbonated mineral water is correlated with hydrothermal activity. In this case, several springs expressed with wells and shallow boreholes product the mineral water. This kind of activity presents crucial impact on the bedrock composition, which is becoming alternated and consequently more friable. Beside the friable form, the alteration can be recognized by the color of the bedrock which normally is dark grey, and the alternation

*Figure 27. The presence of Alteration on the bedrock, (a) The bedrock owns colors in shade of purple and becomes friable, (b) high concentration of sulfur in the bedrock.*

generates colors on the rock in shades of purple.  Of course, this kind of activity is accompanied by high composition of sulfur.  Except sulfur, areas which suffered or still suffering hydrothermal activity, the presence of clay such as bentonite, is very common.

### 3.4.5 Map Units

#### 3.4.5.1 Landslide Mass

The material which is under failure conditions, is characterized by extensive heterogeneity, considering that it is composed from clay to boulders with diameters more than 5m. More precisely, the dominance of clayey material is lucid.

The distinctive characteristics which appears only in this formation dividing it from others are presence of soft clay, its brown color and, as it is referenced before, extensive heterogeneity. It also seems to have high permeability taking into account that through intense rainfall and also as in other cases in which vast amount of water was thrown on the material, no runoff was formed. In addition, this material is the unique which is under failure, and appears surface ruptures.

The present map unit is composed by very soft to soft, light brown, brown and dark brown clay of low to, in some cases, medium plasticity, which is dominant. Coarser material, such as sand and silt, appears in very restricted quantities. However, the presence of gravel, within the clayey material, is sizable. To be more accurate, very loose to loose angular gravel of weathered and altered sandstone appears into the underlying clayey material. It is important to point out the shape of gravel, which is angular. That excludes any correlation of this material with gravel of riverbed origin, which is rounded.

Beside the gravel, the presence of coarser material is clear. There are sizable boulders, with angular shape, composed by altered and weathered sandstone. More precisely, the most common sizes of boulders observed range between 0,50-1,50m.

*Figure 28. Landslide Mass, (a) presence of boulder within the mass, (b)&(d) The complete heterogeneity observed in landslide mass, with angular fragment on clayey material, (d) the border on northwestern part of the landslide and clean differences with the surrounding material*

### 3.4.5.2 Fill Material

After the excavation, in the study slope, excavated material was placed upon the excavation in order to obtain flat terrain. The composition of this material is approximately the same with the material in which failure occur. Probably the only difference between them is the percentage in clay. The filled material has greater composition in gravel. Of course, the extensive presence of gravel does not indicate the absence of the dominance of clay. Northern than landslide the filled material is composed by excavated material derived by the tunnels, which are adjacent to the construction. The width of this material is no greater than 2m.

### 3.4.5.3 Alluvium

The alluvium material is composed by sediments which are deposited by the river Zvaroula. Those sediments are characterized by great heterogeneity, however, it is easy to be singled out the alluvium material by the landslide mass, which is also characterized by extensive heterogeneity, for the following reasons.

The alluvium material is mainly composed by very loose to loose deep colored sand, rounded gravel, cobbles, and boulders. There is also presence of clay, but in contrast to the other types of sediments in the area, its concentration is restricted. Furthermore, the boulders, the cobles and the gravel, are composed by sandstone, marls, chalk, chert and also, andesites and other volcanic rocks, which are presented southern in the regional area. So, the major differences of alluvium material with the material produced by the landslide, beside the surface ruptures, are the rounded in contrast to the angular, shape of clasts, the lack of clay, the dark colored color and the multipetrological origin of the clasts.

The potential maximum thickness of this formation is considered no greater than 10m.

### 3.4.5.4 Colluvium

The colluvium material is composed by very weathered bedrock, boulders of weathered bedrock origin, in clayey material and top soil. The dominant difference between this unit and the landslide mass is that the material of this unit does not suffer failure in contrast to the material of landslide.

The potential maximum thickness of this formation is considered no greater than 5-6m.

### 3.4.5.5 Basaltic Andesite

As it is mentioned before, intrusive volcanic rocks are observed in the bedrock of this region. More precisely intermediate intrusive rocks are observed on the in the northwestern part of the close study territory. The age of this intrusion is younger than upper Cretaceous and older than Miocene, where the volcanism, in this area, generally stops. So, this formation is formed in Tertiary and more precisely, probably in Paleogene period. Petrologically the appeared rock is igneous rock based on its texture, in which the observation of crystals is possible. The color of rock appears to be dark green and it has mafic to intermediate composition. So, the formation can be characterized as basaltic andesite to andesite,

*Figure 29. Basaltic Andesite*

*Figure 30. Calcareous Sandstone, (a) Marly intercalations, (b) Moderately weathered Sandstone, (c) lenses of chert within sandstone, (d) Slightly weathered dark grey sandstone.*

composed by amphiboles, plagioclase, and probably pyroxenes. This rock type appears massif, very strong, jointed but infoliated. Alteration does also occur on this formation, however it has not became friable and remains strong. Its contact with the surrounding sandstone seems to be intrusion from north, but from south, the sandstone appears upthrusted on this map unit *(figure 29;32).*

### 3.4.5.6 Calcareous Sandstone

The bedrock in close study area, appears to be, clastic sedimentary rock, sandstone. Considering the regional geological map *(figure 30;31),* this sedimentary formation is formed at Upper Cretaceous, in which younger intrusions by igneous rocks are also mentioned. This formation is characterized as a sandstone, based on the its grains size, which are recognizable by natural observation. That means that the grains have sand size, or greater, diameter. However, grains with diameter greater than sand size, were not be observed during surface investigation. It is worth to mention that whether the recognition of grains by natural observation cannot be committed, then their size would have smaller diameter, such as silt and clay. To be more accurate, the present unit can be characterized as a fine-grained sandstone. The grains in this formation, are mainly composed by quartz, feldspar, calcite, mica and mafic minerals, which probably are biotite and hornblende. The presence of calcite in among the grains, but also in matrix material of the rock, gives the prefix Calcareous on the formation. Beside the participation of calcite in the matrix material and grains, several cases in which calcite veins occurred was noticed.

The thickness of the bedding presents extensive distribution. That means that the thickness of bedding, ranges between 0,05-1,00m.

The sandstone, generally appears moderately to very fractured. The color by which it is characterized is deep grey, but in several cases the color of the bedrock appears to be light

*Figure 31. Presence of grey clayey material as lenses into the bedrock, Sandstone.*

brown which is the result of weathering. Furthermore, there are cases in which hydrothermal alteration on the bedrock occurs, so it color is changes into deep red or deep purple.

Beside the presence of intrusive igneous rocks, which is reference earlier, intercalations and lenses of marls and cherts, 1,00m and 0,10m thick respectively, are also observed *(figure 30).*

Beside the above formations, in the sandstone, lenses of grey clay are also noticeable. Those layers are characterized, as stiff clay of high plasticity, and its origin is questionable. More precisely the origin of clay is considered either by geodynamic processes, which means that they were produced during brittle deformation occurred, or by hydrothermal alteration which in general occurs in the area. The origin by surface processes, such as weathering, or even shearing by landslides, cannot product high plasticity clay. The high plasticity clays own their physical and mechanical properties, and consequently their plasticity on the mineralogical composition.

### 3.4.6 Structural features

#### 3.4.6.1 Faults

Before visit has paid, observations of morphology, aerial photographs, satellite imagery and of course the study of regional geology indicated the presence of geological faults in the close study area. More precisely, the morphology, aerial photographs, satellite imagery indicate possible positions in close study area, with possible orientation of ENE-SSW, where faults can be located. The study of regional geology confirmed the given orientation. But the position of those features cannot be located by observation of that small-scale map *(figure 21).* Even the exact orientation produced by those maps cannot be accurate, so this observation is considered valid as an indication but not as a fact and it should have confirmed in the field.

So, investigation has committed in the field, in order to detect and confirm the origin of features which indicate the presence of tectonic faults in the area. To be more accurate, the

*Figure 32. The tectonic contact between sandstone and basaltic andesite. Northern fault.*

underlying investigation has committed for two major faults, northern and southern of the close study area.

The northern fault was detected between two separate lithological formations, sandstone and basaltic andesite. The presence of sheared material, in the contact of the underlying formation indicates its tectonic origin. Furthermore, the curves at the bedding of sandstone provide the origin of the fault, which is considered as a reverse fault. The orientation of this fault is measured in situ as 165/65 dip direction and dip angle respectively. So, in this case the imprint in the morphology was identified in the field, and it was successively confirmed as a reverse fault with the underlying orientation. Furthermore, the spatial

*Figure 33. The geological reverse fault southern of close study area.*

distribution of andesite is restricted, which means that northeastern no presence of this rock type occurred. Although the presence of andesite is limited, the fault continues to occur, with shear zones into sandstone, up to 2m width. It is likely that this fault belongs to group of faults with the same direction, by which Cretaceous formation is placed on Miocene formation.

The existence of the second tectonic fault southern of the landslide was also confirmed by field observation. Although in the specific area southern than slide, there is no change in lithology, the presence of shear zone is detectable. More precisely in this area of study the bedding appears to have the same dip direction towards south. However, in this position there is a close zone in which the dip direction appears to be inclined towards north. After this zone, exclusive shearing of approximately 3m occurs with soiled and disintegrated material. Although the material is disintegrated, structure is observed with the same direction as the bedding, within the zone, in which extensive weathering is also observed. Unfortunately, the presence of clear measurable surface cannot be detected, but the orientation of the fault was determined from geomorphological indexes, as a strike lines. So, the orientation of this feature is 150/65 dip direction and dip angle respectively.

### 3.4.6.2 Bedding

The bedding is considered crucial structural element, and its knowledge, contributes at the better understanding of geological model. As it is reference before and it is shown on *figure 34*, the orientation of bedding is towards south with dipping angle ranges between 25-55°. Of course, there are several exceptions. The first exception is observed northern of landslide where dipping of bedding towards northern is observed. Furthermore, close to those measurements there are others, which show dipping towards south, as it is illustrated on the geological map *(Appendix, figure 165).* This means that in the area the process of folding occurred. The editing of measurements, in order to study the geometry of the folding, indicated B axis of folding oriented as 265/15 strike and dip angle respectively. Worth mentioning is that the dip direction of fault, which is detected on that territory, is 165°, which

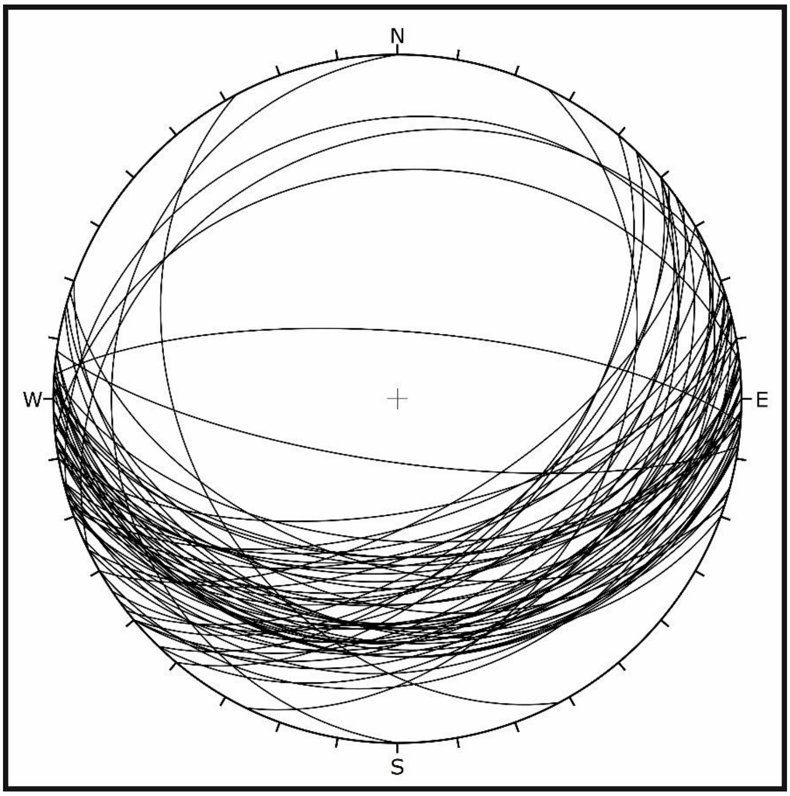

*Figure 34. Projection of bedding measurement of close study area into Schmitt diagram (Equal Area/Lower Hemisphere)*

means that the strike of it is 255°. Taking into consideration lateral limits of 10°, the B axis of folding is parallel to the fault which is considered reasonable, and it confirms the presence of the deformation, in that direction. Further exceptions are noticed in the southern fault, and they are already explained.

### 3.4.6.3 Joints

Regarding other discontinuities in the close study area, joints also have been recorded. They are presented to the map *(Appendix, figure 165)* with two major ways. The first way of illustrating joints on the map is the same with the bedding, with specific symbol of dip and strike in referenced position. The second was is using structural analysis.

In total, for the study area, every measured joint was plotted in the same diagram in order for classification occur. Three major sets of joints were provided from the underlying process and they are illustrated in *figure 35.* It is important to point out that the first set of joints are oriented parallelly to the formed slope in the south border of the slide.

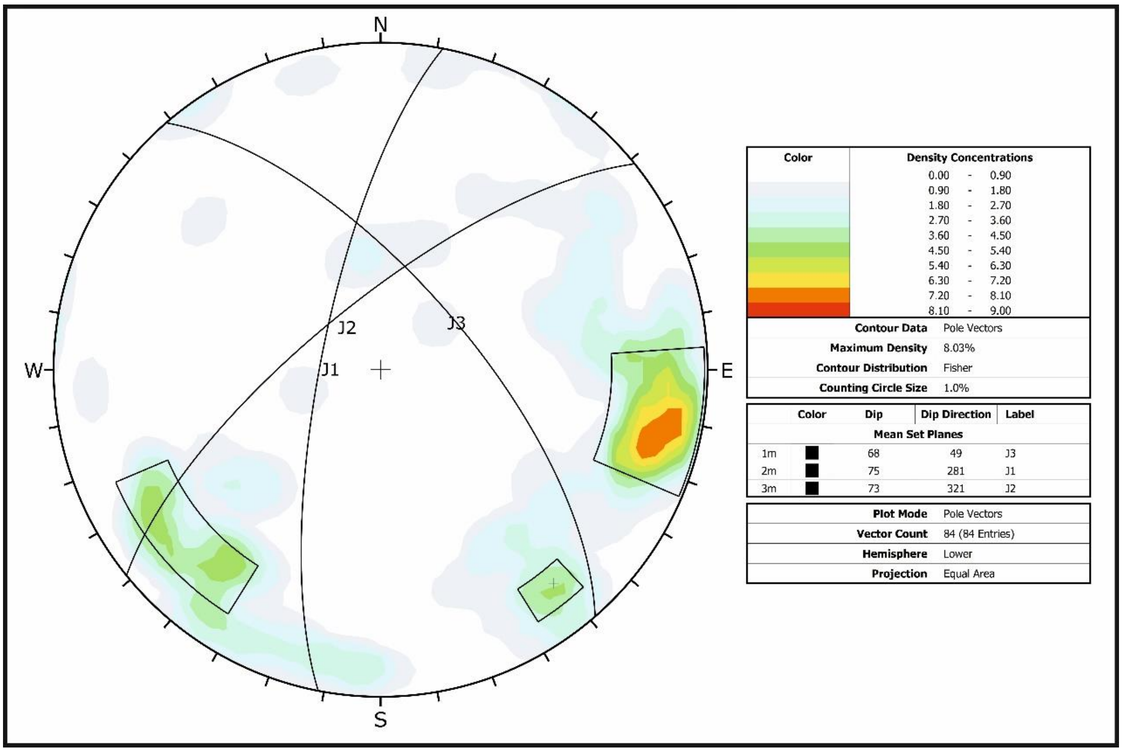

*Figure 35. Projection of total joint sets of close study area into Schmitt diagram (Equal Area/Lower Hemisphere)*

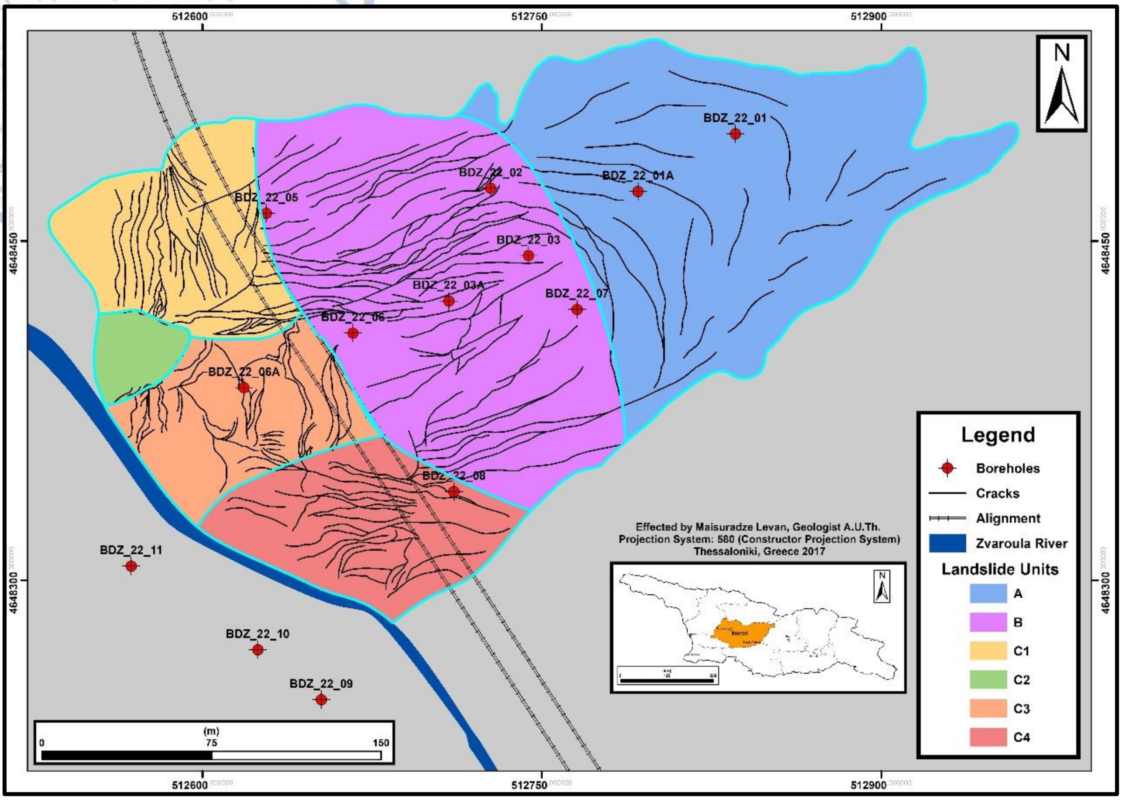

*Figure 36. Landslide divided into categories regarding behavior type and surface ruptures*

### 3.4.7 Mapping of cracks

Surface ruptures on the landslide were also mapped. The mapping of those features was completed based on field mapping in cooperation with images provided by UAV, the underlying ruptures were mapped in order to understand accurately the mechanism of the landslide. The orientation and the position of surfaces ruptures can provide crucial information about the behavior of the slide regarding spatial distribution. So, the division of the landslide into 3 major units, occurred, considering the underlying features, and each unit has unique behavior, which understanding and its spatial distribution could provide the understanding of failure mechanism *(figure 36).*

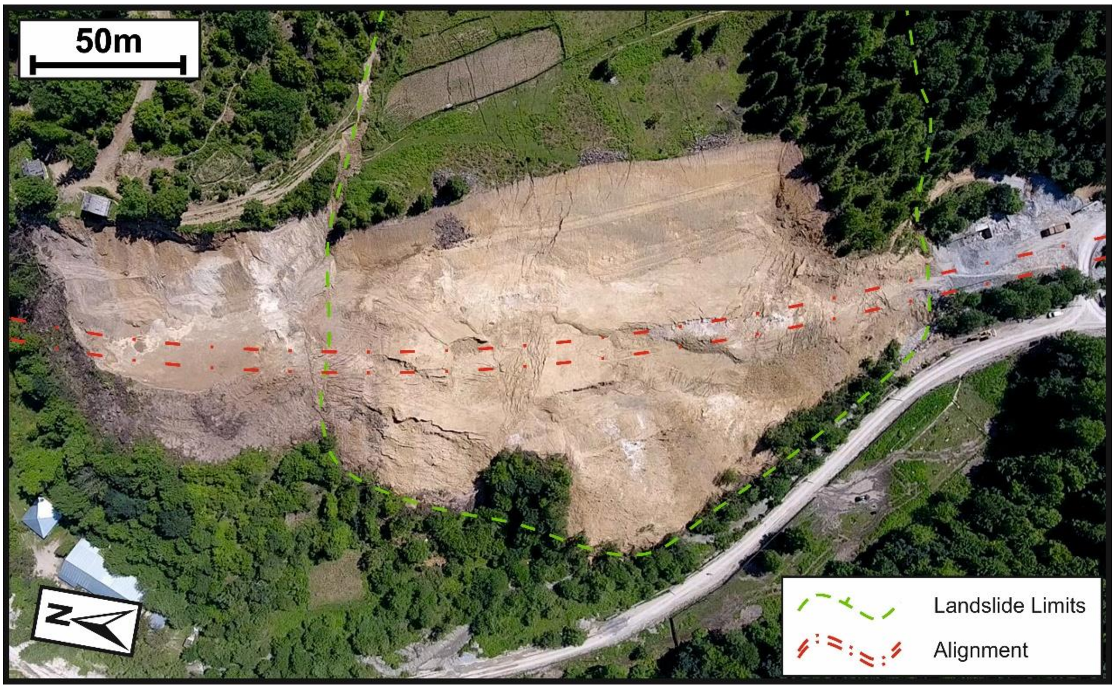

*Figure 37. Aerial Images by UAV depicts the toe of the slide, and surface of ruptures, Provided by the Contractor.*

*Figure 38. The Surface ruptures on the landslide, (a) Ruptures on the first unit on the head of the landslide, (b) radial surface ruptures on the end of the main body towards C1 Subcategory, (c) radial ruptures on the main body of the landslide, (d) Ruptures on C4 subcategory.*

The first unit (A) extend from the scarp of the landslide, up to 1/3 of length of it, and it is generally composed by the head of the landslide. At this unit, there is a presence of the main but also minor scarps, which have similar geometry. The presence of minor transverse cracks is also observed. Generally, in this unit significant settlements are observed.

The second unit (B) extends in the middle of the landslide and it is composed by the main body of it. The ruptures which are observed in this section, is mainly radial cracks which are parallel or subparallel to the axis of the movement.

The third unit extends on the rest of the slide, it is composed mainly by the toe of the landslide and it is subdivided in four categories. The first category (C1) presents the final movement of the landslide towards West and surface ruptures approximately of north - south direction with dipping towards east with high dip angles, indicates failure mechanism of toppling. The second category (C2) does not contains surface ruptures, and it does not seem to appear any movements. The third category (C3) presents the final movement of the landslide towards southwest and the ruptures are oriented in approximately northwest-southeast direction. Still the failure mechanism is toppling. The forth category express the movement of the landslide toward south southeast and it is expressed by circular surface ruptures on approximately west(WNW)-east(ESE) direction. The failure mechanism in this unit seems to be slides. It is also observed that the third category (C3) appears tilting towards the scarp of the landslide. This tilting is also combined with uplifting.

### 3.4.8 Hydrogeological Regime

Regarding the hydrological conditions in the close study area, investigation has also committed. So, the presence of springs, and other indications regarding groundwater has been made. It is worth to mention that, although the regional geology in this area indicates the presence of clastic rocks, and restricted quantities of limestones, vast number of springs with noticeable discharge were observed in the wider area. Furthermore, as it is mentioned earlier, the presence of springs expressed by shallow wells and boreholes, which provide natural carbonate water also occur in the close study territory. Consequently, the springs in the close study area, are divided into two main units, depended on the origin of provided water. The natural carbonated water is earth crusts' origin and it is partially independent source of groundwater. The second unit is composed by typical meteorological origin groundwater.

So, in close study area there is a presence of shallow boreholes providing natural carbonated water. Their position is western of slide, and their maintenance is vital for the local and wide community of the area.

Another spring, from the second unit, was detected in the toe of the slide. The presence of this spring, is crucial in the evaluation of landslide's stability because it provides important information regarding the groundwater within the landslide, and it will be considered as a piezometrical surface during stability analysis. The discharge of this spring is also worth mentioning, and it is approximately equal to 0,5m$^3$/min. The elevation of the spring is approximately 2-3m above the level of the river.

*Figure 39. The springs in the toe of the Landslide*

## 3.5 Conclusions

Taking everything into account, the final product of geological and engineering geological surface investigation was produced, which is nothing else but the engineering geological map at a scale of 1:1.000, of close study area (*Appendix, figure 165*). From the general procedure of mapping, conclusions regarding the understanding of the geological model have been made.

First of all, taking into account observations of the topography even on small scale, but also aerial imagery and aerial photographs before the occurring excavation, the presence of old stabilized landslide in the region is now considered unquestionable. Furthermore, the morphology indicates even the mechanism of the old landslide, which taking into account the back-tilt phenomenon, which is observed on the slope orientation maps *(figure 17),* is a rotational type. So, considered the relations related the length of the old landslide, the depth could have been approximately assumed. The underlying facts present a recognizable old landslide with sizable dimensions.

Secondly, by the geological and engineering geological mapping the limits of the landslide was accurately detected. It is worth mentioning that the borders of the landslide are generally detectable with relatively great accuracy by the slope inclination map of *figure 18*. It is also observed that the material of the landslide in the north border slips at the bedding of the bedrock, and contrary in the south border, the landslide slips on the surface of approximately vertical joints which are slightly inclined towards north. Furthermore, the properties and characteristics of the failure material were also studied, so the material can be described as soft brown gravelly clay with angular fragments and boulders. Beside the under-failure material, the properties, the characteristics and the structure of the surrounding bedrock was also being examined. Important observations considering the occurrence of clayey lenses into bedrock were also committed. In addition, the conditions of bedrock on flat areas, eastern than the active landslide has committed. Those areas are composed by poor geotechnically characterized, bedrock.

Regarding the brittle tectonic deformation on the close study area, two major reverse faults were detected northern and southern of the landslide. The presence of those faults is important for interpretation of the geological processes which are responsible for the formation of the landslide. The activity of those faults, not only disintegrate the rock mass, which consequently reduces the strength of the rock mass, but also allowed hydrothermal fluids to pass and disintegrated the intact rock. The reduction in the geotechnical quality of the bedrock by the activity of tectonic faults and hydrothermal alteration, are responsible for the formation of the old landslide in the close study area.

Furthermore, the landslide was divided into three major categories, considering the position, the shape and the orientation of surface ruptures. Those three categories are expressed by the head, the main body and the toe of the landslide *(figure 36).* The toe of the landslide is subdivided into 4 categories regarding the direction the magnitude and the type of movement. More precisely the C1 subunit seems to present movements of moderate magnitude towards west with translation mechanism, and toppling in the edge. The C2 subunit does not contain any cracks, which means that this subunit remains immobile. In the subunit C3 uplift of important magnitude is noticed, and generally it appears lateral movements from WSW to SW. The last C4 subunit appears movements toward SW to SSW with a rotational slide mechanism. Generally, considering the behavior on the three units of the landslide, it can be considered as a rotational landslide.

# Chapter 4 Geological & Engineering Geological Subsurface Investigation

## 4.1 General

The drilling of geotechnical exploratory boreholes, is one of the most vital processes in engineering works *(Price D.G. & de Freitas M.H., 2009).* In particular, for landslide stability assessment projects, exploratory boreholes are crucial, in order to obtain helpful information considering the evolution of landslide, the composition of failed material, the characteristics in the shearing zone and more. More precisely in this study, the purpose of the drilling program was the detection of shear zones within the ground, and the evaluation of the material adjacent to those zones.

In the context of the current stability assessment, ten exploratory geotechnical boreholes have been implemented. From the underlying boreholes, only the seven provide reliable drill core loggings. The reliability of the core loggings is not only depended on the in situ evaluation of the specialist, but also in the drilling method. In *table 2,* the coordinates, the altitude and the depth of each borehole is demonstrated.

| Borehole | X | Y | Altitude (m) | Depth(m) |
|---|---|---|---|---|
| BDZ_22_01 | 367822,00 | 4647435,00 | 645,24 | 35,00 |
| BDZ_22_01A | 367779,78 | 4647407,94 | 654,25 | 47,00 |
| BDZ_22_02 | 367714,74 | 4647410,50 | 640,15 | 48,00 |
| BDZ_22_03 | 367730,90 | 4647380,56 | 640,59 | 50,00 |
| BDZ_22_03A | 367695,39 | 4647361,26 | 640,70 | 47,00 |
| BDZ_22_05 | 367615,64 | 4647401,63 | 626,62 | 46,00 |
| BDZ_22_06 | 367653,00 | 4647347,00 | 623,00 | 35,00 |
| BDZ_22_06A | 367603,92 | 4647324,87 | 622,36 | 40,80 |
| BDZ_22_07 | 367751,93 | 4647356,32 | 641,30 | 44,30 |
| BDZ_22_08 | 367695,72 | 4647277,02 | 630,99 | 48,00 |

*Table 2. Implemented exploratory geotechnical boreholes with the corresponding coordinates on UTM (Zone 38) projection system, altitude and depth in meters.*

The log coring on boreholes BDZ_22_01, BDZ_22_03 and BDZ_22_06 were not available for evaluation, so only pictures of them were provided. Furthermore, the quality of coring in the underlying boreholes is estimated questionable, considering that the exact position of the target, which was the depth of the slide, was not easy to detect, but only the contact among the stable and unstable material was distinguished. So, detailed analysis only for the rest of the boreholes will take place below. The analysis contains the presentation of the result of drilling process, which is the description of core data and indexes related to the core data, such as total core recovery (TCR), solid core recovery (SCR), rock quality designation (RQD), which are explained below in detailed. Furthermore, the presentation of problems which occur during drilling will be presented too, considering that those problems usually are crucial in the total evaluation. In addition, only for the rock type samples, rock mass classifications with GSI and RMR classification systems will occur in order to obtain parameters regarding the shear strength of the rock mass, which will be used on the geotechnical investigation.

## 4.2 Drilling Method

Two major drilling methods were used in this investigation program. Both completed by the same machinery which is ST 1023-HD type, and the same driller. The methods were used interchangeably based on the type of the drilling material.

The first drilling method, the simplest one, in which the sampler is single core barrel and the drilling takes place with tungsten bit at completely dry conditions. The diameter of drilled hole is 96,00mm, and the size of sample is 63,50mm. Furthermore, in every run, 0,5 – 1,0 thick, all drilling casings are exported from the borehole, in order to export the sample which is located at the last tube, and after exporting it, which usually taking place with hydraulic pressure, all casings are placed in the borehole to start the new run. It should be noted that this kind of drilling is applicable only on soil type formations.

The process of dry drilling has an essential impact on the sample. More precisely, this kind of drilling reduces the quality of the sample which is becoming partially disturbed. This occurs mostly because of high temperature, which is developed in the bit, and impacts to the sample, which passes through the bit. More precisely, the external bounders of the sample are burnt out. Furthermore, the single core barrel forces the sample into rotation. Considering that the velocity of cutting new material is deferent to the velocity of casing, the sample suffers shear deformation.

Although, the underlying method disturbs the sample, it is recommended in some cases. It is recommended for cohesionless soils, such as sand and gravel, above the water table. Furthermore, the sample, although disturbed, provides information about the origin of the material. For example, in this type of sampling, it is easy to single out sandy formations from clayey formations. To conclude, this type of sampling allows soil classification. Furthermore, laboratory tests in order to detect the strength of soil are also possible to be implemented, considering that the result would be a conservative approach. Generally, it is an economical method of drilling, which can be used when the accuracy on sample observation, for example thin shear zones, and accurate strength of the soil is not required.

The second type of drilling is more complicated. Not only the equipment is different, but also the procedure. In this case the process is implemented by double core barrel sampler and diamond bit. In contrast to previous method, now the drilling does not take place into dry conditions, and the circulation of drilling fluid, which is mainly composed by water and minorly by bentonite and polymer, occurs. The circulation of drilling fluid occurs between the inner and the external core, and after cutting in the bit, the sample is placed through the inner core, which is not rotating through the procedure of drilling. The diameter of hole is the same as previous yet the produced sample is thinner. It needs to be enhanced, that whether the diamond bit is cutting, drilling cannot be executed without drilling fluids. Furthermore, when it comes to export the sample from the sampler, only the inner core is thrown by wireline system. This means that the extraction of casing up to the depth of drilling is not required.

The wireline system, is a complicated system, requires double or triple core barrel, split samplers included, and it is usually used in two cases. Whether deep boreholes are implemented, the extraction of the casing to the final depth, is considered extremely time consuming, so the wireline system solves the problem, and the extraction is required only when the bit is needed to be changed, or other problems occur. Furthermore, when cohesionless material, such as sand or gravel is drilled below water table, the extraction of the casing creates cavings. So, it is possible for the hole to be closed even up to the depth of water table. In this case using wireline system the casing is not removed from the borehole, and the drilling continues, with only restricted quantities of caving, which is produced by restricted lifting of casing. Generally, the caving in this case, is minor.

Double core barrels although provide fast penetration, they are designed for drilling in strong, homogenous and slightly fractured rock mass. Furthermore, the double core barrel it is possible to be converted into triple by inserting thinner PVC type tube into the inner core. This makes the result of drilling more accurate. Although by inserting the third tube the result of drilling is more accurate, in low quality of rock mass, and in loose soils, double core split barrel is recommended, which in this case was not used. Although the double core split barrel produces way better sample, the penetration is slower than in the double, and also has higher maintenance cost.

It is worth mentioning that, samples for laboratory testing, which are referred as undisturbed samples at the loggings, are taken by double core barrel, including rotation and drilling fluids.

The external casing, which were used in those geotechnical exploratory boreholes, had external diameter of PQ size, which is 122mm, and proportionate inner diameter in order to the bit could pass. In the edge of the casing tungsten carbide bit is placed. So, this casing can also work as single core barrel. It is worth to mention that the tungsten carbide bit cannot pass compacted material such as a boulder, with a consequence that if boulder in the drilling be meted, below that depth there will be no securing of casing.

## 4.3 Core Logging Parameters

### 4.3.1 Total Core Recovery

Total core recovery (TCR) index *(figure 40)* characterizes only the core recovery, and it does not provide any other information, or at least direct information, about rock mass or soil, quality. TCR index, is a percentage of core recovery divided by the length of the core run (*Price D.G. & de Freitas M.H., 2009*). The length of core run should not exceed 5m, in order to assign TCR index on core material *(Hencher S., 2015).*

The underlying index is useful in order to understand the difficulties in the drilling process. From those difficulties, it is possible to draw conclusions about the drilled material. For example, whether the TCR is limited conclusions about the cohesion of geomaterial can be assumed. Furthermore, it is possible for geotechnically characterized good material, to have low values of TCR, if the process of drilling was not accurate. In contrast, if the TCR index contains high values, it does not mean that the quality of drilled material is not restricted.

### 4.3.2 Solid Core Recovery

Solid core recovery (SCR) index *(figure 40)* is defined as a percentage of the total length of solid components divided by the length of total core run *(Price D.G. & de Freitas M.H., 2009)*. It is worth to mention that this index, in contrast to TCR index, is applicable only on rock cores. The definition of solid core recovery, was unclear for years, and variety of definitions were used. So, the applicability of the underlying index was limited, and also problems related to the assigning RQD index, which is analyzed below, were common.

In 1986, accurate definition, of solid core recovery was stated by *Norbury D., et al.,* in order to clarify its meaning, and it is presented below:

“Solid core is taken as core with at least one full diameter (but not necessarily a full circumference) measured along the core axis between two natural fractures”

Considering the underlying definition, core recovery with one set vertical joints, the SCR is equal to 100%. If there are more than a single set, then only the sections of core in which joints are intersected, are excluded from SCR index *(Norbury D., et al. 1986).*

The underlying index, is useful to draw conclusions about the quality of rock mass. The present index is applicable for the detection of shear zones, in rock mass, during log coring. Furthermore, it does not have strict limits, which allows better understanding of rock mass quality by engineering geologists. It can also be combined with not only TCR index, but also the RQD index, for better demonstration of the engineering conditions which occur on the rock formation.

### 4.3.3 Rock Quality Designation

The rock quality designation (RQD) index *(figure 40),* is a logging core parameter, and describes the quality of drilled rock mass. It was first introduced in 1968, and now it is considered as a parameter on drilling procedure. It is also used on rock mass classification systems (*Bieniawski Z.T 1973; Barton N., et al 1974*). Unambiguous definition of RQD is illustrated by *Deere D.U., & Deere D.W., 1988*, and it is mentioned below:

“The RQD is a modified core recovery percentage in which all the pieces of ‘sound’ core over 100mm long are summed and divided by the length of the core run.”

Sound cores are considered unbroken, unweathered and unaltered rock type formations, which could be produced by both surface and hydrothermal processes. The sample is considered sound as long it is not friable. Friable is the sample, which can be easily excavated by the pick of geological hammer, or it is possible to be broke by hand.

The underlying index is generally accepted and widely used mostly because its simplicity. It was initially proposed for sampling by double core barrel of NQ-size core of 54,70 mm diameter. Now, drilling with double core barrels of diameter between BQ (36,50mm) and PQ (85,00mm) sizes are generally accepted, but the NQ-size remains the optimum diameter of sampling in order to assign RQD index, for the geotechnical purposes *(Deere D.U., & Deere*

*D.W., 1988)*. The RQD index initially was applied on granitic formations and not in sedimentary formations, where bedding and other structures occur. So, bigger diameters than PQ size, are also applicable, and in many cases indispensable.

Beside core diameter, the length of core run has crucial effects on RQD index. The sensitivity of RQD on shear zones is depended on the length of core run. For instance, if there is area of 30cm composed by shear material, and consequently with RQD=0 on this area, if the core run is 3,00m then the total RQD is equal to 90%. In contrast, if the total run is 30cm, then the total RQD is equal to 0%. So, it is recommended the run length should be range between 1,00-1,50m (*Deere D.U., & Deere D.W., 1988*).

In order to measure the RQD index, the pieces of core must be measured along the centerline, in order to avoid to false limitation in the quality of rock mass, for cases in which fractures are approximately vertical, parallel to the borehole and are cut off by second set. Furthermore, breaks caused by the process of drilling should not be encountered as breaks, and should be summed and added to the RQD index. In many cases though, the distinguish between the structural fractures produced by geological processes and fractures caused by drilling, is difficult. Although, the surfaces of drilling-caused fractures are fresh, in many cases the geological fractures, are might be seen so. Consequently, in cases of doubt fractures are considered natural, caused by geological processes. It is also worth mentioning that the RQD index should be assign on the product of drilling immediately after the process of drilling because there are phenomena, such as slaking, in which the rock suffers break down with time. This should be referred on the total loggings, because probably it will affect the construction, however, it should not be taken into consideration for the assigning of RQD index (*Deere D.U., & Deere D.W., 1988*).

Taking into account few parameters related to poor sampling, stress relief, slaking and more, it is concluded that RQD index is extremely absolute and strict between samples. For example, the quality of rock mass from core with RQD=20% and SCR=20% is not better than sample of core with RQD=15% and SCR=80%. Of course, usually the value of SCR is close to the value of RQD, however there are cases in which rock mass is penalized wrong. So, a way of plotting the two underlying indexes together, can produce useful conclusions about the quality of rock mass.

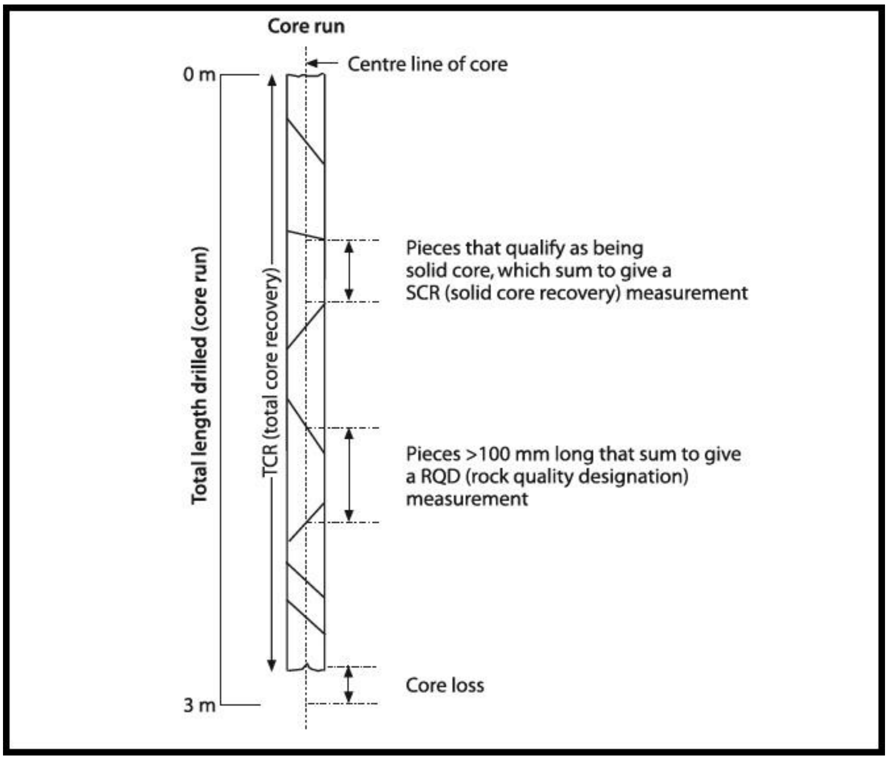

*Figure 40. Example of TCR, SCR, RQD indexes measurements (Price D.G. & de Freitas M.H., 2009)*

## 4.4 Boreholes

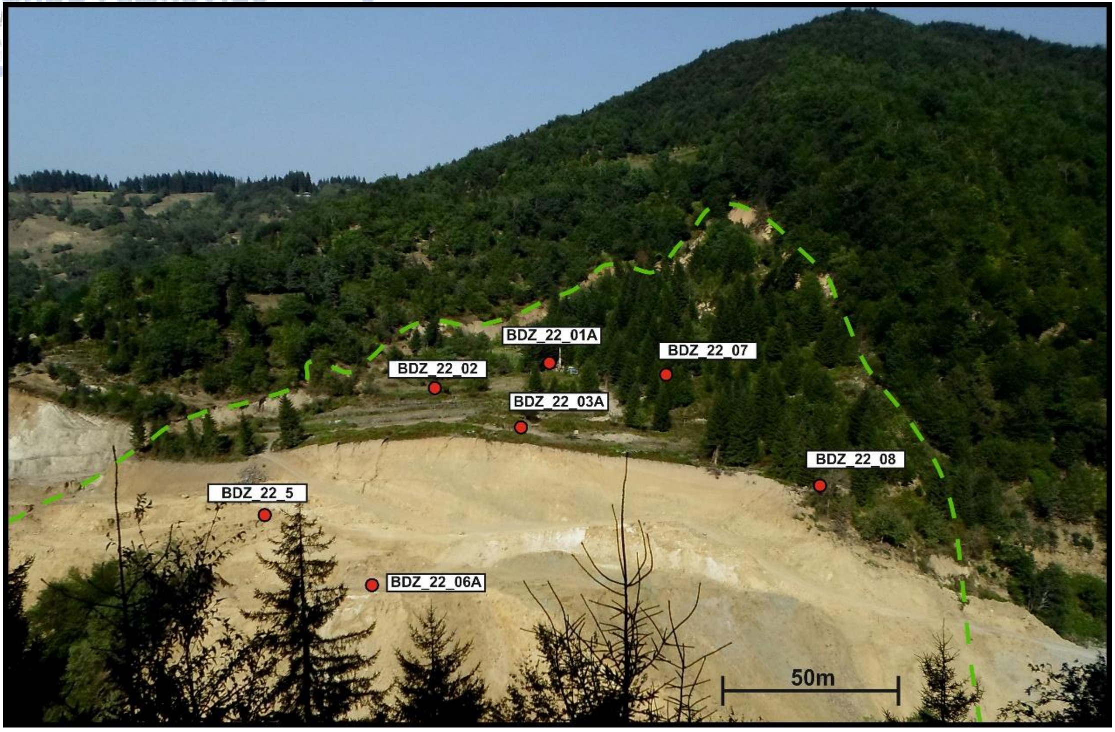

*Figure 41. Picture of Landslide from the opposite slope, with greed dashed line, the boundary of landslide and with red circles, the executed ant evaluable boreholes.*

### 4.4.1 Borehole: BDZ_22_01A

The Borehole BDZ_22_01A is located most closely to the scarp of the landslide compared to other boreholes *(figure 41).* The total Depth of the borehole was 47,00m and the ground elevation 645,24m. The drilling process started at 24/08/2017 and was completed within five (5) days at 28/08/2017, with approximate 10m per day drilling progress. First 30,00m of drilling was executed by single core barrel and tungsten carbide bit. The rest of the drilling was completed by double core barrel and diamond bit, with losses of drilling fluids is approximately equal to 50%. Casing was applied from the top of the borehole to the depth of 30,00m. The TCR index, for the underlying drilling was up to 90% with standard deviation of 15%.

In this borehole, top soil appears from the top of the borehole to the depth of 1,20m, with clayey material and presence of decomposed organic matter and roots, which gives to the soil dark brown to dark colored color. The presence of soil material continues up to the depth of 30,00m, and it constitutes by brownish clayey material. The presence of light brown to brown, very soft to soft, clay of medium plasticity is dominant. However, brown and grey angular gravel and boulders mostly of weathered and altered sandstone origin, are also included in this type of formation. Although, compared to clay the quantities, gravel and boulders are restricted, in two cases the thickness of boulders appears to be approximately up to 1,00m. As it is mentioned before up to 30,00m the drilling was implemented by single core, dry drilling with tungsten carbide bit. The mean TCR index in the section, from the top up to the depth of 30,00m was 96% with standard deviation of 2%.

The outcome of sampling at depth of 30,00m changes from brownish clayey material to also brownish gravelly material. This makes the change of the bit, from tungsten carbide bit to diamond, essential. The outcome of the underlying change appears clearly on the TCR index which is reduced now to mean value of 60% with standard deviation of 15%.

The material from 30,00 to 38,00m can be described as a very loose to loose, brown angular gravel with intense presence from brown, grey, purple, angular fragments of

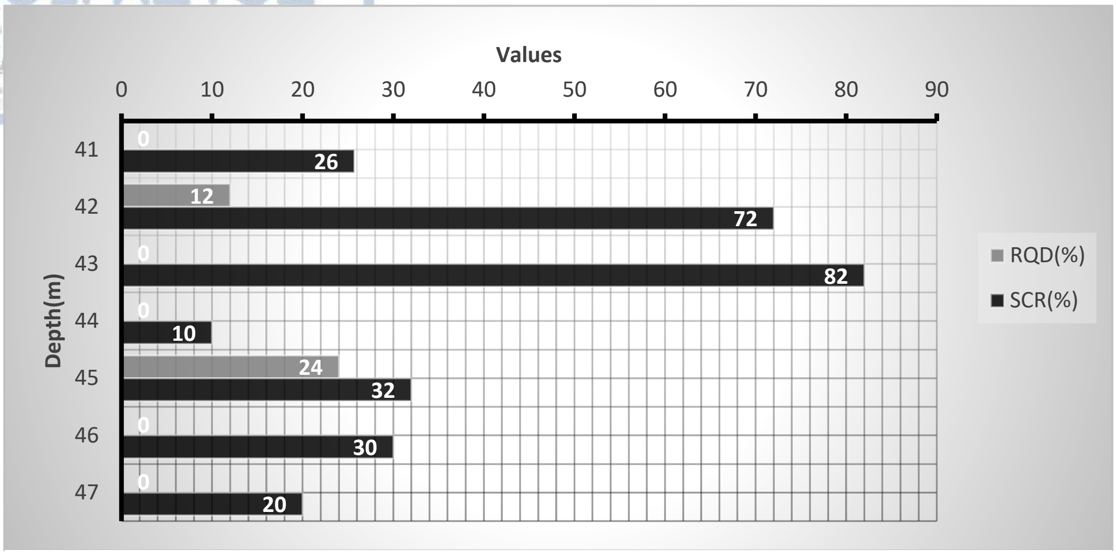

*Figure 42. RQD and SCR indexes versus depth, for Borehole: BDZ_22_01A*

weathered and altered sandstone, which most probably are fragments from bigger boulders. Furthermore, on this formations manganese type alteration is observed. It is also worth to point out that the fact that in the outcomes of the sample there was not observed any presence of clay does not means that there is not clay in this material. The lack of clay in the sampling is based on type of drilling, in which the fluids of the drilling process out washed the clay from the total sample.

Change of the type of sample occurred at depth of 38,00 m. Until the depth of 40,30m the sample became medium stiff to stiff, light grey to grey, clay of high plasticity with partially presence of angular gravel and fragments from dark grey sandstone. The TCR index is approximately equal to 94%.

At depth of 40,30m bedrock was reached. The bedrock in this case is moderately weak, slightly weathered, fine grained dark grey calcareous sandstone. Calcite vanes of restricted diameter as well as pyrite crystals are contained in the texture of sandstone. The bedrock in this case, appears to be intensively fractured-fissured with mean RQD index approximately equal to 6%. Furthermore, mean SCR index is approximately equal to 39%, yet with standard deviation of 25% *(figure 42).* The TCR index is approximately equal to 96±1%.

In order to assign total GSI index to the bedrock in this borehole, the examination of the structure of bedrock and the conditions of discontinuities have been implemented. In this case, the structure is considered as disintegrated and the condition of discontinuities poor, based on the thin infilling and medium weathering on the surfaces of the discontinuities. So, the total GSI index for this borehole is exported as GSI=20-25 *(figure 109).* Of course, GSI values was exported in the borehole with the same methods per 1m interval, and it is illustrated versus depth on *figure 43.*

Similarly, to export the total RMR index for the bedrock of this borehole, parameters which are mentioned above were examined. So, in this case UCS value was assumed between 5-25 MPa, RQD is <25%, spacing of discontinuities <6cm. Considering the groundwater conditions, damping conditions were assigned. For the conditions of discontinuities, the persistence is assumed 10-30m, the separation ranges between 1-5mm, the surfaces are smooth to slightly rough, soft infilling thinner than 5mm is observed and finally the surfaces are moderately weathered. Taking everything into account RMR index for this borehole is calculated to RMR=27-30 *(figure 110).* Of course, RMR values was exported in the borehole with the same methods per 1m interval, and it is illustrated versus depth on *figure 43.*

To conclude about this berehole, from the begin, to the depth of 38,00m the drilled material is considered as a landslide material. From 38,00 to 40,30m, stiff clay was drilled, which is considered stable, as does the bedrock, which was reached at depth of 40,30 m to the end of the borehole at 47,00m.

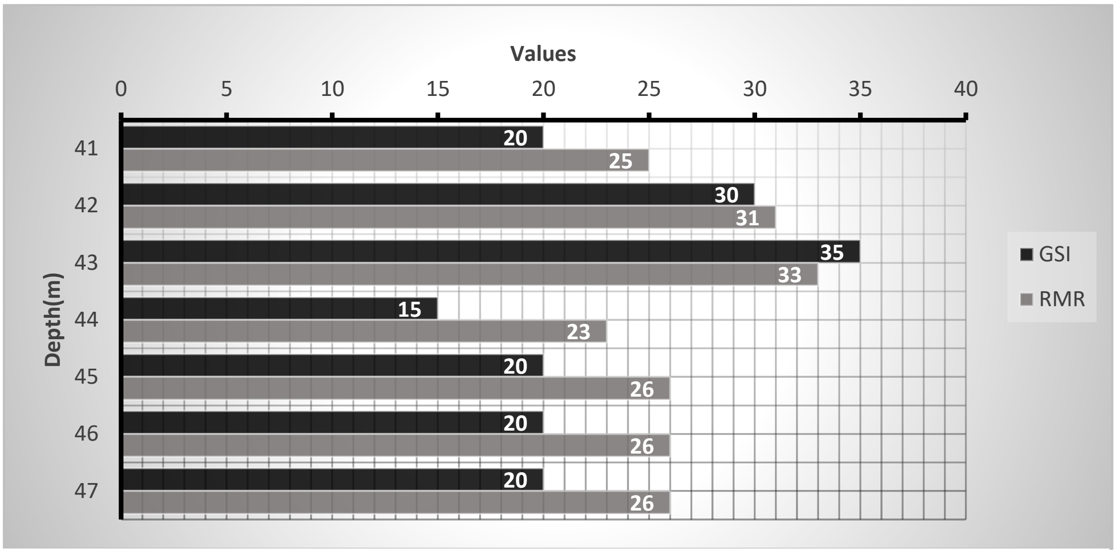

*Figure 43. GSI and RMR indexes versus depth, for Borehole: BDZ_22_01A*

### 4.4.2 Borehole: BDZ_22_02

The Borehole BDZ_22_02 is located northern to the main axis of the landslide *(figure 41).* The total Depth of the borehole was 48,00m and the ground elevation 640,15m. The drilling process started at 03/09/2017 and was completed within three days at 05/09/2017, with approximate 15m per day drilling progress. First 33,50m of drilling was committed by single core barrel and tungsten carbide bit. The rest of the drilling was completed by double core barrel and diamond bit, and the losses of drilling fluids are approximately equal to 80%. Casing was applied from the top of the borehole until the depth of 27,00m. The TCR index, for the underlying drilling was up to 93% with standard deviation of 7%.

In the current borehole, top soil appears from the top of the borehole to the depth of 1,50m, with clayey material and presence of decomposed organic matter and roots. Top soil is presented as brown to dark brown. The presence of soil material continues up to the depth of 32,80m and it is constituted by brownish clayey material. The presence of light brown, brown and dark brown, very soft to soft, clay of medium plasticity is dominant. However, brown, grey, deep red and purple angular gravel and boulders, mostly of weathered and altered sandstone origin, are also included in this type of formation. The boulders appear to be 30-50cm thick. The mean TCR index in the section, from the top up to the depth of 32,80m was 93% with standard deviation of 8%.

Although the drilling was still continued on soil material, the type of material which was the final sample was changed. From 32,80 to 38,40 the result of drilling was medium stiff to stiff dark and light grey, clay of high plasticity with restricted but noticeable quantities of gravel and angular fragments. More precisely from 35,70m to 37,10m the presence of angular fragments was intense. That means that those fragments either are individual pieces or pieces from greater boulders. Mean TCR index in this material of the borehole is approximately equal to 95% with standard deviation of 8%. Furthermore, the drilling fluid losses on this material is approximately equal to 90%. More precisely drilling fluids are completely lost from 33,50m to 35,00m, and below that depth loses are 80%.

At depth of 38,40 bedrock have been reached. Another 9,40m was drilled into bedrock until the drilling ended. Although, in this borehole the bedrock, petrologically is a dark grey, fine grained calcareous sandstone, its quality ranges significantly. From 38,40m to 40,60m,

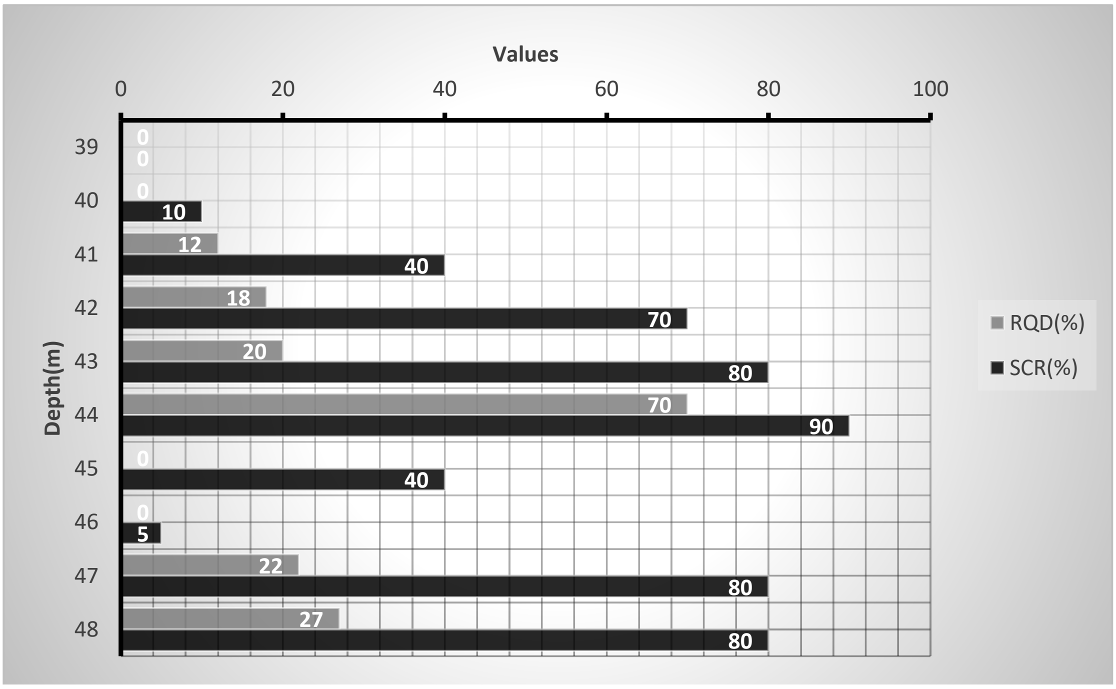

*Figure 44. RQD and SCR indexes versus depth, for Borehole: BDZ_22_02.*

the bedrock appears weak, very to intensively fractured and slightly to moderately weathered. Deeper, the quality of the bedrock is becoming better. So, until the end of the borehole bedrock appears strong, moderately fractured, slightly weathered with an exception of zone at depth of 44,90m to 46,00m, where the bedrock is intensively fractured and slightly to moderately weathered. Of course, the reducing in the RQD index is clear not only in the depth of 44,90-46,00m but also at depth of 38,40-40,60m, where there is more weathered area and it is shown with the SCR index at *figure 44* versus depth. Generally, the underlying indexes have mean values of 17% and 50% with standard deviation of 21% and 35% respectively. Mean value of TCR index in the bedrock is 93% with standard deviation of 5%. Furthermore, the drilling fluid losses on this material is approximately equal to 80%, without any specific area in which drilling fluid is completely lost.

In order to assign total GSI index to the bedrock in this borehole, the examination of the structure of the bedrock and the condition of discontinuities have executed. In this case, the structure is considered as very blocky, considering that the rock mass tectonically partially and not completely disturbed, and the condition of discontinuities poor, based on the thin infilling between the surface of discontinuities. So, the total GSI index for this borehole is exported as GSI=30-35 *(figure 109).* Of course, GSI values was exported in the borehole with the same methods per 1m interval, and it is illustrated versus depth on figure 45.

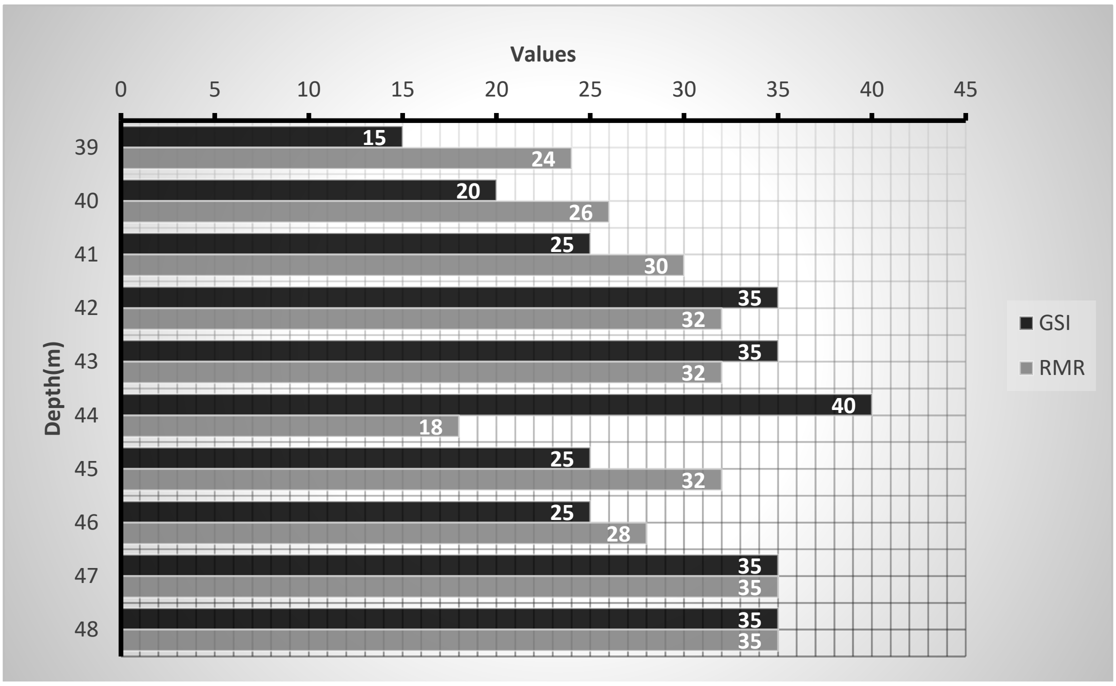

*Figure 45. GSI and RMR indexes versus depth, for Borehole: BDZ_22_02*

Similarly, to export the total RMR index for the bedrock of this borehole, parameters which are mentioned above were examined. So, in this case UCS value was assumed between 5-25 MPa, RQD is <25%, spacing of discontinuities is 6-20cm. Considering the groundwater conditions, damping conditions are assigned. For the conditions of discontinuities, the persistence is assumed 5-20m, the separation ranges between 0,5-5mm, the surfaces are smooth to slightly rough, soft infilling thinner than 5mm is observed and finally the surfaces are slightly to moderately weathered. Taking everything into account RMR index for this borehole is calculated to RMR=33-39 *(figure 110).* Of course, RMR values was exported in the borehole with the same methods per 1m interval, and it is illustrated versus depth on *figure 45.*

To conclude about this berehole, from the begin, to the depth of 32,80m the drilled material is considered as a landslide material. From 32,80 to 38,40m, stiff clay was drilled, which is considered stable, as does the bedroch, which was reached on depth of 38,40 m to the end of the borehole at 48,00m.

### 4.4.3 Borehole: BDZ_22_03A

The Borehole BDZ_22_03A is located in the middle of the main body of the landslide area (*figure 41)*. The total Depth of the borehole was 46,00m and the ground elevation 637,73m. The drilling process started at 19/08/2017 and was completed in five (5) days in 23/08/2017, with approximate 8m per day drilling progress. First 29,00m of drilling was executed by single core barrel and tungsten carbide bit. The rest of the drilling was completed by double core barrel and diamond bit, and the losses of drilling fluids are approximately equal to 60%. Furthermore, areas in which water have lost completely are not observed. Casing was applied from the top of the borehole until the depth of 28,00m. The TCR index, for the underlying drilling was up to 89% with standard deviation of 8%.

In this borehole, top soil appears from the top of the borehole to the depth of 2,50m, with soft dark brown clay and noticeable presence of decomposed organic matter.

The presence of soil material continues up to the depth of 35,70m and it is constituted by brownish clayey material. The presence of light brown, brown and dark brown, very soft to soft, clay of medium plasticity is dominant. However, brown, grey, deep red and purple angular gravel and boulders, mostly of weathered and altered sandstone origin, are also included in this type of formation. The boulders appear to be 30-70cm thick. The mean TCR index in the section, from the top up to the depth of 35,70m is 88% with standard deviation of 8%.

Although the drilling was still continued on soil material, the type of material which was the final sample is different. From 35,70 to 37,00 thin lense of medium stiff to stiff dark and light grey, clay of high plasticity was drilled, with restricted but noticeable quantities of gravel and angular fragments. The TCR index on this thin section appears to be equal to 80%.

At depth of 37,00 bedrock have been reached. Another 10,00m was drilled into bedrock until the drilling ended. Although, in this borehole the bedrock, petrologically is a dark grey, fine grained calcareous sandstone, there are noticeable differentiation in weathering. From 37,00m to 42,00m, the bedrock appears slightly to moderately weathered and from 42,00 until 47,00 the bedrock is slightly weathered. In general, the sandstone appears intensively fractured which is obvious from the RQD index, which in this case is approximately equal to

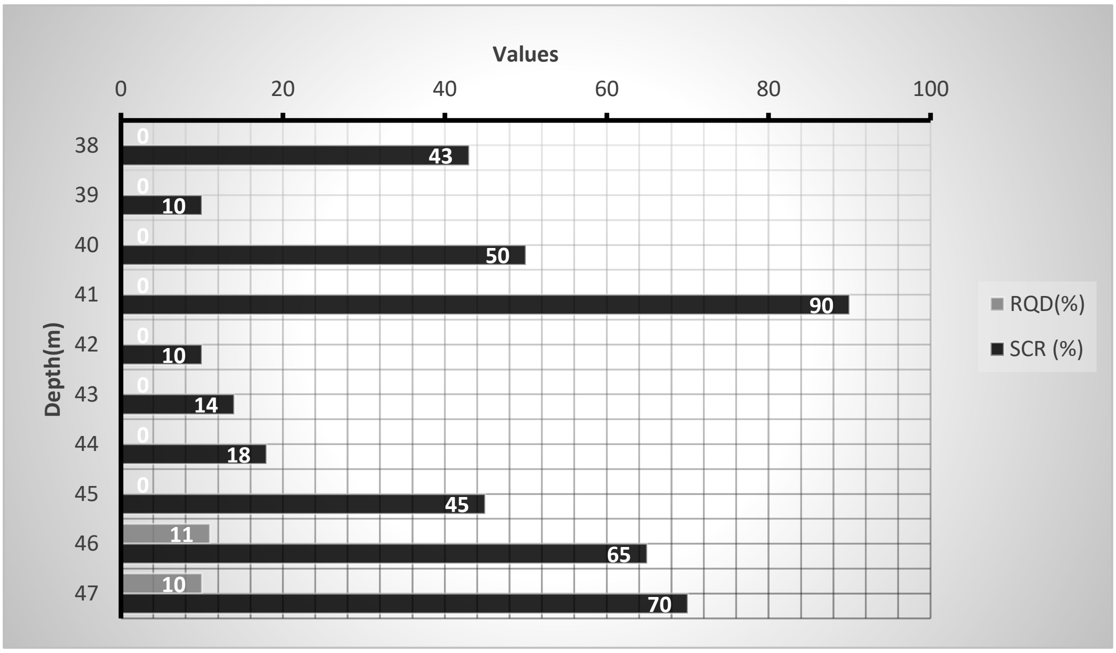

*Figure 46. RQD and SCR indexes versus depth, for Borehole: BDZ_22_03A*

zero. In contrast, the mean SCR index is approximately equal to 42% with standard deviation of 27%. The range of SCR and RQD indexes versus depth is demonstrated at *figure 46.* Furthermore, mean TCR index on the bedrock is approximately equal to 88% with standard deviation of 8%.

In order to assign total GSI index to the bedrock in this borehole, the examination of the structure of the bedrock and the condition of discontinuities have committed. In this case, the structure is considered as disintegrated, based on intensive fracture which characterizes the bedrock, and the condition of discontinuities poor, based on the thin infilling and medium weathering on the surfaces of the discontinuities. So, the total GSI index for this borehole is exported as GSI=20-25 *(figure 109).* Of course, GSI values was exported in the borehole with the same methods per 1m interval, and it is illustrated versus depth on *figure 47.*

Similarly, to export the total RMR index for the bedrock of this borehole, parameters which are mentioned above were examined. So, in this case UCS value was assumed between 5-25 MPa, RQD is <25%, spacing of discontinuities <6cm. Considering the groundwater conditions, damping and wet conditions are assigned. For the conditions of discontinuities, the persistence is assumed >20m, the separation ranges between 2-10mm, the surfaces are smooth to slightly rough, soft infilling thinner than 5mm is observed and finally the surfaces are moderately weathered. Taking everything into account RMR index for this borehole is calculated to RMR=23-28 *(figure 110).* Of course, RMR values was exported in the borehole with the same methods per 1m interval, and it is illustrated versus depth on *figure 47.*

To conclude about this berehole, from the begin, to the depth of 35,70m the drilled material is considered as a landslide material. From 35,70 to 37,00m, stiff clay was drilled, which is considered stable, as does the bedroch, which was reached on depth of 37,00m to the end of the borehole at 46,00m.

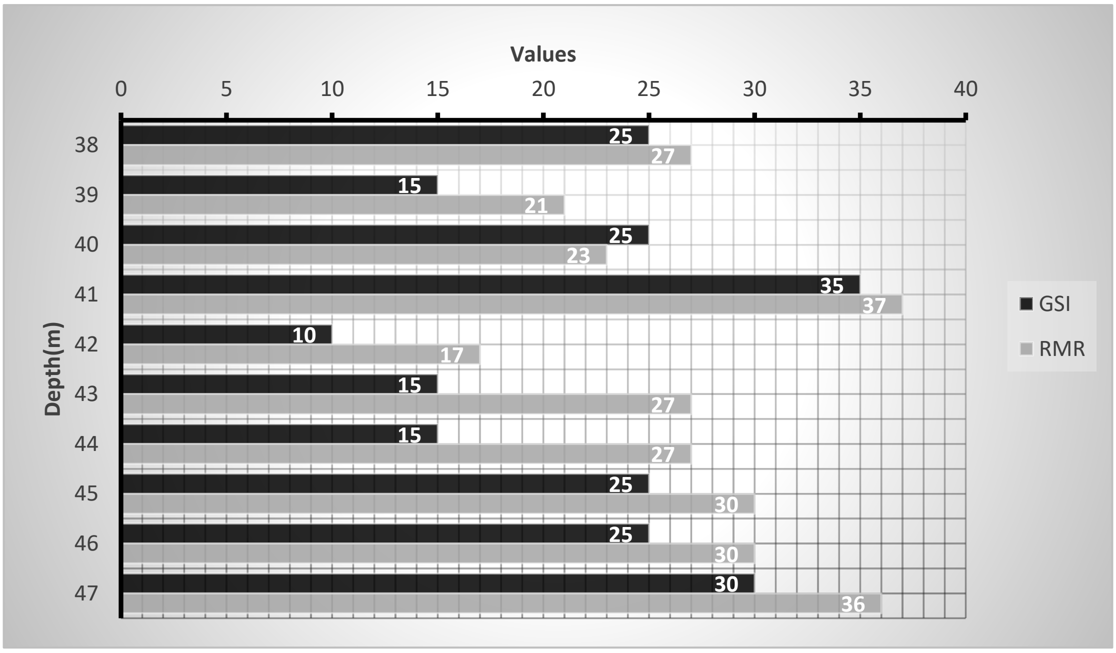

*Figure 47. GSI and RMR indexes versus depth, for Borehole: BDZ_22_03A*

### 4.4.4 Borehole: BDZ_22_05

The Borehole BDZ_22_05 is located in the northern flank of the landslide area, at C1 unit (*figure 41)*. The total depth of the borehole was 46,00m and the ground elevation 626,62m. The drilling process started at 06/09/2017 and was completed within four days at 09/09/2017, with approximate 11m per day drilling progress. During the drilling process, a lot of difficulties have faced. First indication, which confirms the previous sentence is the frequent change between single core barrel and triple core barrel, as well as diamond and tungsten carbide bit. Drilling process started with single core until the depth of 5,00m in which tungsten carbide bit could not pass. Until this depth, sample can be described as soft to very soft, light brown gravelly clay to clayey gravel with angular fragments of weathered-alternated sandstone. At depth of 5m rocky formation occur, which made necessary the change from tungsten carbide bit to diamond bit. That means, drilling process continues with drilling fluids instead of dry drilling. Furthermore, casing have installed at depth of 5,00m.

The rocky formation which was faced at depth of 5,00m, appears to be approximately 0,50m thin and the process continued with diamond bit until the depth of 25,00m where the TCR index dropped gradually to 50%. From the depth of 5,50m, to 9,80m the material is similar to the material in the begging of the borehole. However, from 9,80m to 17,10m the type of sample changed. So, the result of sampling was rocky formation which can be described as a moderately weak to moderately strong, deep red to deep purple, moderately to very fractured, very weathered-alternated sandstone. Below, the product of drilling is changes into clayey material. This is the major fact which indicates that the 7,30m thick rocky formation is nothing else but huge boulder into clayey material. From 17,10 to 25,00m the result of the drilling is described as soft, brown, gravelly clay of low to medium plasticity with angular gravel and fragments. It is important to point out, considering that the depth of casing was only 5m, the losses of drilling fluid was absolute 100%.

At depth of 25,00m change in sampler and bit occur, and the drilling process continue with single core barrel sampler and tungsten carbide bit. Although the change on the sampling occur, the material remained the same. However, the change on the sampling method had crucial impact on TCR index, which increased up to 80%. The losses in core recovery previously,

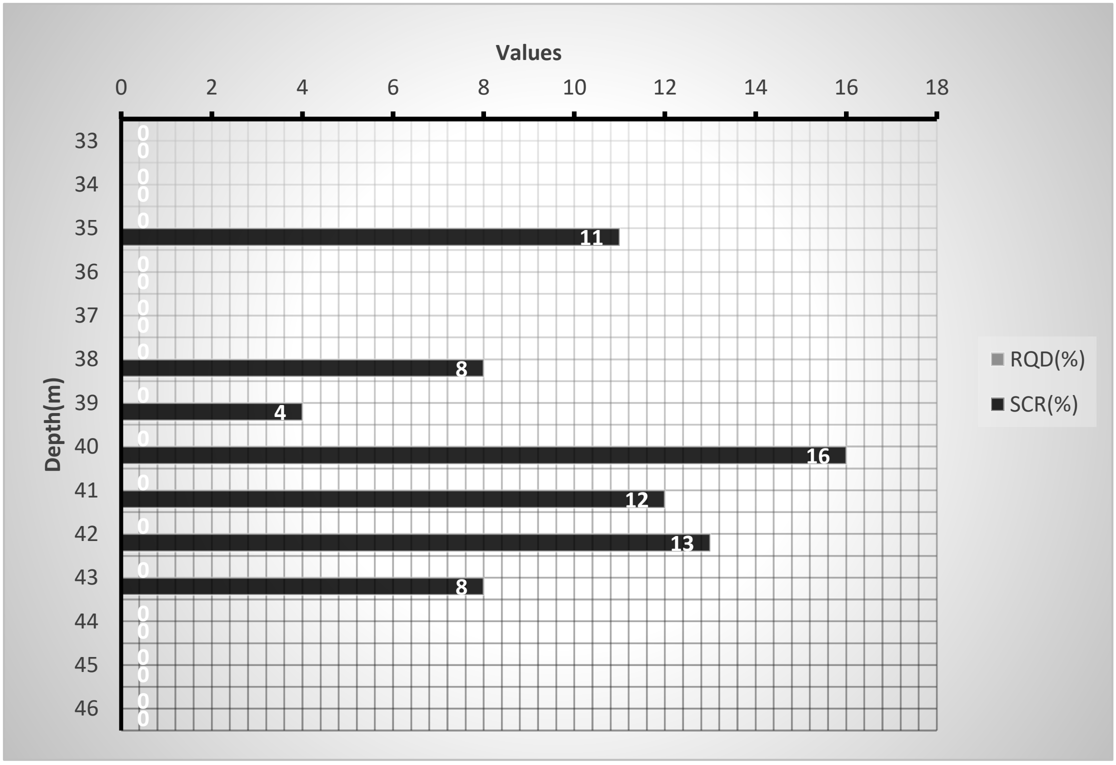

*Figure 48. RQD and SCR indexes versus depth, for Borehole: BDZ_22_05*

was the result of drilling fluid, which outwash important quantities of the sample. Drilling with single core barrel and tungsten carbide completed at depth of 29,50m, and continued with double core barrel and diamond bit with drilling fluids.

At depth of 30,40m the material changed in the sample occur. From soft, brownish clay of medium plasticity with gravel and fragments, material changed into stiff grey clay of high plasticity, which also contained gravel and fragments though.

At depth of 32,00m bedrock has reached. From core examination, conclusions considering not only the type of formation but also its quality have been exported. The sample constitutes by moderately very weak to weak, intensively to completely fractured-fissured, moderately weathered, fine grained, dark grey calcareous sandstone. Furthermore, layers of clay, 5-8 cm thin are also contained. The intensive distribution on the bedrock is also indicated by the RQD index which is constantly equal to zero. The evaluation of SCR index approaches the same result, considering that the mean SCR value is approximately equal to 5% with standard deviation of 5%. The values of RQD and SCR versus depth are shown in *figure 48.* Combined all the underlying information it is concluded that the quality of bedrock in this position is extremely restricted. Considering though, that through the process of drilling problems, regarding the machinery have faced, it could be assumed that the quality of the bedrock is better than the indication of sample, yet still it is limited. The mean TCR index on the bedrock is equal to 86% with standard deviation of 8%.

In order to assign total GSI index to the bedrock in this borehole, the examination of the structure of bedrock and the condition of discontinuities have implemented. In this case, the structure is considered as disintegrated, based on intensive fracture which characterizes the bedrock in this position, and the condition of discontinuities is considered as very poor, based on the thick clayey infilling. So, the total GSI index for this borehole is exported as GSI=15-20 *(figure 109).* Of course, GSI values was exported in the borehole with the same methods per 1m interval, and it is illustrated versus depth on *figure 49.*

Similarly, to export the total RMR index for the bedrock of this borehole, parameters which are mentioned above were examined. So, in this case UCS value was assumed between 5-25 MPa, RQD is <25%, spacing of discontinuities <6cm. Considering the groundwater

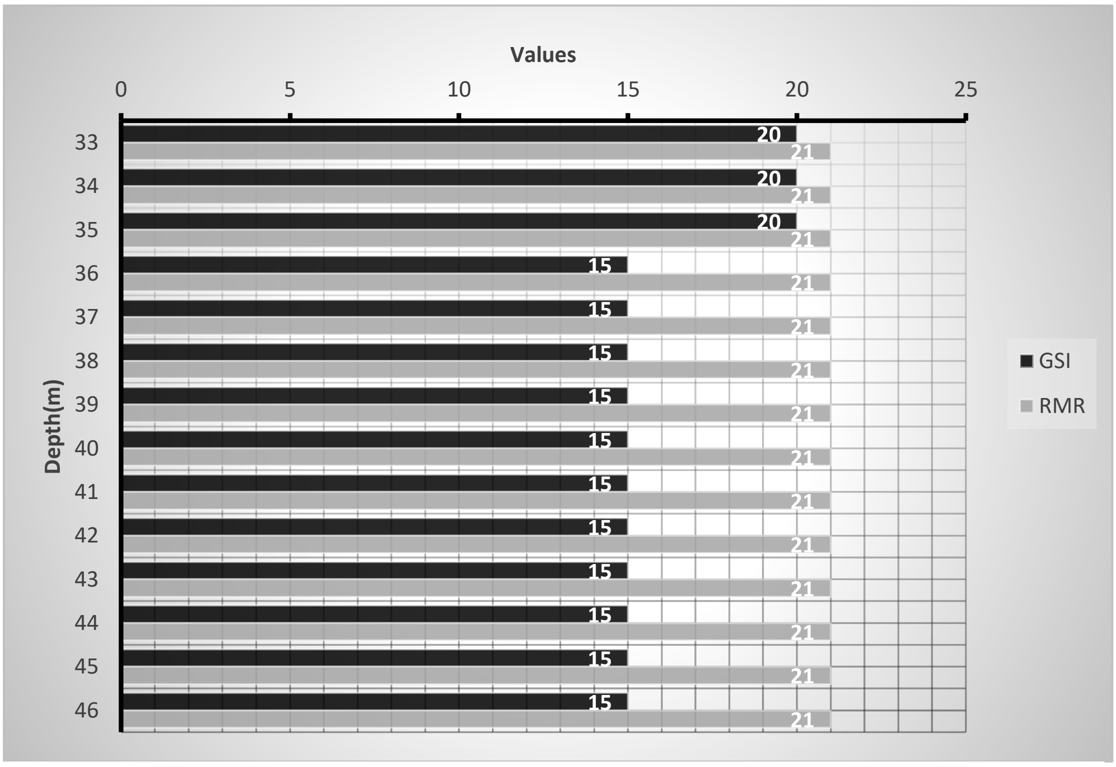

*Figure 49. GSI and RMR indexes versus depth, for Borehole: BDZ_22_05*

conditions, wet conditions are assigned. For the conditions of discontinuities, the persistence is assumed >20m, the separation is >3mm, the surfaces are smooth to slightly rough, soft infilling thicker than 3mm is observed and finally the surfaces are moderately weathered. Taking everything into account RMR index for this borehole is calculated to RMR=21-26 *(figure 110).* Of course, RMR values was exported in the borehole with the same methods per 1m interval, and it is illustrated versus depth on *figure 49.*

To conclude for this borehole, landslide material faced from the top to the depth of 30,40m, for which the mean TCR index is approximately equal to 86% with standard deviation of 11%. Furthermore, the thickness of stiff light grey clay, which is considered stable, is restricted to 1,60m with core recovery of 85%. In the end 16,00m of poor quality bedrock was also drilled with recovery characteristics mentioned above. It is also worth to meantion that the totat TCR index for the borehole is approximately equal to 86% with standard deviation of 11% and during the process of drilling returned drilling fluids was not observed.

### 4.4.5 Borehole: BDZ_22_06A

The Borehole BDZ_22_06A is located in the center, on the toe of the landslide, at C3 subunit. The total depth of the borehole was 40,80m and the ground elevation is 622,36m. The drilling process started at 13/08/2017 and was completed within seven days at 19/08/2017, with approximate 6m per day drilling progress. It is worth mentioning that this borehole, chronologically was the first one, from seven boreholes which were executed on the landslide with applicable core evaluation.

First 17,80m of borehole were drilled by single core barrel and tungsten carbide bit under dry conditions. The result of drilling up to depth of 16,60m, in general is constituted by very soft to soft, brown, gravelly clay of medium plasticity, with gravel and angular fragments. Gravelly material appears ate depths 0-1,40m, 2,40-3,20m, 5,80-6,00m and 14,70-14,80m, which are composed by weathered and altered sandstone of brown, deep red, deep purple and grey color. Material up to depth of 16,60 is considered as a landslide of material. From 16,60m to 17,80m medium stiff to stiff, grey clay of high plasticity, with gravel and angular fragments was sampled. At depth of 17,80 the sampling changed from single core barrel to double core barrel, and the tungsten carbide bit to diamond bit. Furthermore, drilling fluids now are added, in contrast to dry drilling which was committed up to the depth of 17,80m.

Although the sample does not seem the same, up to the depth of 18,50m is the same. Drilling fluids are responsible for the wash out of clay. From 18,50m to 20,10m, the material changed into brown gravel and fragments. Furthermore, the TCR index is even reduced to 30% in this zone, which means that is possible that drilling fluids wash out the clay, which is also component yet it is not seem on the result of drilling. Slightly weathered, moderately to very fractured, with no signs of alteration, fine grained dark grey sandstone appeared from 20,10 to 22,00m. From 22,00m to 29,00m the sample can be described as grey to dark grey, stiff,

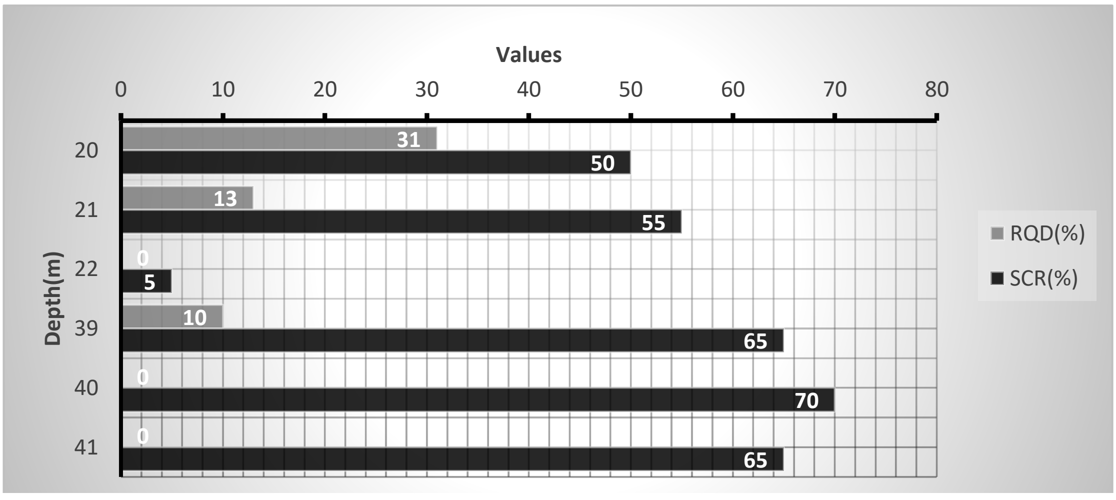

*Figure 50. RQD and SCR indexes versus depth, for Borehole: BDZ_22_03A*

clay with gravels and angular fragments of grey sandstone. More careful look questions the dominance of clay and enhanced the appearance of gravel and fragments. Considering though that the sampling was carried out with diamond bit, drilling fluids and also this was the first borehole, it is possible to conclude that the clay has been washed out.

Below the depth of 29,00m, 8,90m thick layer of deep brown, coarse grained sand has faced. The drilling on that material was complicated and difficult, considering that the two diamond bits have been burnt on this material. This is mostly based on low or even cohesionless material of sand, which sampling with drilling fluids was terribly difficult. So, the reduce on the quantities of drilling fluids, cause reduce on cooling rate of bit, which was finally burnt.

At depth of 37,90m bedrock have reached, immediately after the sandy zone. Exactly before the bedrock the clay component of sandy formation has been increased. The drilling continued to the depth of 40,80m, which was the final depth of the borehole. The fact that the final depth of borehole was below the level of the river (588m) was the most vital factor, which indicated the end of drilling process.

The clear bedrock in this borehole appears from 37,90m to 40,80m and can be described as moderately weak, intensively fractured-fissured, slightly to moderately weathered, fine grained, grey calcareous sandstone. The intense fracture can be also exported by RQD value which is approximately equal to zero. Furthermore, the SCR is approximately equal to 67% *(figure 50)* and lastly the TCR index is approximately equal to 93%.

Worth mentioning is also the rock type formations which was drilled at depth 20,10m to 22,00. Considering that the sandy formation belongs to the bedrock, which would be more analyzed below, the dark grey sandstone which was drilled in this depth is part of the bedrock and it is not a boulder. That means that values of RQD and SCR are applicable on this sample. So RQD and SCR indexes are equal to 22% and 53% respectively.

It is worth mentioning that although the RQD and SCR indexes regarding the drilled sands does not appear at the diagrams, the sandy formation is considered lenses into the bedrock.

Concerning the total GSI for the rocky formations of the borehole, the examination of the structure of the bedrock and the condition of discontinuities implemented. In this case, the structure is considered as disturbed/seamy, based on structural disorder of rock. The condition of discontinuities poor, based on moderately weathered surfaces and appearance of infilling. So, the total GSI index for this borehole is exported as GSI=30-35 *(figure 110).* Of course, GSI values was exported in the borehole with the same methods per 1m interval, and it is illustrated versus depth on *figure 51.*

Similarly, to export the total RMR index for the bedrock of this borehole, parameters which are mentioned above were examined. So, in this case UCS value was assumed between

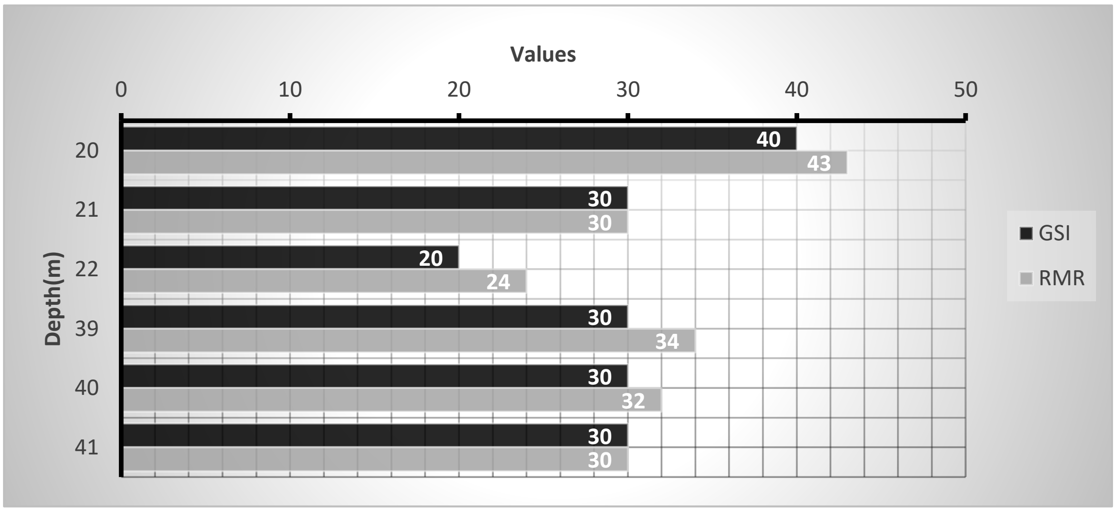

*Figure 51. GSI and RMR indexes versus depth, for Borehole: BDZ_22_06A*

5-25 MPa, RQD is <25%, spacing of discontinuities is 5-15cm. Considering the groundwater conditions, damping conditions are assigned. For the conditions of discontinuities, the persistence is assumed 10-20m, the separation ranges between 1-5mm, the surfaces are slightly rough, soft infilling of <2mm is observed and finally the surfaces are slightly to moderately weathered. Taking everything into account RMR index for this borehole is calculated to RMR=30-35 *(figure 110).* Of course, RMR values was exported in the borehole with the same methods per 1m interval, and it is illustrated versus depth on *figure 51.*

To conclude about this borehole, landslide material apppears until the depth of 16,60m, with mean TCR value approximately equal to 91±9%. The grey stiff grey clay of high plasticity appears until the depth of 18,50m, with thickness of 1,9m. Below, 1,60m of brown angular fragments have been drilled and then layer of dark brown coarse-grained sand, of 8,90m thickness was sampled with TCR index 82±6%. At depth of 38,90m to 42,80 weak bedrock has been drilled. The total mean value of TCR index for this borehole is 84±14%, and the drilling fluid loses are restricted to 20% without important variations even in sandy areas.

### 4.4.6 Borehole: BDZ_22_07

The Borehole BDZ_22_07 is located in the southern flank of the main body of the landslide. The total Depth of the borehole was 44,30m and the ground elevation is 641,30m. The drilling process started at 29/08/2017 and was completed within five days at 02/09/2017, with approximate 10m per day drilling progress. First 36,00m of borehole were drilled by single core barrel and tungsten carbide bit under dry conditions. The rest of the drilling was completed by double core barrel and diamond bit, and the losses of drilling fluids are approximately equal to 40% to the depth of 39m in which drilling fluids have been completely lost. Casing was applied from the top of the borehole until the depth of 31,80m. The TCR index, for the underlying drilling was up to 90% with standard deviation of 7%.

In this borehole, top soil appears from the top of the borehole to the depth of 2,00m, with clayey material and presence of decomposed organic matter and roots. Top soil is considered as brown to dark brown colored. The presence of soil material continues, and until the depth of 33,50m, it is constituted by brownish clayey material. The presence of light brown, brown and dark brown, very soft to soft, clay of low to medium plasticity is dominant. However, brown, grey, deep red and purple angular gravel and boulders, mostly of weathered and altered sandstone origin, are also included in this type of formation. The mean TCR index in the section, from the top up to the depth of 33,50m was 90%.

Although the appearance of soil- type material continues to the depth of 36,00m changes the composition of it. From 33,50 to 36,00 the result of drilling was medium stiff to stiff dark and light grey, clay of high plasticity with restricted but noticeable quantities of gravel and angular fragments. That mean that those fragments either are individual pieces or pieces from a bigger boulder. Mean TCR index in this material of the borehole is approximately equal to 90%. It is important to point out that in this borehole the underlying stiff clayey material have been sampled by single core barrel and dry drilling by tungsten carbide bit.

At depth of 36,00 bedrock have been reached. Another 8,30m was drilled into bedrock until the drilling ended. The bedrock appears weak, intensively fractured-fissured, slightly to moderately weathered with no signs of intense alteration, based on the color of rock, dark grey fine grained calcareous sandstone. The quality of the sandstone, considering the fracture, seems to become improved after 43,00m depth. The intensive fracture from 36,00m to 43,00 is indicated by the RQD index which in this area is equal to zero, and the SRC index, is approximately equal to 11% with standard deviation of 8%. Below, not only the RQD is

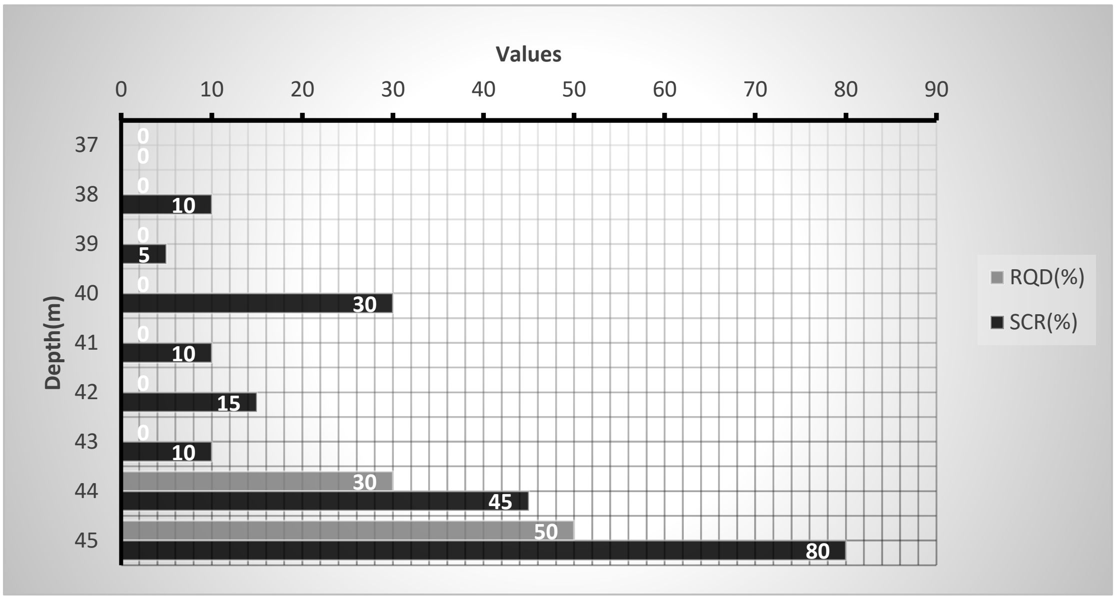

*Figure 52. RQD and SCR indexes versus depth, for Borehole: BDZ_22_07*

improved, with mean value of 40%, but also the SCR with value of 60%. Totally for the bedrock in this borehole the mean RQD is equal to 9%, the SCR is equal to 23% and the mean TCR is equal to 91% with 7% of standard deviation. Furthermore, at depth of 39,00m the returned drilling fluid have been lost.

In order to assign total GSI index to the bedrock in this borehole, the examination of the bedrock's structure and discontinuities condition have taken place. In this case, the structure is considered as disintegrated but partially there are areas in which the bedrock appears very blocky. The condition of discontinuities is fair to poor, based on moderately weathered surfaces and at some areas thin infilling. So, the total GSI index for this borehole is exported as GSI=23-28 *(figure 109).* Of course, GSI values was exported in the borehole with the same methods per 1m interval, and it is illustrated versus depth on *figure 53.*

Similarly, to export the total RMR index for the bedrock of this borehole, parameters which are mentioned above were examined. So, in this case UCS value was assumed between 5-25 MPa, RQD is <25%, spacing of discontinuities is 6-20cm. Considering the groundwater conditions, damping conditions are assigned. For the conditions of discontinuities, the persistence is assumed >15m, the separation ranges between 1-5mm, the surfaces are smooth to slightly rough, soft infilling thinner than 5mm is observed and finally the surfaces are moderately weathered. Taking everything into account RMR index for this borehole is calculated to RMR=28-32 *(figure 110).* Of course, RMR values was exported in the borehole with the same methods per 1m interval, and it is illustrated versus depth on *figure 53.*

To conclude about this borehole, landslide material apppears until the depth of 33,50m, then continues a thin layer of stiff grey clay 1,60m thick, and eventually, 8,30m of generally poor quality bedrock was drilled until the end of process.

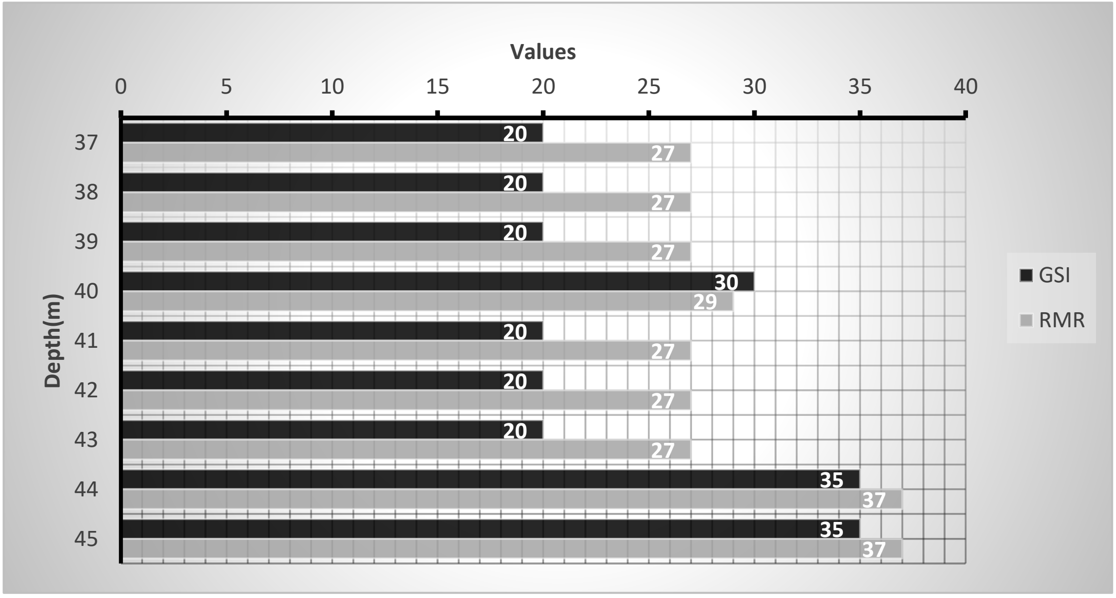

*Figure 53. GSI and RMR indexes versus depth, for Borehole: BDZ_22_07*

### 4.4.7 Borehole: BDZ_22_08

The Borehole BDZ_22_08 is located in the southern part to the main axis of the landslide, in C4 subunit. The total depth of the borehole was 48,00m and the ground elevation is 630,98m. The drilling process started at 10/09/2017 and was completed within four days in 13/09/2017, with approximate 10m per day drilling progress.

First 18,00m of borehole were drilled by single core barrel and tungsten carbide bit under dry conditions. The result of drilling until this depth was, 2,00m thick, top soil which is composed by very soft to soft, deep brown gravelly clay of medium to high plasticity with decomposed organic matter, roots and angular fragments. From the depth of 2,00m until the depth of 18,00m the result of sampled material, in general is constituted by very soft to soft, brown, gravelly clay of medium plasticity, with gravel and angular fragments. It is worth to mention that at depth of 13,20-14,50m loose, brown, clayey gravel and angular fragments occur. Furthermore, at depth of 12,00-12,40m soft to medium stiff, grey clay is also appeared.

The change in drilling method was not related to change on the material considering that the type of material below 18,00m was the same. So, the change occurred in order to take specific kind of samples, which is referenced in previous chapter, for laboratory tests. From 18,00m the drilling continued by double core barrel, diamond bit and drilling fluids, on the same material as previous, until the depth of 23,00m in which change on type of drilling occurred again.

Single core barrel and tungsten carbide bit was placed again, and the dry drilling continued to the depth of 31,50m. Until the depth of 27,00m, the type of material was approximately the same, soft to very soft brown clay with gravel and angular fragments. At depth of 27,00m change only on color occur, which became darker. So, from 27,00m to 29,50m the material can be described as soft, dark brown clay of medium plasticity with gravel and angular fragments. At depth of 29,50m the material complete change occurred. From soft brown clay, now it appears to be medium stiff to stiff, grey to dark grey, clay of high plasticity. This material, continues to contain gravel and angular fragments, but those are different than previously. In grey clay, the fragments and gravel have origin of grey unaltered sandstone in contrast to the brown clay, in which the gravel and the fragments have origin of weathered and altered brown sandstone. Sample for laboratory tests have been taken from the depth of 31,15-31,55m too.

Change on the method of drilling occurred at depth of 31,50m, in which double core barrel and diamond bit started drilling with drilling fluids. Furthermore, casing was installed at depth of 30,00m. Grey stiff clay is drilled from 29,50m to 32,80m, in which a change on material occurred, and 80cm of brown angular fragments have been drilled. Below that, 5,10m thick layer of deep brown, coarse grained sand has faced. The drilling on that material was complicated and difficult, considering that the two diamond bits have been burnt on this material. This is mostly based on low or even cohesionless material of sand, which sampling with drilling fluids is terribly difficult. So, the reduce on the quantities of drilling fluids, cause reduce on cooling rate of bit, which finally was burnt.

At depth of 38,50m, the difficult for drilling are have partly finished, and dark grey clay of high plasticity appeared again for 1,00m. Drilling continued, and from 39,50m to 42,80m, the result of sampling was dark grey, medium dense, clayey fragments and gravel of unaltered sandstone. This area of approximately 3m thick, is considered as a bedrock, but its structure indicates that it is not ordinary bedrock, but a mantle of weathered bedrock, and it is not considered as a 100% rocky formation. At depth of 42,80m though, good quality bedrock

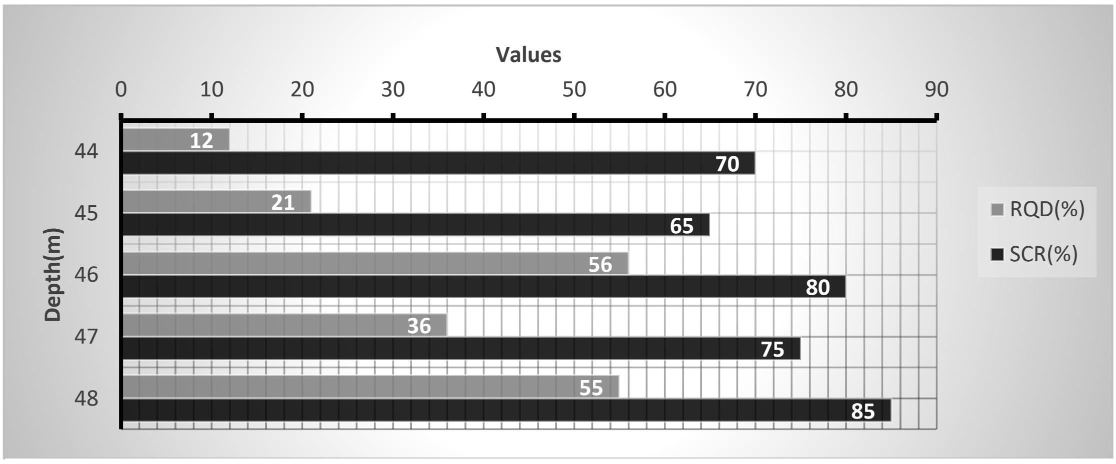

*Figure 54. RQD and SCR indexes versus depth, for Borehole: BDZ_22_08*

approached and the process of drilling continued to the depth of 48,00m, which is the final depth of the borehole.

From the depth of 42,80m to 48,00m, bedrock can be described as strong, slightly weathered, moderately fractured – fissured, fine grained and thin bedded, dark grey calcareous sandstone. On the samples, calcite vanes and presence of pyrite-crystals are appeared. The surfaces of discontinuities are weathered-discolored. The fair quality of the bedrock is indicated also by RQD and SCR indexes. The mean value of RQD is approximately equal to 36% with standard deviation of 18%. Respectively, the mean value of SCR is 75% with standard deviation of 7%. The values of RQD and SCR indexes are plotted versus depth on *figure 54.* In addition, the TCR index for this formation is equal to 96±1%.

In order to assign total GSI index to the bedrock in this borehole, the examination of the structure of the bedrock and the condition of discontinuities have taken place. In this case, the structure is considered as very blocky. The condition of discontinuities is fair to poor, based on moderately weathered surfaces and lack of infilling. So, the total GSI index for this borehole is exported as GSI=45-50 *(figure 109).* Of course, GSI values was exported in the borehole with the same methods per 1m interval, and it is illustrated versus depth on *figure 55.*

Similarly, to export the total RMR index for the bedrock of this borehole, parameters which are mentioned above were examined. So, in this case UCS value was assumed between 5-25 MPa, RQD is 25-50%, spacing of discontinuities is 6-60cm. Considering the groundwater conditions, damping conditions are assigned. For the conditions of discontinuities, the persistence is assumed 3-10m, the separation ranges between 0,1-1mm, the surfaces are slightly rough to rough, infilling is observed rarely and finally the surfaces are slightly to moderately weathered. Taking everything into account RMR index for this borehole is calculated to RMR=44-50 *(figure 110).* Of course, RMR values was exported in the borehole with the same methods per 1m interval, and it is illustrated versus depth on *figure 55.*

To conclude about this borehole, landslide material apppears until the depth of 29,50m, with mean TCR value approximately equal to 96±1%. The grey stiff grey clay of high plasticity appears until the depth of 32,80m, with thickness of 3,3m and TCR value equal to 96±1%. Below, 80cm of brown angular fragments have been drilled and then layer of dark brown coarse-grained sand, of 5,10m thickness was sampled with TCR index 89±4%. Then, 1,00 thick stiff, grey clay of high plasticity appeared again. At depth of 39,50m to 42,80 weak rocky formation occur and from 42,80 to 48,00, bedrock has been drilled. The material below 29.50 is considered stable. The total mean value of TCR index for this borehole is 95±3%, and the drilling fluid loses are restricted to 20% without important variations even in sandy areas.

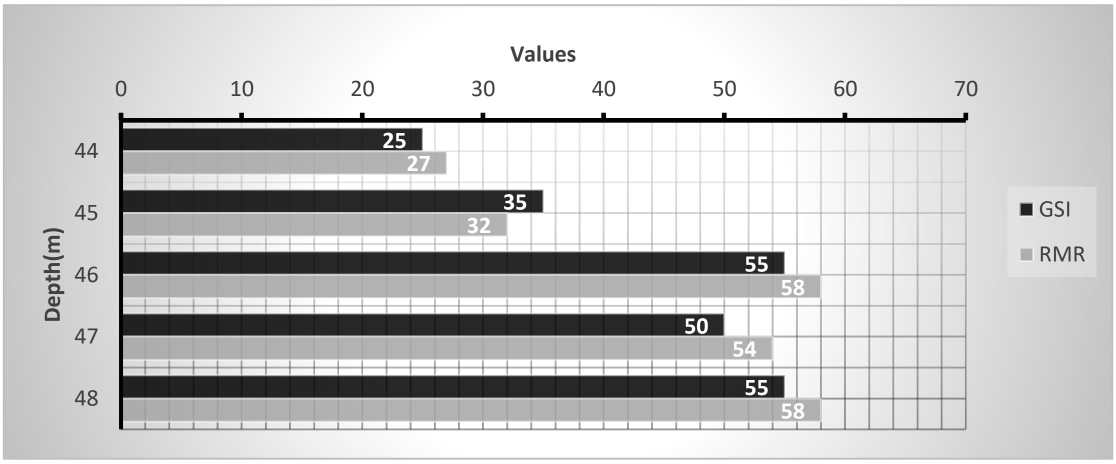

*Figure 55. GSI and RMR indexes versus depth, for Borehole: BDZ_22_08*

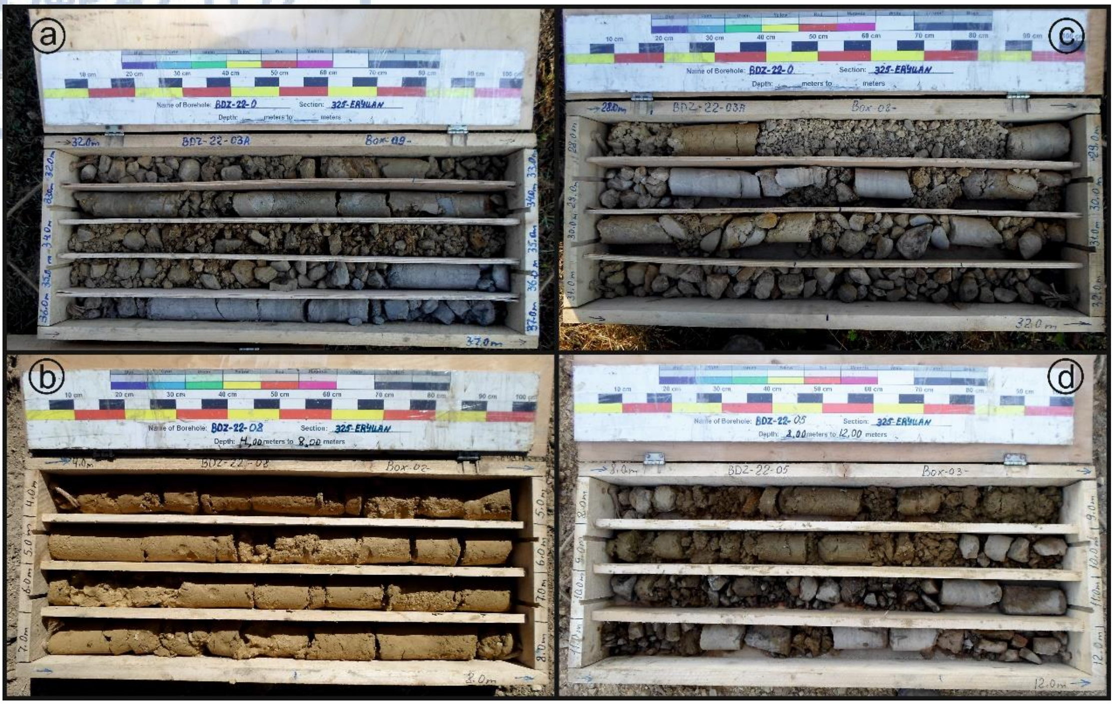

*Figure 56. The product of drilling, characterized as unstable landslide material.*

## 4.5 Conclusions

The result of drilling process, which is described in detail, attribute two major units. The first unit contains the material of active landslide and the second, the stable bedrock. The second case contains the stiff clayey drilled material, the fine grained dark grey sandstone and the dark colored sand.

In order to divide the results of drilling to the underlying categories, major criteria have been posed. So, the unstable material of active landslide, has individual characteristics, different from the characteristics of stable bedrock. Those crucial factors, which indicates if the drilled material is stable or not, are presented below.

The characterization of drilled geomaterial as unstable is based on the factors:

- The color of unstable material is brownish.
- The unstable geomaterial attribute lack of geological structure.
- The gravel and the fragments, which are contained, have angular shape with partially sharp edges.
- The dominance of clay and lack of silt and sand size particles.
- The intensive presence of soil type material, and most precisely of clay.
- The lack of strength, the samples are considered very soft and loose.
- In general, extensive heterogeneity is appeared on the samples of unstable material.

The stable material, based only on information provided by boreholes, is subdivided into four categories:

- Stiff, white to dark grey clay of high plasticity.
- Deep brown to dark colored coarse-grained sands.
- Weak, completely fractured- fissured, moderately weathered, dark grey, fine grained calcareous Sandstone.
- Moderately weak to moderately strong, very fractured, slightly to moderately weathered, dark grey, fine grained calcareous sandstone.

The two last units are considered the bedrock and their differentiation is not crucial for the stability assessment. In general, weak moderately weathered and completely fractured sandstone of third category, which has a structure, appears as a thin layer of 1-2m overburden

*Figure 57. The product of drilling, characterized as stable bedrock, calcareous sandstone. At (c) can be observed the lenses of clay into bedrock.*

to the major bedrock, which structure is clear. The interpretation of the weak rock overburden to the bedrock is not difficult that, considering that appearance of weathered layer, above the bedrock is usual.

Stiff clayey material *(figure 58),* which usually follows the unstable material of active landslide, is considered stable, because:

- The color of material, is different than the color of unstable material and it ranges from white grey to dark grey.
- The strength of the material, considering only the in-situ evaluation, it is noticeable and importantly enhanced than the strength of unstable material.
- Although this material also contains gravel and angular fragments, their quantities are limited, and they are composed by grey, unweathered sandstone.

The interpretation considering this unit, cannot be unique. First of all, from field investigation, layers of clayey material of 1-2m thin are observed. Although the underlying clay is seemed to be located in the contact of the landslide material and the bedrock, it appears also in the bedrock, however the drilling method in the bedrock, is responsible for the out washing of this material. This represents the reason why the presence of stiff clay within the bedrock is not lucid. Secondly, the appearance of this type of material is relatively common on fault zones. Yet, considering that the boreholes are distributed in a wide area, the geometry of a single fault cannot explain the appearance of this material in every borehole. Even if the fault was sub horizontal, which is not because the faults in the study area appear with relatively vertical and different orientations, does not explain properly the appearance of this material in every single borehole. In contrast, this kind of material is commonly observed in location where hydrothermal activity exists. The hydrothermal activity usually forms clay of high plasticity, which are observed in this situation. So, the presence of the clay formation is interpreted as lenses within the bedrock which suffered hydrothermal alteration.

The most questionable geomaterial in this investigation, is the deep brown sands, which were sampled at boreholes BDZ_22_06A and BDZ_22_08 *(figure 60).* The question here, is about its origin, for which there are two major assumptions, and they are based on several facts. According to the first assumption, this material is the result of sedimentation by the river which lies in the toe of the slide, and it was covered by the ancient landslide. The second

*Figure 58. The product of drilling, characterized as stable stiff clayey geomaterial.*

assumption claims that this material, is bedrock origin, and appears as a different layer in the bedrock. Below, the facts which support both assumptions will be presented:

The first assumption is supported by the facts:

- The geomaterial appears only in two boreholes, which are located near to the riverbed.
- The geomaterial is composed by sands.
- Right after the process of sampling on this geomaterial, intensive smell by organic matter occurred.
- At the borehole BDZ_22_06A the formation faced at absolute elevation of 593,39m to 584,46m, and in borehole BDZ_22_08 the formation faced at 597,3m to 592,4m. The underlying difference in elevation is considered too small, and it can be assumed that in both borehole the geomaterial is faced on the same level.
- The lack of cohesion, which is indicated by the sampling.

| Borehole | Sliding Depth (m) |
|---|---|
| BDZ_22_01A | 38,00 |
| BDZ_22_02 | 32,80 |
| BDZ_22_03A | 35,70 |
| BDZ_22_05 | 30,40 |
| BDZ_22_06A | 16,60 |
| BDZ_22_07 | 33,50 |
| BDZ_22_08 | 29,50 |

*Table 3. The depth of the sliding zone in each borehole.*

The second assumption is supported by the facts:

- The shape of grains is not typical type of riverbed sedimentation, considered that those are not rounded yet flattened.
- During drilling losses on drilling fluids did not occur.
- Although, the drilling conducted with wireline system, which generally does not allow great quantities of caving to fall into borehole, the amount of caving was unimportant.

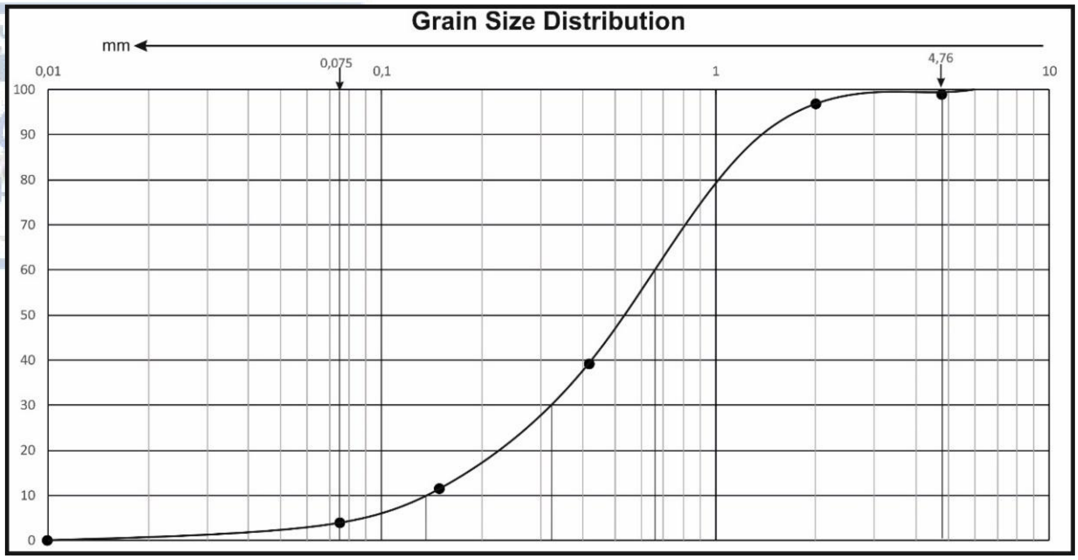

*Figure 59. Size distribution curve, for the questionable origin, sands.*

- Composition of organic decomposed organic matter is also observed through the bedrock.
- The grain size distribution curve *(figure 59),* is not characterizes typical riverbed sediments, considering restricted quantities of clay. So, by the underlying curve the material is characterizes as poorly grade sand (SP) according to the Unified Soil Classification System.

The distinction between the underlying assumptions is important because, if the sandy material is riverbed origin, then the old surface of rupture is known, and it is deeper than the surface, concluded by the assumption that the sandy material contains to the bedrock. In both cases the material is stable, but the question for the stability of overburden to the sandy material units occur.

Of course, information derived from the geotechnical monitoring would clarify, which material is stable and which is not, regarding the active surface of sliding, yet it seems that the second assumption is to be considered as the more reliable.

*Figure 60. The product of drilling, characterized as stable sandy geomaterial.*

# Chapter 5 Geotechnical Monitoring

## 5.1 General

The geotechnical monitoring is considered essential for stability analysis, by providing crucial factors regarding the analysis, and in general for engineering geological and geotechnical behavior of the slope. More precisely, the instrumentation is responsible for the detection of vital, for the analysis factors, factors such as the depth of the shearing, the piezometrical head and more.

For the estimation of the depth of the rupture, even though it is possible to be detected by geological evaluation of drilled cores, by installation of inclinometers not only the uncertainties, regarding which geological feature indicates shearing, are reduced, but also the surface of shearing, is acquired with great accuracy. Furthermore, inclinometers allow calculation of the total magnitude of displacement, the velocity of movement, and even the direction of movement. In addition, it is possible to correlate the rate of movement with other parameters such the rate of the excavation, precipitation and variation of water level.

The estimation of the piezometrical head, by piezometers is crucial for the stability analysis, mostly because of the massif impact of the total level of water table on the stability. The accuracy in the piezometrical data is required because of the underlying impact. That is why the water table cannot be acquired during drilling process.

In addition, the continuous surface monitoring could provide information regarding the magnitude and the direction of surface movements, which are valuable in order to determine how the landslide is behave. The measured direction provides the detection of hazardous zones downslope. Furthermore, the process allows to categorize the landslide into separate units with unique characteristics. The separation of the landslide into units, makes easier the study of the behavior of every part of the landslide. The better knowledge of the behavior is required in order to provide the better solution regarding the geotechnical problem.

## 5.2 Inclinometers

### 5.2.1 General

Slope inclinometers are commonly used in slope stability assessment since 1950s, by detecting movements vertically to the casing of the borehole in which they are installed, by passing probe alongside to the casing and measure the inclination of the casing with respect to the vertical (*Stark D.T., Choi H., 2008*). The underlying movements indicate surfaces of failure on the slopes. Usually, areas below and under the sheared surfaces does not suffer any deformation. At those slopes inclinometers does not indicate any movement, on the contrary to the sheared zones. Generally, the procedure of determining the depth of shear zones, only by observing the core sample, the result of drilling, is difficult and false conclusions can be drawn. So, the instrumentation by inclinometers could help in evaluating more accurately the stability in any cutting, slope, or excavation, by indicating zone of shear deformation, with great precision. The monitoring by the underlying instruments provide not only the depth of shear zones, but also the rate and the direction of movements which are also vital in stability assessments. Furthermore, there is no other way to observe if the movement in the depth of shear zone and is constant or accelerates (*Cala M., et al.,2016*).

Although, in most of the cases, inclinometers are installed vertically to detect shear zones in stability assessment projects, there are few cases in which inclinometers are installed horizontally in order to calculate settlements, and their spatial distribution. It is also possible to install inclinometers inclined, under special circumstances in which the access is limited or the formation which needs monitoring is also inclined. However, most commonly inclinometers are installed vertically, rarely they are installed horizontally, and there are limited cases in which those instruments are installed inclined. Of course, in horizontal and inclined installations the system of probe and in general, of monitoring is more complicated than in vertical installations *(Machan, G., and Bennett, V. G. 2008).*

A typical probe of inclinometer, contains various types of sensors. For example, strain-gauged cantilevers, pendulums attached to rotary, electrical potentiometers, vibrating wire apparatus, force-balance accelerometers and electrolevels are used. Most common are the sensors of accelerometers *(Clayton C.R.I., et al.1995)*. The underlying sensors calculate the tilt of casing in four, perpendicular to one another, directions. There are uniaxial and biaxial probes. Uniaxial probes contain one sensor and four passes of the probe through the casing are needed. On the contrary, biaxial probes contain two sensors, and only two passes into the casing are required. Most commonly, biaxial probes are used, such as in the present study. The casing of inclinometers contains four grooves, in perpendicular to one another, directions in which the probe is guided by guided wheels, which are fixed on it. In biaxial probes, usually the main axis, axis A, is parallel to the expected movement and the wheels of the probe. That means that the minor axis, axis B, is transverse to the expected movement. So, the first sensor is oriented to the axis A and the second to the axis B, in which the first measurement is taking place. The second measurement is oriented 180 degrees from the first. The measurements are taken place from the bottom to the top, and it is important to ensure that the bottom of the installations is embedder beyond the sliding area. In *figure 61,* the system of inclinometer is demonstrated.

During the installation, it is very important to ensure:

- As it is referenced before, that the depth of the installation must be deeper that the depth of the sliding, because if it is not, the installation will move with the landslide and there would not be any signs of shear deformation, from the present instrumentation.
- The density of grouting to be approximately the same with the surrounding geomaterial. If the grouting is too dense, then the geomaterial will move around it. However, if the density of the grouting is limited, then failure could occur after

the installation and false conclusions about the depth of the failure surface could be extracted.

- The strength of tube material should be match with the density of surrounding geomaterial, for the same reason as the grouting.
- The bottom of the first tube of inclinometer should be sealed as the connections between tubes and any other type of space in tubes, in order for grouting not to penetrate within the tube.

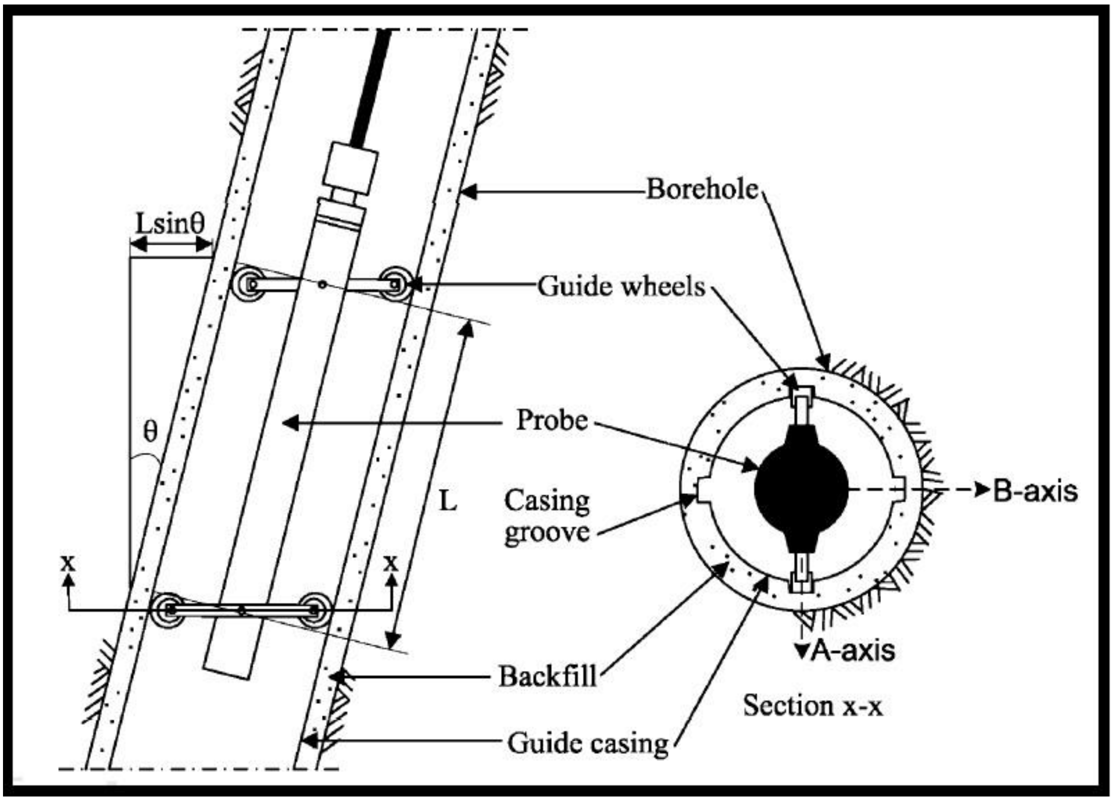

*Figure 61. Principles of inclinometer configuration of inclinometer equipments (Stark D.T., & Choi H., 2008).*

It is also desirable the measurements would be completed with the same probe by the same person. However, sometimes it is difficult to maintain the same probe, because probes are very sensitive instruments and they are damaged frequently. So, in this case the results, are no as accurate as would have been if the probe was the same.

The precision of the measurements by the underlying instruments is depended not only on the precision of the probe, but also on the procedure. That means that even if the measurements and the installation were carried out very accurately, the precision would be lesser than the accuracy of the probe. So, it is crucial, in order for the measurements to be relatively close to the real data, the procedure of installation and data collecting, be very accurate.

It is convenient to point out that the probe does not obtain directly the deviation from vertical, but it measures the angle of the deviation. So, considering that the distance of measurement interval is known, it is easy to calculate the deviation from the equation below:

$$a=L*sin\vartheta$$

Where:
$a$: Deviation from vertical,
$L$: Measurement interval,
$\vartheta$: Deviation (acute) angle from vertical.

The measurement interval, usually coincides with the distance between guided wheels, in which measurements are taken from the probes (*Stark D.T., & Choi H., 2008*).

There are plenty of ways with which the collected data could be plotted. The most common are:

- Incremental Displacement: Which is the best plot in order to observe and point out the zone of shear deformation or the vertical deformation. In this type of plot, the collected data is corrected by the deduction of zero readings, and then data for individual measurement is plotted versus depth.
- Cumulative Displacement: In this case the plot is achieved by adding the deviation from the bottom to the top, and plot for every measurement the value which is derived from the summing of deviations up to that depth from the bottom. Of course, the deviations in this case are also corrected by zero reading. The pattern of a landslide (e.g. rotational, translational, toppling etc.), can be derived by the information of this plot. If the displacement on the depth of shear zone is greater than the surface, then the landslide is rotational, if the displacements are the same then the landslide is translational and finally, if the displacement is greater at the surface, then the landslide type is toppling.
- Vector Displacement: Which shows on map view the total displacement versus the direction of movement. In this plot type the main axes A&B are plotted and the total displacement is the result of combination of total displacement on axis A and the total displacement on axis B. Usually, in this plot type, the last value of cumulative displacement is plotted, which indicates the total displacement on the surface or the value at the depth of shear deformation of the cumulative displacement.
- Total Displacement per Time: In this plot type the magnitude of displacement from the previous, vector displacement plot type, is plotted versus time. In this plot type, it is possible to observe the velocity or the rate of movement. The underlying plot is considered important because it shows whether the slide accelerates, maintains the same speed or reduces speed. This factor is mostly important not only for the stability assessment but also for the safety downslope.

| Characteristics | Values |
|---|---|
| Wheelbase | 0,5 m |
| Probe Diameter | 25,4 mm |
| Probe Length (Including Connector) | 719 mm |
| Probe Weight | 1,06 kg |
| Probe Material | Stainless Steel |
| Full-scale range | ±30 degrees |
| Data resolution | 0.005 mm per 500 mm |
| Repeatability | ±0,002° |
| Accuracy | ±2 mm per 25 m |
| Axis Alignment | Digitally nulled |
| Temperature Rating | -40° to +70 C° |
| Sensor Type | Biaxial, Accelerometer |

*Table 4. The Structural Characteristics of used Inclinometer (rst.com)*

### 5.2.2 Boreholes

At the site of the landslide, which is studied in the present dissertation five, inclinometer systems, which are composed by plastic tubes, were installed. The diameter of each tube is 70mm and every tube has a length of 3m. Every tube contains special spaces in the top and in the bottom of it, which allows the tubes to be locked to adjacent tubes. The area between the tube and the empty space in the borehole (borehole diameter = 96mm), is covered with a mixture of cement and bentonite, which is injected from the bottom to the top with plastic tube of small diameter which is placed externally to the tubes, installed at the bottom of borehole. Before grouting, it is important to unsure, as it is referenced before, that the bottom of the deeper tube is sealed as the connections among the tubes.

All inclinometers were installed with direction of axis A towards 50° northeast, which is mainly parallel to the movement, considering that the major movement have direction of 230° to southwest. For every borehole, data was collected with probe which characteristics are given in *table 4.* Based on collected measurements, and more precisely the deviations from vertical, the following graphs were implemented for every borehole in which inclinometers were installed:

- Graphs of Incremental Displacement.
- Graphs of Cumulative Displacement
- Graphs of Vector Displacement
- Graphs of Rate of Movement.

It is worth of mention that mainly at the first and the second plot type, the zero readings are not plotted.

In order to plot the Incremental Displacement, the readings were corrected with the values of zero readings and the plot of deviation from vertical versus depth, followed.

To plot the Cumulative Displacement, the values of deviation derived from the previous zero-reading correction, are summed from the bottom to the top and plotted for every depth, the corresponding summary.

To plot the Vector Displacement on the surface the final value of cumulative displacement at the top from both A and B axis, was taken into consideration and plotted for every measurement individually. This creates a vector on the surface in which the direction of movement is shown. Plotted the underlying values for every measurement exports not only the magnitude of total displacement, but also its direction, considering that the orientation of guides within the tubes are maintained.

Furthermore, taking into consideration the total movements for every reading, it is possible to show the displacement value per day or hour. Also, having the magnitude of movement and the time of the movement, it is easy to export the velocity of movement per time unit, and plot it as well.

In addition, the calculation of mean magnitude, rate of movement as the direction is crucial in every evaluation. That is why their calculation took place and the outcome values as the plots are presented below for every borehole individually.

It is extremely important to point out the difference between the total vector movement and individual movement per day. The total vector movements include as start point the zero reading, and consequently the vector starts from the point without any movement, and the end of the vector is the point which is indicated by the cumulative displacement which came from the last conducted readings. The movement per day, is based only on readings which are conducted that day and the day before that. The result between the underlying values is different because the direction of movement is not the same and although it changes little, has crucial effects on the total vector displacement and the total displacement which came out from the summing of individual displacements per day.

The graphs and the calculations took place in matlab, mathworks environment.

#### 5.2.2.1 Borehole: BDZ_22_01A

The installation of inclinometer in borehole BDZ_22_01A took place at 28/08/2017 after the end of drilling processes. The inclinometer is embedded at depth of ~46,70m below ground level and the top of it is on ~0,80m above ground level. The first readings took place on 01/09/2017 and those ones are considered as zero reading measurement. Including the zero-reading measurement, six (6) measurements have collected in total, with time interval of one (1) day. So, the last measurement took place at 06/09/2017. At 09/09/2017 the probe could

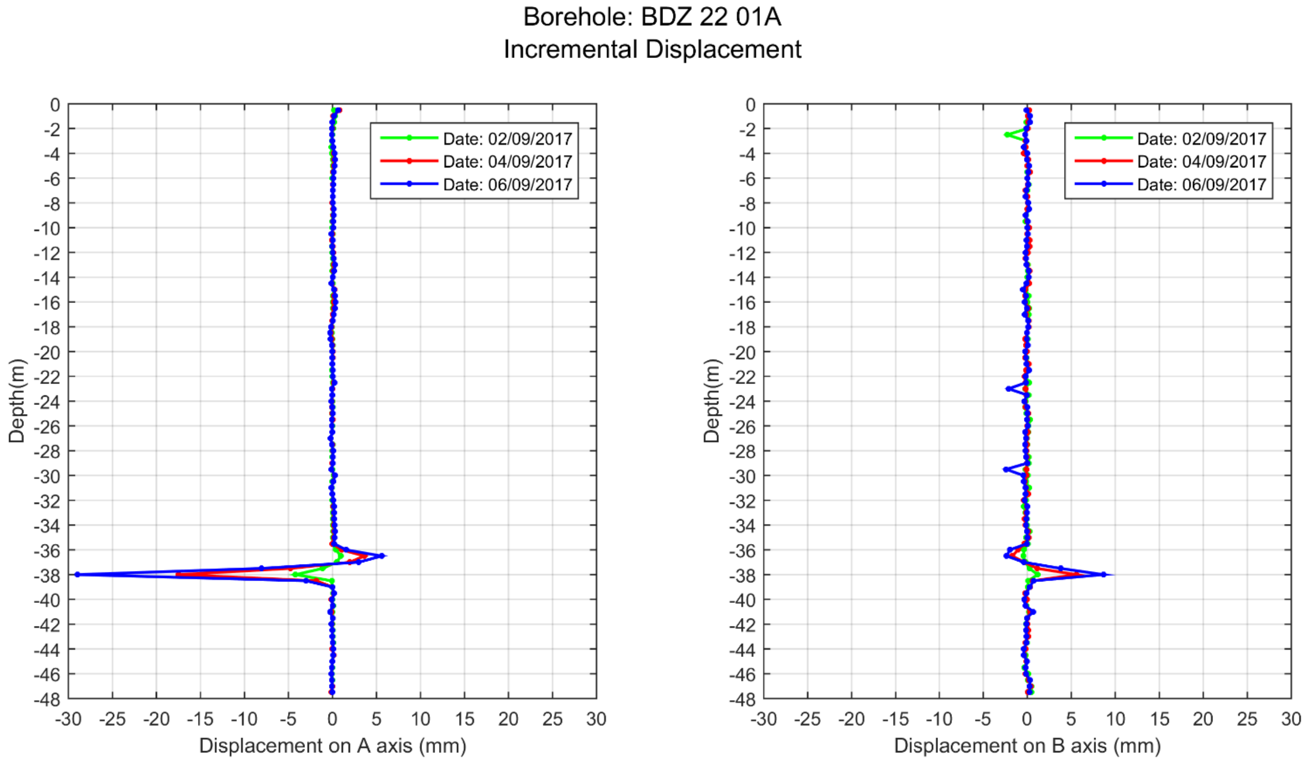

*Figure 62. Incremental Displacement for Borehole: BDZ_22_01A*

not pass from the depth of ~37m from G.L., which indicates damage on the casing from shear deformation at that depth. It is important to point out that intensive rainfall took place on 08/09/2017. It is important to emphasize that in all plot types, which follow, depth equal to zero (0) is considered as ~0,80 m above ground level.

Although the shear zone is obvious after the previous observation of not passing probe in certain depth, this area appears clearly at the incremental displacement plot in depth of

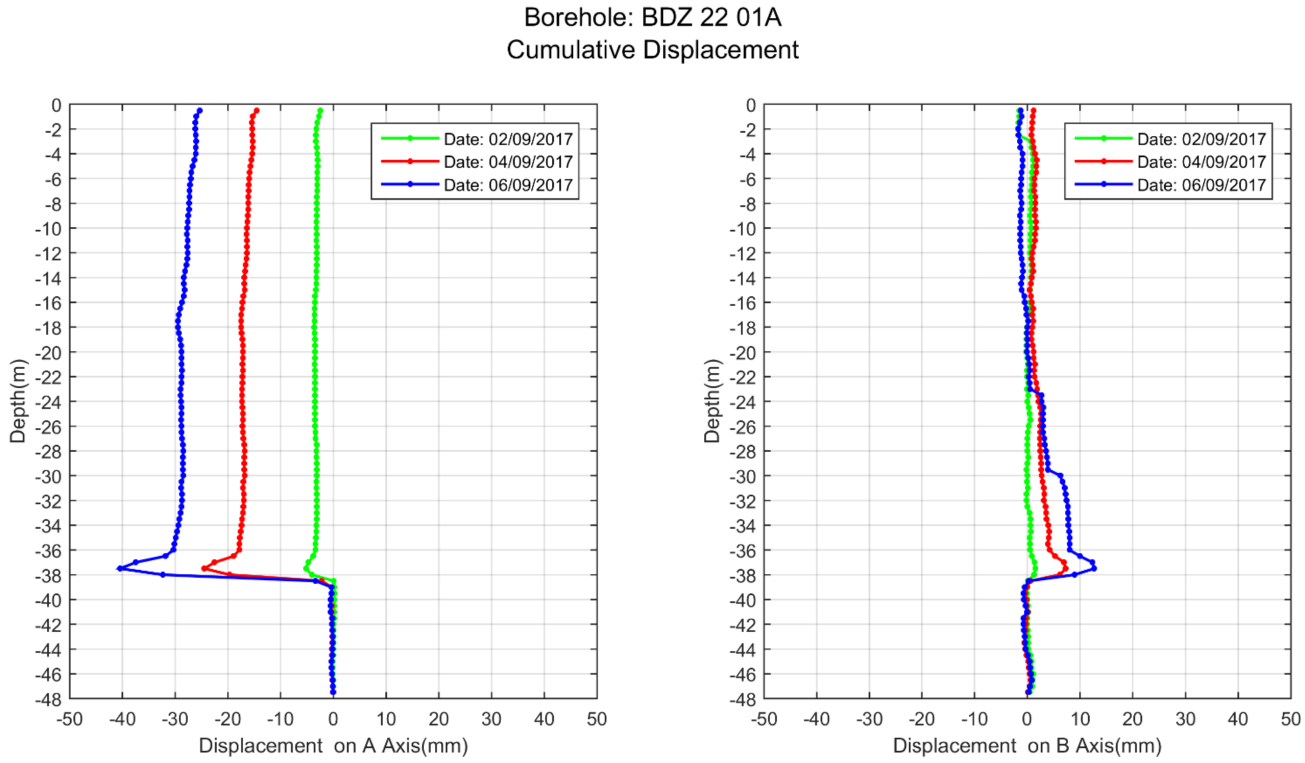

*Figure 63. Cumulative Displacement for Borehole: BDZ_22_01A*

38m *(figure 62)*. In the specific figure data are plotted with time interval of two days, in order to avoid confusions.

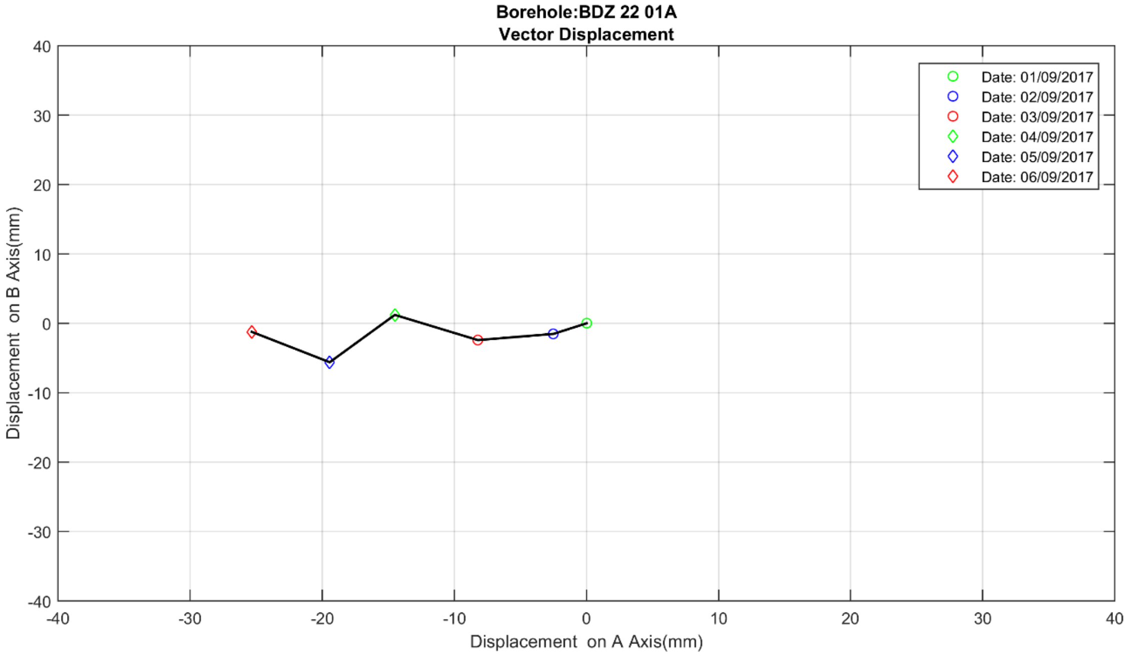

*Figure 64. Vector Displacement for Borehole: BDZ_22_01A*

Furthermore, the total horizontal movement per depth is shown in the Cumulative displacement figure. This plot type is important in order to understand the continuation of total movement in every particular depth and to compare the movement in shear zone with the movement in surface. From *figure 63* it is easy to realize that the displacement at the depth of shear zone is importantly bigger than the displacement at the surface. That means that the landslide moves faster in the depth of shear deformation than the surface. This is a factor which indicates the pattern of landslide, which in this case, from this observation and

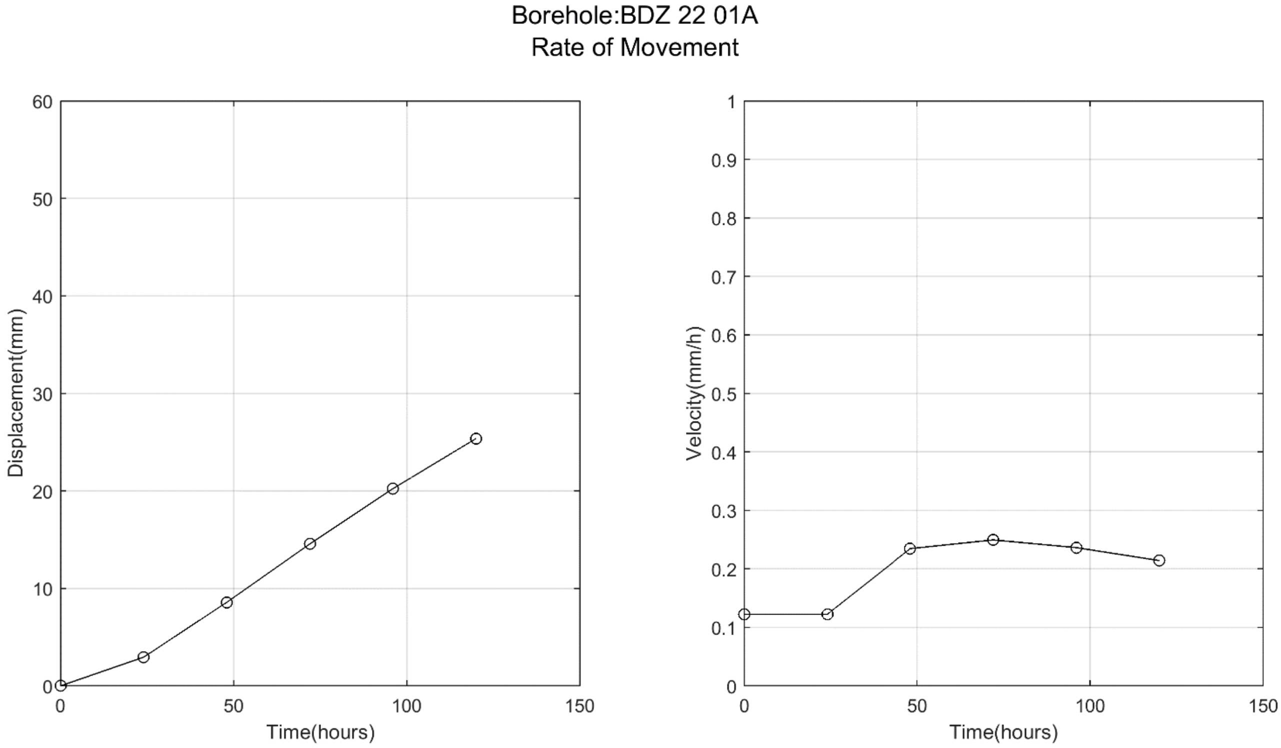

*Figure 65. Rate of Movement for Borehole: BDZ_22_01A*

considering the position of the slide, is concluded as a rotational landslide. In the specific figure data are plotted with time interval of two days, in order to avoid confusions.

The total movement at the surface is shown in vector displacement plot, at figure 4. The direction of movement is calculated, as the vector of total displacement indicates, 227° to southeast. The total vector magnitude of movement is 25,3714 mm and the total vector velocity is 0,2114mm/hour or 4,2288mm/day.

At *figure 65* is shown the evolution of magnitude of displacement and the velocity respectively versus time.

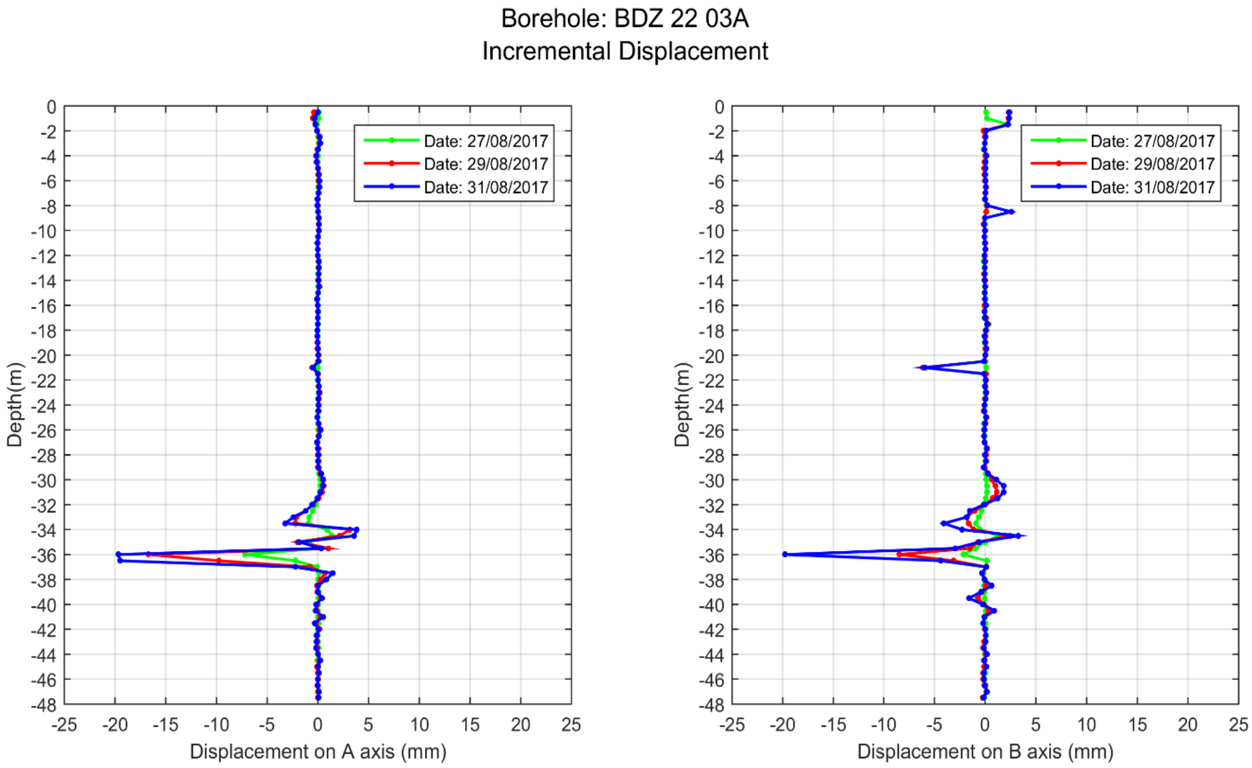

*Figure 66. Incremental Displacement for Borehole: BDZ_22_03A*

### 5.2.2.2 Borehole: BDZ_22_03A

The installation of inclinometer in borehole BDZ_22_3A took place at 23/08/2017 after the end of drilling processes. The inclinometer is embedded at depth of ~46,70m below ground level and the top of it is at ~0,80m above ground level. The first readings took place on 26/08/2017 and those ones are considered as zero readings measurement. Including the zero-reading measurement, in total six (6) measurements have conducted, with time interval of one (1) day. So, the last measurement took place at 31/08/2017. At 01/09/2017 the probe could not pass from the depth of ~35,70m from G.L., which indicates damage at the casing from shear deformation at that depth. It is important to point out that intensive rainfall did not occur on that period of time. It is important also, to emphasize that in all plot types, which follow, depth equal to zero (0) is considered as ~0,80 m above ground level.

Although the shear zone is obvious after the previous observation of not passing probe in certain depth, this area appears clearly at the incremental displacement plot in depth of 36,50m *(figure 66).* In the specific figure data are plotted with time interval of two days, in order to avoid confusions.

Furthermore, the total horizontal movement per depth is shown in the cumulative displacement figure. This plot is important in order to understand the continuation of total movement in every particular depth and to compare the movement in shear zone with the movement in surface. From *figure 67* it is easy to realize that the displacement at the depth

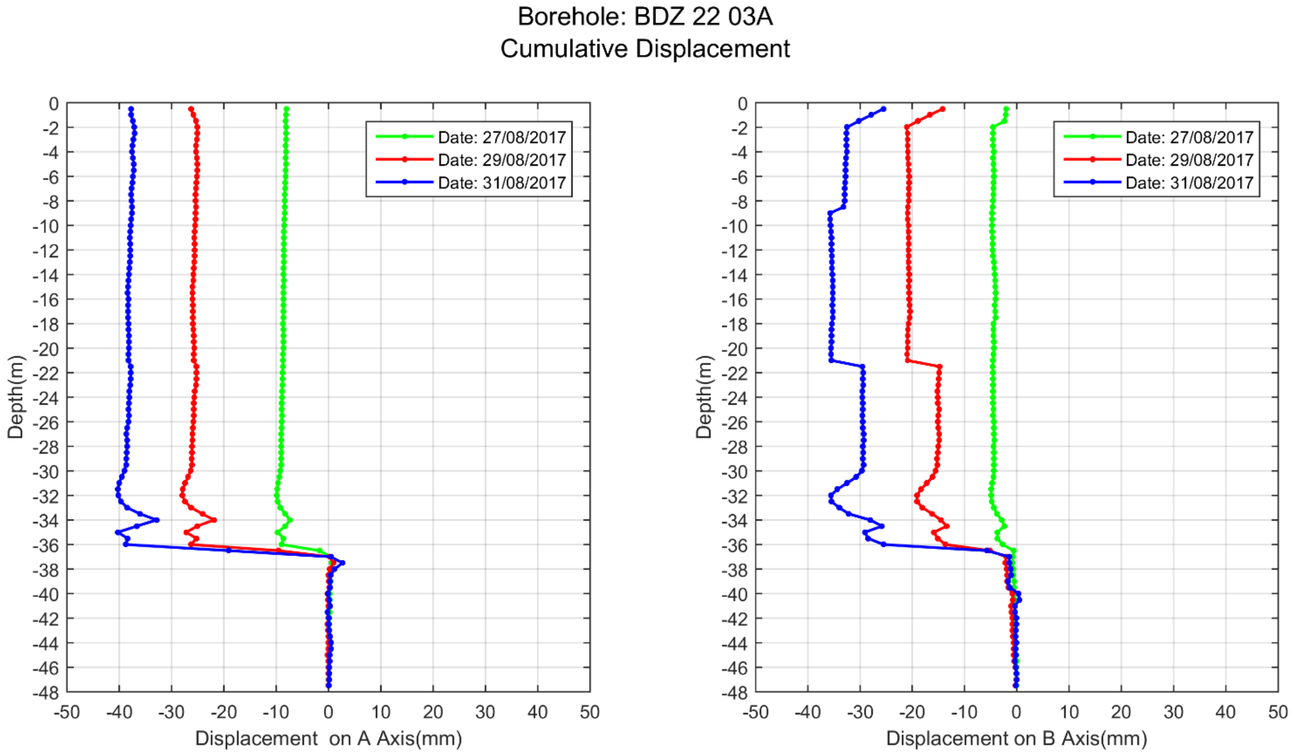

*Figure 67. Cumulative Displacement for Borehole: BDZ_22_03A*

of shear zone is approximately the same with the displacement at the surface. That means that the landslide moves with the same speed in the depth of shear deformation and the surface. From this observation is concluded as a translational landslide, but considering the position of the borehole, for configuration, data from other observations should be considered as well. In the specific figure data are plotted with time interval of two days, in order to avoid confusions.

The total movement at the surface is shown in vector displacement plot, at *figure 68*. The direction of movement is calculated, as the vector of total displacements indicates, 196° to

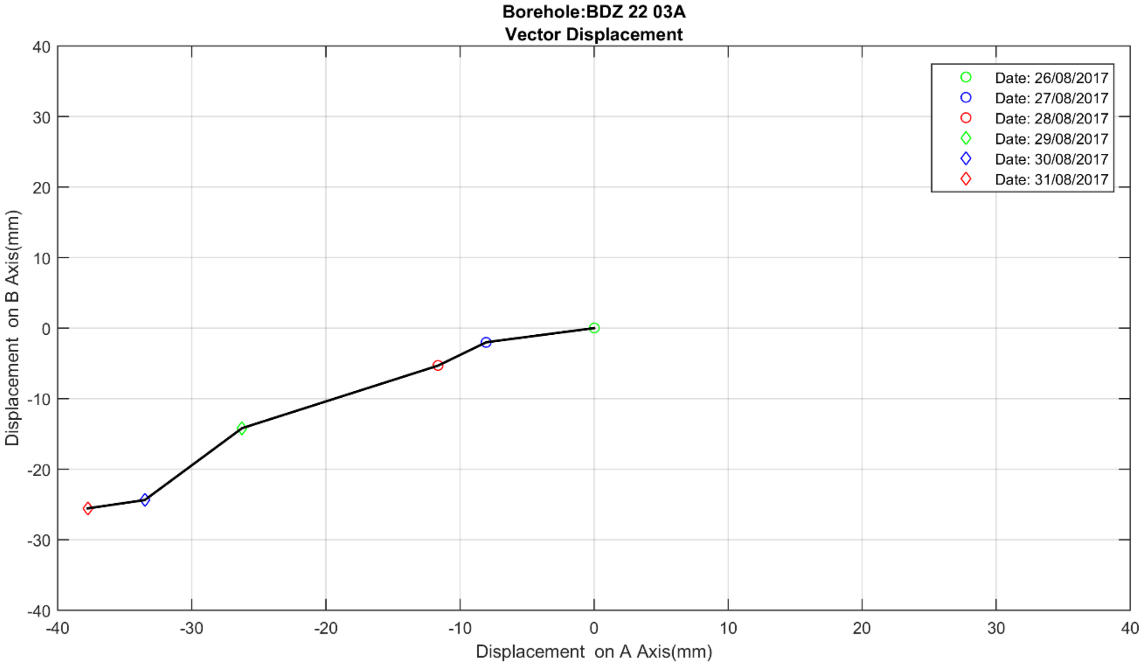

*Figure 68. Vector Displacement for Borehole: BDZ_22_03A*

south-southeast. The total vector magnitude of movement is 45,5879 mm and the total vector velocity is 0,3799mm/hour or 9,1176mm/day.

At *figure 69* is shown the evolution of magnitude of displacement and the velocity respectively versus time.

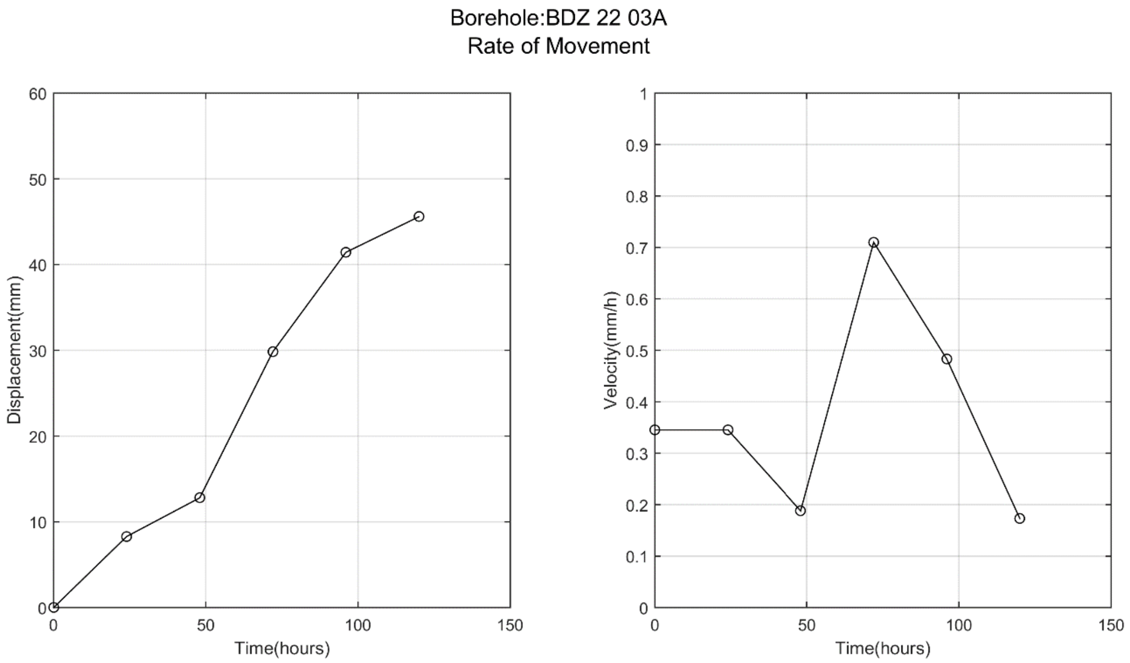

*Figure 69. Rate of Movement for Borehole: BDZ_22_03A*

### 5.2.2.3 Borehole: BDZ_22_05

The installation of inclinometer in borehole BDZ_22_05 took place at 09/09/2017 after the end of drilling processes. The inclinometer is embedded at depth of ~44,70m below ground

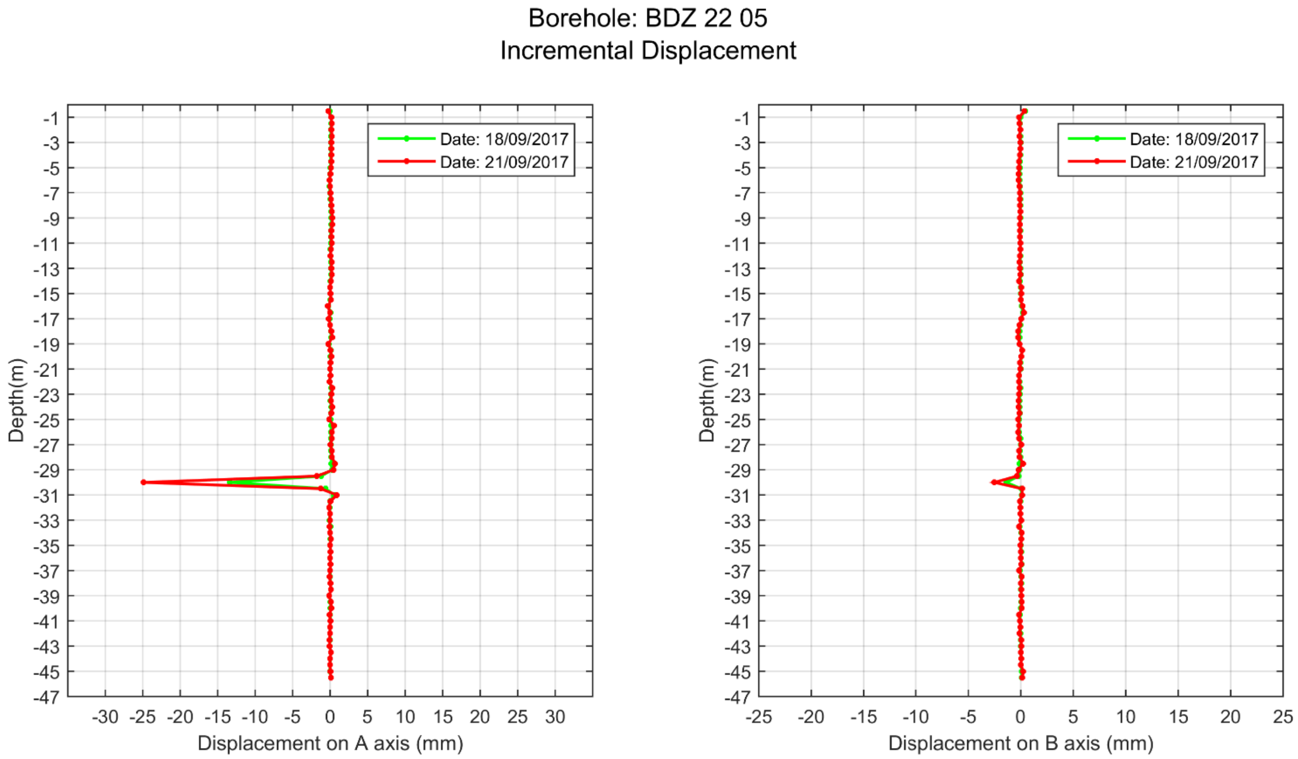

*Figure 70. Incremental Displacement for Borehole: BDZ_22_05*

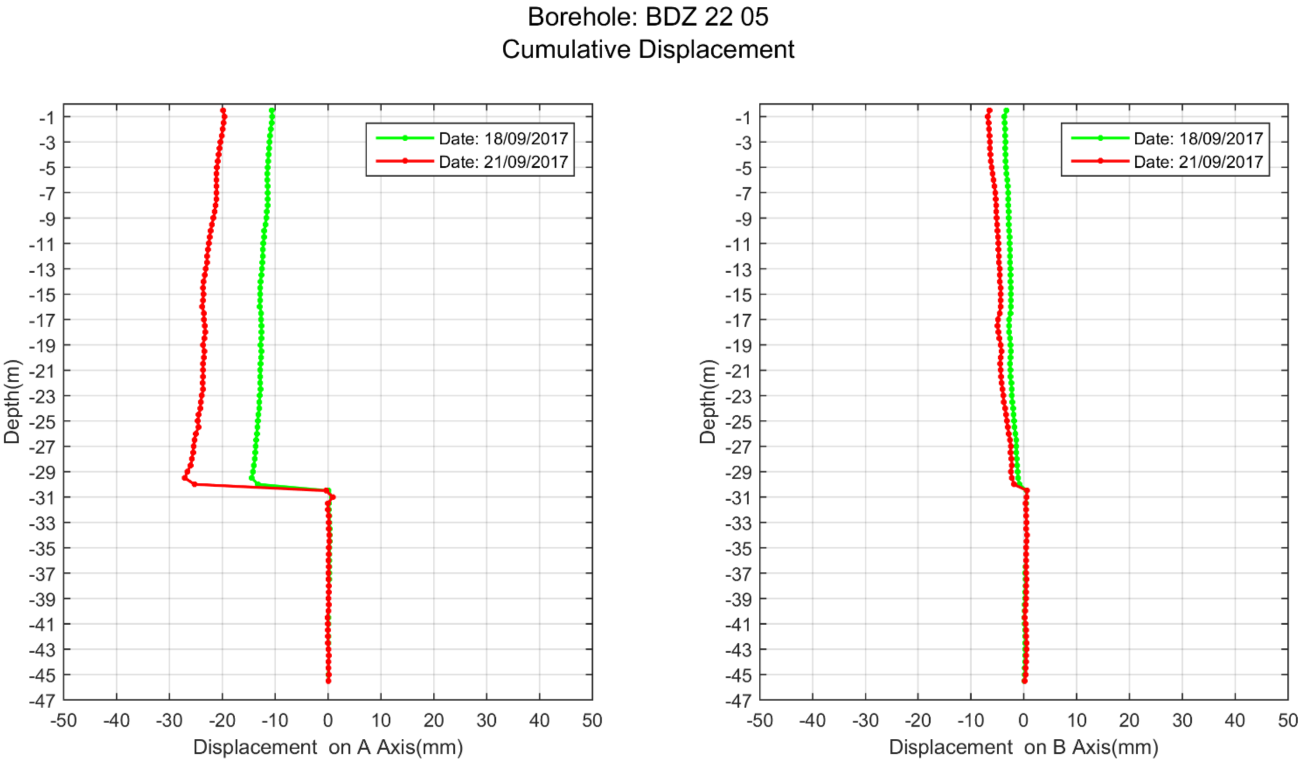

*Figure 71. Cumulative Displacement for Borehole: BDZ_22_05*

level and the top of it is on ~0,80m above ground level. The first measurement took place at 15/09/2017 and those ones are considered as zero reading measurement. The second and the third measurements took place at 18/09/2017 and 21/09/2017 respectively. Including the zero-reading measurement, in total, three (3) measurements were carried out. So, the last measurement took place at 21/09/2017.

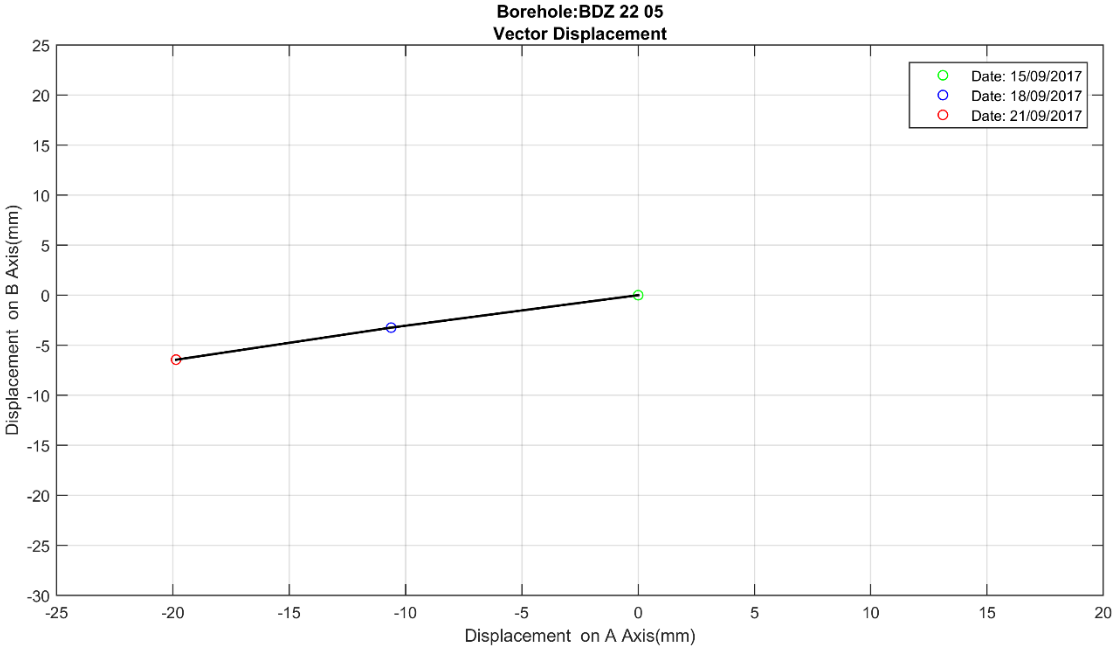

*Figure 72. Vector Displacement for Borehole: BDZ_22_05*

It is important to emphasize that in all plot types, which follow, depth equal to zero (0) is considered as ~0,80 m above ground level.

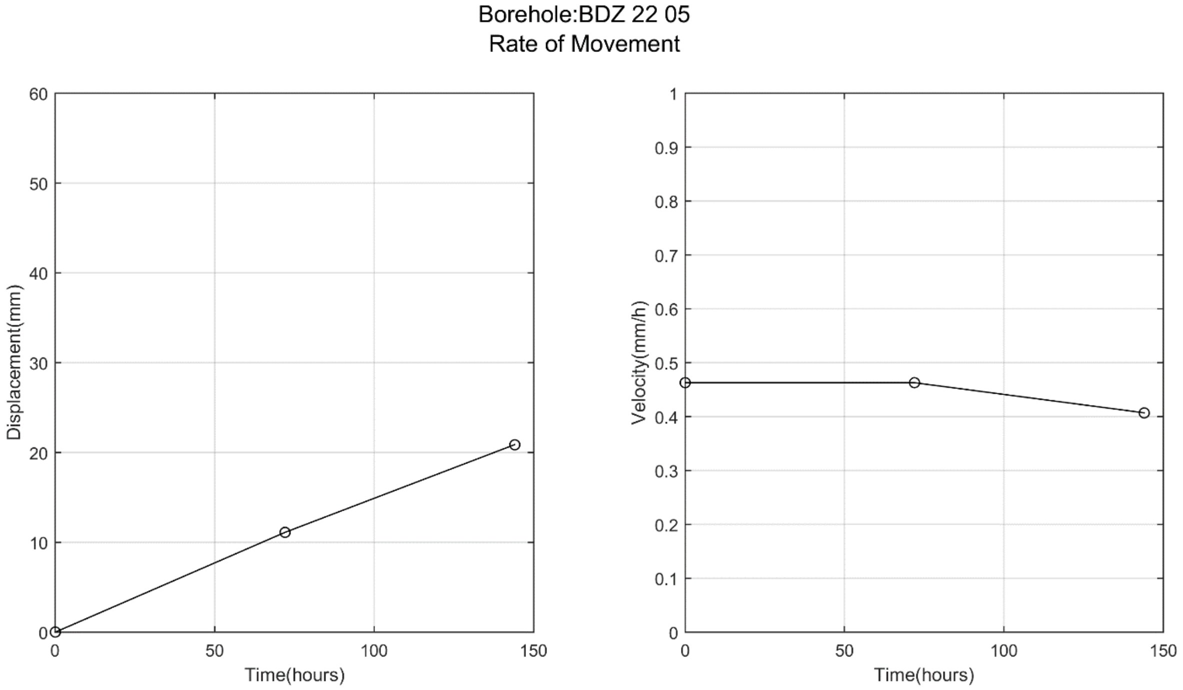

*Figure 73. Rate of Movement for Borehole: BDZ_22_05*

In order to detect the shear zone, incremental displacement plot have been created *(figure 70).* The underlying figure indicates the appearance of shear zone at depth of 30,00m.

Furthermore, the total horizontal movement per depth is shown in the cumulative displacement figure. This plot is important in order to understand the continuation of total movement in every particular depth and to compare the movement in shear zone with the movement in surface. In *figure 71* though, it is difficult to understand the relation between displacement at the depth of shear zone and the displacement at the surface. The reason for the limited evaluation of the *figure 71* is the restricted number of measurements and the way they were carried out.

The total movement at the surface is shown in vector displacement plot, at *figure 72*. The direction of movement is calculated, as the vector of total displacements indicates, 212° to southeast. The total vector magnitude of movement is 20,8782mm and the and the total vector velocity is 0,1450mm/hour or 3,4797mm/day.

At *figure 73* is shown the evolution of magnitude of displacement and the velocity respectively versus time.

### 5.2.2.4 Borehole: BDZ_22_06A

The installation of inclinometer in borehole BDZ_22_06A took place at 19/08/2017 after the end of drilling processes. The inclinometer is embedded at depth of ~40,30m below ground level and the top of it is on ~0,75m above ground level. The first measurement took place at 24/08/2017 and those ones are considered as zero reading measurement. The second measurement took place two (2) days after the first and after that time interval was one (1) day. Including the zero-reading measurement, six (6) measurements have collected in total. So, the last measurement took place at 30/08/2017. At 15/09/2017 the probe could not pass from the depth of ~16.30m from G.L., which indicates damage at the casing from shear deformation at that depth. It is important to emphasize that in all plot types, which follow, depth equal to zero (0) is considered as ~0,80 m above ground level.

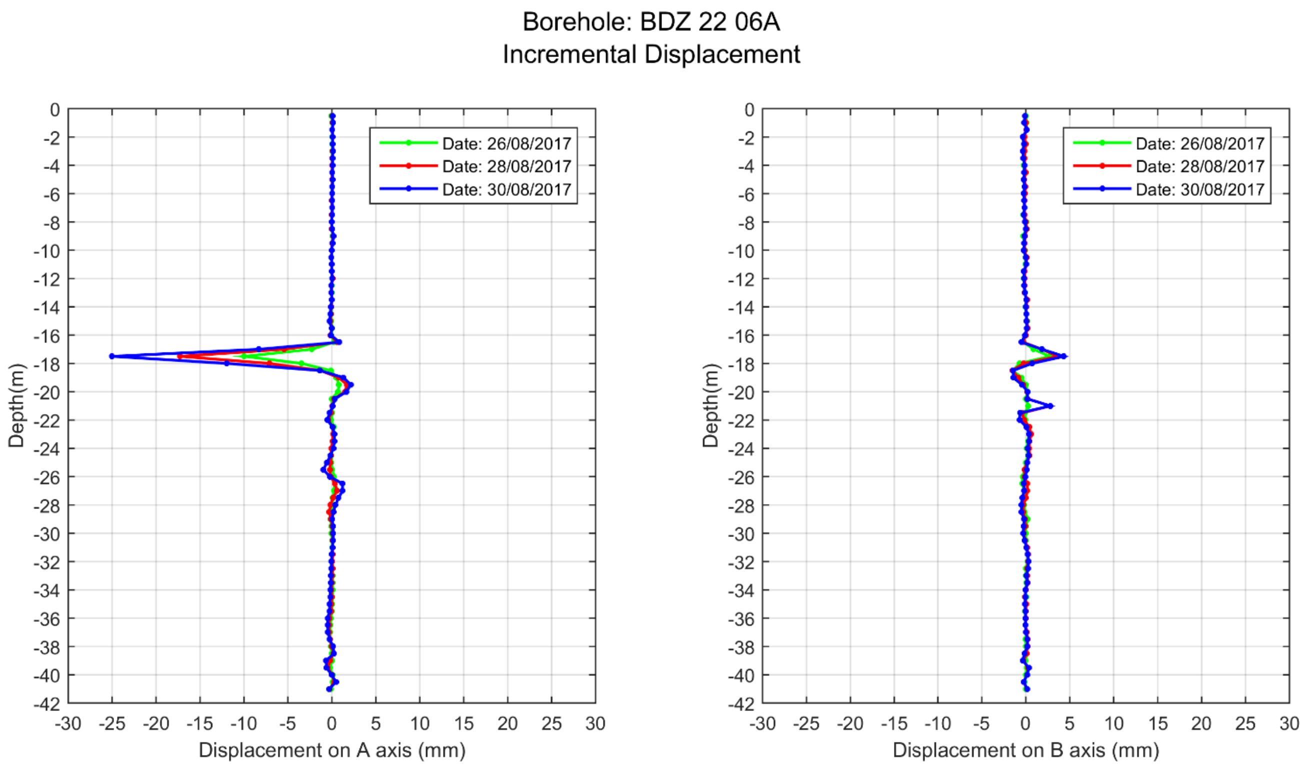

*Figure 74. Incremental Displacement for Borehole: BDZ_22_06A*

Although the shear zone is obvious after the previous observation of not passing probe in certain depth, this area appears clearly on the incremental displacement plot in depth of 17m *(figure 74).* In the specific figure data are plotted with time interval of two days, in order to avoid confusions.

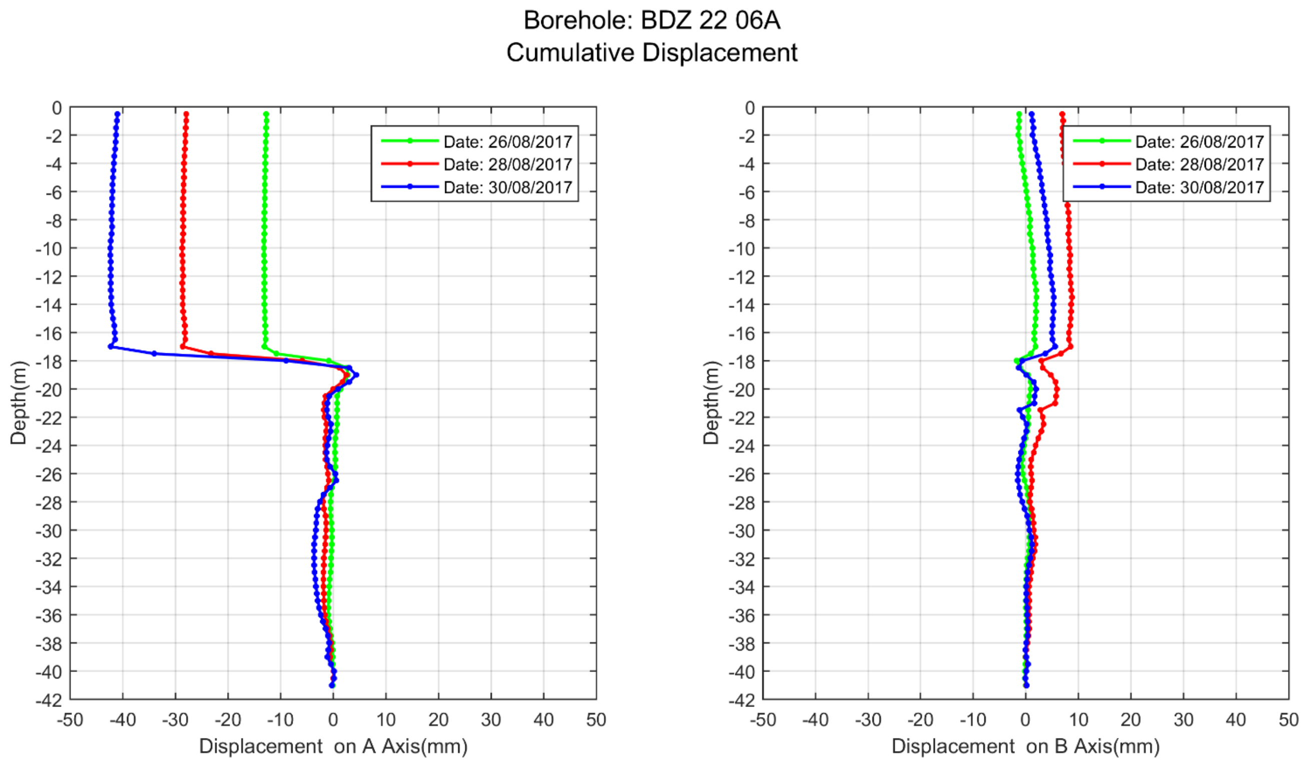

*Figure 75. Cumulative Displacement for Borehole: BDZ_22_06A*

Furthermore, the total horizontal movement per depth is shown in the Cumulative displacement figure. This plot is important in order to understand the continuation of total

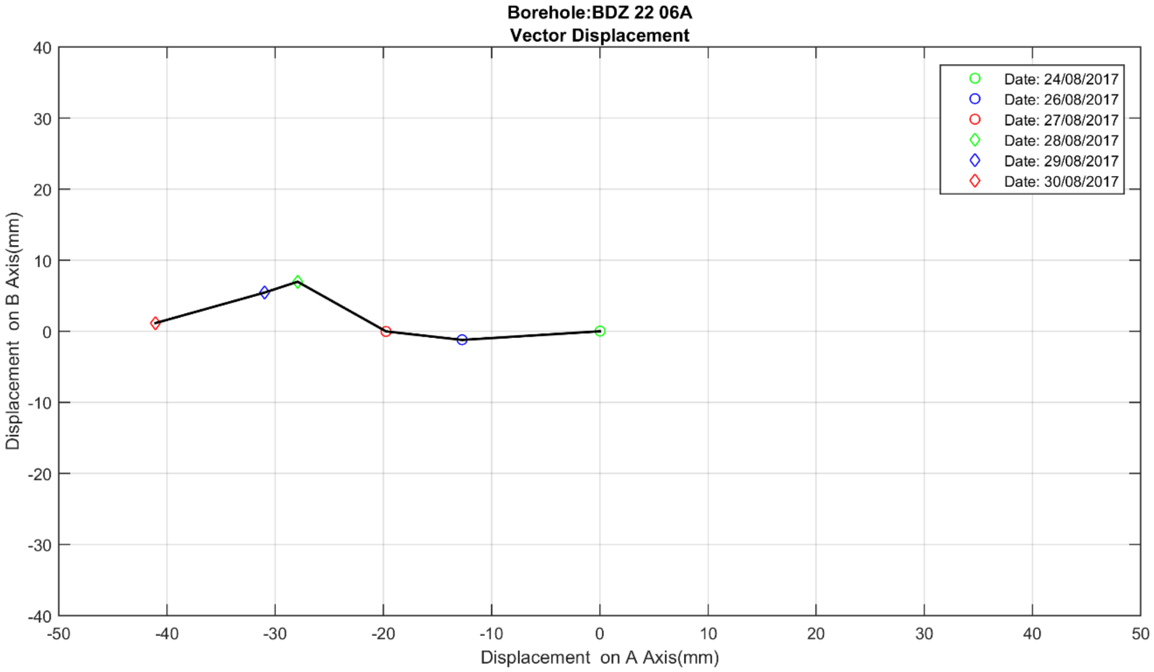

*Figure 76. Vector Displacement for Borehole: BDZ_22_06A*

movement in every particular depth and to compare the movement in shear zone with the movement in surface. From *figure 75* it is easy to realize that the displacement at the depth of shear zone is approximately the same with the displacement at the surface. That means that the landslide moves with the same speed in the depth of shear deformation and the surface. This is a factor which indicates the pattern of landslide in that area, which in this case, from this observation is concluded as a translational landslide. In the specific figure data are plotted with time interval of two days, in order to avoid confusions.

The total movement at the surface is shown in vector displacement plot, at *figure 76*. The direction of movement is calculated, as the vector of total displacements indicates, 231° to southeast. The total vector magnitude of movement is 41,0659 mm and the and the total vector velocity is 0,1515mm/hour or 3,7333mm/day.

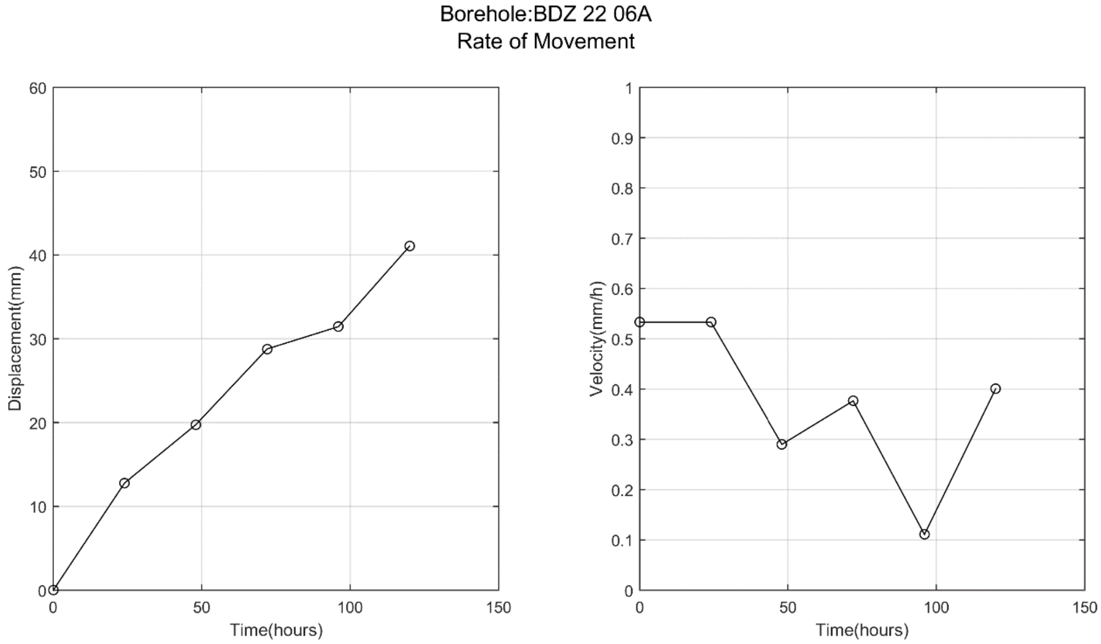

*Figure 77. Rate of Movement for Borehole: BDZ_22_06A*

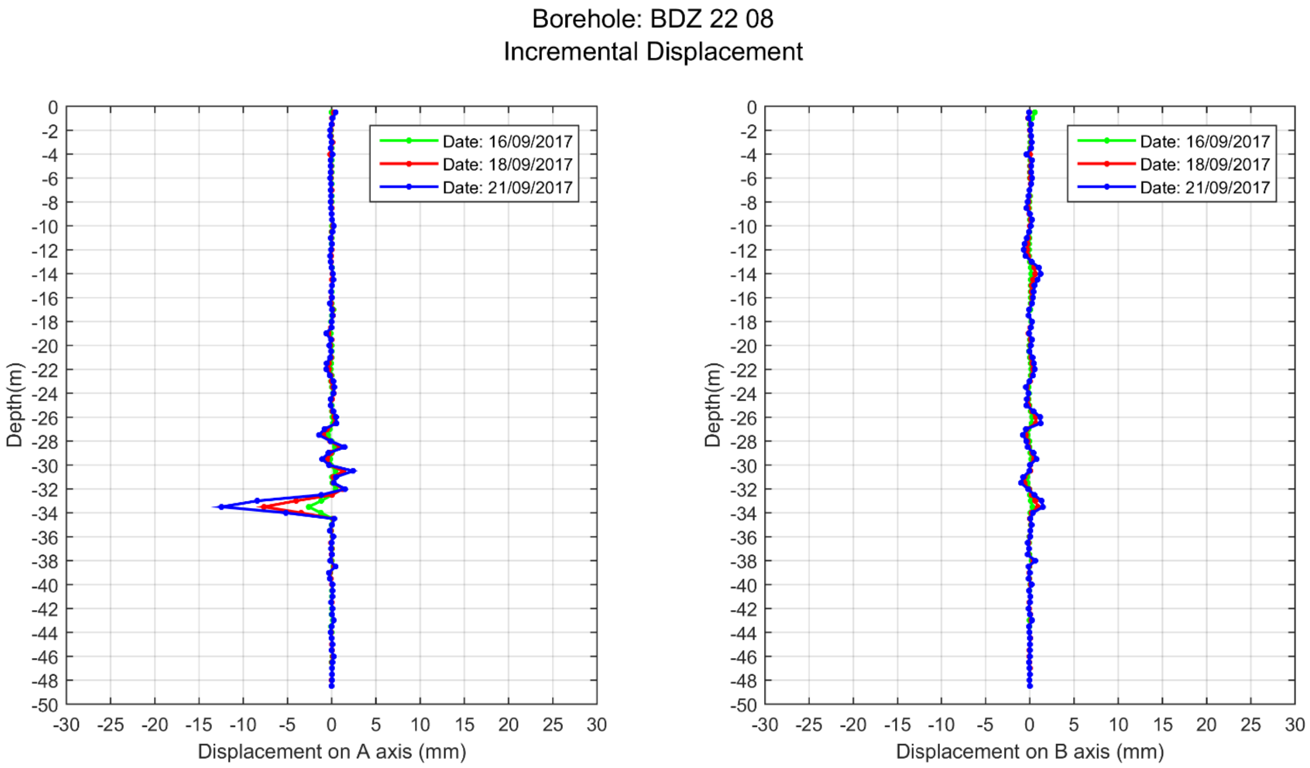

*Figure 78.Incremental Displacement for Borehole: BDZ_22_08*

At *figure 77* is shown the evolution of magnitude of displacement and the velocity respectively versus time.

### 5.2.2.5 Borehole: BDZ_22_08

The installation of inclinometer in borehole BDZ_22_08 took place at 14/09/2017 after the end of drilling processes. The inclinometer is embedded at depth of ~47,20m below ground

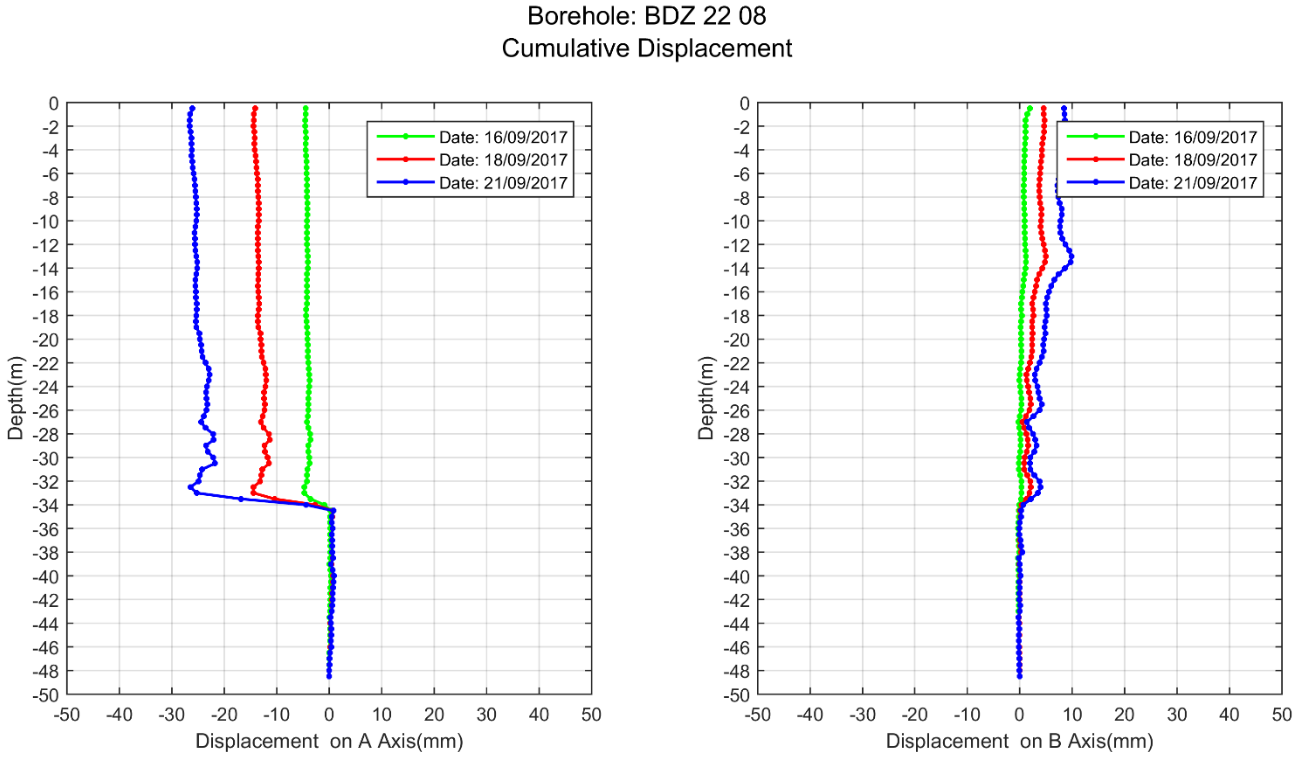

*Figure 79. Cumulative Displacement for Borehole: BDZ_22_08*

level and the top of it is at ~0,80m above ground level. The first readings took place at 15/09/2017 and those ones are considered as zero reading measurement. The second and the third set of measurements took place at 16/09/2017 and 18/09/2017 respectively and the last measurement took place at 21/09/2017. Including the zero-reading measurement, four (4) measurements were in total conducted. It is important to emphasize that in all plot types, which follow, depth equal to zero (0) is considered as ~0,80 m above ground level.

In order to detect the shear zone, incremental displacement plot have been created *(figure 78).* The underlying figure indicates the appearance of shear zone at depth of 32,50m.

Furthermore, the total horizontal movement per depth is shown in the cumulative displacement figure. This plot is important in order to understand the continuation of total movement in every particular depth and to compare the movement in shear zone with the movement in surface. From *figure 79* it is easy to understand that the displacement on the depth of shear zone approximately the same as the displacement at the surface. That means that the landslide moves with the same speed in the depth of shear deformation and at the surface. This is a factor which indicates the pattern of landslide, which in this case, from this observation is concluded as a translational landslide.

The total movement at the surface is shown in vector displacement plot, at *figure 80.* The direction of movement is calculated, as the vector of total displacements indicates, 248° to southeast. The total vector magnitude of movement is 27,4024 mm and the and the total vector velocity is 0,1631mm/hour or 3,9146mm/day.

At *figure 81* is shown the evolution of magnitude of displacement and the velocity respectively versus time.

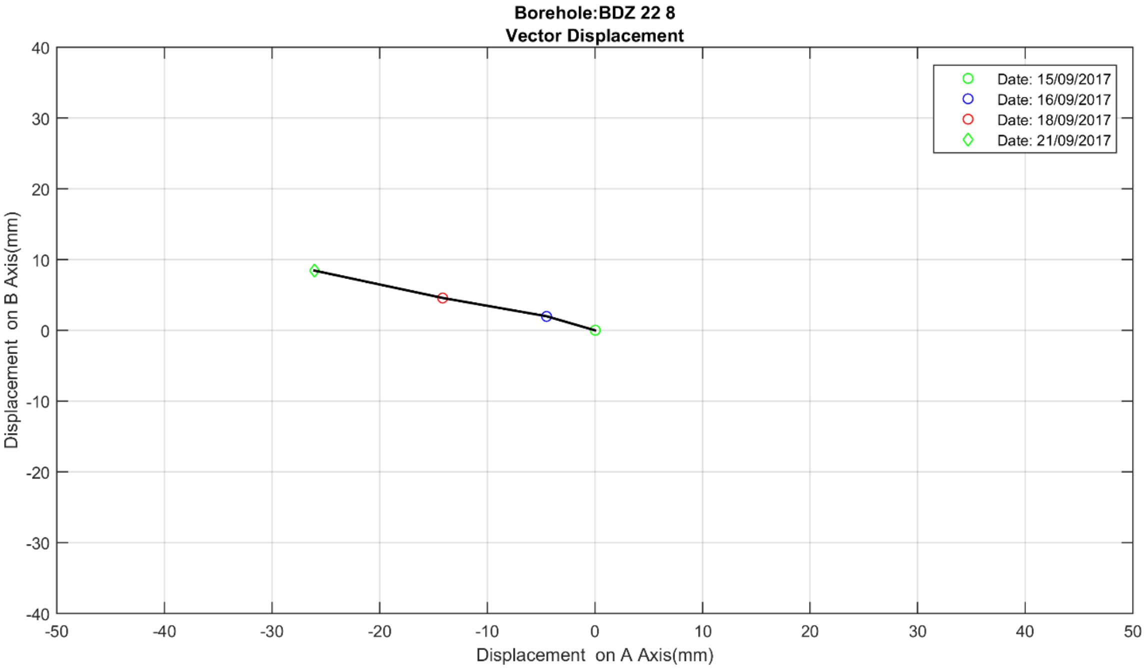

*Figure 80. Vector Displacement for Borehole: BDZ_22_08*

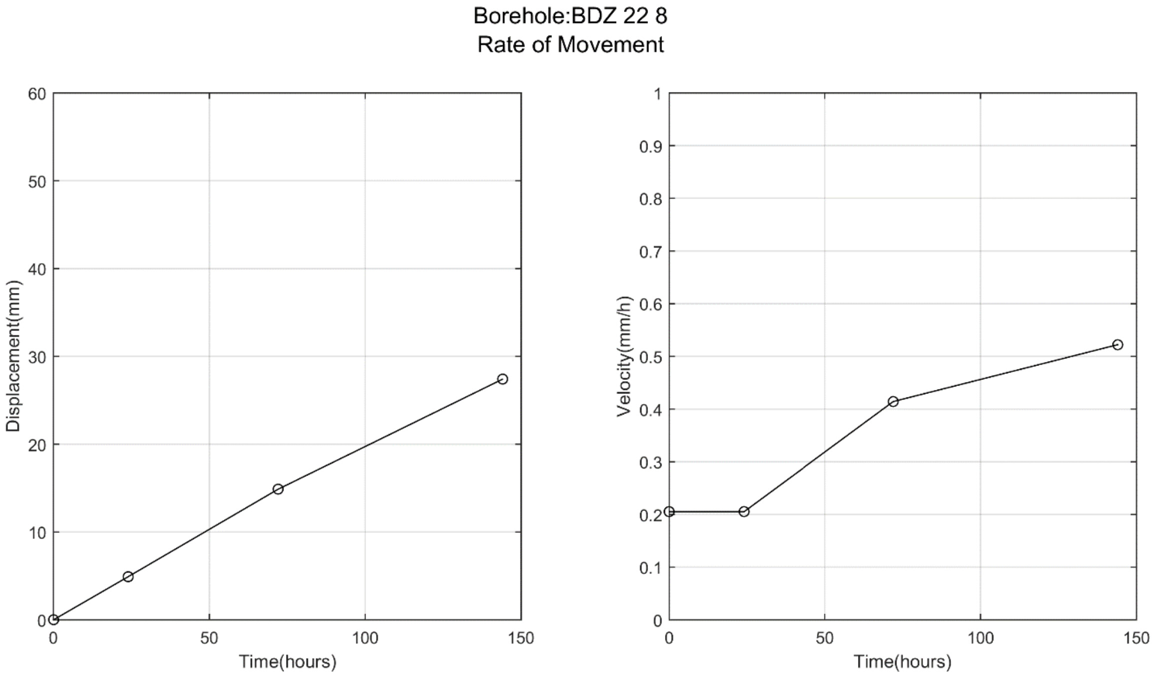

*Figure 81. Rate of Movement for Borehole: BDZ_22_08*

### 5.2.3 Conclusions

To conclude, according to underlying descriptions about each borehole, the landslide is still moving with crucial rates of movement. Also, the depth of the shear zone in every borehole is presented clearly, which enhances the success of the present instrumentation, because the major purpose of instrumentation by inclinometers, is the detection of the depth of the shear deformation. The direction of movement in each borehole indicates general movement to the southeast (230°). However, it seems from the boreholes which are placed at the flanks of the landslide, that there is a coverage from those positions to the middle of the slide. The borehole BDZ_22_03A constitutes an exception, because it seems to be moving towards south-southeast. That possibly means that the south part of the slide is more activated than the north part of it. In any case, data from other observations should be collected and correlated to the underlying assumption. Furthermore, from the cumulative displacement figures, it is possible to understand the type of landslide. In the present case from the acquired data, it seems that the landslide begins as a rotational and it is evolving into translational. However, data from other observations should be collected and correlated to the underlying assumption, as well. *Tables 5,6* contain crucial information about the data provided by the inclinometers, and data which concerns the timeline of variant processes.

*Table 5. Information about the timeline of processes concerning inclinometers.*

| Borehole | Date of Installation | Date of Last Measurement | Date of Failure | Number of conducted measurements |
|---|---|---|---|---|
| BDZ_22_01A | 28/08/2017 | 06/09/2017 | 09/09/2017 | 6 |
| BDZ_22_03A | 23/08/2017 | 31/08/2017 | 01/09/2017 | 6 |
| BDZ_22_05 | 09/09/2017 | 21/09/2017 | - | 3 |
| BDZ_22_06A | 19/08/2017 | 30/09/2017 | 15/09/2017 | 6 |
| BDZ_22_08 | 14/09/2017 | 21/09/2017 | - | 4 |

| Borehole | Total Magnitude of Movement (mm) | Rate of Movement (mm/d) | Direction of Movement (degrees) | Depth of Shear zone from G.L.(m) | Installation Depth from G.L. (m) |
|---|---|---|---|---|---|
| BDZ_22_01A | 25,37 | 4,23 | 227° | 37,20±1,0 | 46,70 |
| BDZ_22_03A | 45,59 | 9,12 | 196° | 35,70±1,0 | 46,70 |
| BDZ_22_05 | 20,88 | 3,48 | 212° | 29,20±0,5 | 44,70 |
| BDZ_22_06A | 41,07 | 3,73 | 231° | 16,30±1,0 | 40,30 |
| BDZ_22_08 | 27,40 | 3,91 | 248° | 31,70±1,0 | 47,20 |

*Table 6. Information provided by inclinometers regarding the magnitude, the rate and the direction of the movement.*

## 5.3 Water Pressure and Water Table

### 5.3.1 General

Water pressure and water table are commonly measured by piezometers and standpipes. Standpipes and piezometers are fundamentally different. There are several types of piezometers, by which the most common are closed and opened piezometer systems, which use is based on the required information. Furthermore, measurements of water table during drilling, are considered valid indication of water table, however the accuracy with which the water table is detected in this case, is restricted.

Standpipes are composed by perforated simple pipe, which is installed in the borehole and filter type material is placed peripherally to fill the hole. The diameter of pipe in this case, is not considered important. Although, measurements of the water table by standpipes is characterized as simple and economical procedure, it presents also disadvantages. The major disadvantage is regarding the fact that in this type of measurement is that cannot measure pore pressures from different layers, considering that through the borehole and filled filter, the communication between aquifers though aquiclude material can occur *(Price D.G. & de Freitas M.H., 2009).*

Open piezometer systems measure pore water pressure in particular zone or formation. There are several types of open piezometer system, which differences are focused at the time response. The most common open piezometers are the Casagrande type. The underlying type of piezometers use perforated plastic pipes at depth in which the water pressure is to be measured, or plastic porous pot which sometimes can be guarded by steel. Whether the perforated plastic pipe is used, it is connected to the surface with the same plastic tube, which is not perforated. In contrast, whether the plastic pot is used, it is also connected to the surface with plastic unperforated tube. The space which remains from the surface of the borehole to the piezometer is filled mostly with granular material at depth in which the pore pressure is under investigation, and the rest of the space is sealed by bentonite and cement *(Price D.G. & de Freitas M.H., 2009).*

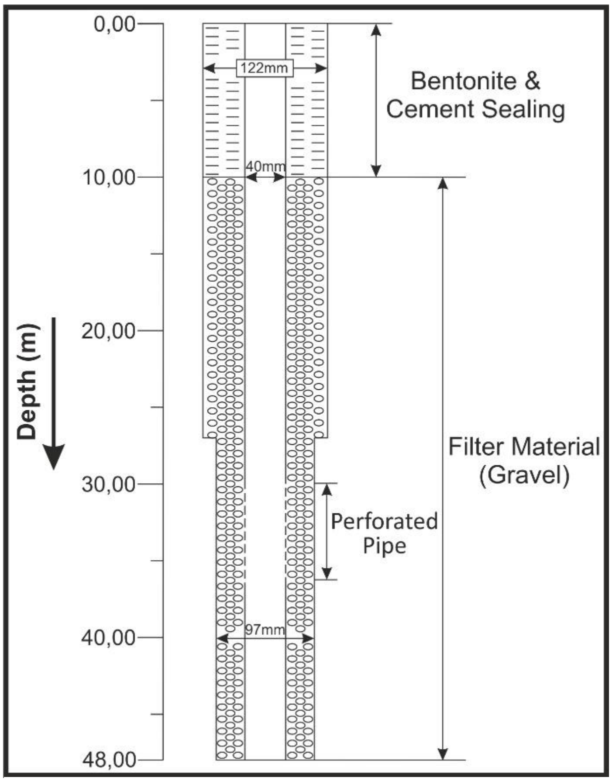

*Figure 82. Sketch of the piezometer installation in borehole BDZ_22_02.*

In both open type piezometers and standpipes, the measurements are implemented by dip meter. The dip meter is usually composed by two electric cables which are connected to electric source, which is usually a battery, an electric device. When the closure of the circuit occurs, the electric device informs that the depth of piezomentrical head is reached. Furthermore, both standpipes and open piezometer, although simple, have the disadvantage regarding time response. More precisely, when rapid response by the instrument is required, for example, on the construction of dams, more sophisticate systems, such as closed piezometers, are commonly used.

### 5.3.2 Installation

During the present stability assessment two open piezometers were installed. The piezometers were installed at the boreholes BDZ_22_02, BDZ_22_07 and their final depth was 47,00m and 44,30m respectively.

| Borehole | Piezometer Depth(m) |
|---|---|
| BDZ_22_02 | 47,00 |
| BDZ_22_07 | 44,30 |

*Table 7. Boreholes and depth of piezometer installation.*

Due to installation, perforated plastic pipe of 40mm, was installed with deviation of 3m from the zone of shear deformation. The rest of the piezometer is composed by unperforated tube of the same diameter. The space between the surface of the borehole and the plastic pipe was covered by gravel until the depth of 10,00m, from which mixture of bentonite and cement was used in order to seal hydraulic conductivity with the surface.

### 5.3.3 Provided data

Information regarding ground water is derived from the monitoring of piezometers as well as the drilling process. Piezometers, have installed only in two positions which is not representative, regarding the area of the study. So, the measurements of water table during

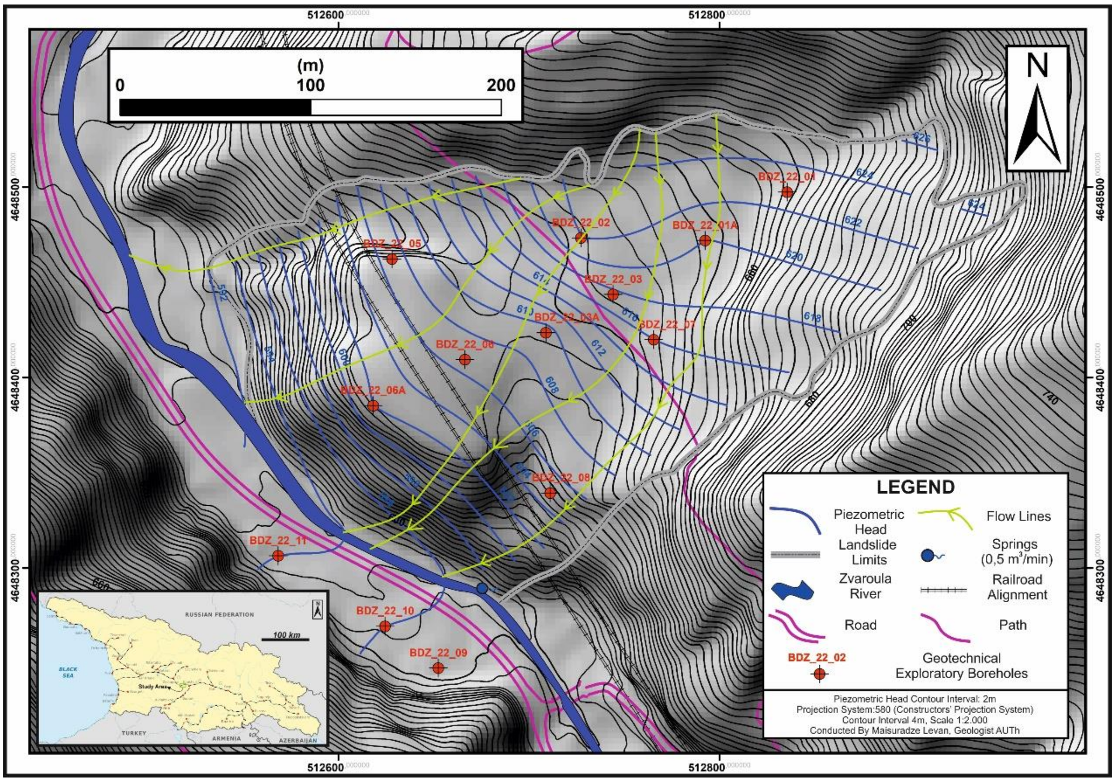

*Figure 83. Piezometrical map of the under-study landslide territory.*

drilling process were also used in order to obtain the characteristics of groundwater flow in the study area.

So, based on the measurement of the *table 8,* piezometrical map, and flow lines were produced, and they are illustrated at *figure 83.*

| Borehole | Depth (m) | Borehole Altitude (m) | Water table Altitude(m) |
|---|---|---|---|
| BDZ_22_01A | 25,00 | 645,24 | 620,24 |
| BDZ_22_02 | 18,00 | 640,18 | 622,18 |
| BDZ_22_03A | 29,00 | 637,75 | 608,75 |
| BDZ_22_05 | 20,00 | 626,64 | 606,64 |
| BDZ_22_06A | 20,00 | 622,40 | 602,40 |
| BDZ_22_07 | 25,00 | 641,36 | 616,36 |
| BDZ_22_08 | 26,00 | 631,16 | 605,16 |

*Table 8. The depth of the water table regarding the altitude of boreholes and the altitude of water table within the boreholes.*

Considering that the measurements within the piezometers are more accurate and useful information regarding the aquifer are produced. First of all, the fluctuation of water level with respect to the time for each borehole is plotted on the *figures 84 and 85* respectively. During the measurements, extensive drought prevailed in the area, with the only exception at 08/09/2017, in which extensive rainfall took place all day long.

In the measurements of borehole BDZ_22_07 the relation between the water table and water availability in the area can be observed. More precisely generally the dropping in the water table with rate 1,5cm/day is observed, with an exception at 08/09/2017, where the level of water table rises 5-10cm.

In the measurements of the water level within borehole BDZ_22_02 the dropping rate during the same period is greater and approximately equal to 3,3cm per day. The first measurement in the *figure 85,* represents the first measurement after the process of drilling and the removing of the casing from the borehole. That means that the response of the piezometer system is not direct. Considering the rate of dropping at water level, at 08/09/2017, the water level normally should have been dropped, however, there is no such

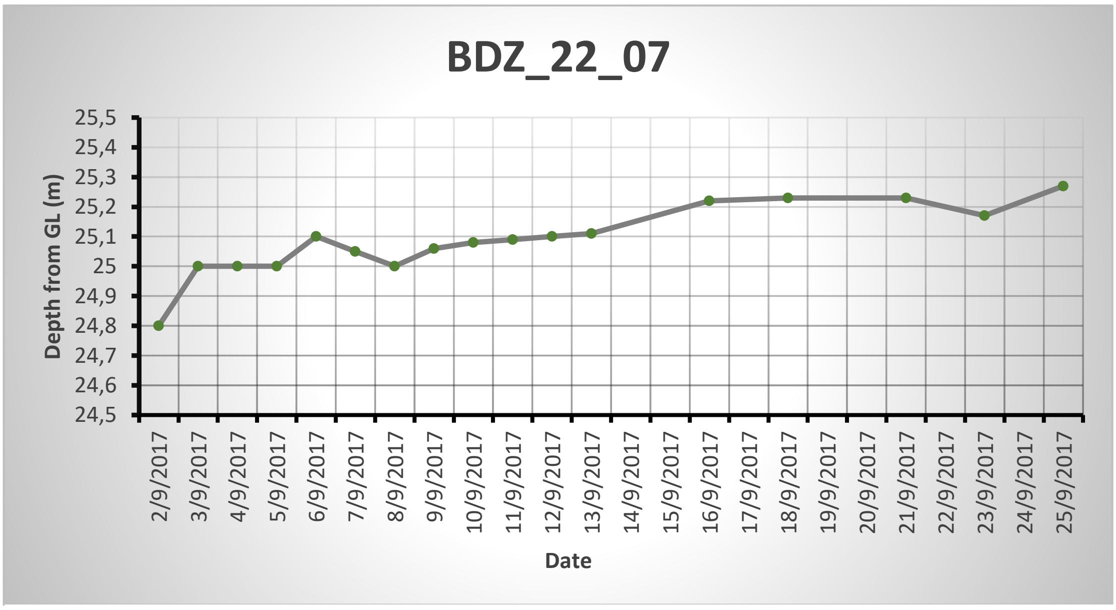

*Figure 84. Fluctuation of water Table at borehole BDZ_22_07.*

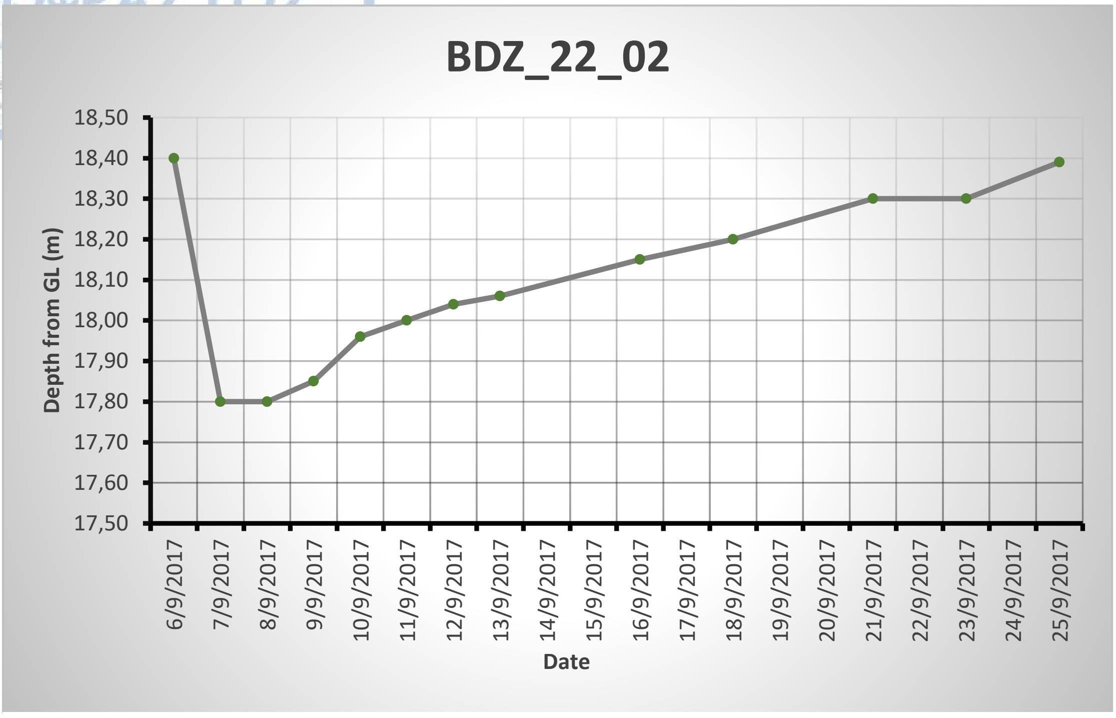

*Figure 85. Fluctuation of water Table at borehole BDZ_22_02.*

observation. In contrast, the water level remains in the same level, which means that the dropping rate, and the water providing rate on that day was equal.

Considering the atmospheric conditions in the study area, regarding the raining and the drought, the direct relation on both boreholes with them is obvious. This relation confirms the assumption regarding the hydraulic conductivity of the landslide material, which generally is considered high. In addition, it seems that the aquifer in this case is unconfined. Furthermore, although the material appears to be extensive heterogenous, regarding its composition, as a mass it seems to have homogenous behavior. That means, the permeability of the mass is relatively high so, crucial pore water pressures cannot be developed.

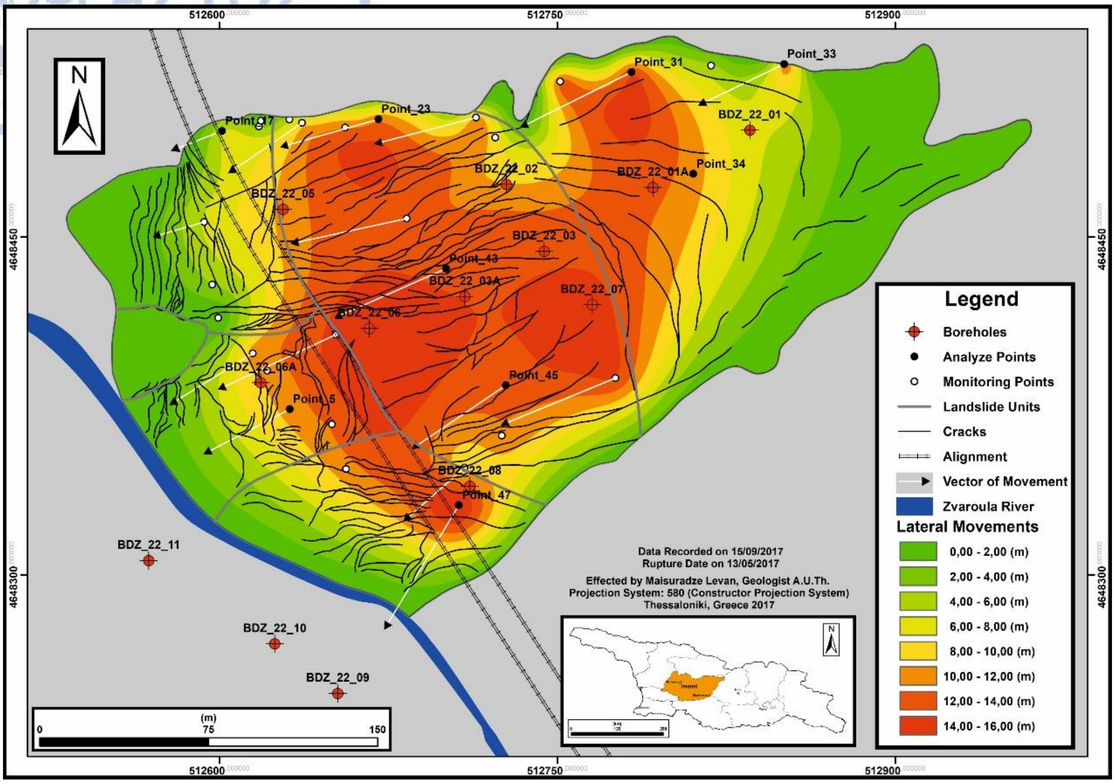

*Figure 86. Map of lateral movements corresponding to the direction of movements and surface ruptures of landslide.*

## 5.4 Monitoring Points

### 5.4.1 General

From the rupture day, which was at 13/05/2017, fifty-two monitoring points were installed in order to monitor the surface, lateral and vertical respectively, movements. The points were composed by iron nails which were inserted into ground. The measurement took place on the head of the nail with great accuracy of centimeter. At 15/05/2017 three points have been lost, and other two points have been installed to replace the lost ones. At 17/05/2017 another point has installed and 3,5m added on all measurements of elevation for convenience of construction and unification of elevation system. In addition, at 28/05/2017 other 10 monitoring point have been added in order to replace other lost ones. Monitoring points have been lost due to massif movements, which are shown to the landslide, especially in a short period of time after excavation.

The underlying monitoring system provides crucial information firstly, regarding the safety, and secondly considering the model of the landslide. Other information regarding the magnitude and the direction, of lateral and vertical displacement, as well as velocity were also provided and calculated respectively. The new installed points start to measure from the installation date, so correction regarding the initial movements is required. Taking into account, generated displacement maps, created by measurements of remaining points, on the date of the installation of new points, the correction regarding the initial movements is possible.

Worth mentioning is the total magnitude of the movements. Although from field observation, it is obvious that the great magnitude of displacement, accurate numerical estimation of the magnitude cannot be acquired. In contrast, from the monitoring of several points, accurate absolute displacements can be measured. The greatest magnitude of lateral and vertical displacements recorded, reach 16m and 7m respectively. Furthermore, the spatial distribution of the displacement shows how the landslide is developed. More precisely, the spatial distribution of the lateral and vertical displacements of final displacements, which were

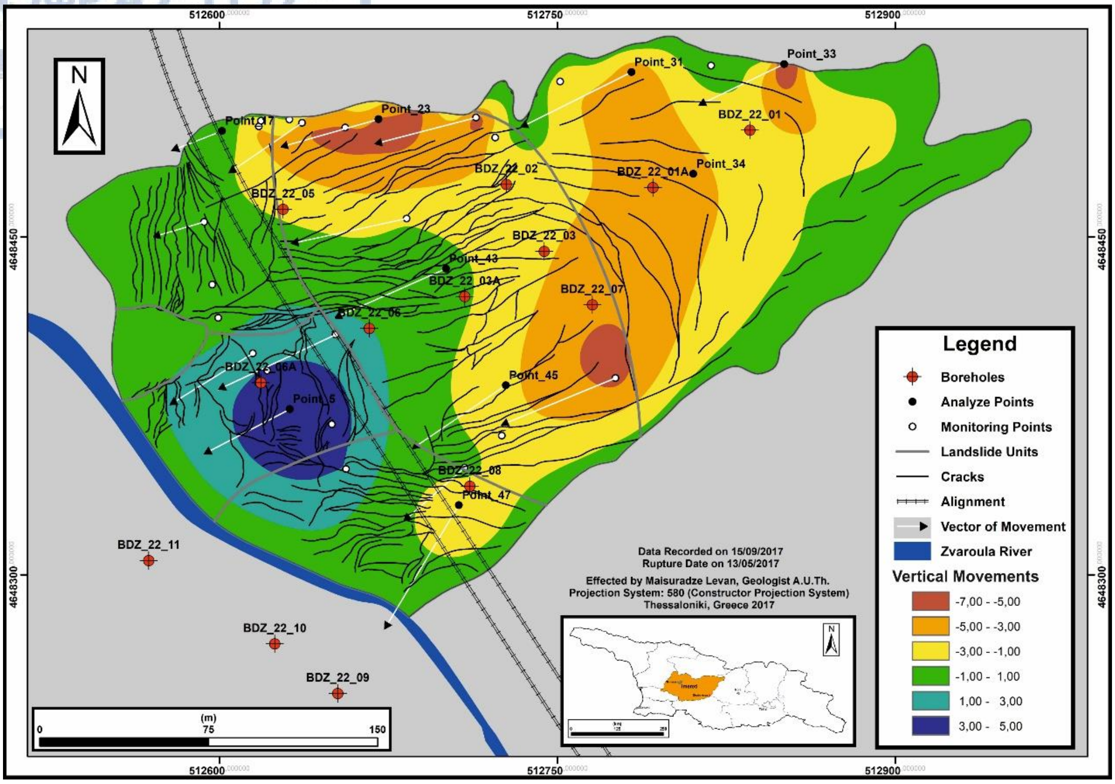

*Figure 87. Map of vertical movements corresponding to the direction of movements and surface ruptures of landslide.*

recorded at 15/09/2017 are illustrated at *figures 86 and 87.* The observation at the underlying maps is considered vital for the understanding of the phenomenon.

In order to construct the maps of *figure 86 and 87,* the limits of the landslide are considered immobile. That means, that the calculation of displacement from the measured points to the border in the toe of landslide occur with a proportional deduction on the rate of displacement, with a result the illustrated movements on the underlying maps in the toe of the landslide, are not accurate. Furthermore, considering that no monitoring points were installed in the scarp, the magnitude of displacement at the scarp, is shown limited on the underlying maps.

Although considering that lateral displacements shown on the map of *figure 86,* regarding the toe of the landslide beyond monitoring points, are not accurate, generally it is shown that in the measured monitoring points which are located in toe, the magnitude of lateral movements is restricted in comparison with the magnitudes of lateral movements measured in the main body, and partly in the head of the landslide. The comparison of the magnitude of movements between the main body and the head of the landslide, cannot be committed accurately, due to lack of monitoring points on the major and minor scarps, as well as in the south border of the head of the landslide. Generally, from these maps it is observed that the major mass of the landslide, which is considered the head and the main body, pushes the material towards southeast, where there is barrier, so the material goes to the sides, with greater movements on the southern toe. The exact definition of lateral movements per landslide unit will follow in next chapters.

The map of *figure 87,* indicates factors regarding the classification of the landslide. In the center of the toe landslide, uplift with magnitude of 3-5m occurs. This is a distinctive characteristic of rotational landslides, it is called back tilt of the toe, and it is explained well as a phenomenon in *chapter 2*. Furthermore, it is shown that the magnitude of vertical movements at the toe, is restricted, with an exception in the southern side of the toe, where the vertical displacements are sizable. Of course, settlements of great magnitude occur at the head and the main body of landslide.

Beyond the recording and the illustration of total magnitude and partly the orientation of displacements which occur in landslide territory, the calculation of the velocity for the monitoring points is vital, in order to recognize whether the landslide accelerates, if the phenomenon has stopped or still occurs. In order to obtain the knowledge regarding the way of the developing of landslide, it is considered vital to understand how the units of landslide, as they are divided in chapter 3, are reacting versus time. This is the reason why several monitoring points were taken, from every unit respectively, and it was analyzed individually regarding the magnitude and the direction of displacement, velocity, and they are illustrated in following chapters.

| Unit | Point | Initial Direction (Degrees) | Final Direction (Degrees) |
|---|---|---|---|
| A | Point_33 | 242° | 244° |
| A | Point_34 | 248° | 247° |
| A | Point_31 | 239° | 243° |
| B | Point_45 | 237° | 236° |
| B | Point_23 | 238° | 254° |
| B | Point_43 | 247° | 245° |
| C1 | Point_17 | 245° | 251° |
| C3 | Point_5 | 244° | 242° |
| C4 | Point_47 | 218° | 211° |

*Table 9. Calculated direction of movement by the monitoring points.*

The orientations are calculated regarding the first measurement and the final measurement and not between two continuous measurements in order not to taking account small unimportant changes in orientation.  Movements lesser than 1cm was not considered valid because of the accuracy of GPS system.

### 5.4.2 Unit A

Three major points were analyzed individually for the head of the landslide, points 33,34,31 *(figure 88,89,90,91).* Regarding the direction of movement, no vital change occurs, considering that the underlying points show movement towards SE (~242°). Furthermore, the point 34 was lost after 23/06/2017.

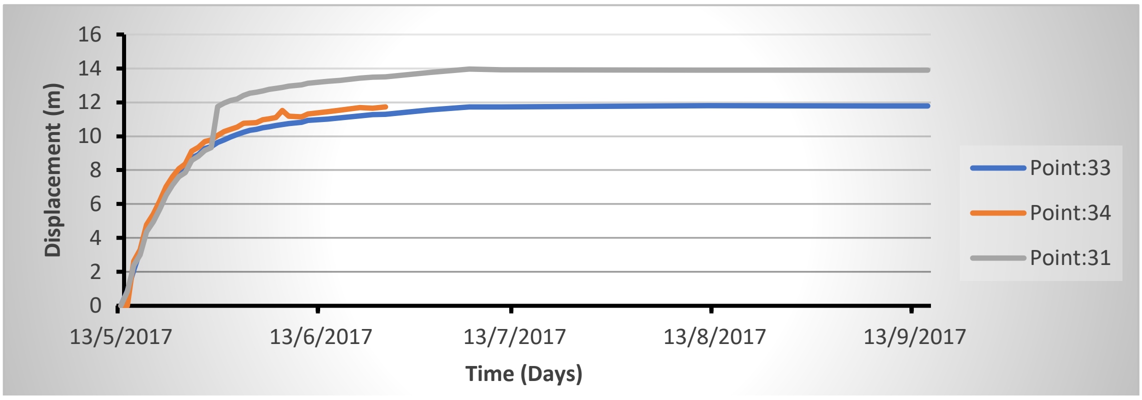

*Figure 88. Lateral Displacement versus time for the Unit A, the head of the Landslide.*

In the *figure 88,* lateral displacement of magnitude 12-14m is shown. This magnitude of movement represents the total movement of the head of landslide from 13/05/2017, the rupture day, until 15/09/2017.

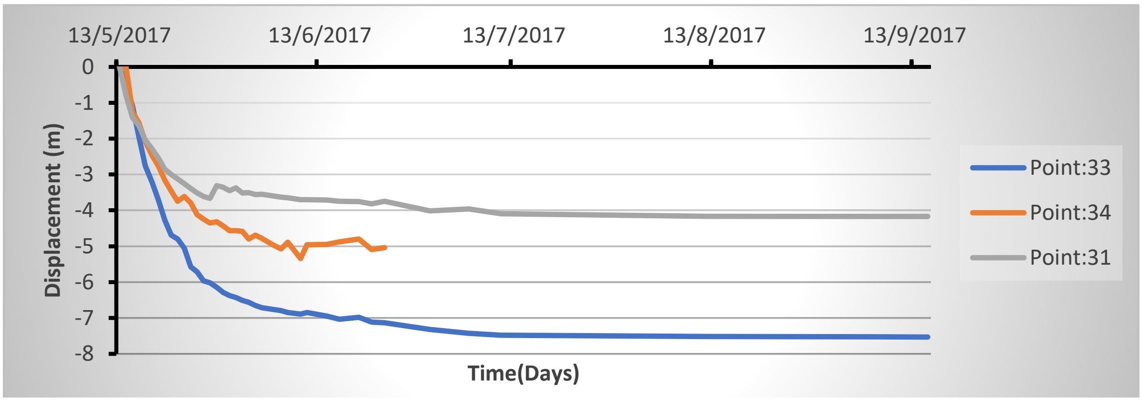

*Figure 89. Vertical Displacement versus time for the Unit A, the head of the Landslide.*

In the *figure 89,* vertical displacements of magnitude 4-7,5m is shown. This magnitude of movement represents the total settlements of the head of the landslide from 13/05/2017, the rupture day, until 15/09/2017.

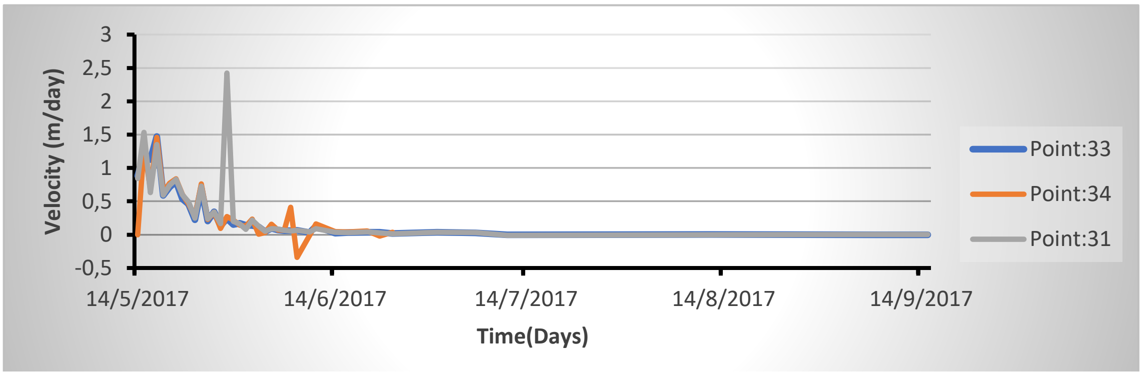

*Figure 90. Lateral rate of movement versus time for the unit A, the head of the landslide.*

Regarding the velocity of the head of the landslide given by the underlying monitoring points on *figure 90,* the landslide seems to appear great lateral movements until the beginning of July. Then the rate of movement appears to be reduced below 1cm/day. Furthermore, the head of the landslide seems to move laterally with approximately the same rates of movements except the point 31 at 28/05/2017, where speed of 2,5 m/day occurs, but there is no correlation with other point on that day, so probably it is something very local. Generally, maximum movements of 1,5m/day are recorded.

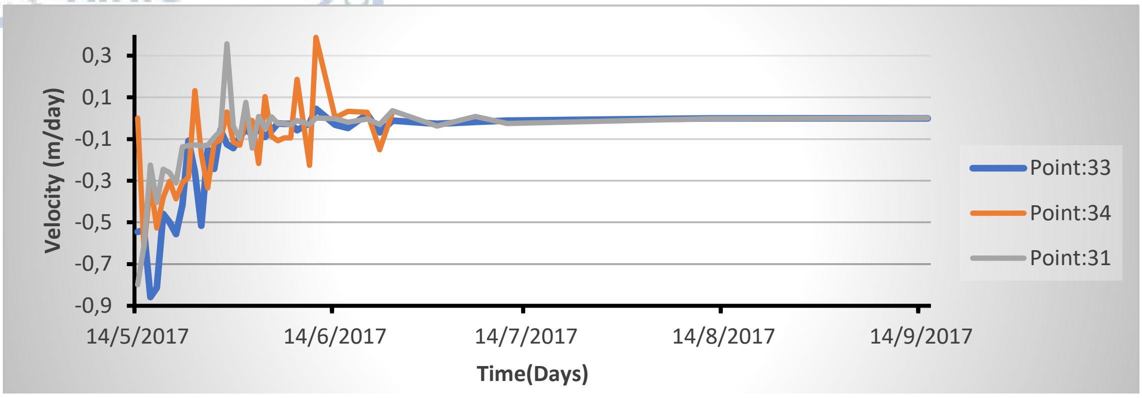

*Figure 91. Vertical rate of movement versus time for the unit A, the head of the landslide.*

Regarding the velocity of vertical movements, of the head of the landslide, which are illustrated at *figure 91,* the landslide seems to appear great vertical movements until the beginning of July, the magnitudes range from 0,8m/day to 0,1m/day regarding settlements. In addition, the rate of vertical movement until the August is greater than 1cm, which is also noticeable rate. Furthermore, cases in which velocity corresponding to uplift movements is observed too. These movements are interpreted as rotational movements of individual blocks of material, during the general sliding.

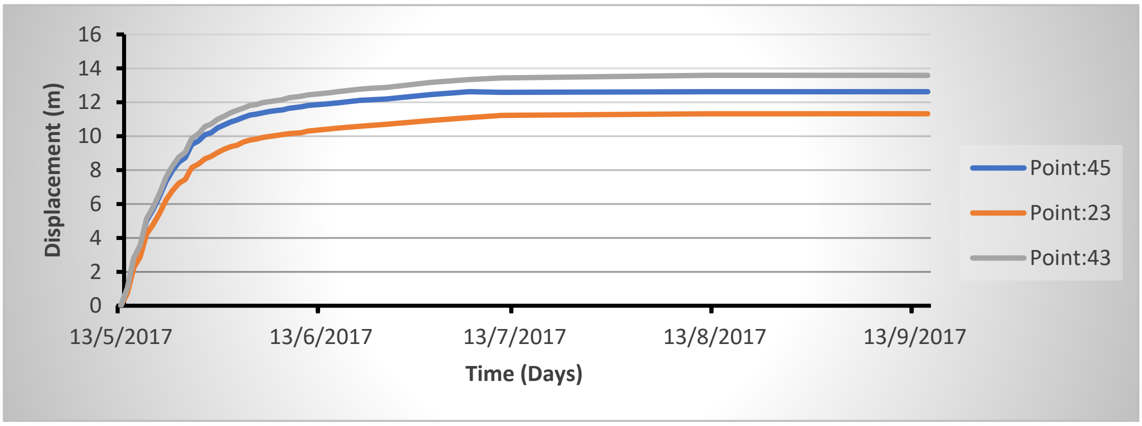

*Figure 92. Lateral displacement versus time for the unit b, the main body of the Landslide.*

### 5.4.3 Unit B

Three major points were analyzed individually for the main body of the landslide, points 45,23,43 *(figure 86;87).* Regarding the direction of movement, it ranges between 236°-247°, so it can be generally considered as SE. Of course, the direction of movement is correlated with the position of the measured point. For example, the point 23 is located near to the northern border of the landslide, appears initial movement to 238°, which changes and the movement on that position seems to be oriented with the general movement of the landslide as the phenomenon is developing. It is worth mentioning that the point 43 is located in the middle of main body and point 45 is located near to the south border of the landslide. These points have been selected, based on their good spatial distribution in the main body.

The magnitude of lateral displacements, which is illustrated at *figure 92*, shows that the main body of the landslide appears displacements between 11-14m. However, in the main body there are other points, which appears displacement even of 16m from the rupture to the 15/09/2017.

In the *figure 93,* vertical displacement of magnitude 0,5-5m is shown. This magnitude of movement represents the total settlements from the main body of the landslide from 13/05/2017 to 15/05/2017. It is also worth to point out that there are other points in the main body in which settlement of 7m are also observed-measured. However, it is worth mentioning that the center of the main body does not appears great magnitude of settlements, which are restricted lesser than 1m.

Regarding the velocity of the head of the landslide given by the underlying monitoring points at *figure 94,* the landslide seems to appear great lateral movements even in August with rate greater than 1cm/day. Furthermore, the main body of the landslide seems to move laterally with approximately the same rates of movements in every position. The maximum rates of movement reach the value of 1,8m/day and displacements over 1m/day are measured until 18/5/2017. Which means that the landslide shows massif acceleration after the rupture for 5 days. However, the velocity in the end of May remains greater than 20cm/day. In addition, even though the movements in all parts of the of the main body are

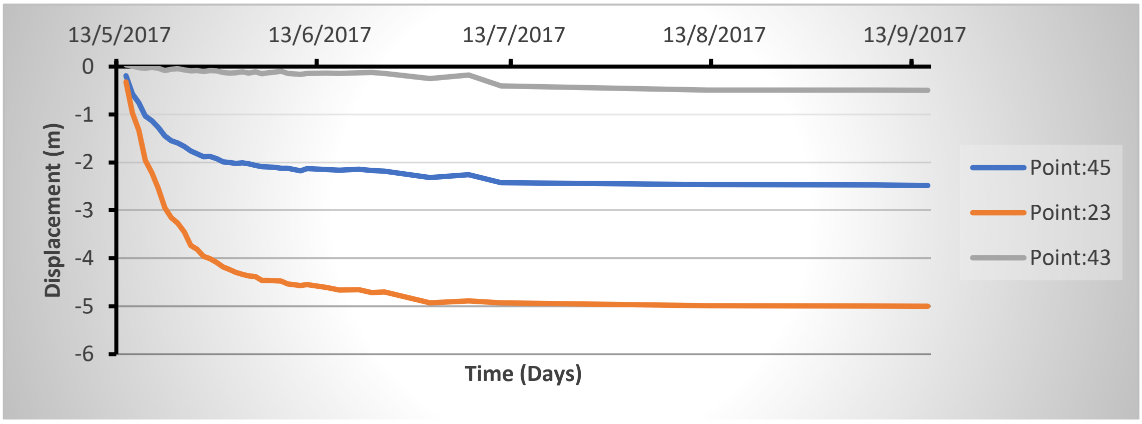

*Figure 93. Vertical displacement versus time for the unit b, the main body of the landslide.*

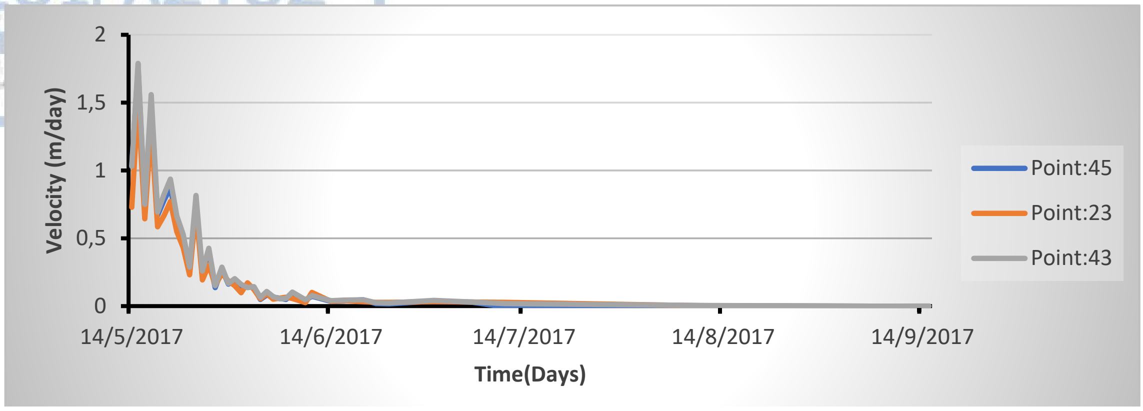

*Figure 94. Lateral rate of movement versus time for the unit A, the main body of the landslide.*

similar, there is no correlation with the other units of the landslide, regarding when the phenomenon accelerates or reduces its velocity.

Regarding the velocity of vertical movements, of the main body of the landslide, which are illustrated at *figure 95,* the landslide seems to appear great vertical movements until the end of May, the magnitudes range from 0,65m/day to 0,1m/day regarding settlements. In addition, the rate of vertical movement until the August is greater than 1cm, which is also noticeable rate. Furthermore, cases in which velocity corresponding to uplift movements, in contrast to the head of the landslide, are not observed in the main body, or at least they are not intense.

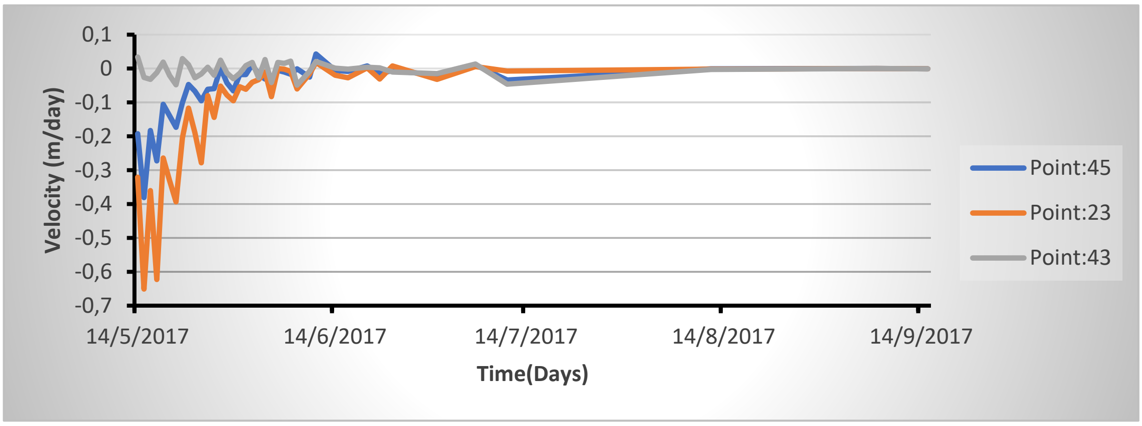

*Figure 95. Vertical rate of movement versus time for the unit B, the main body of the landslide.*

### 5.4.4 Unit C

Three major points were analyzed individually for the toe of the landslide *(figure 86; 87).* More precisely, in this unit one point is analyzed, for the corresponding subdivide unit, which means that the point 17 is analyzed for the C1 subunit in the north of the toe, the point 5 is analyzed for the C3 subunit in the middle of the toe, and the point 47 is analyzed for the subunit C3 in the south of the toe. Of course, the subunit C2 which seems to be immobile, not only by observation of surface ruptures but also from the surface monitoring *(figures 86;86),* is not being further analyzed. Detailed analysis regarding measured movements per subunit follows.

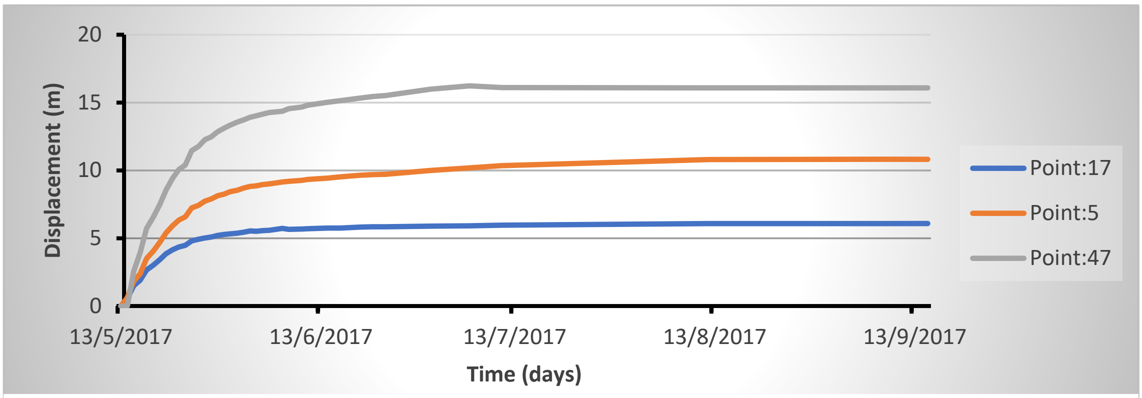

*Figure 96. Lateral displacement versus time for the unit A, the toe of the landslide.*

#### 5.4.4.1 Subunit C1

During the analysis of monitoring points of the toe, and generally the map of *figure 86 and 87,* it is noticeable that comparing to the other parts or units of the landslide, the less intense movements are observed in the subunit C1. To begin with, the direction of the movement in the beginning of the phenomenon is towards 245°, and rotation of 5° towards west occurs as the landslide is developing.

Regarding to the total lateral displacement on point 17, which represents the movements of this subunit, is approximately equal to 6m. Of course, 6m of movement is considered as a huge magnitude of movement, yet in comparison with the other parts of the slide, which movements reach 16m, is restricted. Also restricted, appears the magnitude of total vertical movement. The area is slightly uplifted with magnitude of 0,6m on 15/09/2017.

Concerning the velocity of lateral movements in the northern toe of the landslide, given by the point 17*(figure 98),* it seems to appear great lateral movements of rate greater than 0,1m/day until 28/5/2017. Also, the rate of movement appears greater than 1cm until

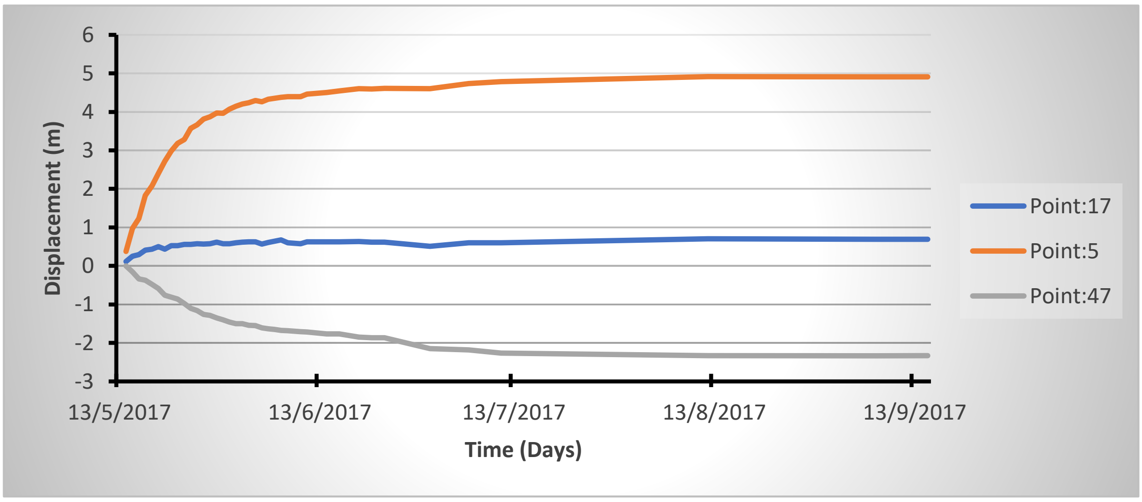

*Figure 97. Vertical displacements versus time for the Unit A, the toe of the landslide.*

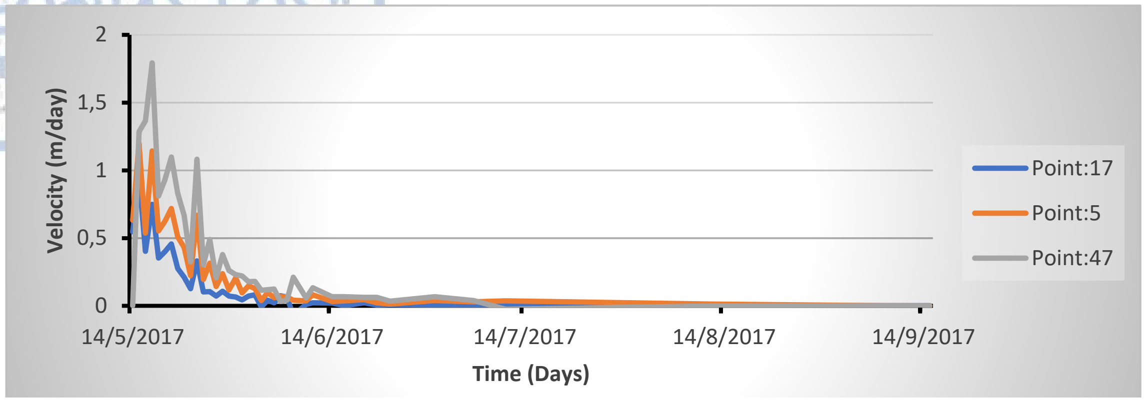

*Figure 98. Lateral rate of movement versus time for the unit C, the toe of the landslide.*

20/06/2017. The maximum rate of movement appears equal to 1m only at 15/05/2017. Regarding the corresponding rate of vertical movements, which are illustrated at *figure 99,* the rate is greater than 10cm until 17/05/2017 and until the beginning of the July the rate is dropped to lesser than 1cm.

### 5.4.4.2 Subunit C3

From the analysis of point 5 regarding the subunit C3, not only sizeable lateral displacements but also crucial uplift is noticed. In addition, concerning to the direction of the movement, which does not change during the development of the phenomenon, is towards 243°.

The total magnitude of lateral displacement in point 5 which represents the movements of subunit 5, until 15/09/2017 reaches 11m. This magnitude of movement, is lesser than the magnitudes on the main body or the head of the landslide, yet the difference is restricted compared to the C1. The maximum rate of lateral displacement recorded reaches 1,2m/day at 15/05/2017. Generally, until 03/06/2017 the lateral velocity is greater than 10cm, and the movement continues until the middle August with rates greater than 1cm/day. In the middle of August extensive period of drought begins, as a result the dropping in the rates of movement.

Regarding the vertical movements, as it is mentioned before, sizable uplift occurs on monitoring point. More precisely the total uplift is approximately equal to 5m from the rupture until 15/09/2017. The rate of uplifting, which is illustrated at figure 39, is shown that the rate is greater than 20cm until 24/05/2017 and until 20/06/2017 the rate is greater than 1cm per day. The maximum rate of uplifting is recorded at 15 and 17/05/2017 approximately equal to 60cm/day.

### 5.4.4.3 Subunit C4

From the analysis subunit C3 the measurements from point 17 were taken into consideration. Regarding to the direction of the movement, important observations have been made. In the beginning of the phenomenon this subunit moves towards ~220°, but

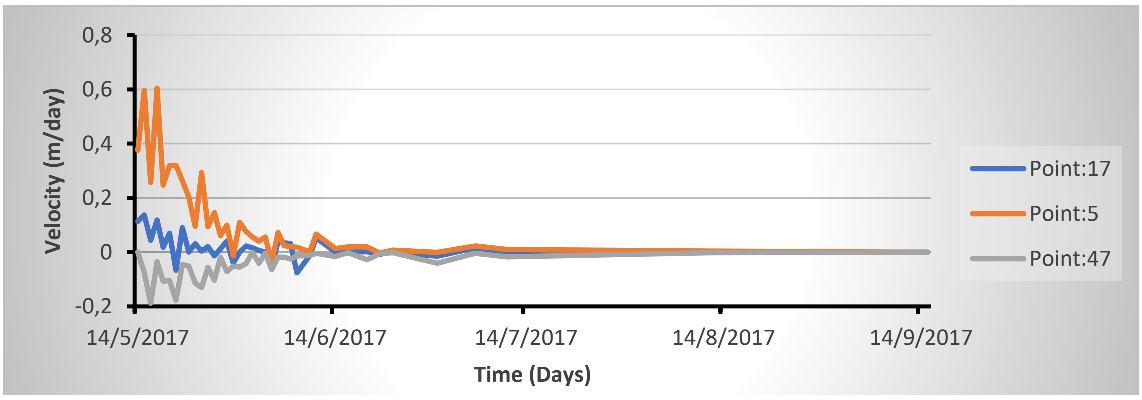

*Figure 99. Vertical rate of movement versus time for the unit C, the toe of the landslide.*

during the development of the phenomenon, rotation in the direction of movement towards south occurs and on 15/09/2017, the direction of movement it is towards ~210°. This observation is critical for the understanding of the phenomenon considering that the same kind of rotation occurs on C1 subunit, with lessen magnitude though.

The total magnitude of lateral displacement in point 47 which represents the movements of subunit C4, until 15/09/2017 reaches 16m, in contrast with the other subunits of the toe of the landslide in which he lateral displacements are not greater than 11m. this shows that the subunit C4 is the most active part of the toe. In order to understand how active is the underlying position, the observation of the rate of movements would be appropriate. So, from the rupture until 24/05/2017 the rate of lateral movement is greater than 1m/day, with maximum rate 1,8m/day at 15/05/2017. Until 11/06/2017, rates greater than 10cm continue to appear. The phenomenon continues to occur until the middle of July with rates of lateral movement greater than 1cm *(figure 98).*

Regarding the vertical movements, in contrast again to the other subunits which are uplifted, this part of the toe, appears settlements. Although the magnitude of lateral movements is definitely sizable, the magnitude of the settlement in this position is restricted to 2,30m *(figure 97).* Consequently, the rates of the settlement are restricted too, with maximum vertical movement recorded at 16/05/2017 approximately equal to 0,2m. the process continues to occur until 20/06/2017 with rate greater than 1cm and then they are dropped.

## 5.5 Conclusions

The monitoring of the landslide, provided by subsurface (inclinometers, piezometers) and surface (monitoring points) instrumentation, proved essential. So, objective conclusions regarding the development of the phenomenon are drawn.

The inclinometers provide the depth of the shear deformation, the rate of movement at the depth of the shear deformation and the surface, the direction and the magnitude of the movement. Furthermore, from the observation at the cumulative displacement plot, the type of the landslide can be concluded, whether the comparison among the magnitude of movement at the depth of shear deformation and the surface occurs. In this case from the underlying data, it can be concluded that the landslide is a typical rotational landslide, which is developed into translational in the toe.

The piezometers provide the accurate estimation of the water level, which has significant impact on the stability assessment. Furthermore, due to the interpretation of results provided by piezometers, vital information related to the type of aquifer is drawn, which allows to conclude that in this area the magnitude of developed pore pressures, cannot be developed in extraordinary levels.

The monitoring of individual points at the surface of the landslide shows the spatial distribution of lateral and vertical movements, produced by the development of the phenomenon. The underlying movements can be interpreted in order to understand the mechanism of the landslide, which based on the uplift at the toe, is considered rotational landslide. Furthermore, it is possible to calculate the rates and the direction of movement. From the rates of the movement, significant observation can be made regarding to the development of the phenomenon. More precisely, it seems that the great velocity characterizes the landslide at the outset of the occurrence, and then the velocity decreases. However, it seems that the landslide, still appears to be moving. Regarding the direction of the movement, disagreement is observed at the direction provide by inclinometers and monitoring surface points. The direction of movement derived by inclinometers is impacted by the stress field at the depth of shearing in contrast to the surface direction of movement derived by surface monitoring points, in which the underlying impact is not important. Furthermore, at the toe of the landslide the surface monitoring points indicate lateral spread of the landslide, which is interpreted due to lack of $\sigma_2$ stress axis at the toe.

# Chapter 6 Geological & Engineering Geological Model

## 6.1 General

In this chapter the correlation of surface, subsurface investigation and the evaluation of geotechnical monitoring regarding the geological and engineering geological model of the landslide is about to take place. The underlying correlation is vital in order to export the geological and the engineering geological model of the study area, which would be taken into consideration during the planning of the construction. Furthermore, the geological model is important in order to understand and interpret the formation of the landslide in the area.

The surface investigation depicts the spatial distribution of features which are affecting directly and indirectly the formation of the landslide. The subsurface investigation, through geotechnical exploratory drilling, attributes the composition of the drilled material and its distribution respectively to the depth. Information produced by the geotechnical monitoring is related to the accurate depth of the surface of movement (inclinometers), the water level (piezometers) and the magnitude and direction of the movement (monitoring points).

The underlying information were correlated in order two produce two-dimensional cross and long sections, which not only show the distribution of material in two dimensions, but also will be used in stability analysis models. So, generally seven two-dimensional (2D) sections were produced in order to study in detail, the development of the landslide and the consequently the geological model. Five sections have parallel or subparallel orientation towards the movement (AA’, BB’, CC’, FF’, GG’) and two are perpendicular to the movement (DD’, EE’).

The bedding of the bedrock is an important feature and its presence at the sections is vital. However, the magnitude of dipping in reality and in sections, is the same only in case, in which the strike of the bedding is perpendicular to the section, in other cases the apparent angle of bedding should be calculated and attributed on the sections. The calculation of the apparent angle occurred from the relation below.

$$a=\tan^{-1}(\sin(\beta)*\tan(\delta))$$

Where:

$a$: represents the apparent angle of dipping

$\beta$: represents the angle between the strike of bedding and the strike of the section.

$\delta$: represents the real angle of dipping

Regarding the surface of rupture, or the shearing zone of the landslide, two major curved planes, are about to be presented below, in more detailed analysis and illustration. The first surface (A), is the outcome of the monitoring by inclinometers and the analysis of drill cores, in which generally changes of material from soft brown clay, to bedrock formation are observed. The second surface is indicated from field observation, immediately after the rupture.

Except from the 2D spatial distribution of features related to the landslide, in the sections other information as the exact position of boreholes, the river, the road, paths, springs, are also illustrated. Of course, the major triggering factor, which is the excavation, is also represented in all sections, respectively to the initial morphology. The expected excavation as well as the final position of the alignment are also illustrated on the sections.

It is worth mentioning that the produced sections are effected at a scale of 1:1.000.

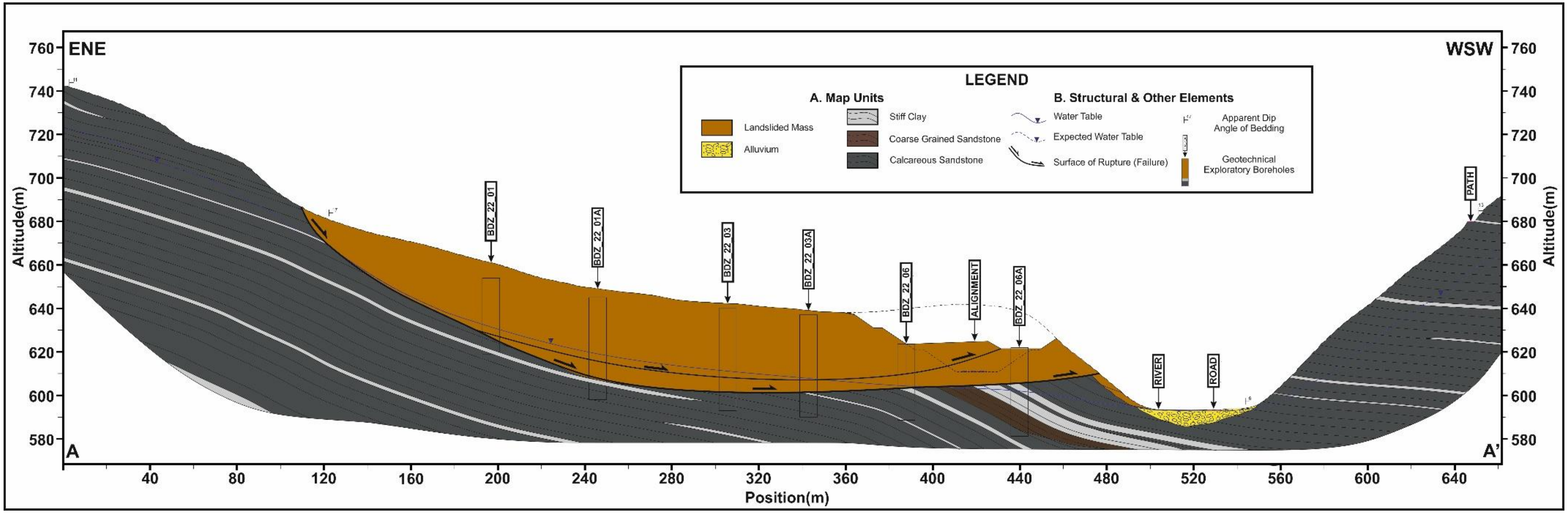

*Figure 100. Geological & Engineering Geological Cross Section AA'.*

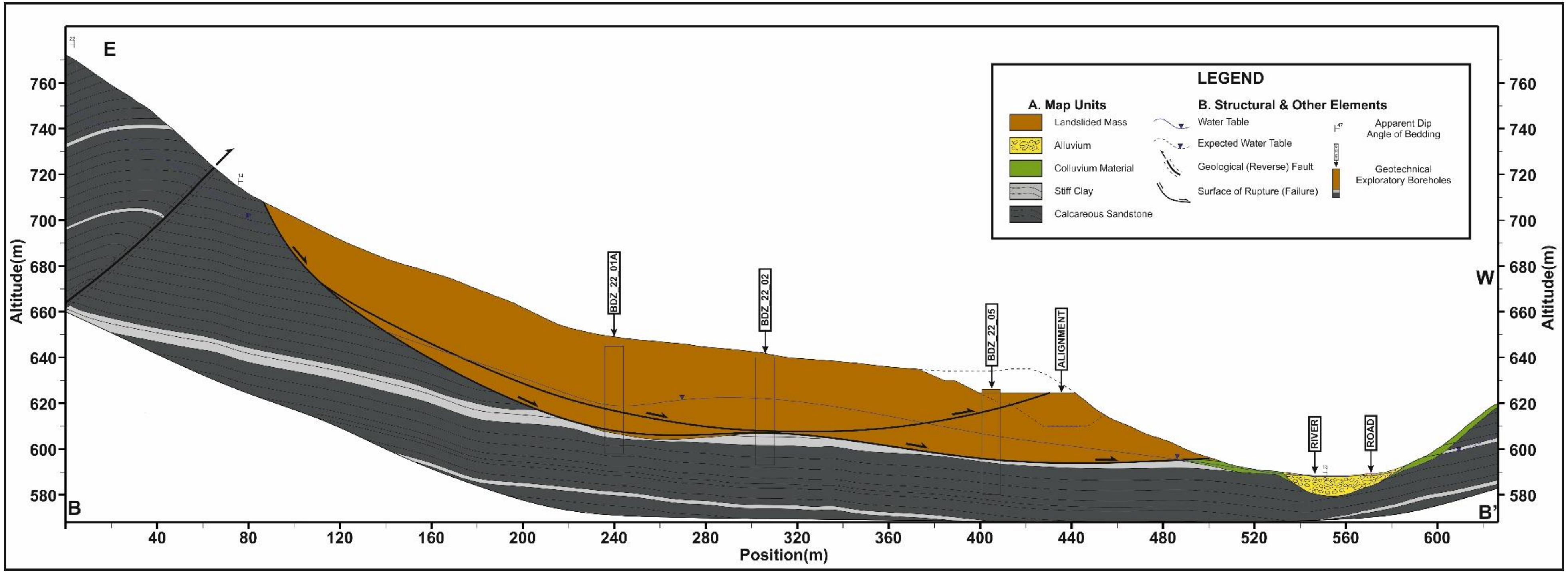

*Figure 101. Geological & Engineering Geological Cross Section BB'.*

## 6.2 Analysis of Two-Dimensional Sections

### 6.2.1 Cross Sections

#### 6.2.1.1 Section AA’

The cross-section AA’ *(figure 100)* was made on the major axes of the landslide. It has orientation ENE-WSW, the orientation of major movement and the length of the section is approximately equal to 660m. In contrast, the length of the landslide in the section is approximately equal to 370m. However, since the section, crosses the scarp of the landslide where curve towards the toe occurs, the underlying length is considered conservative, and in reality, the length is greater. In this section the bedrock, the landslide and the alluvium material are mainly represented, as well the relation among them.

The depth of the shearing, and more precisely the depth of the surface (A) at the current section is indicated by three inclinometers, installed at boreholes BDZ_22_01A, BDZ_22_03A, BDZ_22_06A. Furthermore, data from the boreholes BDZ_22_01, BDZ_22_03, BDZ_22_06, were taken also into consideration regarding the depth, in which brown soft clayey material changes into grey bedrock formation. The presence of the surface (B) is attributed by field observations. Of course, the positions of the scarp and the toe of the landslide, are indicated by the geological map. At the section AA’, the surface of shearing, beyond the scarp of the slide, relatively straight line.

Regarding the thickness of the alluvium material, data provided by BDZ_22_11, indicates thickness of approximately 7m, however the final thickness of the formation, in this middle of the ridge position, and considering not only the results from boreholes BDZ_22_9 & BDZ_22_10 but also the length of the formation on the section, is assumed approximately equal to 10m.

In the bedrock, the lenses of stiff clay are also illustrated as well as the presence of presence of coarse-grained sandstone, as interpretations also. Of course, the orientation of dipping of bedding is perpendicular to the axes of movement, and consequently the magnitude of dipping angle of bedding in this section will be constricted.

The water table in the landslide material is provided from drilling data, and more precisely the measured water table during drilling process. Furthermore, the level of the river is also considered as a free piezometrical head. So, taking account piezometrical data from boreholes BDZ_22_01A, BDZ_22_03A, BDZ_22_06A and the river, the water table is approached. Furthermore, taking into account the great permeability of the landslide material compared to the bedrock’s, the depth of the water table beyond the field of provided data could be determined, and it is expressed as expected water table in the section.

#### 6.2.1.2 Section BB’

The cross-section BB’ *(figure 101)* was made in approximately parallel direction of the major axes of the landslide, and more precisely the section has an orientation of E-W. The length of the section is approximately equal to 620m. The length of the landslide in the section is approximately equal to 420m, however the fact that this section is not exactly parallel to the axis of landslide indicates that the underlying length is an apparent length, and the real length s lesser. In this section the bedrock, the landslide, the colluvium and the alluvium material are mainly represented, as well the relation among them. It is also worth mentioning that in this section the presence of the geological reverse faults is also presented, with its apparent angle.

In order to detect the surface (A) of movement, depth indicated by two inclinometers, installed at boreholes BDZ_22_01A, BDZ_22_05 were taken into consideration. Furthermore, data acquired from the borehole BDZ_22_02, were taken also into consideration regarding the depth of the change from unstable clayey material to bedrock material. Of course, the positions of the scarp and the toe of the landslide, are indicated by the geological map.

In the bedrock, the interpretations of stiff clay are illustrated. Of course, the orientation of dipping of bedding is approximately perpendicular to the axes of movement, and consequently to the axes of the section which means that the magnitude of dipping angle of bedding in this section will be limited.

The water table in the landslide material is provided from drilling data, and more precisely the measured water table during drilling process in boreholes BDZ_22_01A and BDZ_22_05. The measurements derived from the piezometer at BDZ_22_02, confirms in some level, data acquired from the drilling process and it is also taken into consideration. Furthermore, as mentioned before the level of the river is also considered as a free piezometrical head. So, taking account piezometrical data from boreholes BDZ_22_01A, BDZ_22_02, BDZ_22_05 and the river, the water table is approached. Furthermore, taking into account the great permeability at the landslide material regarding to the bedrock, the depth of the water table beyond the field of provided data could be determined, and it is expressed as expected water table in the section. In the end, curve in the piezometrical line occurs in the position of borehole BDZ_22_02 occurs. This curve is derived by the orientation of the section, which is not oriented in direction parallelly to the groundwater flow.

### 6.2.1.3 Section CC'

The cross-section CC' *(figure 102)* with orientation of NNE-SSW, which forms angle greater than 30° with the orientation of major movement. The length of the section is approximately equal to 420m. In contrast, the length of the slide in the section is approximately equal to 280m, which appears to be the apparent length similarly to the section of *figure 100.* In this section the bedrock, the landslide, the colluvium and the alluvium material are mainly represented, as well the relation among them. It is also worth mentioning that in this section the presence of the geological reverse faults is also presented, with its apparent angle.

In order to detect the surface (A) of movement, depth indicated by two inclinometers, installed at boreholes BDZ_22_01A, BDZ_22_08, were taken into consideration. Furthermore, data from the boreholes BDZ_22_07, were taken also into consideration regarding the depth in which change from unstable clayey material to bedrock material occurs. Of course, the positions of the scarp and the toe of the landslide, are indicated by the geological map.

In the bedrock, the interpretations of stiff clay are also illustrated as well as. The orientation of dipping of bedding, in this section is not perpendicular to the axes of movement,

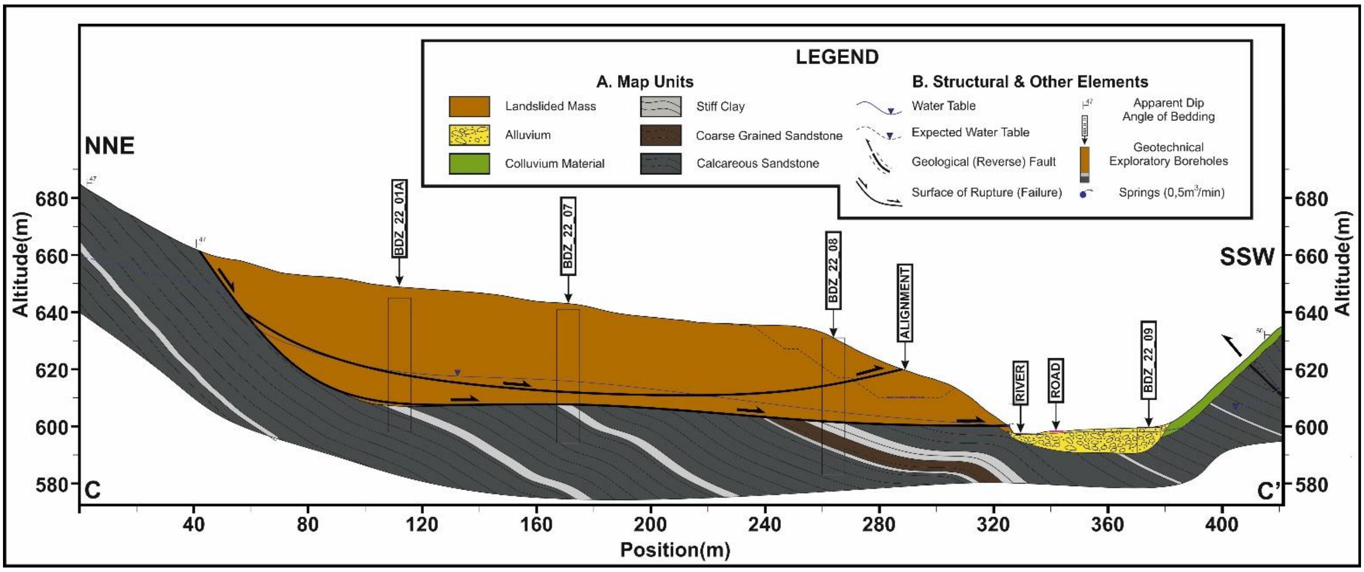

*Figure 102. Geological & Engineering Geological Cross Section CC'.*

and consequently to the axes of the section which means that the magnitude of dipping angle of bedding in this section will not be constricted.

The water table in the landslide material is provided from drilling data, and more precisely the measured water table during drilling process in boreholes BDZ_22_01A and BDZ_22_08. The measurements derived from the piezometer at BDZ_22_07, confirms in some level, data acquired from the drilling process and it is also taken into consideration. Furthermore, as mentioned before the level of the river is also considered as a free piezometrical head. So, the water table is approached. Furthermore, taking into account relation among the permeability at the landslide material and the bedrock, the depth of the water table beyond the field of provided data could be determined as it is mentioned before and it is expressed as expected water table in the section.

### 6.2.1.4 Section FF’

The cross-section FF’ *(figure 103)* was formed northern than the major axes of the landslide and is has an orientation of ENE-WSW. Regarding the other sections, the length of section FF’ is restricted at 400m. In contrast, the length of the landslide in the present section is approximately equal to 300m, however it represents only the northern part of the landslide. The purpose of this section is to attribute better than in section BB’ the geometry of the landside, considering that the BB’ section is not oriented in the direction of main movement.

In this section the bedrock, the landslide, the colluvium and the alluvium material are mainly represented, as well the relation among them. The detection of the surfaces committed similarly with the section BB’, as well as the water table, with a single exception the lack of data derived from the borehole BDZ_22_01A. This is mainly based on the geometry of the section. It is worth mentioning that the water table as well as the surfaces of the ruptures are better represented at this section than in BB’, since the geometry of the section is oriented according to the groundwater flow and also the landslide movement.

### 6.2.1.5 Section GG’

The cross-section GG’ *(figure104)* was formed southern than the major axes of the landslide and is has an orientation of ENE-WSW, similar to the movement. Regarding the other sections, the length of section GG’ is restricted at 380m. In contrast, the length of the landslide in the present section is approximately equal to 320m, however it represents only the northern part of the landslide. The purpose of this section is to attribute better than in section CC’ the geometry of the landside, considering that the CC’ section is not oriented in the direction of main movement.

In this section the bedrock, the landslide and the alluvium material are mainly represented, as well the relations among them. The detection of the surfaces committed similarly with the section CC’, as well as the water table, with a single exception the lack of data derived from the borehole BDZ_22_01A. This is mainly based on the geometry of the section. It is worth mentioning that the water table as well as the surfaces of the ruptures are better represented at this section than in CC’, since the geometry of the section is oriented according to the groundwater flow and also the landslide movement.

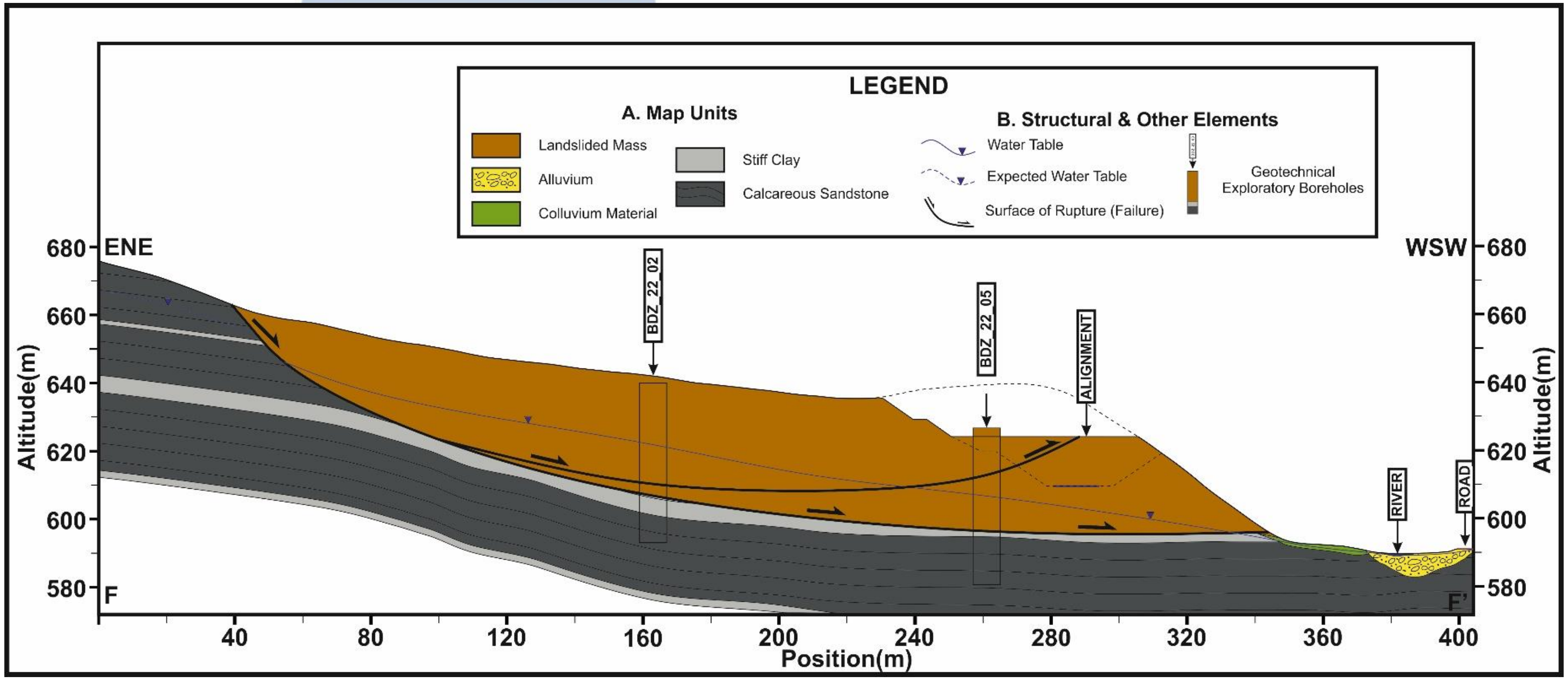

*Figure 103. Geological & Engineering Geological Cross Section FF'.*

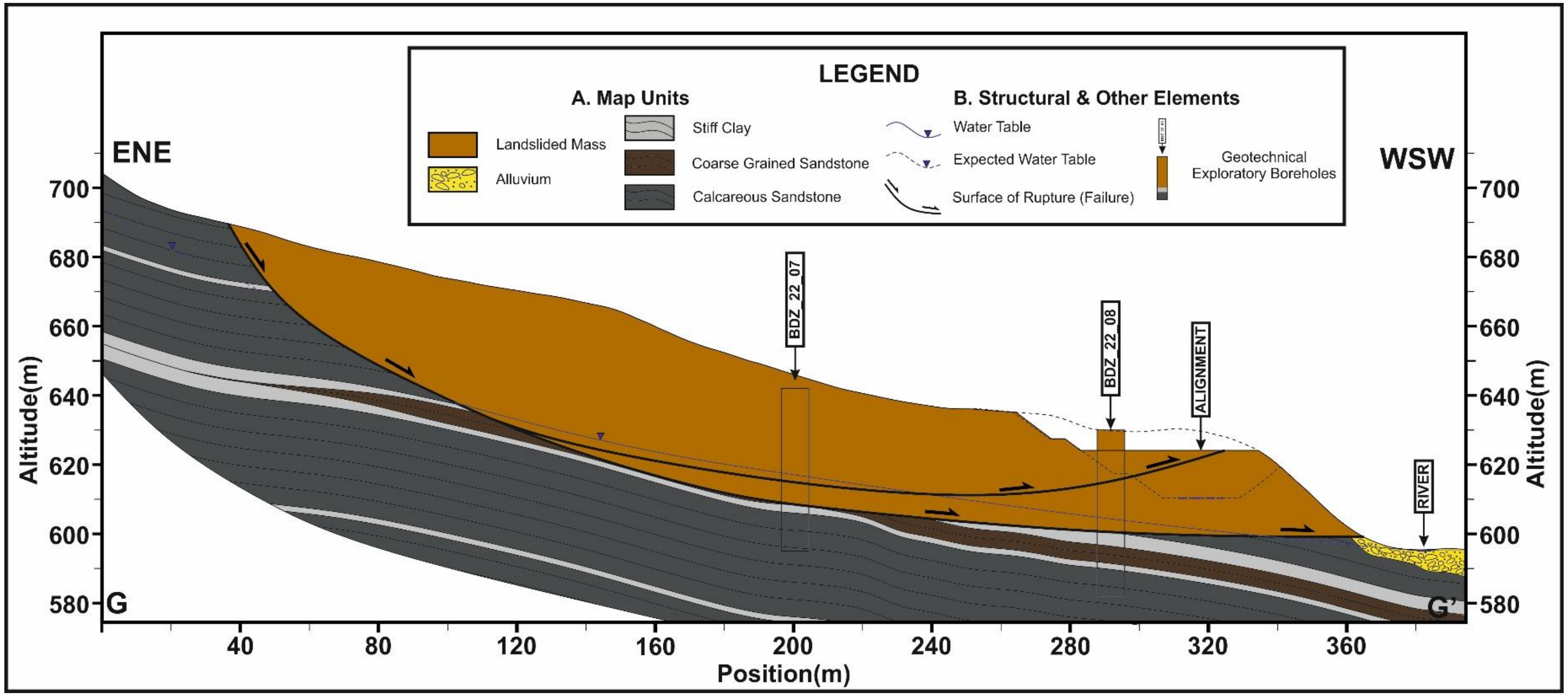

*Figure 104. Geological & Engineering Geological Cross Section GG'.*

### 6.2.2 Long Sections

#### 6.2.2.1 Section DD’

The cross-section DD’ *(figure 106)* was made in perpendicular direction to the major axes of the landslide. It has orientation NW-SE length approximately equal to 440m. In this section, which is parallel to the alignment, the width of the landslide is shown crossing the Boreholes BDZ_22_02, BDZ_22_03, BDZ_22_07. So, the width of the landslide in this section appears to be approximately equal to 150m. Of course, this is not the maximum width of the landslide. Furthermore, considering that in this section is parallel to dipping of the bedding, as well as the dipping of the faults, the represented angles in the *figure 106*, are the approximately equal to the real ones.

Regarding to the landslide, it is showed that it has a position in a valley, ant it northern part slips to the bedding of the bedrock, in contrast to the southern part in which the bedding of the bedrock is dipping contrary to the slope. As it is referenced before in the south there are a group of joints, dipping towards NNW with angle greater than 70°. Furthermore, the great angle of the formed slopes in the south boundary of the landslide indicates a relation among the formed slope and the underlying joints. More precisely, it is believed that initially this huge landslide is formed by rock slides at north and rock toppling at south. So, the deposition of this broken material occurred, and now it is moving, as a mass towards SW, as typical rotational landslide constricted partly by the bedding in the north and the group of joints in the south.

This section is the first section until now, in which the geology of the area is illustrated in detailed. It is shown that generally the bedrock is slightly folded, and there is a clear presence of brittle deformation in the area. So, there are to major reverse faults which are generally responsible for the forming of the morphology. Furthermore, the activity related to those faults, is correlated to the main joints but more importantly, these faults are probably responsible for the existence of springs with natural carbonated water in the close study area. The origin of the material in which the northern fault is overthrusted is not clearly determined because of the lack of outcrops in this area, and the presence of relatively thick overburden colluvium material.

#### 6.2.2.2 Section EE’

The cross-section EE’ *(figure 105)* has similar orientation with the DD section, yet it is formed in the position of the alignment. The section is approximately 480m long, and the width of the landslide in this position is approximately equal to 230-240m. In this position, the width is considered as the total width of the landslide. In this section, the magnitude of occurred excavations, which triggered the landslide, is also demonstrated.

Regarding the bedrock, ductile deformations is observed in the region of southern south, where the presence of fold occur. Of course, this kind of deformation in faults zones or, close to fault zones, are expected. However, the folding upslope seems to be eliminated, or there is no presence of it from the field investigation. Furthermore, the presence of lenses composed by stiff clay and coarse-grained sandstone, are also observed in this section.

It is worth mentioning that the origin and the composition of the bedrock northern that north reverse fault is questionable, and here it is assumed as sandstone. It is questionable because in this territory there is no presence of clear outcrop from which lucid conclusions could drown.

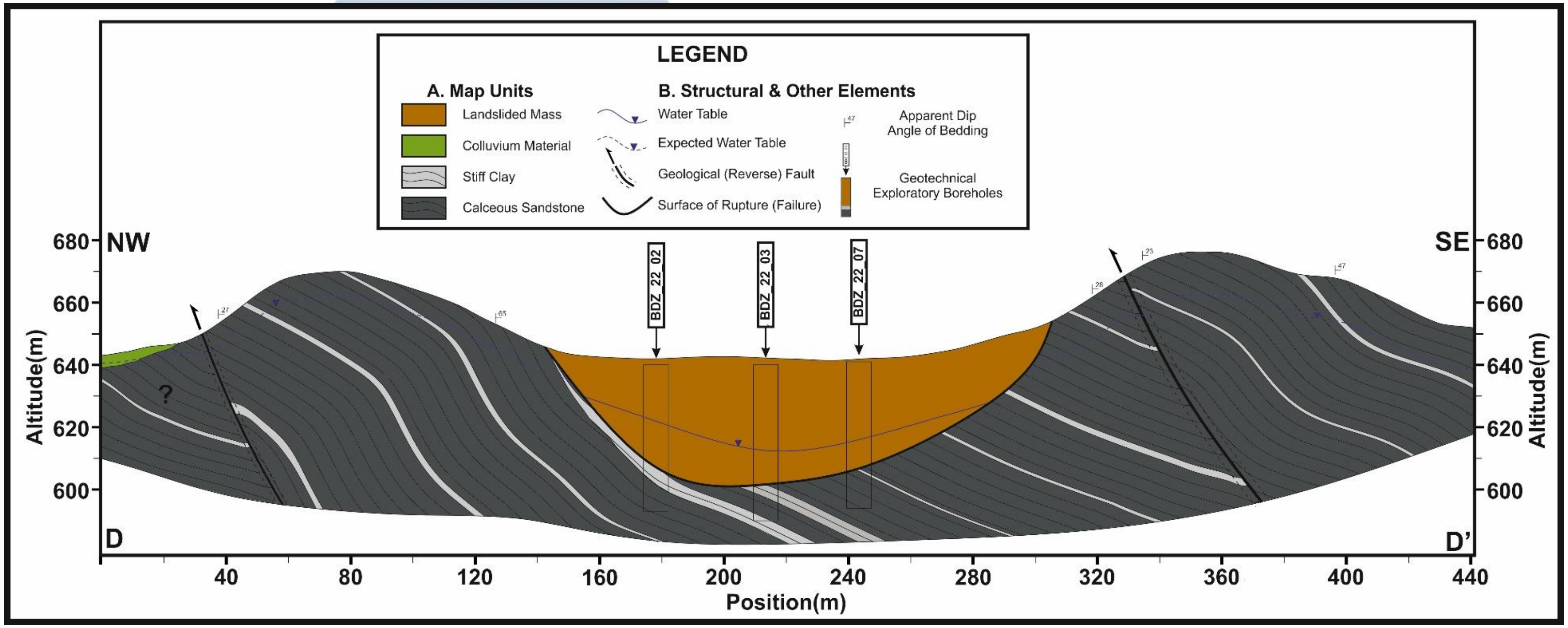

*Figure 106. Geological & Engineering Geological Long Section DD'.*

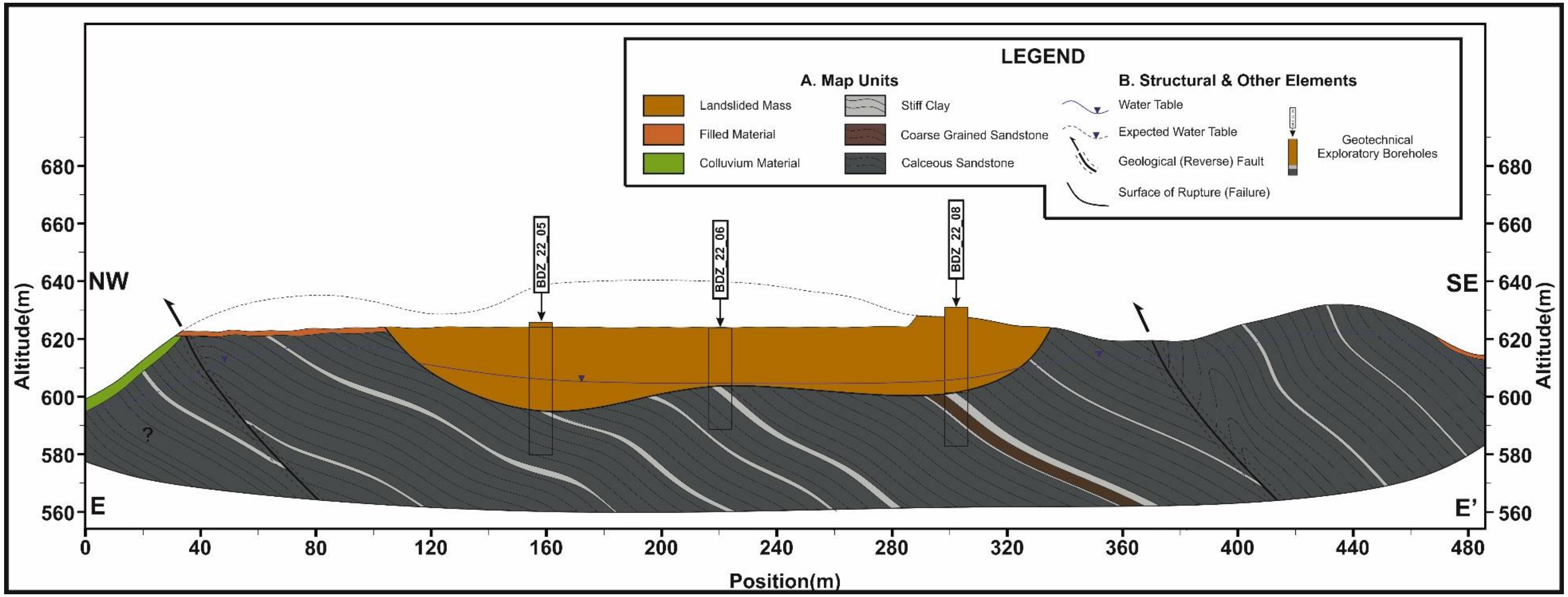

*Figure 105. Geological & Engineering Geological Long Section EE'.*

## 6.3 Conclusions

From the combination of surface, subsurface geological and engineering geological investigation and geotechnical monitoring, the geological and engineering geological model is acquired. The underlying model is about to used, to determine the mechanical characteristics of the sliding zone, which is vital in order to propose the most appropriate counter balance measures.

At the underlying sections, the visualization of the statements referred at previous chapters, is taking place. So, at the underlying sections the presence of the stiff grey clayey material as lenses into the bedrock, is appear as the lenses of formation composed by coarse grained sand. Furthermore, the active reverse faults are illustrated well at DD’ and EE’ sections. In general, ductile deformation of restricted magnitude can be also observed, with increment in the magnitude of deformation adjacent to the reverse faults.

Regarding the water table, it is observed higher at the northern flank of the landslide than the southern flank, in contrast to the fact of higher geomorphologically territories at south.

The surfaces of the rupture seem to be curves. More precisely two major surfaces are depicted at the sections. The first surface (A) is indicated by the inclinometers and drill core evaluation, and the second (B), by geological and engineering geological assessment, during and after the major incident. In general, the surface A with an exception at the toe of the landslide seems to be continuously below water level in contrast to the surface B, which means that the surface A can be activate easily than B, which seems to be more circular than A.

At the underlying model the problems involved, from the activation of the landslide are clearly presented. At the section is lucidly shown that further excavation, in order to the alignment being reached, will further activate the landslide. Considering that the landslide is still on motion, essential features downslope, are still exposed to risk. The first feature is the river Zvaroula. The potential formed or barrier, from the landslide would block the river, resulting a reservoir to the upslope to river territory. Beside the environmental and social problems produced from the underlying condition, the use of the tunnel southern to the landslide would not be feasible. The second feature involves is the road, which droves to the village of Nunisi at south, destination which attracts lot of visitors. So, the blockage of the road would provide issues regarding the local society. The last feature involved, is the springs of natural carbonated water, located at the left bank of river Zvaroula. The maintenance of the underlying springs in the area is considered vital.

# Chapter 7 Geotechnical Investigation

## 7.1 General

The major aim of the present chapter is to estimate mechanical, design parameters for the geological and engineering geological units involved in the formation of landslide. Generally, two major units were resulted from the geological and the engineering geological investigation. Those units are the stable bedrock, including clayey and sandy formations as lenses, and the unstable landslide origin, clayey material, formed by old landslide or even landslides.

The bedrock is mostly composed by calcareous fine-grained sandstone and it is considered stable. However, the steep slopes formed by the occurrence of the landslide, activates rock slides at the bedrock, composed by sliding surface, the bedding. Such examples can be noticed at the north flank of the landslide, northern of BDZ_22_2 borehole. The shear strength of the bedrock and the shear strength of the surfaces of discontinuities such as bedding, at the underlying position, are impacted by hydrothermal alteration, and finally is reduced. Generally, the alteration seems to be intense at the northwestern part of the landslide where there is an occurrence of active geological reverse fault.

Beside the hydrothermal alteration, the tectonic activity is also responsible for the reducing in the shear strength of the bedrock. Considering that the area of study is located among two sizable faults, with thick sheared zones, in relatively close distance, the imprint of their activity at the bedrock is obvious, which in general appears to be very fractured.

Of course, the bedrock contains lenses of grey stiff clay of high plasticity, as well as lenses of deep brown to dark colored, coarse grained sandstone. All lenses involved are considered stable.

The estimation of physical and mechanical properties of landslide material is considered difficult and complicated procedure, considering the heterogeneity of the material. First of all, as it is reference in previous chapters, the shear strength of the surface of rupture is different than the shear strength of the material in general. The engineering geological model indicates as a type of the failure, rotational type of landslide, which means that the shearing is focused at the surface of the rupture, and the inner deformation is restricted. So, the estimation of the shear strength at the surface of rupture will be carried out by back analysis. However, the estimation of the shear strength of the material overburden to the surface of rupture is complicated procedure. Since the fact that the strength of the surface of rupture cannot be acquired by laboratory tests, it cannot be acquired for the overburden material either due to extensive heterogeneity which characterizes the material. Furthermore, back analysis on the overburden landslide material cannot be occurred considering the fact at the time of the failure of specific part it is not known. Although, the underlying parameter can be approached by complicated equations, which are taking account the matric suction, the vegetation and other factors, it will be used for limited, or even none, applications. That is the main reason why the shear strength of the material overburden to the surfaces of rupture are not estimated.

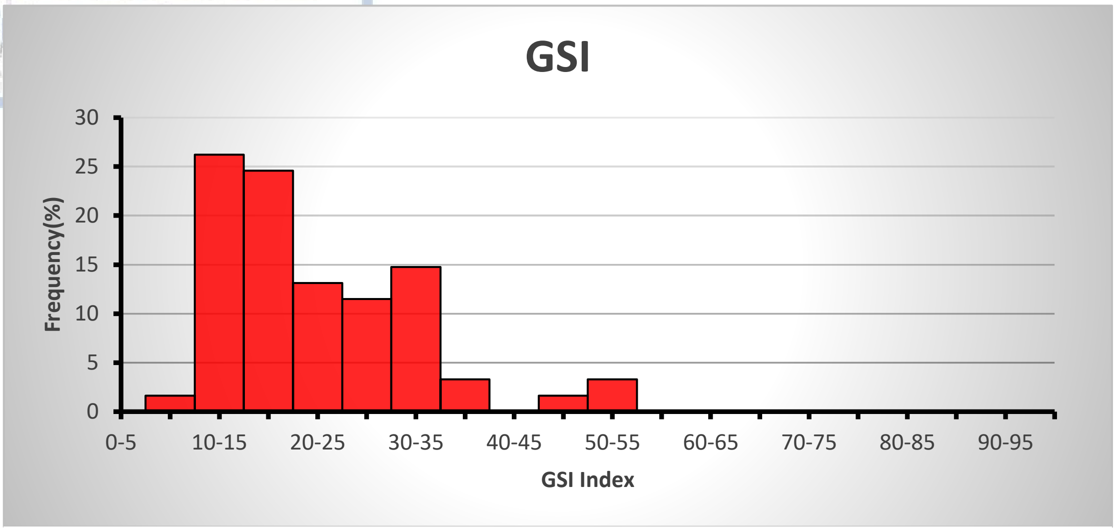

*Figure 107. Distribution of estimated by drill cores GSI index (Conservative).*

## 7.2 Estimated design parameters of rock mass

In order to investigate the engineering geological and geotechnical conditions for the sandstone which is the stable bedrock in this investigation, values of unconfined compressive strength (UCS) and unit weight were assumed from bibliographical sources. More precisely the value of UCS on sandstones according to *Waltham T., 2009*, ranges between 10-90 MPa. According to *Marinos P.V., & Tsiabaos G., 2010*, the UCS of sandstones at flysch and molassic type formations in Greece, ranges between 10-46MPa. Furthermore, the unit weight of sandstone is considered 24kN/$m^3$.

The drilled core samples of the bedrock are classified by RMR and GSI classification systems, and RQD index is assign to. The classification of the bedrock is vital in order to produce Mohr-Coulomb parameters, which will be used in the analysis. It is worth mentioning that each classification system approaches the required parameters differently, so the outcome of the same parameters from each system will be different.

### 7.2.1 Estimation of Shear Strength from GSI

The Geological Strength Index (GSI) were introduced as it is now, in order to be applicable, and provide *m* and *s* factors for Hoek Brown equation regarding the shear strength *(from Carter T.G., and Marinos V.P., 2014*). Furthermore, the underlying index could also provide parameters regarding shear strength of Mohr Coulomb criterium. In general, GSI constitutes more friendly approach for rock mass classification from geologists and engineering geologists and it can be defined quickly and easily in the field. GSI index is characterized by more geological rather than clearly engineering point of view. It generally depicts structure of the rock mass and the condition of the discontinuities among the formed blocks *(Carter T.G., and Marinos V.P., 2014*).

The mean GSI value estimated by all the boreholes combined, approaches 25-30, considering seamy and disturbed structure combined by poor conditions regarding to the surfaces of discontinuities. In the conservative scenario, taking into account that the UCS is equal to 10 MPa, assuming values of *MR* and $m_i$ indexes, is possible to produce the required Mohr-Coulomb parameters.

Regarding the value of MR index, concerning sandstones, according to *Marinos P.V., and Tsiabaos G., 2010,* it ranges between 80-300 with mean value of 140 for flysch type formations, and 100-260 with mean value of 170 for molassic type formations in Greece. Previous studies in propose values of MR in sandstones with range of 200-350 (*from Marinos P.V., and Tsiabaos G., 2010; Deere D.U., 1968; Palmstrom A., Singh R., 2001*). In contrast to the value of $m_i$ index for sandstones, which is estimated by *Marinos G.P., and Hoek E., 2000*, equal to17±4.

| Formation | UCS(MPa) | GSI | MR | mi |
|---|---|---|---|---|
| Sandstone | 10 | 25-30 | 155 | 17 |

*Table 10. Mechanical and Physical Properties of Sandstone*

Taking into account parameters derived from *table 10,* it is possible to calculate the required parameters in Roc Data 5.0 of RocScience. More precisely the cohesion is calculated equal to **c=380kPa**, and the friction angle equal to **ϕ=27°.**

### 7.2.2 Estimation of Shear Strength from RMR

The Rock Mass Rating (RMR) classification system was initially introduced by *Bieniawski Z.T., 1973*, for rock mass classification, during underground constructions, and more precisely, tunneling. At 1985 modifications have been made in order for the underlying system be applicable at slope stability problems (*Romana M., 1985*). The system takes into account (*Bieniewski T.Z., 1989*):

- The unconfined compressive strength of the intact rock
- The RQD index from boring,
- Spacing and conditions of discontinuities,
- Groundwater conditions and
- Orientation of discontinuities regarding the construction.

At the present study, the major discontinuity is the bedding, which is considered very favorable taking into account that {dip direction of slope - dip direction of bedding}>30.

The mean RMR index, which is estimated by all boreholes combined, approaches 28-33. According to *Bieniewski T.Z., 1989,* the strength of the rock mass regarding Mohr-Coulomb parameters, taking into account only the RMR index, is estimated to cohesion **c=100-200kPa**, and the friction angle **ϕ=15-25°.**

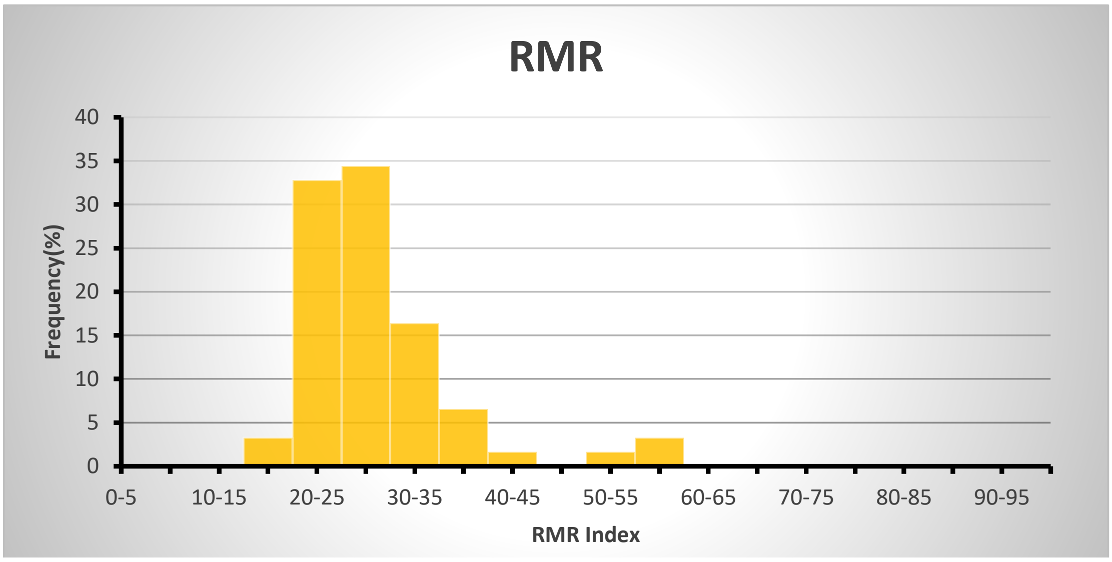

*Figure 108. Distribution of estimated by drill cores RMR index (conservative).*

To sum up, taking into consideration the shear strength of rock mass, provided by both classification systems, the bedrock is maintained stable. However, in weak rock mass, such as in this case, the estimated shear strength parameters are more valid, whether they are produced by GSI classification system *(Galera J.M., et al., 2007; Carter T.G., and Marinos V.P., 2014).* Consequently below, in stability analysis, cohesion **c=380kPa**, and the friction angle **ϕ=27°** will be used for the bedrock.

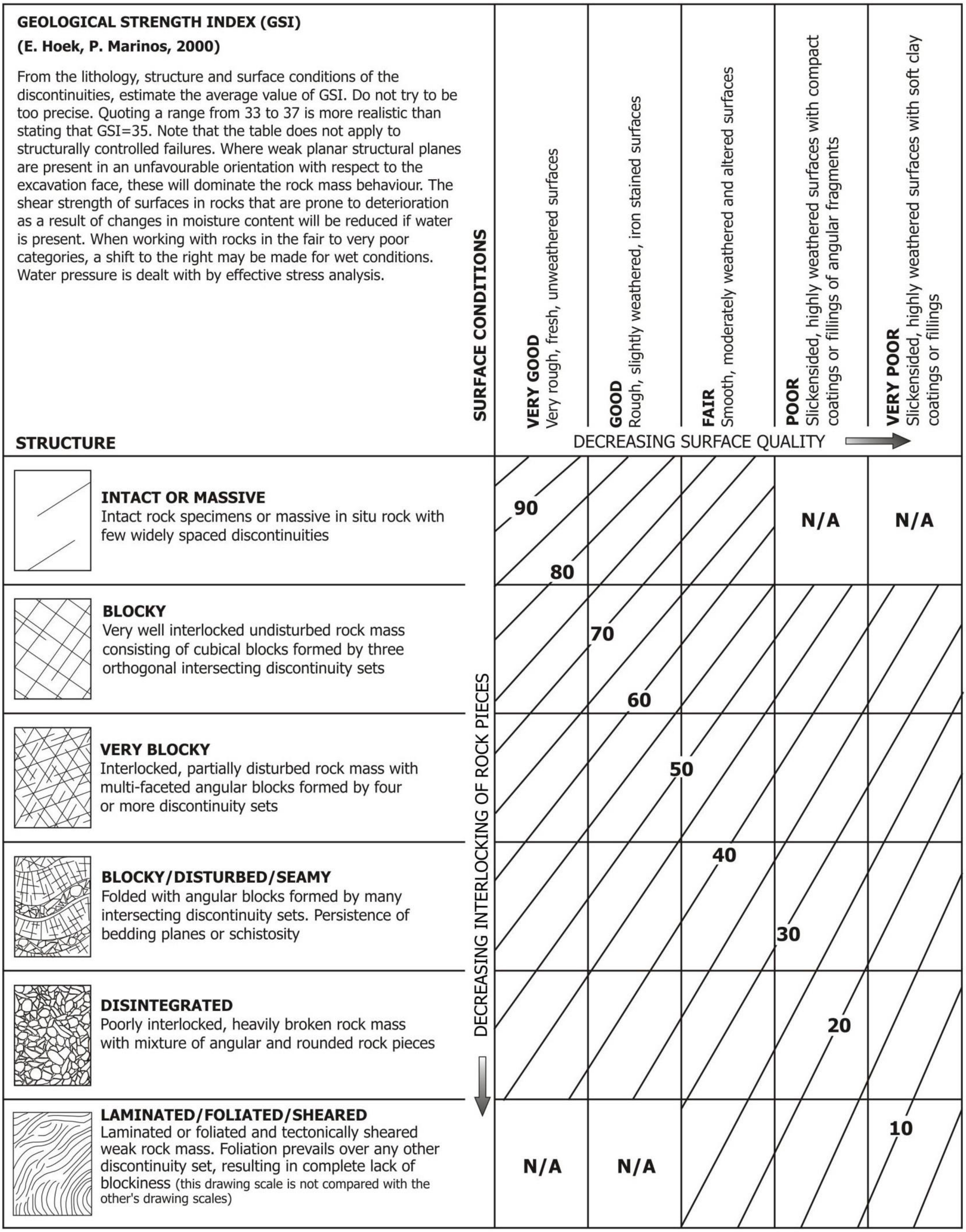

**GEOLOGICAL STRENGTH INDEX (GSI)**
**(E. Hoek, P. Marinos, 2000)**

From the lithology, structure and surface conditions of the discontinuities, estimate the average value of GSI. Do not try to be too precise. Quoting a range from 33 to 37 is more realistic than stating that GSI=35. Note that the table does not apply to structurally controlled failures. Where weak planar structural planes are present in an unfavourable orientation with respect to the excavation face, these will dominate the rock mass behaviour. The shear strength of surfaces in rocks that are prone to deterioration as a result of changes in moisture content will be reduced if water is present. When working with rocks in the fair to very poor categories, a shift to the right may be made for wet conditions. Water pressure is dealt with by effective stress analysis.

**VERY GOOD** Very rough, fresh, unweathered surfaces

**GOOD** Rough, slightly weathered, iron stained surfaces

**FAIR** Smooth, moderately weathered and altered surfaces

**POOR** Slickensided, highly weathered surfaces with compact coatings or fillings of angular fragments

**VERY POOR** Slickensided, highly weathered surfaces with soft clay coatings or fillings

**INTACT OR MASSIVE** Intact rock specimens or massive in situ rock with few widely spaced discontinuities

**BLOCKY** Very well interlocked undisturbed rock mass consisting of cubical blocks formed by three orthogonal intersecting discontinuity sets

**VERY BLOCKY** Interlocked, partially disturbed rock mass with multi-faceted angular blocks formed by four or more discontinuity sets

**BLOCKY/DISTURBED/SEAMY** Folded with angular blocks formed by many intersecting discontinuity sets. Persistence of bedding planes or schistosity

**DISINTEGRATED** Poorly interlocked, heavily broken rock mass with mixture of angular and rounded rock pieces

**LAMINATED/FOLIATED/SHEARED** Laminated or foliated and tectonically sheared weak rock mass. Foliation prevails over any other discontinuity set, resulting in complete lack of blockiness (this drawing scale is not compared with the other's drawing scales)

*Figure 109. GSI chart (Hoek E., Marinos P., 2000).*

**TABLE 4.1 The Rock Mass Rating System (Geomechanics Classification of Rock Masses)[a]**

**A. CLASSIFICATION PARAMETERS AND THEIR RATINGS**

| | Parameter | | Ranges of Values | | | | | | |
|---|---|---|---|---|---|---|---|---|---|
| 1 | Strength of intact rock material | Point-load strength index (MPa) | >10 | 4–10 | 2–4 | 1–2 | For this low range, uniaxial compressive test is preferred | | |
| | | Uniaxial compressive strength (MPa) | >250 | 100–250 | 50–100 | 25–50 | 5–25 | 1–5 | <1 |
| | Rating | | 15 | 12 | 7 | 4 | 2 | 1 | 0 |
| 2 | Drill core quality RQD (%) | | 90–100 | 75–90 | 50–75 | 25–50 | <25 | | |
| | Rating | | 20 | 17 | 13 | 8 | 3 | | |
| 3 | Spacing of discontinuities | | >2 m | 0.6–2 m | 200–600 mm | 60–200 mm | <60 mm | | |
| | Rating | | 20 | 15 | 10 | 8 | 5 | | |
| 4 | Condition of discontinuities | | Very rough surfaces<br>Not continuous<br>No separation<br>Unweathered wall rock | Slightly rough surfaces<br>Separation < 1 mm<br>Slightly weathered walls | Slightly rough surfaces<br>Separation < 1 mm<br>Highly weathered wall | Slickensided surfaces<br>or<br>Gouge < 5 mm thick<br>or<br>Separation 1–5 mm<br>Continuous | Soft gouge > 5 mm thick<br>or<br>Separation > 5 mm<br>Continuous | | |
| | Rating | | 30 | 25 | 20 | 10 | 0 | | |
| 5 | Groundwater | Inflow per 10 m tunnel length (L/min) | None | <10 | 10–25 | 25–125 | >125 | | |
| | | | or | or | or | or | or | | |
| | | Ratio $\frac{\text{Joint water pressure}}{\text{Major principal stress}}$ | 0 | <0.1 | 0.1–0.2 | 0.2–0.5 | >0.5 | | |
| | | | or | or | or | or | or | | |
| | | General conditions | Completely dry | Damp | Wet | Dripping | Flowing | | |
| | Rating | | 15 | 10 | 7 | 4 | 0 | | |

**B. RATING ADJUSTMENT FOR DISCONTINUITY ORIENTATIONS**

| Strike and Dip Orientations of Discontinuities | | Very Favorable | Favorable | Fair | Unfavorable | Very Unfavorable |
|---|---|---|---|---|---|---|
| Ratings | Tunnels and mines | 0 | −2 | −5 | −10 | −12 |
| | Foundations | 0 | −2 | −7 | −15 | −25 |
| | Slopes | 0 | −5 | −25 | −50 | −60 |

**C. ROCK MASS CLASSES DETERMINED FROM TOTAL RATINGS**

| Rating | 100 ← 81 | 80 ← 61 | 60 ← 41 | 40 ← 21 | <20 |
|---|---|---|---|---|---|
| Class no. | I | II | III | IV | V |
| Description | Very good rock | Good rock | Fair rock | Poor rock | Very poor rock |

**D. MEANING OF ROCK MASS CLASSES**

| Class no. | I | II | III | IV | V |
|---|---|---|---|---|---|
| Average stand-up time | 20 yr for 15-m span | 1 yr for 10-m span | 1 wk for 5-m span | 10 h for 2.5-m span | 30 min for 1-m span |
| Cohesion of the rock mass (kPa) | >400 | 300–400 | 200–300 | 100–200 | <100 |
| Friction angle of the rock mass (deg) | >45 | 35–45 | 25–35 | 15–25 | <15 |

*Figure 110. RMR Chart (Beniewski T.Z., 1989).*

## 7.3 Estimated design parameters for the Landslide Material

### 7.3.1 General

As it is referenced previously, the estimation of physical and mechanical parameters in the landslide material is considered complicated and difficult procedure, taking into account the heterogeneity by which the material is constituted. So, the estimation of the strength of material from laboratory and in situ tests would attribute apparent parameters, different from the real ones and generally the results from the underlying tests are overestimate the real parameters of the material, which could drive to massif failures.

In rotational landslides, the surface of failure is likely to be circular or non-circular curve. The circular curves are usually observed in homogenous geomaterial and contrary, non-circular curves are commonly observed at heterogenous geomaterial (*Knappett J.A., & Craig, R.F., 2012*). So, in this case the geological and engineering geological model indicates non-circular surface, in agreement with the underlying statement. Regarding the slope stability analysis, limit equilibrium methods are widely used such as Bishop simplified method, Janbu simplified method, Janbu corrected method etc. Bishop's simplified method is commonly used whether the surface of shearing is considered circular. In contrast, Janbu's methods are used whether the surface of failure is non-circular (*Cornforth, D.H., 2005*). In this case considering that the surface of failure is non-circular, Janbu's corrected method is used for the stability analysis.

In back analysis, stability analysis occurs in the beginning of the failure process considering that in this state the factor of safety is equal to unit. The underlying process removes one of the unknow factors from the stability analysis. Regardless the factor of safety (FS), other required parameters involved in stability analysis are the geometry of the slope, the density of the failed formation, the surface of rupture, the shear strength of the formation and the pore water pressure (*Cornforth, D.H., 2005*). The geometry of the slope could be estimated from topo survey, the surface of rupture could be provided by boring and instrumentation, such as inclinometers, and the pore water pressure from piezometers. Regarding the density of under failure formation, it can be assumed or few cases could be taken into account, considering that the density influences both driving and resisting forces, so the effects of the density of the material are restricted. However, the estimation of shear strength parameters, which is crucial factor during stability analysis, is generally considered as a large source of uncertainties *(Tang W.H., et all., 1999).*

It is difficult to estimate the shear strength parameters from laboratory testing, because the simulation of the in-situ conditions in the laboratory contains a lot of uncertainties. The parameters which should be taken into consideration for the estimation of the prevailed field conditions in the laboratory are the effective normal stress, the surface of failure, pre-existing deformation, drainage during shearing, magnitude and rate of shear displacement etc. *(Tang W.H., et all., 1999).* Even though the simulation of the field conditions were completely reliable, and consequently the results regarding the testing material were also reliable, the testing would still be occurred on constrained amount of material, which is hardly representative of the total material. This is the major source of uncertainties regarding in situ testing too. So, in order for them to be representable a vast number of tests should be carried out, which is correlated with crucial increasing in the cost of the investigation. Contrary, back analysis can calculate the average shear strength representative for total surface of failure, with relatively low cost *(Cornforth, D.H., 2005).*

The estimation of shear strength by back analysis is considered one of the most valid methods in geotechnical engineering (*Tang W.H., et all., 1999; Cornforth, D.H., 2005*), however, even in this type of analysis uncertainties exist. Firstly, it is difficult to estimate the accurate geometry of the slope, as well as the pore water pressure at time of activation. Of course, the calculation of the density of the material still constitutes an uncertainty. Furthermore, even the surface of failure could be different than the estimated one. However, the magnitude of uncertainties in back analysis, is clearly constrained compared to the estimation of shear parameters by other methods as laboratory and in-situ testing.

In this case the geometry of the slope when failure occurred is known with great accuracy. The surface of failure is obtained by instrumentation and geological-engineering geological evaluation. So, in order to eliminate any uncertainty regarding the surface of rupture, both cases should be examined. Concerning the groundwater, information is drawn by the piezometers. However, the information regarding the piezometrical head is acquired after the occurrence of the incident. As the phenomenon of the landslide developed, surface ruptures at the area of landslide opened, with a result of dropping of the phreatic water table. Those cracks are also responsible for the elimination of pore water pressure, which could be developed in the shear zone.

Nevertheless, in this case, considering the phreatic water table at the measured level and the correlation of the phreatic water table with the total piezometrical head, constitutes conservative approach, and therefore the results would be acceptable, considering that there is no other way to estimate the underlying factors at the time of failure. This approach is conservative because of the activation of the surface ruptures or cracks, but also due to the period of the monitoring. The monitoring was carried out at the begging of the September, which considered dry period, contrary to the May, in which the rainfall and the snow melting provide vast amount of water, and consequently the level of groundwater is shallower compared to the September. However, another case with hypothetic shallow water table, should be examined too, in order to cover uncertainties regarding the stability and understand better the model. Considering that the influence of pore water pressure and in general the influence of the level of water table is great, the shear strength provided by the back analysis for hypothetical shallow water table, would be considered as the maximum shear strength in the surface of rupture.

The density of the material affects both driving and resisting forces during calculation of safety factor. So, the error regarding the density seems to be eliminated, and the produced uncertainty, compared to the shear strength or groundwater variation, is relatively small for

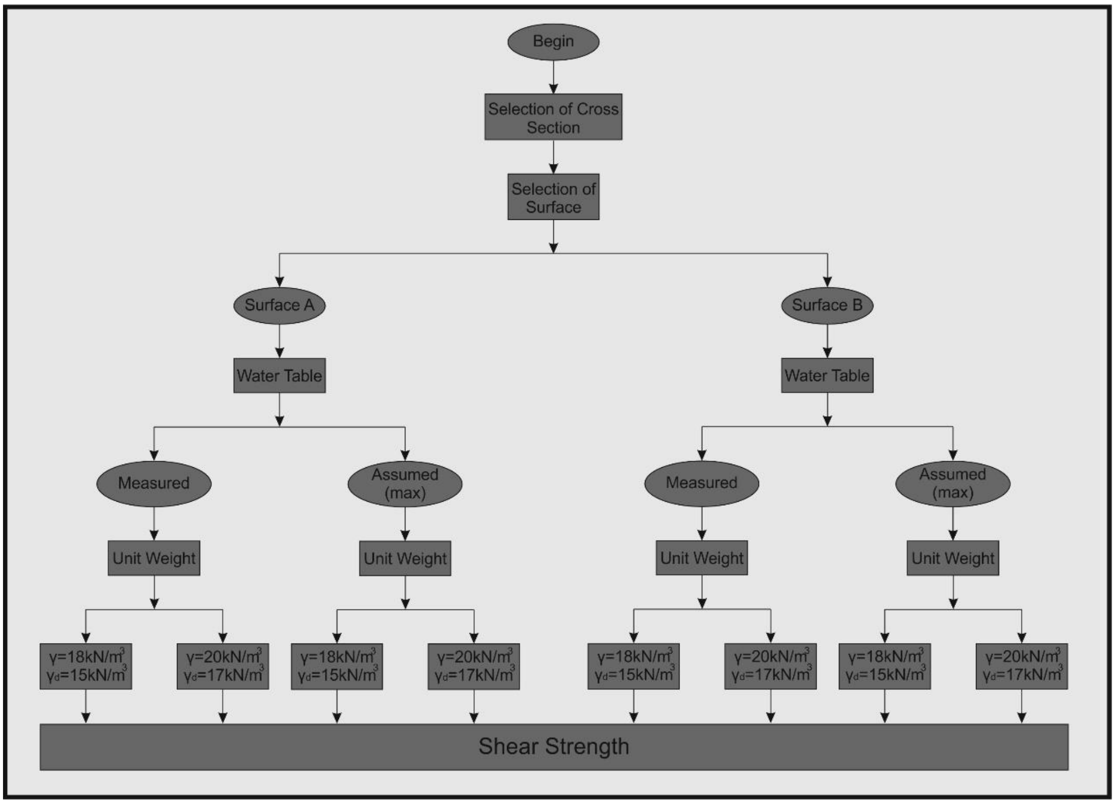

*Figure 111. The procedure of stability analysis.*

stability analysis (*Cornforth, D.H., 2005).* However, stability analysis cannot be carried out without estimation of the material density. Of course, in this case, the underlying property of the material cannot be estimated accurately mostly due to materials' heterogeneity. So, it is more valid to examine the stability for more than one value of density. Through the stability analysis, saturated unit weight and unsaturated unit weight is required. Taking into account the geological history of the deposition of the examined geomaterial, which is mainly composed by unconsolidated, very soft to soft gravelly clay with angular fragments and boulders, and is deposited mostly at dry conditions which did not allowed further compaction-consolidation, the unit weight is expected to be restricted. More precisely, two major hypotheses were examined in order to cover possible uncertainties. The first assumption examines the stability, taking into account saturated and unsaturated unit weight equal to $\gamma=18kN/m^3$ and $\gamma_d=15kN/m^3$ respectively. The second hypothesis examines the stability taking into account saturated and unsaturated unit weight equal to $\gamma=20kN/m^3$ and $\gamma_d=17kN/m^3$ respectively.

Although now, the data regarding the unit weight, the surface of rupture and the piezometrical head, are more less known, back analysis cannot be implemented for the current situation, considering that the landslide, as it is indicated by inclinometers, is still on motion. This means that the static factor of safety now, is lower than unit, and its accurate is not known. So, it is essential to implement back analysis for the initial rupture at 13/05/2017.

It is worth to point out that the back analysis will occur in order to detect the shear strength parameters in the surface of shearing. It does not mean that the produced strength represents the shear strength of the material overburden to the shear zone. Of course, the shear strength parameters beyond the shearing zone, can be estimated by other methods.

The analysis below, took place at Computer Program, Slide 7.0 of RocScience, regarding no-circular surfaces and factor of safety calculated with Janbu's corrected method.

### 7.3.2 Back Analysis Procedure

Using the information provided from the previous chapter, back analysis was executed. Of course, the analysis was carried out in several cases in order to cover any existing uncertainties. First of all, the analysis was implemented for five cross sections. The sections AA', FF', and GG' is oriented parallelly to the axes of the movement, in contrast the section BB' is oriented approximately parallelly to the axes of the movement and the section CC' is oriented with >20° regarding the movement. This generally means that results regarding the shear strength provided by CC' section would be a very conservative approach, and should be considered as the minimum shear strength.

| Section | Surface A | | | | | | | |
|---|---|---|---|---|---|---|---|---|
| | Water Table 1 | | | | Water Table 2 | | | |
| | $\gamma_d=15$, $\gamma=18$ (kN/m$^3$) | | $\gamma_d=17$, $\gamma=20$ (kN/m$^3$) | | $\gamma_d=15$, $\gamma=18$ (kN/m$^3$) | | $\gamma_d=17$, $\gamma=20$ (kN/m$^3$) | |
| | φ° | FS | φ° | FS | φ° | FS | φ° | FS |
| AA' | 10,35 | 1,005 | 10,25 | 1,002 | 16,90 | 1,006 | 15,60 | 1,003 |
| BB' | 14,65 | 1,000 | 14,40 | 1,003 | 23,00 | 1,001 | 21,20 | 1,001 |
| CC' | 9,60 | 1,005 | 9,45 | 1,005 | 15,65 | 1,006 | 14,40 | 1,004 |
| FF' | 11,90 | 1,003 | 11,50 | 1,002 | 16,50 | 1,000 | 15,40 | 1,003 |
| GG' | 14,25 | 1,003 | 14,10 | 1,002 | 24,00 | 1,002 | 23,95 | 1,000 |

*Table 11. Friction angle and safety factor regarding the surface of rupture(B) derived by instrumentation, unit weights and water tables.*

| Section | Surface B | | | | | | | |
|---|---|---|---|---|---|---|---|---|
| | Water Table 1 | | | | Water Table 2 | | | |
| | $\gamma_d=15, \gamma=18$ (kN/m$^3$) | | $\gamma_d=17, \gamma=20$ (kN/m$^3$) | | $\gamma_d=15, \gamma=18$ (kN/m$^3$) | | $\gamma_d=17, \gamma=20$ (kN/m$^3$) | |
| | φ° | FS | φ° | FS | φ° | FS | φ° | FS |
| AA | 10,25 | 1,003 | 10,25 | 1,004 | 17,50 | 1,004 | 16,20 | 1,002 |
| BB | 13,15 | 1,000 | 13,05 | 1,002 | 21,75 | 1,003 | 20,20 | 1,006 |
| CC | 7,30 | 1,000 | 7,30 | 1,004 | 12,80 | 1,001 | 11,85 | 1,002 |
| FF | 9,55 | 1,003 | 9,4 | 1,006 | 13,8 | 1,005 | 12,80 | 1,000 |
| GG | 13,15 | 1,000 | 13,15 | 1,003 | 23,25 | 1,006 | 21,40 | 1,000 |

*Table 12. Friction angle and safety factor regarding the surface of rupture(B) derived by geological-engineering geological evaluation, unit weights and water tables*

In *figure 111,* the procedure of back analyses is described in detail. In the beginning, the examined section (AA', BB', CC', FF', GG') was selected. Afterwards, the selection of the surface of shearing took place. The surface A, is indicated by the inclinometers and boring, and the surface B was observed right after the failure in the site of construction. Thence, the selection of the water table occurred. The options are the measured water table level (1) and a hypothetical shallower water table (2), with approximately 5m from the surface, by which the maximum shear strength is attributed. To continue, two cases regarding the unit weight are also analyzed.

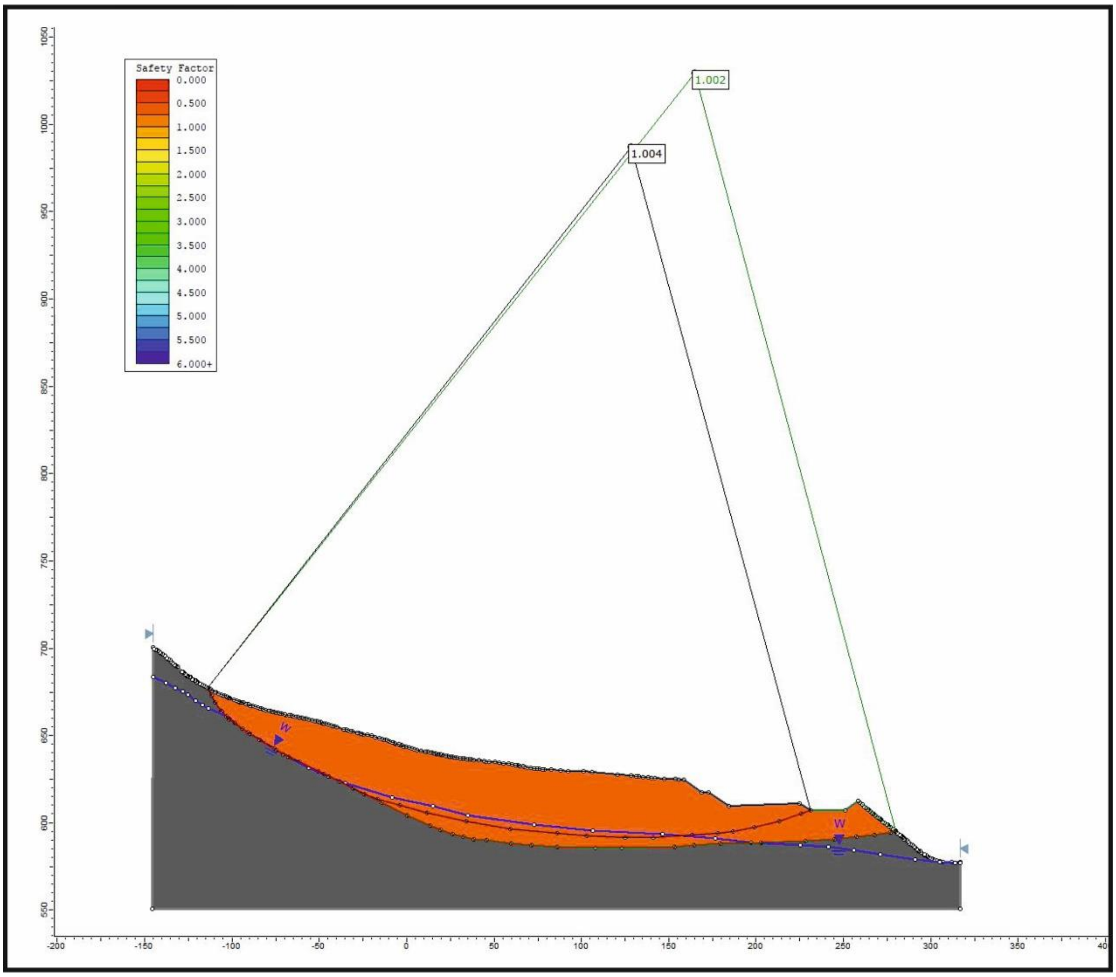

*Figure 112. The Back analysis for the established engineering geological model for shear strength regarding the landslide mass with unit weight 17kN/m$^3$ and saturated unit weight 20kn/m$^3$, and shear strength expressed only by friction angle φ=10,25°*

Taking into consideration the underlying data, and also static safety factor equal to unit, the stability analysis back calculates the average shear strength on the inputted surfaces of rupture. More precisely, considering that the shear strength is commonly expressed by Mohr-Coulomb parameters, the cohesion (c) and the friction angle (ϕ°), usually in these cases the cohesion is assumed as equal to zero (0), and the calculation occurs only for the friction angle, for each case.

As it is referenced, the expected results regarding the shear strength on the failure surfaces, at section CC' are too conservative shear strength for critical static factor of safety. Of, course the expected assumption is confirmed by the results of the analysis.

From the acquired by the analyses results, the maximum deviations considering only uncertainty the unit weight, is observed with magnitude of 1,85°, in GG' section, for the surface B, and water table 2. In general, the deviations regarding the unit weight are above 1°, when the water table 2 is chosen. Deviations no higher than half degree are observed when the water table 1, the measured water table, is chosen. For the section AA', which is considered the critical section, the deviations regarding the unit weight are approximately equal to 1,3°, for water table 2, and lesser than 0,2°, when the measured by piezometers water table is taken into consideration.

To compare, for critical factor of static safety, the shear strength for the two chosen surfaces, maximum deviation approximately equal to 3° is observed at section CC' and 2,7° at section FF', when water table 2 is chosen. Maximum deviations regarding the surface of shearing when the measured water table is chosen, is generally lower by 0,3°. For the section AA', which is considered the critical section, the deviations regarding the surface of rupture is lesser than 0,6°.

The greater deviations are observed in correspondence with the level of water table. More precisely deviations, at a magnitude of 10°, are observed at the section GG'. The average deviation regarding the water table is 6,6±2 degrees. Regarding the AA section, the results are approximately the same, and the deviation ranges from 5,4° to 7,25°. The underlying observation proves the great influence of the groundwater on slope stability projects.

### 7.3.3 Estimation of design Shear strength

Generally, in previous chapters the shear strength at the failure surface, is produced for a combination of conditions regarding the situation at the landslide as it is now (end of engineering geological geotechnical investigation program), and the conditions during the failure. However, it is pointed out that, considering that the monitoring still indicates movements, the static factor of safety in the present is below unit. So, although there is accurate information concerning the current condition regarding the surface of the shearing and the groundwater, back analysis cannot be implemented for the current situation, because the static factor of safety is below unit. Of course, other type of analysis also cannot be conducted considering that there is no information regarding the current topography.

Regarding the groundwater, the conditions have changed from the outset of the rupture, until the end of investigation program. The reason is the presence of surface ruptures or cracks, which are formed after the failure. The landslide material in present could be considered as a material of high permeability, even if it is composed mainly by clay, because of the presents of those cracks. However, taking into account the geological history of the material, which is formed by previous incidents of landslides, the permeability at the outset of the failure, before surface ruptures formed, was high too. Considering that the drainage provided by the cracks offers better drainage, the water table in present cannot reach the surface. This means that the if the shear strength is calculated for the current situation regarding the groundwater, the estimation would be conservative and it will cover other uncertainties.

In contrast to the groundwater conditions which are changed, the shear strength, which is considered residual shear strength, on the surface of shearing, by definition, should not appear great variation. In general, the residual shear strength, which is approached in this situation should not have changed sizably. The residual shear strength in materials after several failures does not really change. Considering that, the under-study material has failed several times at past, the residual shear strength has already formed, so during the under-study failure and the present time the magnitude of shear strength remains approximately the same.

In order to obtain the magnitude of shear strength, back analysis has implemented forty times in total for five cross sections. The average calculated friction angle is equal to 14,6±4,6 degrees. However, the analysis produced conservative and exaggerative values of shear strength. For example, friction angle produced by back analysis on section CC' for the measured water level (ϕ=7.5°) constitutes a conservative approach. In contrast, produced values greater than 20°, constitutes exaggerative approach. Furthermore, at the section AA' the maximum movement occur. This means that the material located at sections FF' and GG', are influenced, or being pushed, by the movement on the main axis. The underlying procedure cannot be represented on 2D back analysis. Considering the underlying fact, the shear strength produced by back analysis at FF' and GG' is constitutes partly conservative approach. So, in order to establish the design shear strength, data derived from the section BB', CC', FF', GG', should be taken into consideration, however, data regarding the shear strength provided by the section AA' should be examined in detail.

Taking everything into consideration, in order to approach the design shear strength for the landslide, friction angle derived by back analysis at section AA', for the measured water table for both surfaces, should be estimated as the design shear strength. So, the average friction angle derived by back analysis taking into consideration the underlying assumptions, is equal to **ϕ=10,25±0,1** degrees.

| A/A | Units | Shear Strength | | Unit Weight (kN/m³) | |
|---|---|---|---|---|---|
| | | Cohesion c (kPa) | Friction Angle ϕ° | Saturated | Unsaturated |
| 1 | Stable Bedrock | 380 | 27 | 24 | - |
| 2 | Unstable Landslide Material* | 0 | 10,25 | 20 | 17 |

*Table 13. Physical and mechanical properties of engineering geological units (* The calculated shear strength is estimates for the surface of the rupture, the shear zone).*

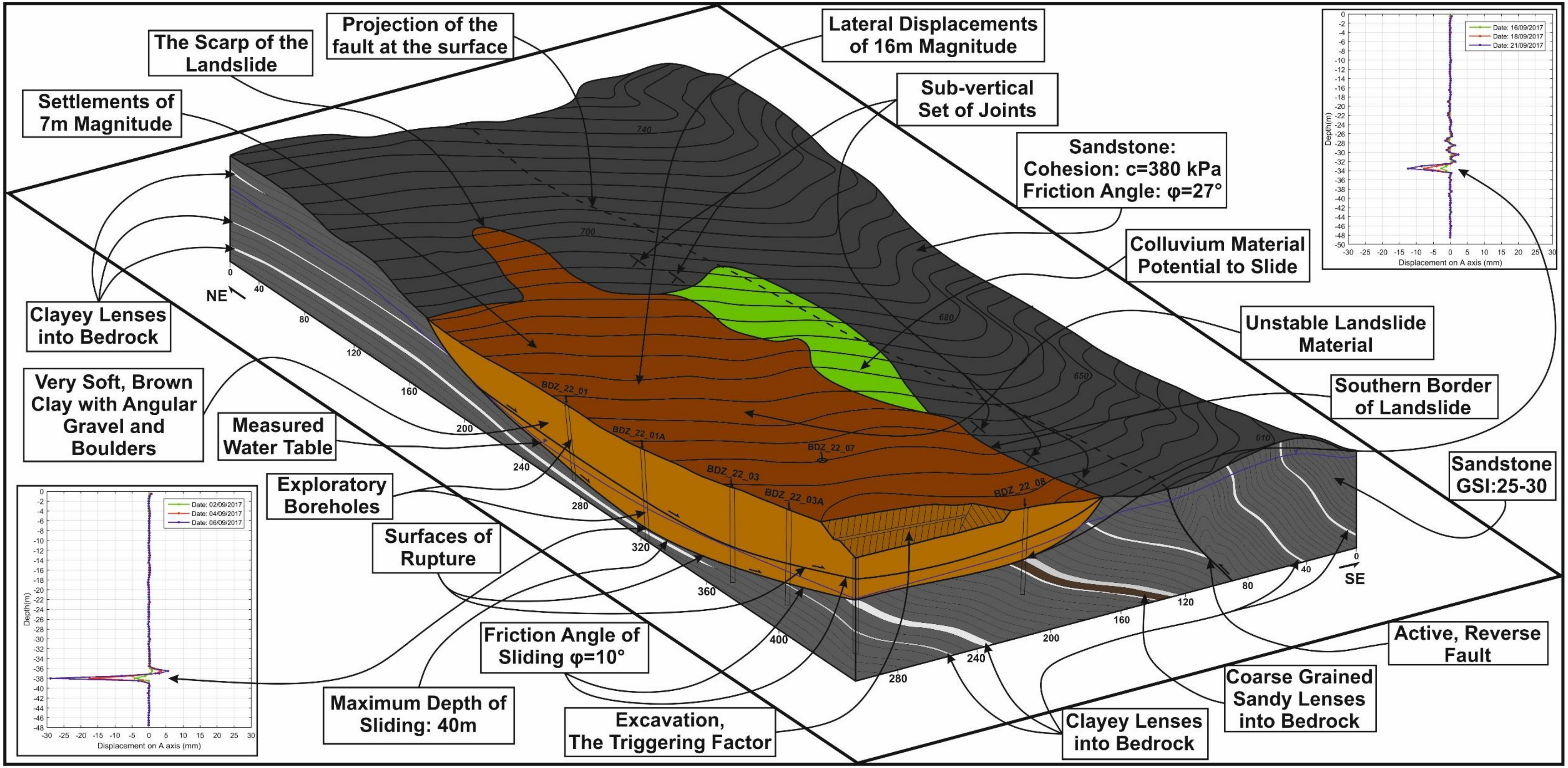

*Figure 113. Conceptual Engineering Geological Model Regarding the South Border of the Landslide*

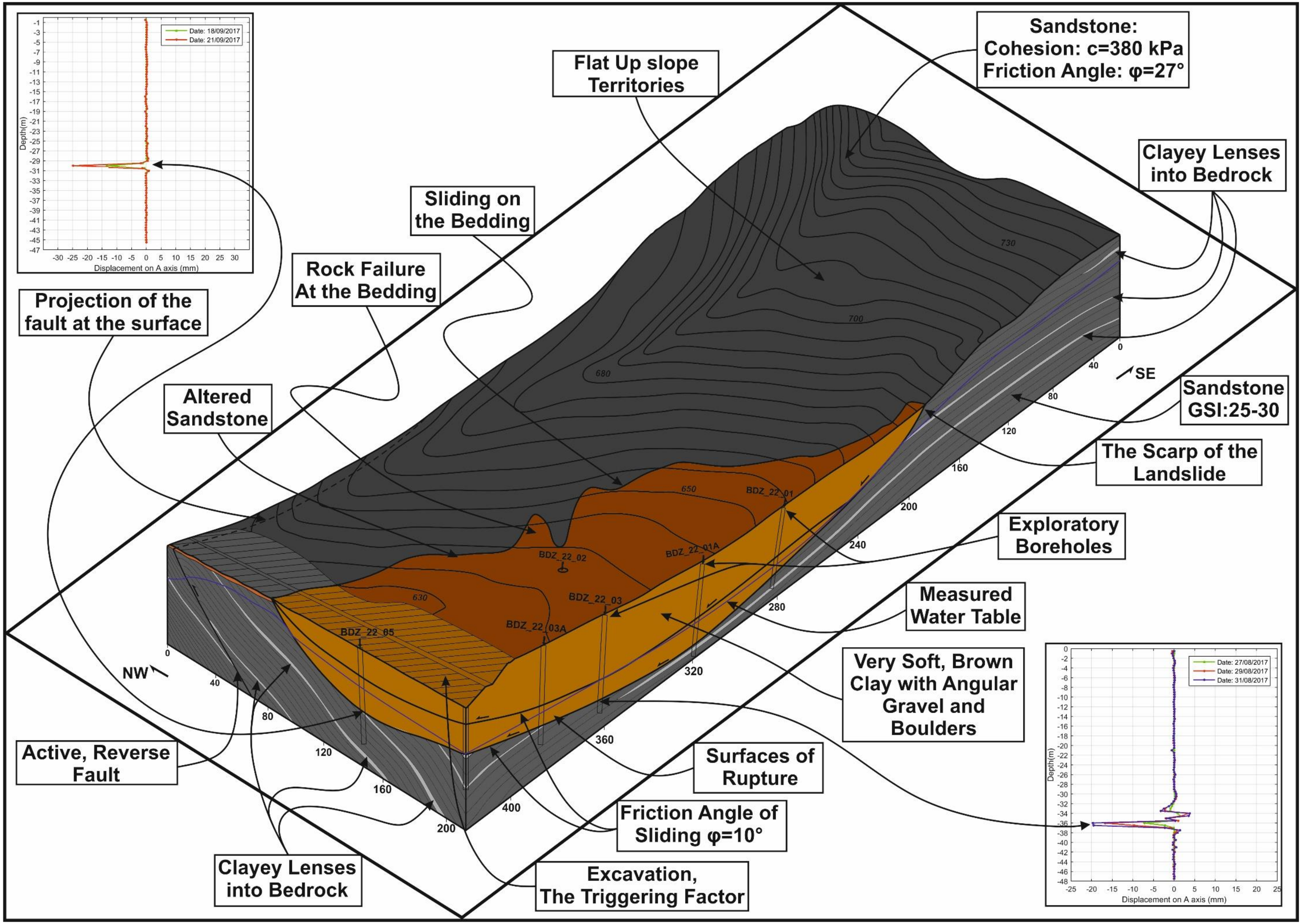

*Figure 114. Conceptual Engineering Geological Model Regarding the North Border of the Landslide*

### 7.4 Conclusions

The purpose of the geotechnical investigation in the present study is to establish design physical and mechanical parameters regarding the engineering geological units involved. The estimation of the underlying parameters regarding the first unit composed by stable bedrock, conducted due to rock mass classification systems. More precisely, bibliographical sources provide the unconfined compressive strength, MR and $m_i$ indexes, and using the RoCData 5.0 of RocSciense, the required Mohr-Coulomb parameters, cohesion and friction angle, were calculated. The

The estimation of physical and mechanical parameters of the second engineering geological unit is considered more complicate procedure. The landslide material constitutes completely heterogenic material, which means that the underlying parameters cannot be defined by laboratory testing. Considering that the failure has occurred, back analysis, at engineering geological conditions at the time of the failure, depicts satisfying results. The analysis carried out for known surfaces, water table, and combination of physical and mechanical properties. The final results regarding the design parameters are illustrated at *table 13.* It is worth to point out that the calculated shear strength represents the shear strength of the surface of rupture. The shear  It is reasonable to compare the output from the underlying procedure, with same case studies. So, the reactivation of landslide of Washington park reservoir slide, constitutes approximately the same conditions, considering that the old landslide reactivated by man-made modifications at the geometry during construction and change in groundwater regime. In this case even the dimensions of the produced landslide are approximately the same with the dimensions of the landslide studied in the present thesis. In case of Washington park reservoir slide, the shear strength of the surface of rupture is also estimated by back analysis. So, the estimated shear strength in this case is represented by cohesion $c=0$ and friction angle $\phi=13.3^o$ (*Cornforth, D.H., 2005*). The underlying results, are relatively close to the calculated by the current study shear strength, which enhances its validity.

# Chapter 8 Suggestions

## 8.1 General

The purpose of this study constitutes counter balance suggestions for the stabilization of the landslide, which, is still on motion. Furthermore, considering that the altitude of the existence alignment, requires further excavations in the toe, solutions regarding realignment should be examined.

Considering the magnitude of the landslide, in order for active measures to be taken, such as anchors, retaining walls and more, the cost would be extremely increased, because those counter measures should have massif dimensions. For example, in order for retaining wall to response on the active lateral earth pressures, it should be founded at depths of 40-50m, and should have thickness of 10-15m, as the length of the anchors should be 30-40m in a very dense grid. So, the cost of the underlying counter measures would be huge, and that is the main reason why those type of counter measures are not applicable in this case. In such cases the most effective solutions, are provided by drainage and earth works.

The importance of the groundwater regime for stability assessments is extensively studied in previous chapters. So, as it is referenced previously, the impact on changes at the groundwater regime, is vital on the stability and that is why the groundwater conditions should be controlled.

In such cases the earthworks require excavations at the head of the landslide and deposition of material at the toe of the landslide, in forms of counterweights or berms. The concept of the approach is described at *figure 115*, in which generally, with the counterweight or berm at toe, the vertical stress is increased, and generally the shear stress is remained the same. That involves the displacement of Mohr cycle to the right, with respect to the vertical stress axis. This is vital in order, the section among the Mohr cycle and Mohr - Coulomb failure envelope, be avoided so no failure occur.

In this case two major scenarios are about to be examined. The first scenario involves the stability assessment without taking into consideration the effects of the dynamic phenomenon, such as earthquake, in contrast to second scenario, in which the impact of earthquake with total acceleration 20% of gravity acceleration g, would be taking into consideration for the stability analysis. More precisely, according to the *Eurocode 8*, whether the total pick ground acceleration is equal to 0,2g, the horizontal is considered equal to 0,1g and the vertical to 0,05g. The underlying data were taken into consideration below, where the analysis is taking into consideration seismic event.

Beside the railroad line and the landslide, other important features should be also taken into consideration, in order to provide solutions, regarding the present problem of stabilization, so the current state of affairs in the area not to be disturbed. Such features are:

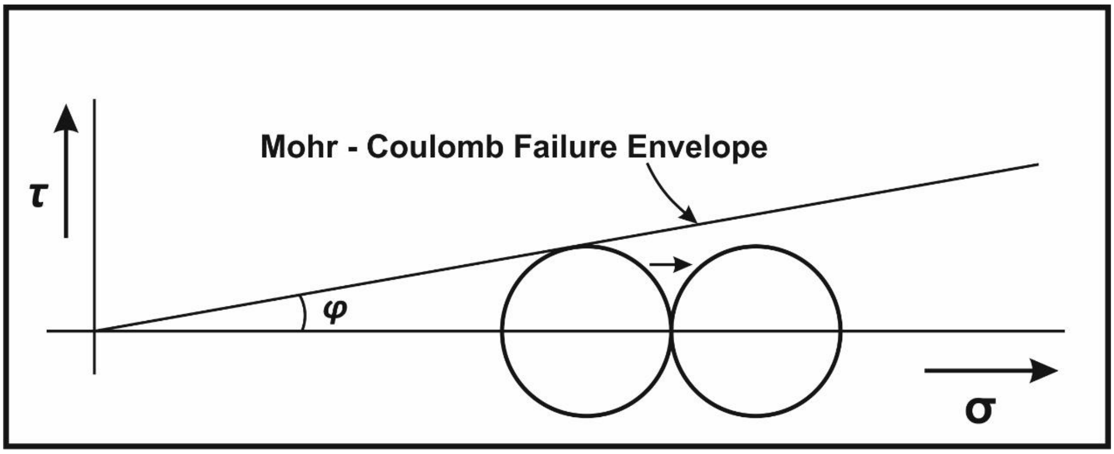

*Figure 115. The concept, the Mohr cycles moving to the right, avoiding the failure envelope, for the counter measures.*

- The river Zvaroula, with impact in stability and general to construction, which is already discussed,
- The road, located at the left bank of the river,
- The springs of natural carbonated water, at the left bank of the river.

The cost of the counter measure works should be taken also into consideration, considering that the cost of the works constitutes of the most valuable factor in this evaluation. For example, in this case in order the landslide be avoided, a bridge can be constructed, founded in stable bedrock beyond landslide area, which in combination to restricted earthworks would be considered satisfying. Furthermore, solutions such as excavation of tunnel beneath or next to the landslide, will be also satisfactory. However, the underlying and also other solutions are rejected from the current study due to the high cost, in contrast to the earthworks. The cost in earthworks is generally focused in the run of mine factor. The underlying factor is depended at the distance from the mining location of the material, to the location of the deposition. In this case though, the material would be provided from the tunnel which is excavated next to the landslide so the run of mine distance is restricted.

Regarding the physical and mechanical characteristics of the material which is about to constitute the berm, it is recommended to have specific gravity 20kN/m$^3$ and saturated specific gravity 22kN/m$^3$. The shear strength of the fill material, it is proposed to have cohesion **c=20kPa** and friction Angle **φ=32°,** which will be acquired due to appropriate compaction. The landslide material, as it is proposed at the engineering geological and geotechnical model, will have specific gravity of 17kN/m$^3$ and saturated specific gravity 20kN/m$^3$ during analysis. Regarding the shear strength of the surface of rupture it will have cohesion **c=0 kPa** and friction Angle **φ=10,25°,** which is also proposed previously. The bedrock is estimate with specific gravity of 24kN/m$^3$, and shear strength of cohesion **c=380 kPa** and friction angle **φ=27°**, estimated by the engineering geological and geotechnical model.

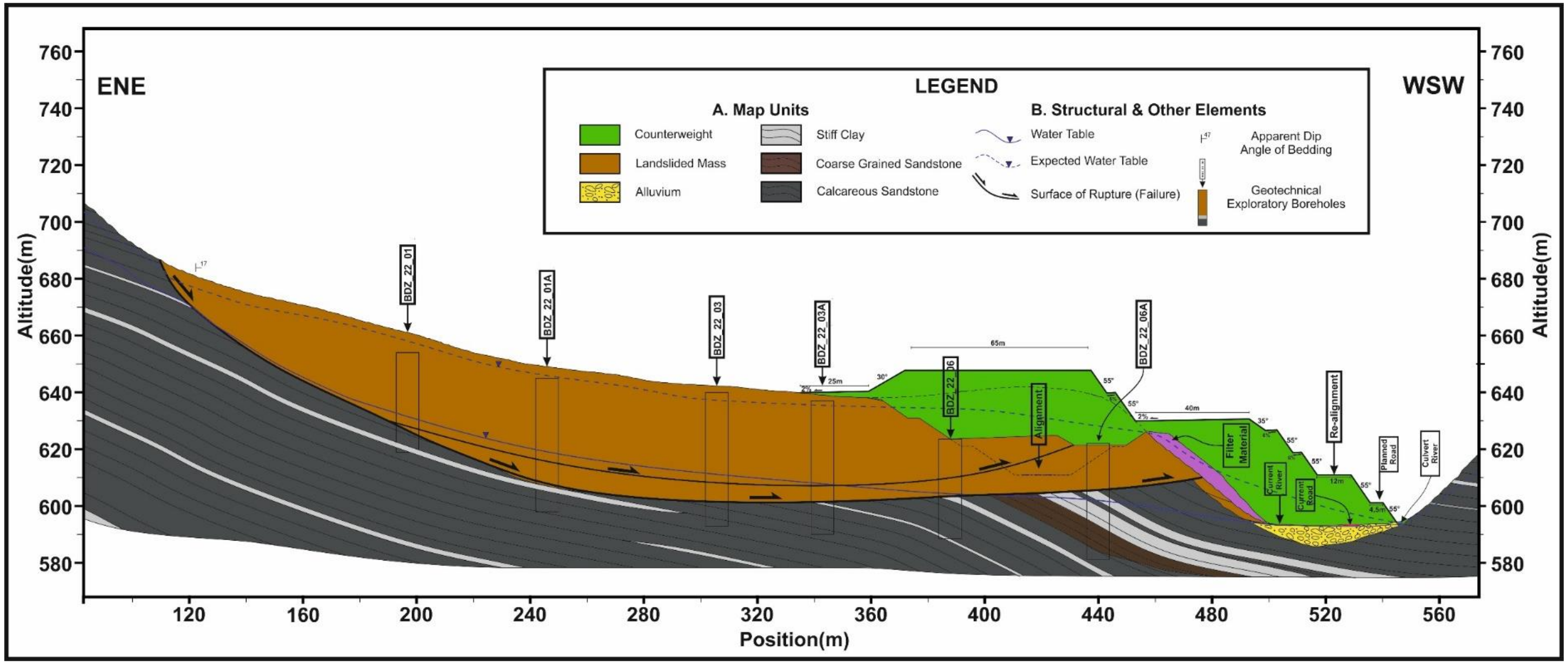

*Figure 117. Model of the Berm, according to the first scenario.*

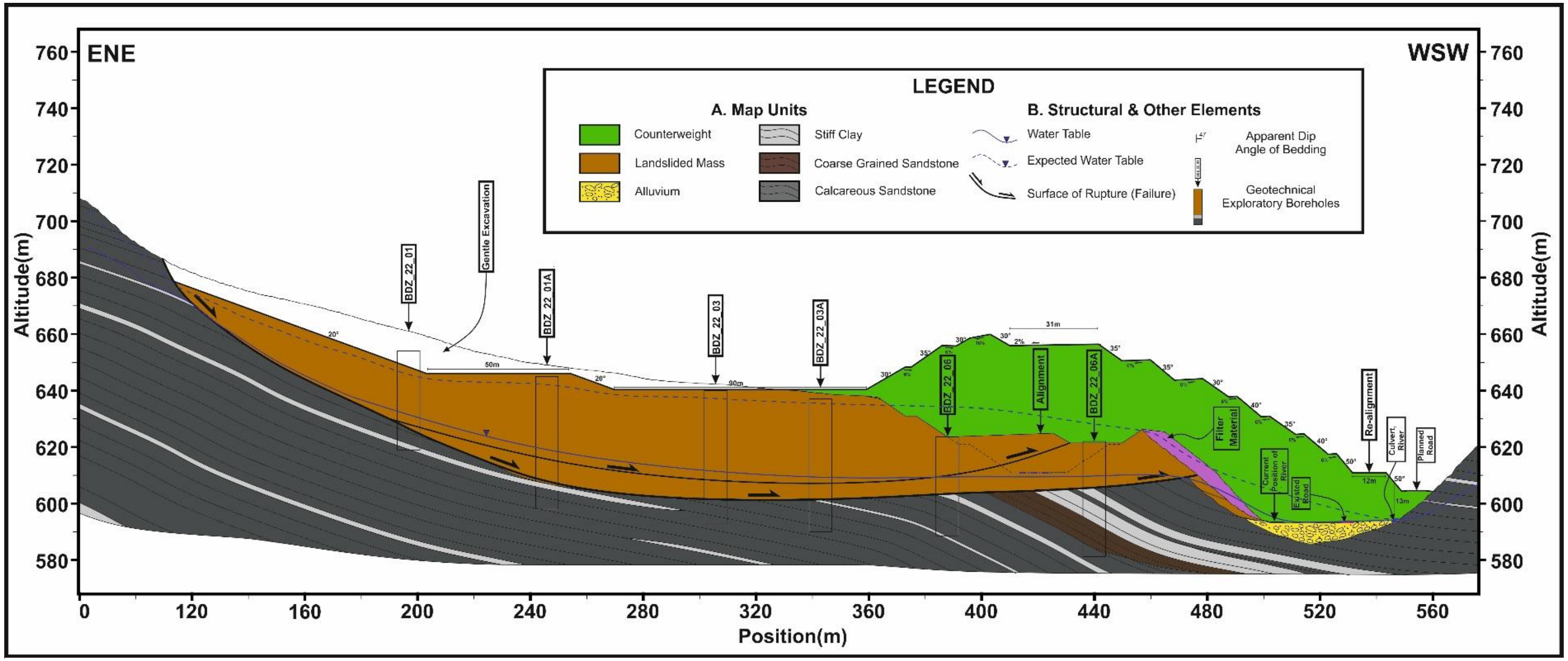

*Figure 116. Model of the Berm and the excavation, according to the second scenario.*

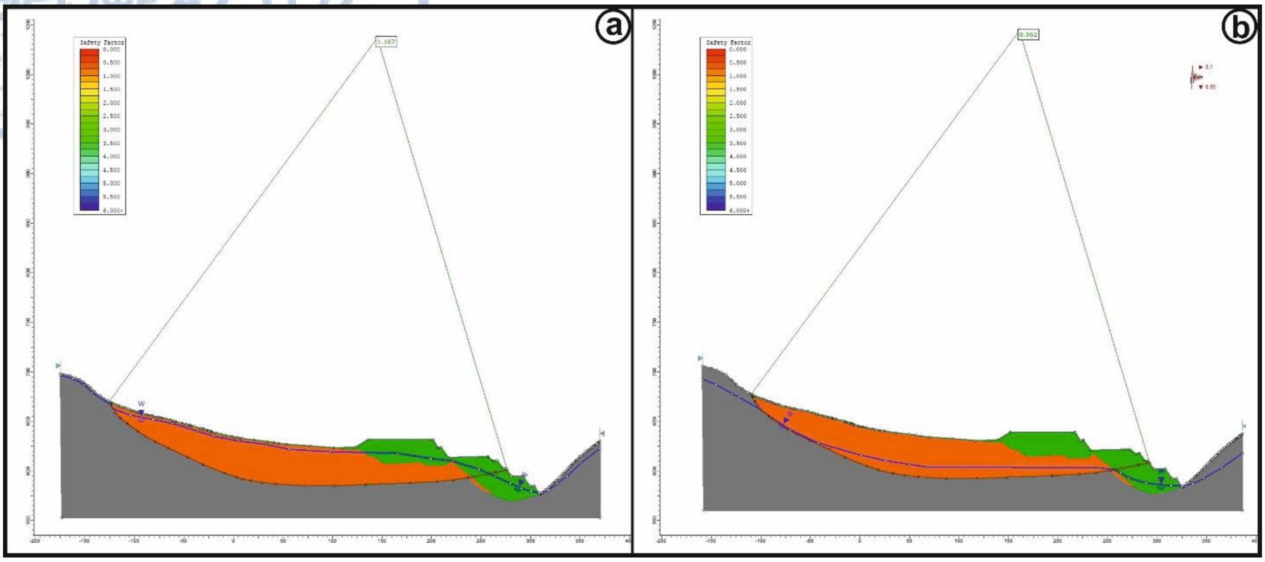

*Figure 118. The stability response of the model of the first scenario for the surface A, (a) for high water level and no seismic event, (b) low water level and seismic event.*

## 8.2 First Scenario

At the first scenario, the stability is accomplished considering only the high groundwater levels, regarding the destabilizing factors. Also, in this case no excavation is recommended at the head of the landslide, and the stability is approached only by placing of berm at the toe of the slide *(figure 117).*

In this case the railroad line and the road would be place on the berm, at benches 12m and 4,5m wide respectively. Downslope, remains extra space for the river, where the maintenance of the springs of natural carbonated water, is possible.

In this case, it is more appropriate to use a culvert for the river in order to protect the potential banks of the river, composed by the berm, from erosion, which will impact significantly on the stability. The river during summer is, potentially characterized as a low capacity river, however, during winter and spring, the period of snow melting, the capacity of the river is expected significantly increased. The erosion capability of the river is directly connected to its capacity, which means that the magnitude of the erosion at the banks of the river will increase whether the capacity of the river during winter and spring seasons, is increased too.

Beside the road, the alignment and the position of the river, another five benches are included for the construction, until the final flat area at the top. The description of their dimensions and inclinations follows:

- The first bench is 2m wide and has inclination of 6% towards ENE.
- The second bench is 3m wide and has inclination of 6% towards ENE.
- The third bench is 40m wide and has inclination of 2% towards ENE.
- The forth bench is 40m wide and has inclination of 2% towards ENE.
- The fifth bench is 2m wide and has inclination of 6% towards ENE.
- The final flat area at the top of the burn is 65m wide.

Regarding the slopes between the underlying benches the alignment and the road, from downslope to upslope:

- The first slope is about 8m height with inclination of 55° towards WSW.
- The second slope is about 10m height with inclination of 55° towards WSW.
- The third slope is about 8m height with inclination of 55° towards WSW.
- The forth slope is about 8m height with inclination of 55° towards WSW.
- The fifth slope is about 4m height with inclination of 35° towards WSW.
- The sixth slope is about 10m height with inclination of 55° towards WSW.

- The seventh slope is about 8m height with inclination of 55° towards WSW.

Upslope, beyond the flat area of 65m two more slopes occur. So, the eighth slope is about 8m height with inclination of 30% towards ENE and the last ninth slope is inclined with 2% towards ENE.

At the underlying stability analysis for the surface, indicated by inclinometers (A), carried out with Janbus' corrected method, taking into account high water table level and no seismic event, factor of safety was produced equal to FS=1,167 (*figure 118*). Of course, analysis for the stability of the berm was also carried out, with the same data regarding the water table and seismic event, however in this case the stability analysis program was ordered to detect the circle of the failure, with Bishops' simplified method. In this case factor of safety was produced equal to FS=1.114 *(figure 119).*

Secondary analyses were also carried out in this model taking into account also the seismic load. The detailed results regarding water table, the surface of rupture and seismic load factors are presented at *table 14.* It is worth mentioning that the same geometry with surface A, and high, water table level during the maximum seismic event results factor of

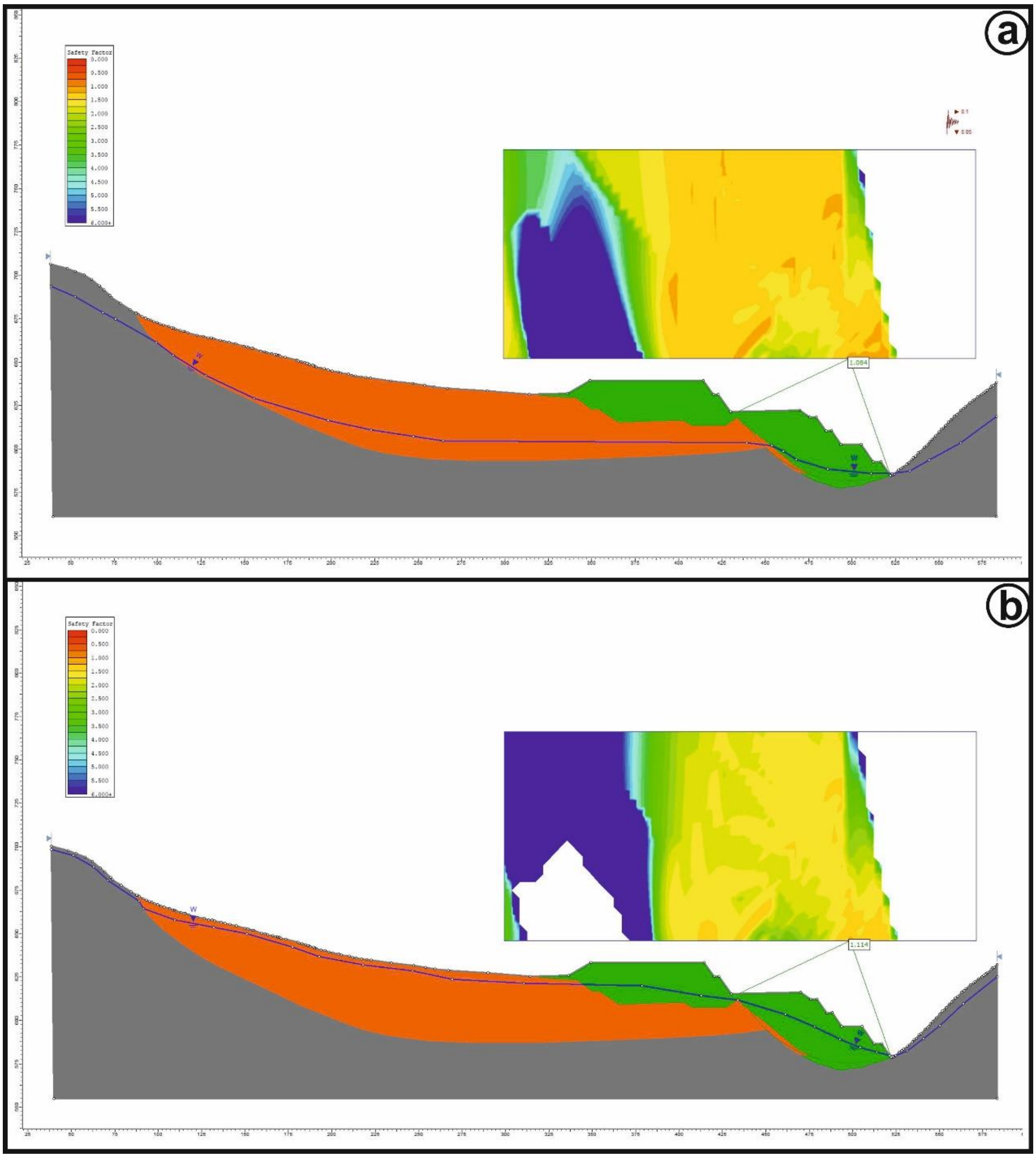

*Figure 119. The stability response of the model of the first scenario for the circle surfaces on the berm, (a) for high water level and seismic event, (b) low water level and no seismic event.*

safety below FS<0.7, which corresponds to failure, although the berm individually will be at critical stability condition. However, if the maximum seismic event occurs when the water table is considered in low levels, the critical stability regarding the surface A is acquired.

| Case | Water Table | Surface | Seismic Load | Method | FS |
|---|---|---|---|---|---|
| 1 | High | A | No | Janbu Corrected | 1,167 |
| 2 | High | Unknown | No | Bishop Simplified | 1,114 |
| 3 | High | A | Yes | Janbu Corrected | 0,695 |
| 4 | High | Unknown | Yes | Bishop Simplified | 0,951 |
| 5 | Low | A | Yes | Janbu Corrected | 0,962 |
| 6 | Low | Unknown | Yes | Bishop Simplified | 1,084 |

*Table 14. Different cases for the model of scenario 1.*

## 8.3 Second Scenario

At the second scenario *(figure 116)* the stability is acquired, taking into account the seismic loading and the high, water table level. In this case, in order to obtain the stability, greater berm should be founded. This means that the berm itself, in this case would be wider and higher than previously and also, further excavation at the main body and the head of the landslide should be implemented. It should be noted that the excavation in this case, must form gentle slopes, considering the limited strength of the geomaterial.

In this case, the berm covers the whole valley, so the foundation of culvert for the river is essential. The underlying installation shall take place at the same position as in scenario 1 in order to acquire the lesser overburden loading for the culvert. So, in this case the minimum thickness of the overburden, approaches 13m.  Furthermore, the road is now planned at the lowest part of the berm, and the railroad line at the first bench. Generally, the slopes are becoming gentler but more than the first scenario.

Beside the road, the alignment, other nine benches are included for the construction, until the final flat area at the top. The description of their dimensions and inclination follows:

- The first four benches are 3m wide and have inclination of 6% towards ENE.
- The fifth and sixth benches are 10m wide and have inclination of 6% towards ENE.
- The flat area (seventh bench) before the final slope is 31m wide and have inclination of 2% towards ENE.

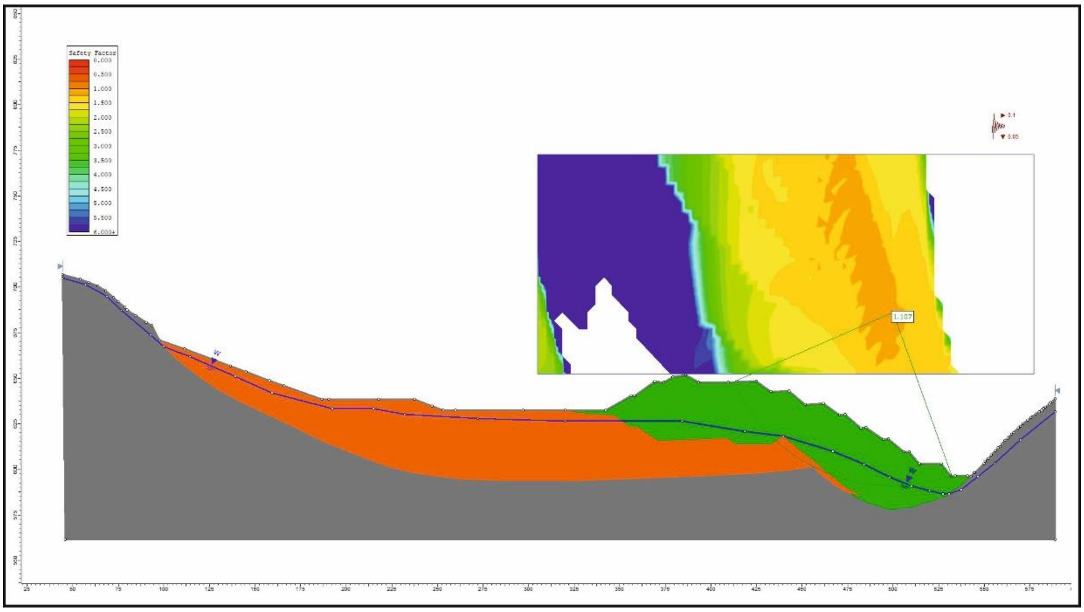

*Figure 120. The stability response of the model of the second scenario for the circle surfaces on the berm.*

- Beyond the top of the berm, two benches with inclination of 6% towards WSW, 2m and 6m wide, should also be constructed in the upslope area *(figure 116).*

Regarding the slopes among the underlying benches the alignment and the road, from downslope to upslope:

- The first slope is about 6m height with inclination of 50° towards WSW.
- The second slope is about 7m height with inclination of 50° towards WSW.
- The third slope is about 7,5m height with inclination of 40° towards WSW.
- The forth slope is about 6,5m height with inclination of 35° towards WSW.
- The fifth slope is about 7m height with inclination of 40° towards WSW.
- The sixth slope is about 6,5m height with inclination of 30° towards WSW.
- The seventh slope is about 7m height with inclination of 35° towards WSW.
- The eighth slope is about 6m height with inclination of 35° towards WSW.
- The ninth slope is about 4m height with inclination of 30° towards WSW.
- The tenth slope is about 1,5m height with inclination of 10° towards ENE.
- The eleventh slope is about 2,5m height with inclination of 30° towards ENE.
- The twelfth slope is about 8m height with inclination of 35° towards ENE.
- The thirteenth slope is about 8m height with inclination of 30° towards ENE.

In this case, excavation at the main body and the head of the landslide is recommended. So, beyond the berm, 90m flat area is formed by excavation. Gentle slope with inclination of 20° and 0,5m height follows. Flat area should be formed again with a length of 50m which will be followed by gentle slope of 20° inclined towards WSW and approximately 30m height.

The major aim in this scenario is the assurance of stability no matter the circumstances. According to the analysis which were carried out, the berm is stabilized successfully and it responds to the maximum seismic event, with high, water table levels. Regarding the surface A, acquired by the inclinometers, in this case the factor of safety approaches FS=1.05, and for the stabilization of the burn itself regarding same conditions the factor of safety approaches FS=1.2.

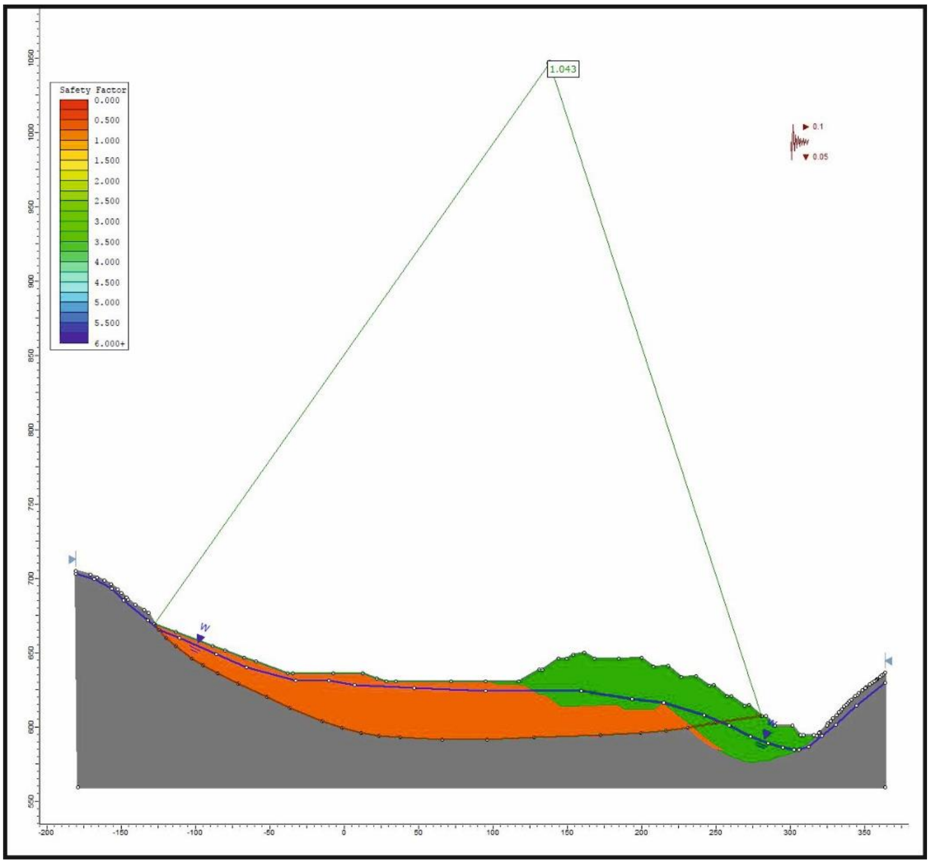

*Figure 121. The stability response of the model of the second scenario for the surface A.*

## 8.4 Conclusions

Taking everything into account, in this case the counter balance measures should be focused at earthworks and drainage. If not, the cost of counter measures would be extraordinary, considering the magnitude of the landslide. In addition, beyond the relocation of the alignment, considering that the present position cannot be acquired without further activation of the landslide, the maintenance of the road, the river and the natural carbonated springs, shall be considered essential.

In this case the construction of berm (counterweight), at the toe of the landslide is considered indispensable, however, the underlying requirements should be taken into consideration. Which means that the construction should be approached that way, so the springs will not be covered, the passing of the river be secured and the road be maintained. At the first proposed scenario, the railroad line and the road are located at benches of the founded berm. Furthermore, at the present scenario, space in the edge of the valley remains, so in this position the passing of river and the maintenance of springs downslope, can be implemented. Although space for the passing of river is secured, it is preferable to restrict the river into culvert, in order to avoid stability problems related to the erosion of the berm. Regarding the springs, the reconstruction of them is recommended in the toe of the berm.

In first scenario, the deposition of filter material, 5m to 10m thick is required among the contact of landslide material and the berm. The underlying drainage system will provide low groundwater level in the berm, and considering the hydraulic gradient, it will also ensure dropping of the groundwater level within the landslide. In addition, in the current scenario, considering low water table, and maximum seismic loading, provided by earthquake, the stability is also acquired. However, in case of intense and sustain rainfall if the response of the filters is limited, and the groundwater level reaches the surface, the stability will not be ensured, not only for the landslide but also for the berm according to the stability analysis.

In order to avoid the failure, even with the combination of the high-water table level and the maximum seismic loading provided by earthquake, the second scenario is proposed. According to the second scenario, the same drainage system is acquired, however the founded berm has greater dimension. Furthermore, in this case gentle excavations at the head and the main body of the landslide shall be implemented. In this scenario, the valley is filled with the berm, with the minimum overburden of 13m. This might create problems regarding the maintenance of the springs, and it will make more expensive the construction of the culvert which should response on significant loading. The railroad line and the road will be located at the benches of berm.

Considering that the present sections represent the conditions right after the failure, and no recent topographical survey is implemented, the results regarding the counter balance measures are considered questionable. The major reason is, that the morphology of the territory is significantly changed. Massif settlements at the head of the slide, uplift at the toe and significant lateral displacements are observed, which means that the geometry of the landslide is way different than the one presented at the underlying sections in the present time. Although the concept, and approximately the dimensions of the berm will be the same, stability analysis should be committed taking into account the same data regarding the surface of rupture, the shear strength, the groundwater regime and the seismic event, at the present morphology given by new topographical survey.

# Chapter 9 Conclusions

The current dissertation focuses at the complete evaluation regarding the stability of slope failure, which occurred during railroad construction at the region of the village Zvare, Imereti, at Central Georgia, Caucasus. The current study provides the results of geological, engineering geological and geotechnical investigation of the landslide, produced from the underlying subgrade failure. Furthermore, in the current study the estimation of feasible solutions regarding the stability and issues provided by the development of the landslide are pointed out.

In the region of the village Zvare, during the construction of railroad line, slope instability occured. More precisely, engineering works, such as excavation, took place at the toe of old stabilized landslide, which was activated from the removing of stabilizing material at the toe. The landslide occurred at 13/05/2017, with the activation of approximately 400m length and 230m wide territory. It is worth to mention that the landslide is still on motion.

The territory firstly was approached by field geological and engineering geological mapping, combined with subsurface investigation program, carried out by exploratory boreholes and installed instrumentation within the boreholes. Furthermore, the territory was also being monitoring by terrestrial GPS system.

The monitoring by terrestrial GPS system indicate that the incident initially attributed displacements of great magnitude and finally displacements of 16m and 7m in lateral and vertical direction respectively were recorded. More precisely settlements of approximately 7m were observed at the head of the landslide, and contrary, uplift movements of approximately 5m were observed at the toe of the slide. The greater lateral movements are observed at the head and the main body of the landslide. Considering the rate of movement, the velocity was abruptly increased at the outset of the development of the phenomenon. To be more accurate initially displacements of approximately 2m per day were recorded.

The failed material is composed by very soft to soft clay, with angular gravel, and boulders contained. In the close to failure territory, the bedrock is composed by fractured, altered, fine grained calcareous sandstone. The bedrock includes lenses of clayey and sandy composition. The clayey material is considered the result of hydrothermal activity, which is also observed in the region expressed by springs of natural carbonated water. The springs of natural carbonated water in the area is derived by the active tectonic regime expressed by reverse faults. It should be noted that in the area two, active reverse faults are presented and among them the study area is located. The combination of tectonic disintegration and hydrothermal alteration, are considered the initial factors related to the reducing of strength of the bedrock, and providing landslides in the area. Field observations indicate the limitation of the landslide at north by the bedding of the bedrock, and at south by set of subvertical joints.

For the estimation of the depth of the slide and the characteristics of involved engineering geological units and the surface of failure, geotechnical exploratory boreholes were carried out. The drilling process indicate maximum depth of shear zone at approximately 40m, and the characteristics of material above and below to the shear zone. Furthermore, instrumentation, inclinometers and piezometers, were installed at the boreholes in order to detect with great accuracy the depth of the shearing and the level of water table. The depth of shearing is indicated clearly, in relatively limited time, by inclinometers considering that, the installed instruments brake up from the shearing at certain depths, which indicates shearing.

At the end of the geological, engineering geological and geotechnical exploratory program the engineering geological model was estimated. The underlying model shows clearly the risks and hazards connected to the occurrence of the landslide. To be more accurate, the development of the phenomenon, beside the impact on the railroad line, which should be realigned, will create a dam or a barrier which will not allow the normal flow of river, forming upslope a reservoir, with catastrophic impact at the construction, the environment and also the local society. Furthermore, the development of the landslide, impacts the presence of road and of natural carbonated water downslope. The maintenance of both features is considered vital, for reasons related to the local society. So, the stabilizing of the landslide, considering the maintenance of the underlying features is essential.

The engineering geological model was also used in order to obtain the characteristics of the failure regarding the surface of failure, the groundwater regime, the spatial distribution of the landslide, and finally the shear strength of the surface of landslide by back analysis. The underlying characteristics are considered key factors in the stability assessment, and their evaluation, in order to propose feasible counter balance measures is vital.

In this case, taking into account the magnitude of the failure and financial factors, or limitations, the counter balance measures are focused at the construction of berm at the toe of the landslide, combined by drainage constructions, among the berm and the landslide material. The construction of the berm should consider the maintenance of important features such as the new alignment, the road, the springs and the passing of the river.

At the present study two major suggestions have been made. The first suggestion is focused at the achievement of the stability, regarding high water table, approximately at the surface. According to the first suggestion the maintenance of the underlying features is achieved, however failure occurs by the combination of the high groundwater levels and seismic event, considering that the factor of safety is dropped below 0,7. In contrast, whether the maximum seismic event with ground acceleration of 0,2g, occurs when the water level is dropped, the critical stability can be achieved.

Contrary, the second suggestion secures the stability whether both destabilization factors, seismic and high groundwater level occur in the same time. The disadvantage in this case is that further studies and constructions should be carried out in order to maintain the passing of the river and the presence of springs downslope, considering that in this case the valley is fully filled by the berm. Furthermore, at the second suggestion, gentle excavations upslope is required.

Excavation of greater magnitude at the upslope territory, is potential to trigger other landslides, considering that already too steep slopes are formed, and examples of failure at the bedrock is already occurred. That makes the stabilization by the berm and the drainage system more feasible, considering also that the counterweight would accumulate the excavated material from the adjacent tunnels.

In order to enhance the validity of the proposed suggestions, new topographical survey at the area is required, considering that the stability analysis regarding the proposed counter measures carried out in morphology at the outset of the incident. Furthermore, the results from the activation of the active tectonic faults, which exist in the wider territory, should be studied in detail, considering that the construction in general, and more specifically, the studied landslide, belong to the near field of active faults.

# References

## a) Articles

Cała, M., Jakóbczyk, J., & Cyran, K. (2016). Inclinometer monitoring system for stability analysis: the western slope of the Bełchatów field case study. *Studia Geotechnica et Mechanica*, *38*(2), 3-13.

Cruden, D. M., & Varnes, D. J. (1996). Landslides: investigation and mitigation. Chapter 3-Landslide types and processes. *Transportation research board special report*, (247).

Carter, T. G., And Marinos, V. (2014). Use of GSI for rock engineering design. In Proceedings 1st international conference on applied empirical design methods in mining. Lima, Peru.

Deere D.U., & Deere D.W., 1988. “The rock quality designation index in practice”, Rock Engineering Systems for Engineering Purposes, ASTM STP 984, Louis Kirkaldie, Ed., American Society for Testing Materials, Philadelphia, pp. 17-34

Hungr, O., Leroueil, S., & Picarelli, L. (2014). The Varnes classification of landslide types, an update. Landslides, 11(2), 167-194.

Galera, J. M., Álvarez, M., & Bieniawski, Z. T. (2007). Evaluation of the deformation modulus of rock masses using RMR: comparison with dilatometer tests. Underground works under special conditions. Taylor and Francis, London, 71-77.

Gamkrelide, I.P., (1986). Geodynamic evolution of the Caucasus and adjacent areas in Alpine time. Tecntonophysics 127:261-277

Gudjabidze G.E., Gamkrelidze I.P., 2003. Geological Maps of Georgia. Georgian state department of geology and national oil company "SAQBAVTOBI".

Machan, G., & Bennett, V. G. (2008). Use of inclinometers for geotechnical instrumentation on transportation projects: State of the practice. Transportation Research E-Circular, (E-C129).

Marinos, & Tsiambaos (2010). Strength and deformability of specific sedimentary and ophiolithic rocks. Bulletin of the Geological Society of Greece, 43, 1259-1266.

Marinos P, Hoek E 2000. GSI: A geologically friendly tool for rockmass strength estimation. In: Proc. GeoEng2000 at the Int. Conf. on Geotechnical and Geological Engineering, Melbourne, Technomic publishers, Lancaster, Pennsylvania, pp 1422-1446

Norbury DN, Child GH, Spink TN (1986) A critical review of Section 8 (BS5930). Soil and rock description in site investigation practice. Eng Geol Special Publication 2:331–342

Philip H. Cisternas A. Gvishiani A. Gorshkov A., 1989. The Caucasus: an actual example of the initial stages of continental collision, Tectonophysics, 161, 1–21.

Romana, M. (1985, September). New adjustment ratings for application of Bieniawski classification to slopes. In Proceedings of the international symposium on role of rock mechanics, Zacatecas, Mexico (pp. 49-53).

Stark, T. D., & Choi, H. (2008). Slope inclinometers for landslides. Landslides, 5(3), 339.

Tan, O., and Taymaz, T., 2006, Active tectonics of the Caucasus: Earthquake source Mechanisms and rupture histories obtained from inversion of teleseismic body waveforms, in Dilek, Y., and Pavlides, S., eds., Postcollisional tectonics and magmatism in the Mediterranean region and Asia: Geological Society of America Special Paper 409.

Tang, W. H., Stark, T., and Angulo, M. (1999). ‘‘Reliability in back analysis of slope failures.’’ Soils Found., 39(5), pp73–80

Varnes, D. J. (1978). Slope movement types and processes. Special report, 176, 11-33.

### b) Books

Atkinson, J. (2007). The mechanics of soils and foundations. CRC Press.

Bell F.G., (2007). Engineering Geology, Second edition, Elsevier Ltd. p581

Bieniawski Z.T., (1989). Engineering rock mass classification: a complete manual for engineers and geologist in mining, civil and petroleum engineering. John Wiley & Sons, p251.

Bondyrev V.I., Davitashvili, Z.V., Singh P.V., (2016). The Geography of Georgia, Problems and Perspectives. Springer p228.

Clayton C.R.I., Matthews M.C., Simons N.E., (1995) Site Investigarion, second edition. John Wiley & Sons, Inc.

Cornforth, D.H., (2005). Landslides in practice: investigation, analysis, and remedial / preventative options in soils. 596 pp., John Wiley & Sons, Inc., Hoboken, N. J..

Fredlund D.G., Rahardjo H., Fredlund M.D., 2012. Unsaturated Soil Mechanics in Engineering Practice. John Wiley & Sons, Inc. p.927

Highland, L.M., and Bobrowsky, P., 2008, The landslide handbook—A guide to understanding landslides: Reston, Virginia, U.S. Geological Survey Circular 1325, 129 p.

Hencher S., (2015) Pratial Rock Mechanics, Applied Geotechnics Series. CRC press taylor & francis Group, A spon press book, 346p.

Knappett J.A., & Craig, R.F., (2012), “Craig’s Soil Mechanics”, Eighth edition, Spon Press, London

Kramer, S.V., 1996. Geotechnical Earthquake Engineering. Practice Hall, New Jersey. 653pp.

Price D.G., de Freitas M.H., (2009). Engineering Geology, Principles and Practice. Springer-Verlag Berlin Heidelberg. 450p

Waltham, T. (2009). Foundations of engineering geology. CRC Press.

### c) Internet Sites

Google Earth
wikipedia.com
railway.ge
rst.com

# Appendix

| | | | | | | | | | | |
|---|---|---|---|---|---|---|---|---|---|---|
| Boreole Depth (m) | Casing Depth [m] | Coordinates | X= | 367779,783 | Drill RIG type | ST 1023-HD | Inclination: | Vertical | Borehole: | BDZ_22_01A |
| | | System | Y= | 4647407,937 | Driller | E.Bakshalyev | Started Date: | 24/8/2017 | Finish Date: | 28/8/2017 |
| | | UTM (Zone 38N) | Z= | 645,236 | Geologists | Maisuradze A.Levan | | | | |

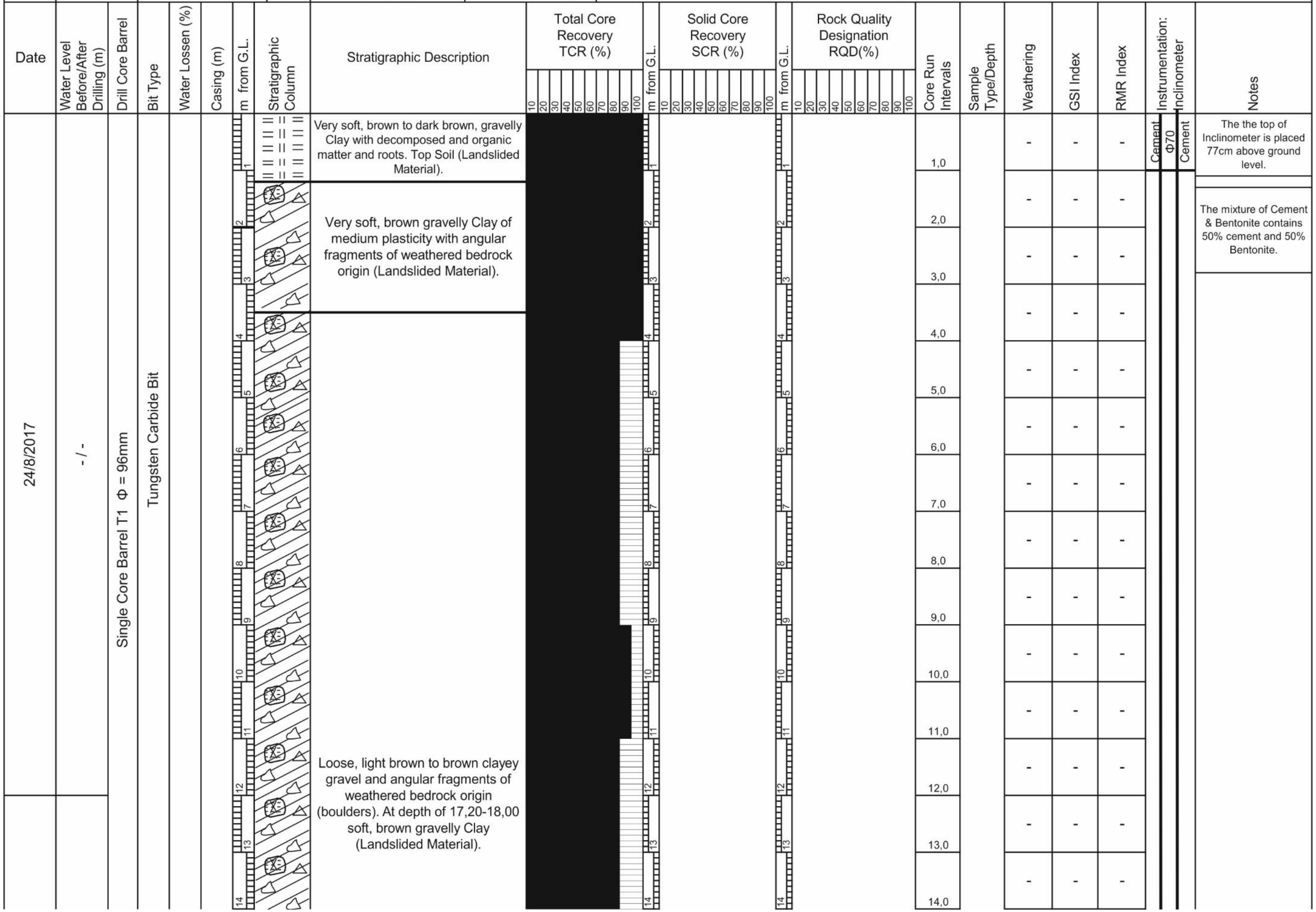

Very soft, brown to dark brown, gravelly Clay with decomposed and organic matter and roots. Top Soil (Landslided Material).

Very soft, brown gravelly Clay of medium plasticity with angular fragments of weathered bedrock origin (Landslided Material).

Loose, light brown to brown clayey gravel and angular fragments of weathered bedrock origin (boulders). At depth of 17,20-18,00 soft, brown gravelly Clay (Landslided Material).

The the top of Inclinometer is placed 77cm above ground level.

The mixture of Cement & Bentonite contains 50% cement and 50% Bentonite.

*Figure 123. Core Logging of borehole BDZ_22_01A (1/3)*

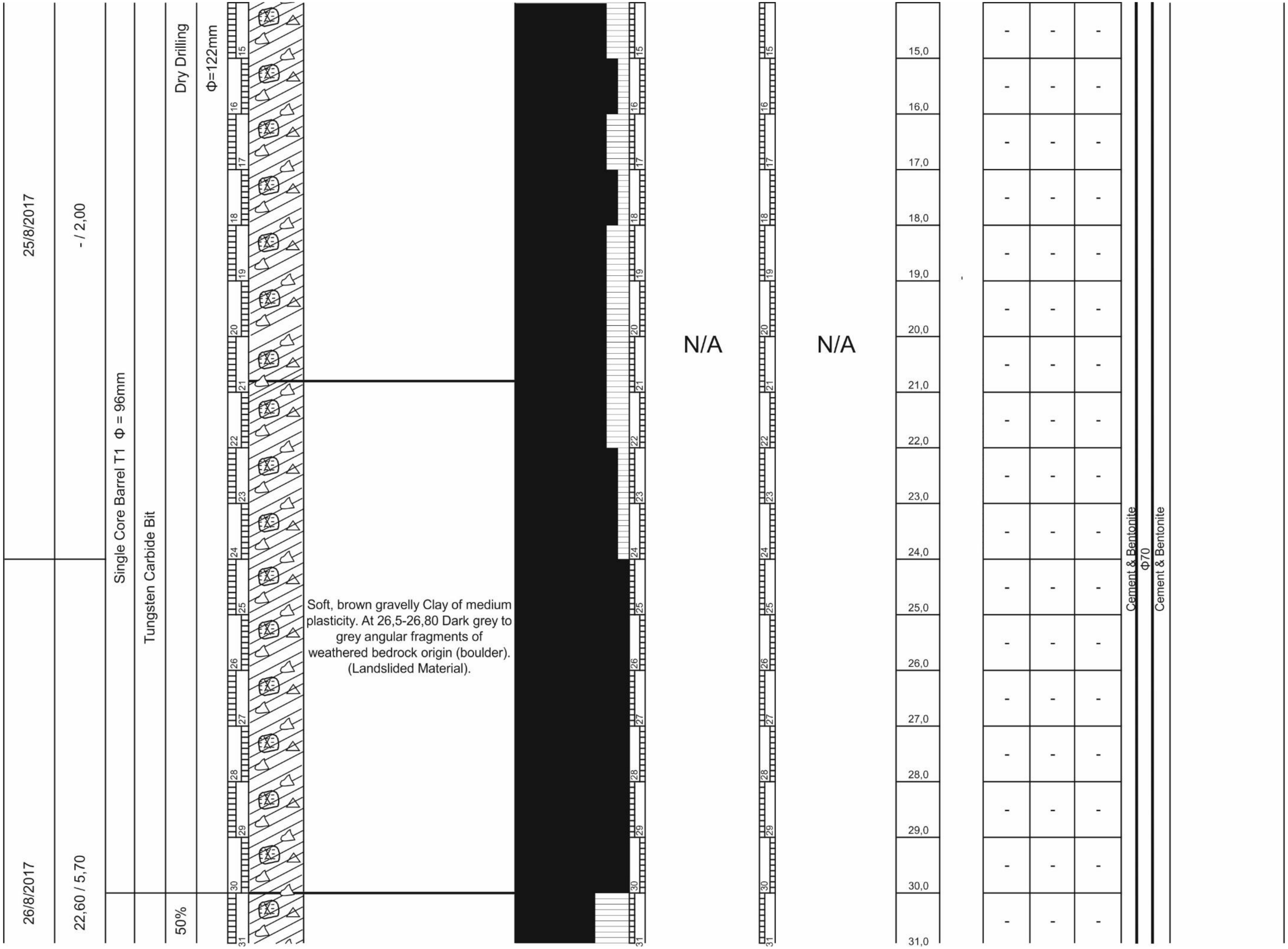

Soft, brown gravelly Clay of medium plasticity. At 26,5-26,80 Dark grey to grey angular fragments of weathered bedrock origin (boulder). (Landslided Material).

*Figure 124. Core Logging of borehole BDZ_22_01A (2/3)*

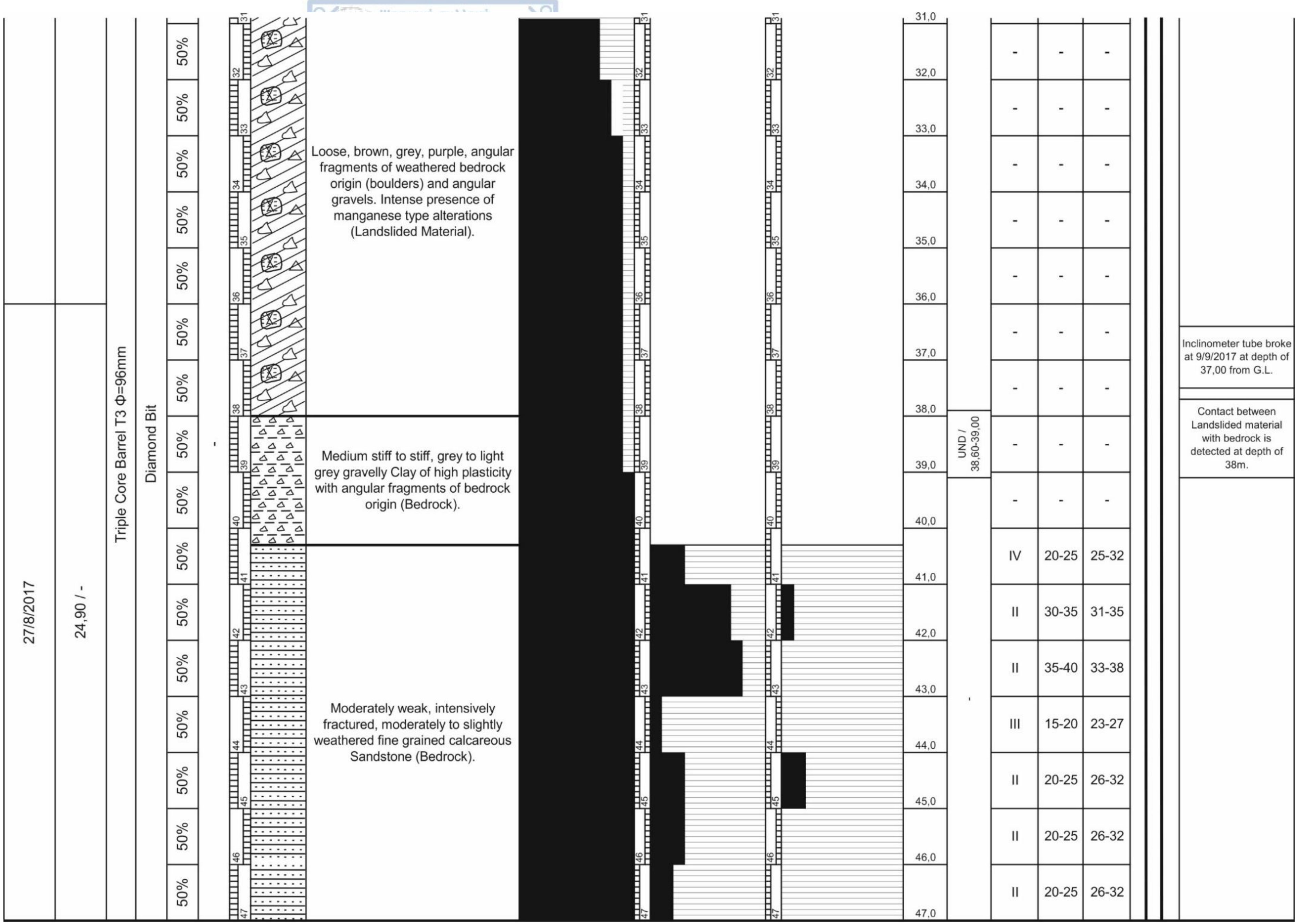

Loose, brown, grey, purple, angular fragments of weathered bedrock origin (boulders) and angular gravels. Intense presence of manganese type alterations (Landslided Material).

Medium stiff to stiff, grey to light grey gravelly Clay of high plasticity with angular fragments of bedrock origin (Bedrock).

Moderately weak, intensively fractured, moderately to slightly weathered fine grained calcareous Sandstone (Bedrock).

Inclinometer tube broke at 9/9/2017 at depth of 37,00 from G.L.

Contact between Landslided material with bedrock is detected at depth of 38m.

Figure 125. Core Logging of borehole BDZ_22_01A (3/3)

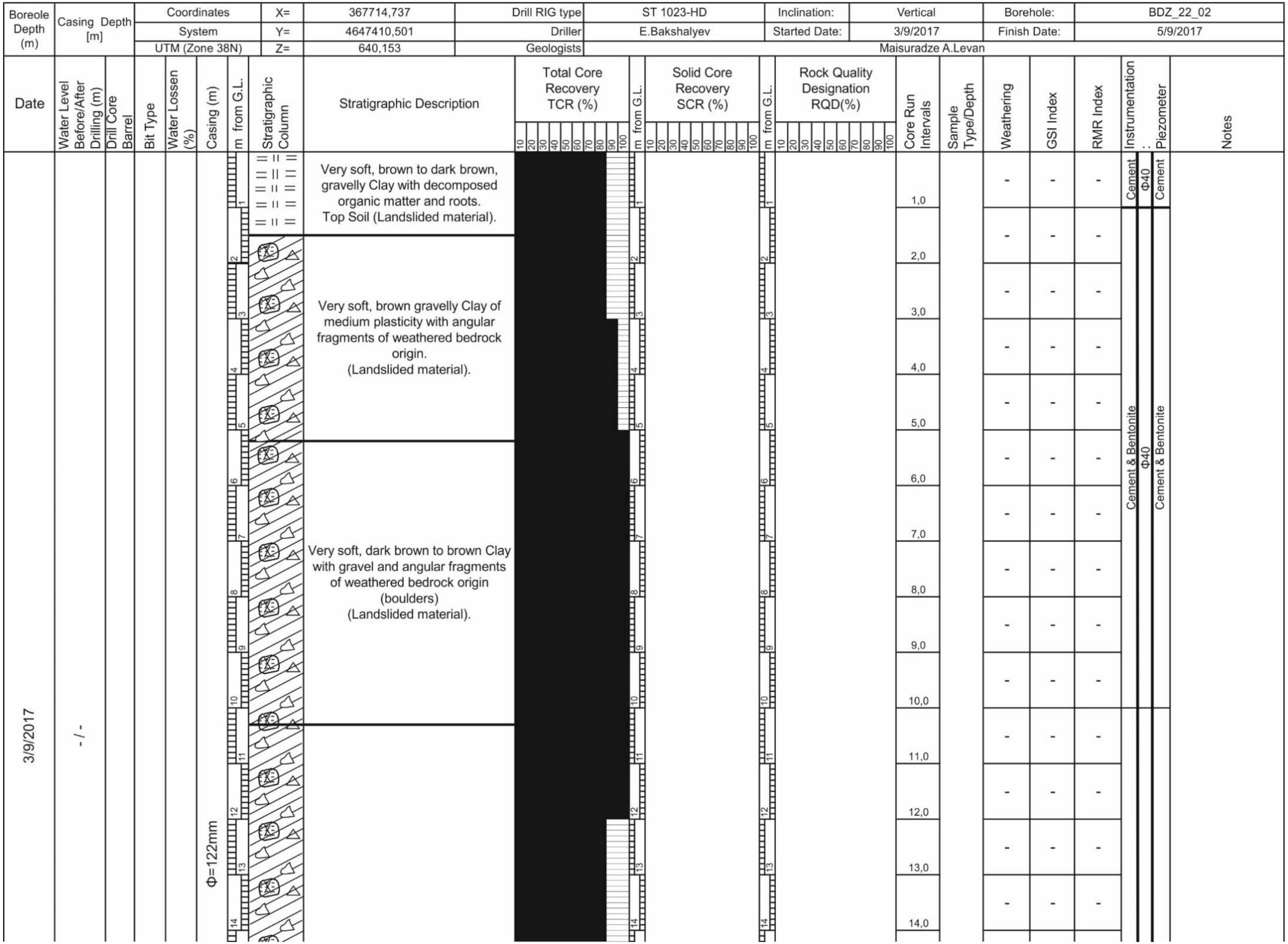

| | | | | | | | | | | |
|---|---|---|---|---|---|---|---|---|---|---|
| Boreole Depth (m) | Casing Depth [m] | Coordinates | X= | 367714,737 | Drill RIG type | ST 1023-HD | Inclination: | Vertical | Borehole: | BDZ_22_02 |
| | | System | Y= | 4647410,501 | Driller | E.Bakshalyev | Started Date: | 3/9/2017 | Finish Date: | 5/9/2017 |
| | | UTM (Zone 38N) | Z= | 640,153 | Geologists | Maisuradze A.Levan | | | | |

Very soft, brown to dark brown, gravelly Clay with decomposed organic matter and roots. Top Soil (Landslided material).

Very soft, brown gravelly Clay of medium plasticity with angular fragments of weathered bedrock origin. (Landslided material).

Very soft, dark brown to brown Clay with gravel and angular fragments of weathered bedrock origin (boulders) (Landslided material).

Figure 126. Core Logging of borehole BDZ_22_02 (1/3)

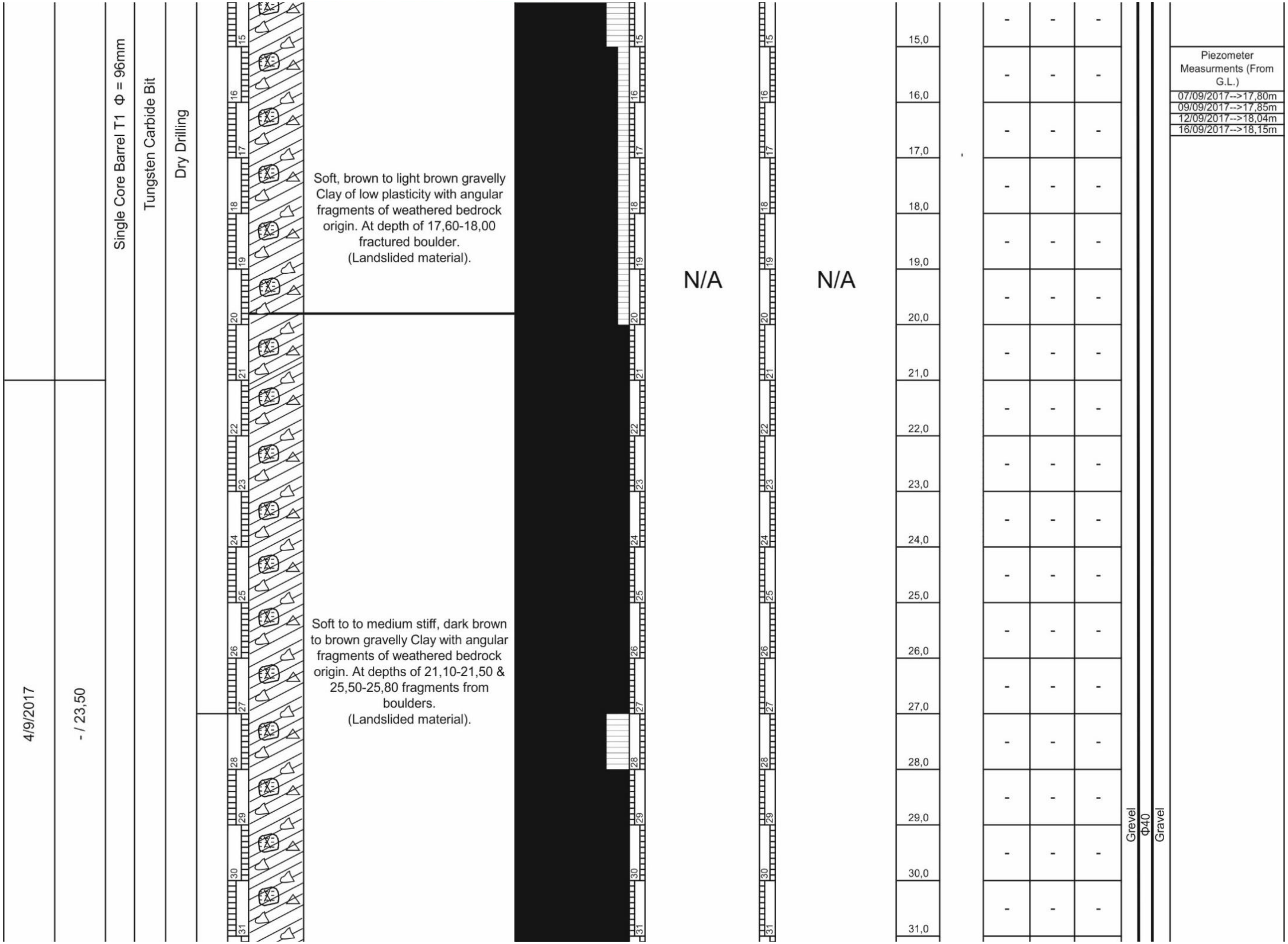

Soft, brown to light brown gravelly Clay of low plasticity with angular fragments of weathered bedrock origin. At depth of 17,60-18,00 fractured boulder. (Landslided material).

Soft to to medium stiff, dark brown to brown gravelly Clay with angular fragments of weathered bedrock origin. At depths of 21,10-21,50 & 25,50-25,80 fragments from boulders. (Landslided material).

| Piezometer Measurments (From G.L.) |
|---|
| 07/09/2017-->17,80m |
| 09/09/2017-->17,85m |
| 12/09/2017-->18,04m |
| 16/09/2017-->18,15m |

*Figure 127. Core Logging of borehole BDZ_22_02 (2/3)*

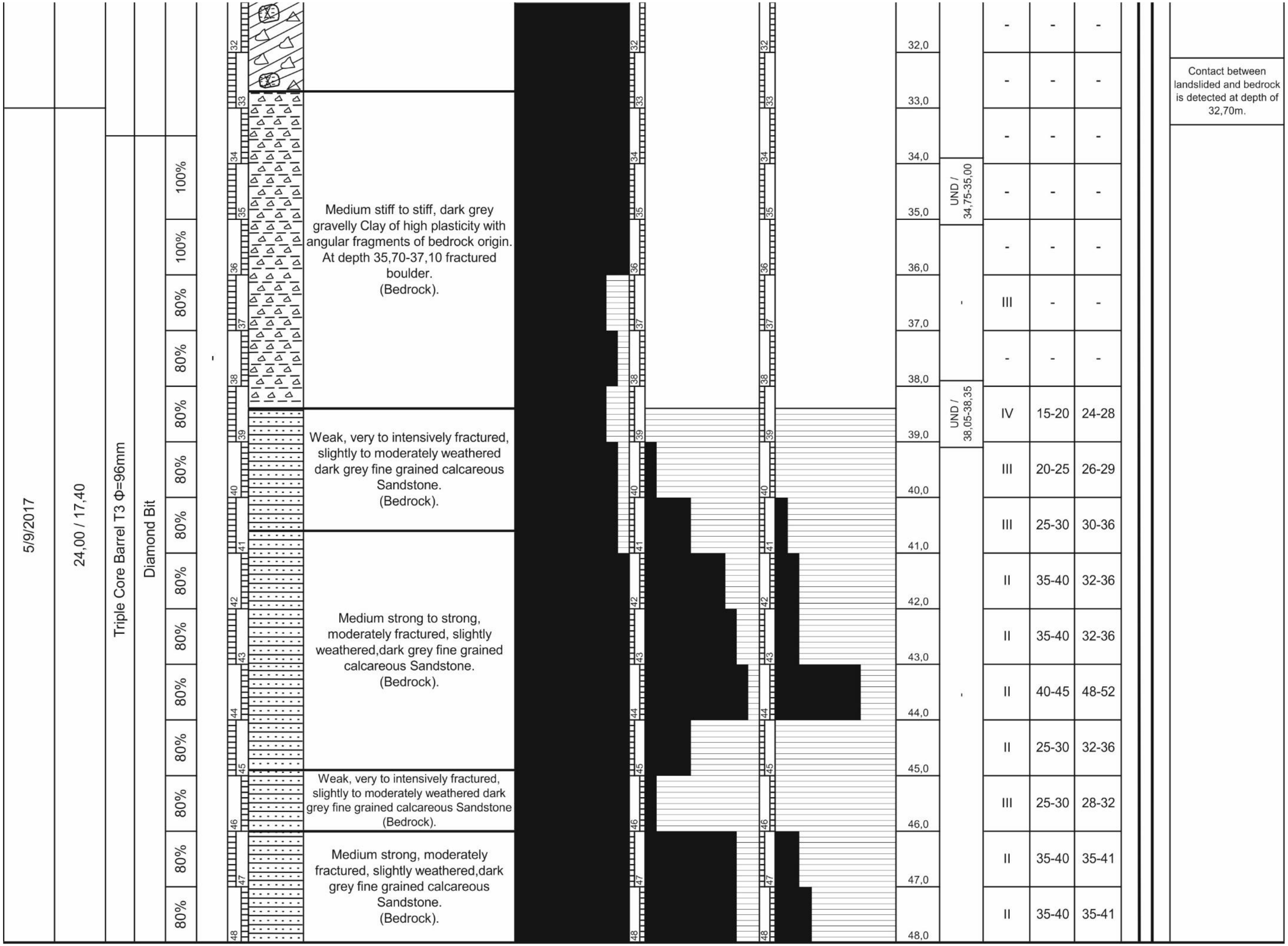

Medium stiff to stiff, dark grey gravelly Clay of high plasticity with angular fragments of bedrock origin. At depth 35,70-37,10 fractured boulder. (Bedrock).

Weak, very to intensively fractured, slightly to moderately weathered dark grey fine grained calcareous Sandstone. (Bedrock).

Medium strong to strong, moderately fractured, slightly weathered,dark grey fine grained calcareous Sandstone. (Bedrock).

Weak, very to intensively fractured, slightly to moderately weathered dark grey fine grained calcareous Sandstone (Bedrock).

Medium strong, moderately fractured, slightly weathered,dark grey fine grained calcareous Sandstone. (Bedrock).

| | | | | |
|---|---|---|---|---|
| 32,0 | | - | - | - |
| 33,0 | | - | - | - |
| 34,0 | | - | - | - |
| 35,0 | UND / 34,75-35,00 | - | - | - |
| 36,0 | | - | - | - |
| 37,0 | - | III | - | - |
| 38,0 | | - | - | - |
| 39,0 | UND / 38,05-38,35 | IV | 15-20 | 24-28 |
| 40,0 | | III | 20-25 | 26-29 |
| 41,0 | | III | 25-30 | 30-36 |
| 42,0 | | II | 35-40 | 32-36 |
| 43,0 | | II | 35-40 | 32-36 |
| 44,0 | - | II | 40-45 | 48-52 |
| 45,0 | | II | 25-30 | 32-36 |
| 46,0 | | III | 25-30 | 28-32 |
| 47,0 | | II | 35-40 | 35-41 |
| 48,0 | | II | 35-40 | 35-41 |

Contact between landslided and bedrock is detected at depth of 32,70m.

*Figure 128. Core Logging of borehole BDZ_22_02 (3/3)*

| Boreole Depth (m) | Casing Depth [m] | Coordinates | X= | 367695,386 | Drill RIG type | ST 1023-HD | Inclination: | Vertical | Borehole: | BDZ_22_03A |
|---|---|---|---|---|---|---|---|---|---|---|
| | | System | Y= | 4647361,255 | Driller | E.Bakshalyev | Started Date: | 19/8/2017 | Finish Date: | 23/8/2017 |
| | | UTM (Zone 38N) | Z= | 637,731 | Geologists | Maisuradze A.Levan | | | | |

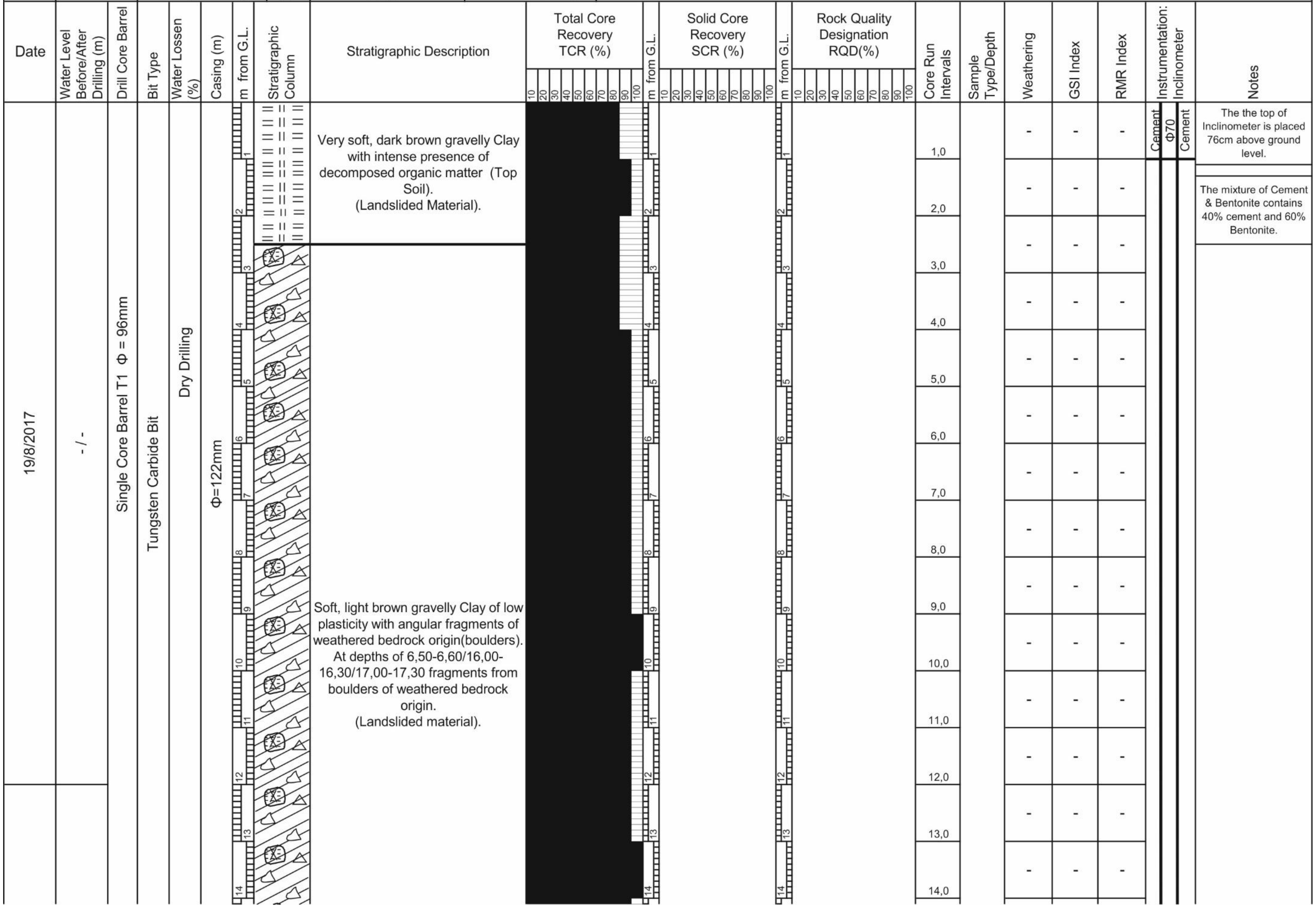

Very soft, dark brown gravelly Clay with intense presence of decomposed organic matter (Top Soil). (Landslided Material).

Soft, light brown gravelly Clay of low plasticity with angular fragments of weathered bedrock origin(boulders). At depths of 6,50-6,60/16,00-16,30/17,00-17,30 fragments from boulders of weathered bedrock origin. (Landslided material).

The the top of Inclinometer is placed 76cm above ground level.

The mixture of Cement & Bentonite contains 40% cement and 60% Bentonite.

*Figure 129. Core Logging of borehole BDZ_22_03A (1/3)*

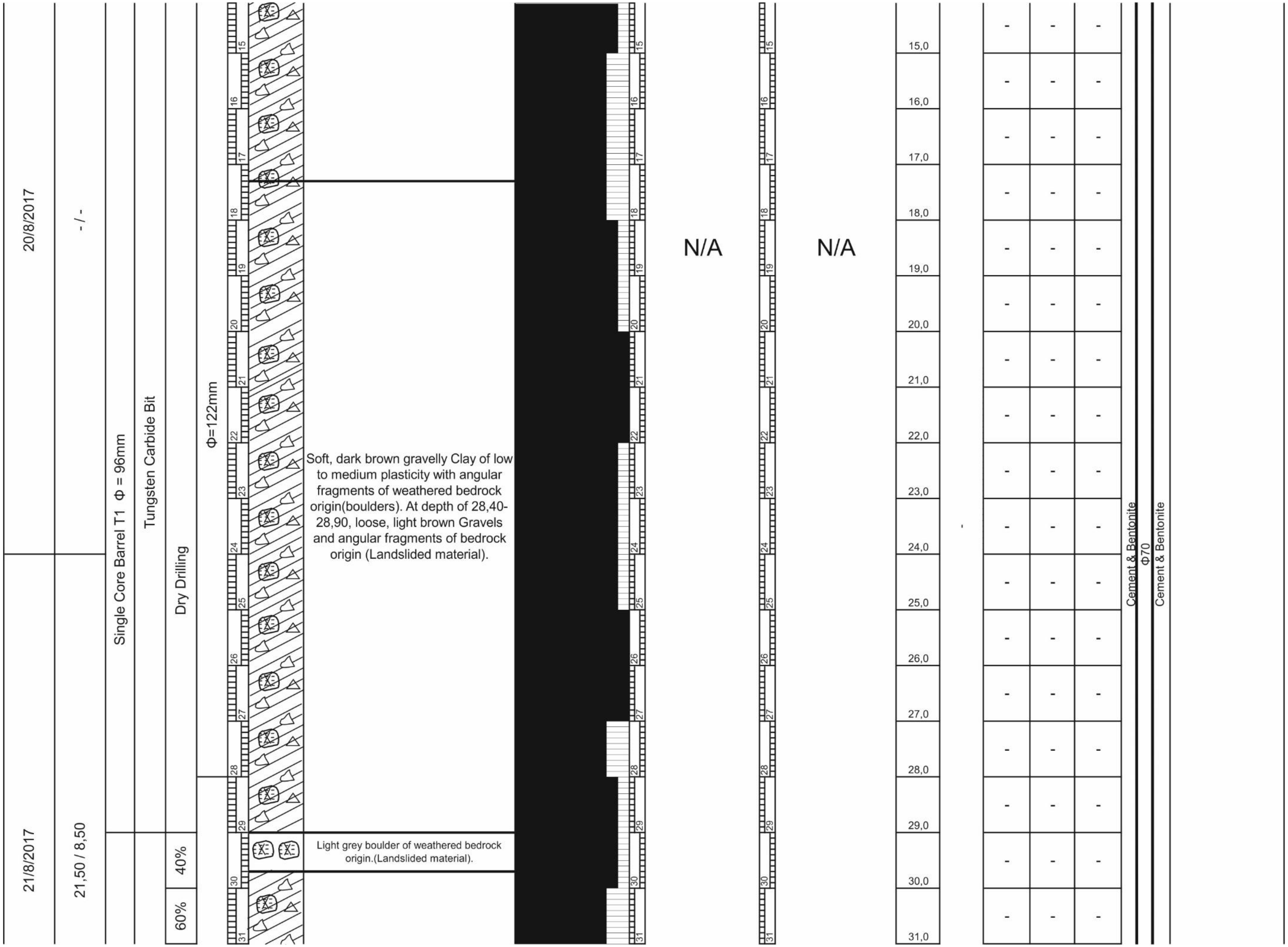

*Figure 130. Core Logging of borehole BDZ_22_03A (2/3)*

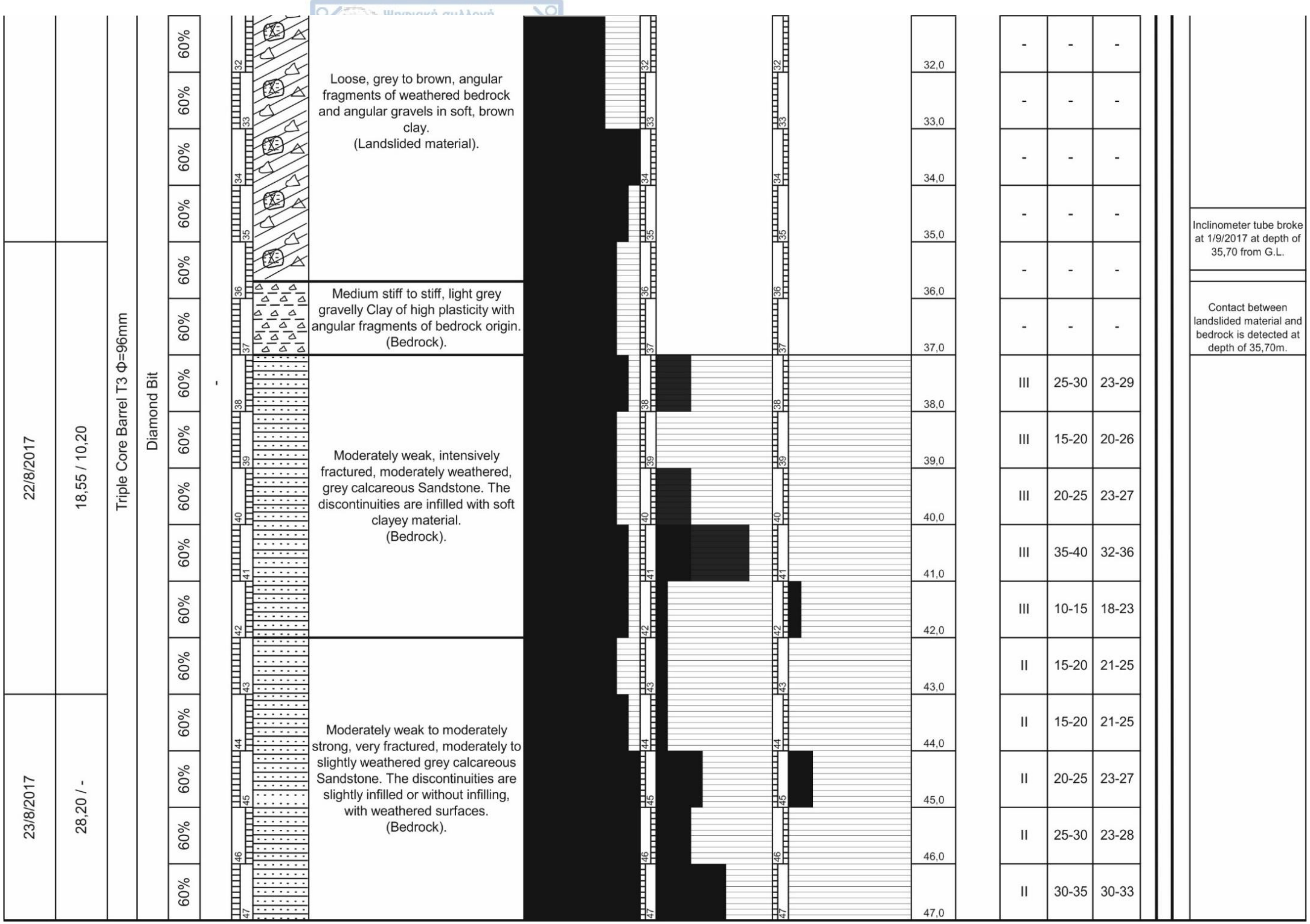

Loose, grey to brown, angular fragments of weathered bedrock and angular gravels in soft, brown clay. (Landslided material).

Medium stiff to stiff, light grey gravelly Clay of high plasticity with angular fragments of bedrock origin. (Bedrock).

Moderately weak, intensively fractured, moderately weathered, grey calcareous Sandstone. The discontinuities are infilled with soft clayey material. (Bedrock).

Moderately weak to moderately strong, very fractured, moderately to slightly weathered grey calcareous Sandstone. The discontinuities are slightly infilled or without infilling, with weathered surfaces. (Bedrock).

| | | | |
|---|---|---|---|
| 32,0 | - | - | - |
| 33,0 | - | - | - |
| 34,0 | - | - | - |
| 35,0 | - | - | - |
| 36,0 | - | - | - |
| 37,0 | - | - | - |
| 38,0 | III | 25-30 | 23-29 |
| 39,0 | III | 15-20 | 20-26 |
| 40,0 | III | 20-25 | 23-27 |
| 41,0 | III | 35-40 | 32-36 |
| 42,0 | III | 10-15 | 18-23 |
| 43,0 | II | 15-20 | 21-25 |
| 44,0 | II | 15-20 | 21-25 |
| 45,0 | II | 20-25 | 23-27 |
| 46,0 | II | 25-30 | 23-28 |
| 47,0 | II | 30-35 | 30-33 |

Inclinometer tube broke at 1/9/2017 at depth of 35,70 from G.L.

Contact between landslided material and bedrock is detected at depth of 35,70m.

Figure 131. Core Logging of borehole BDZ_22_03A (3/3)

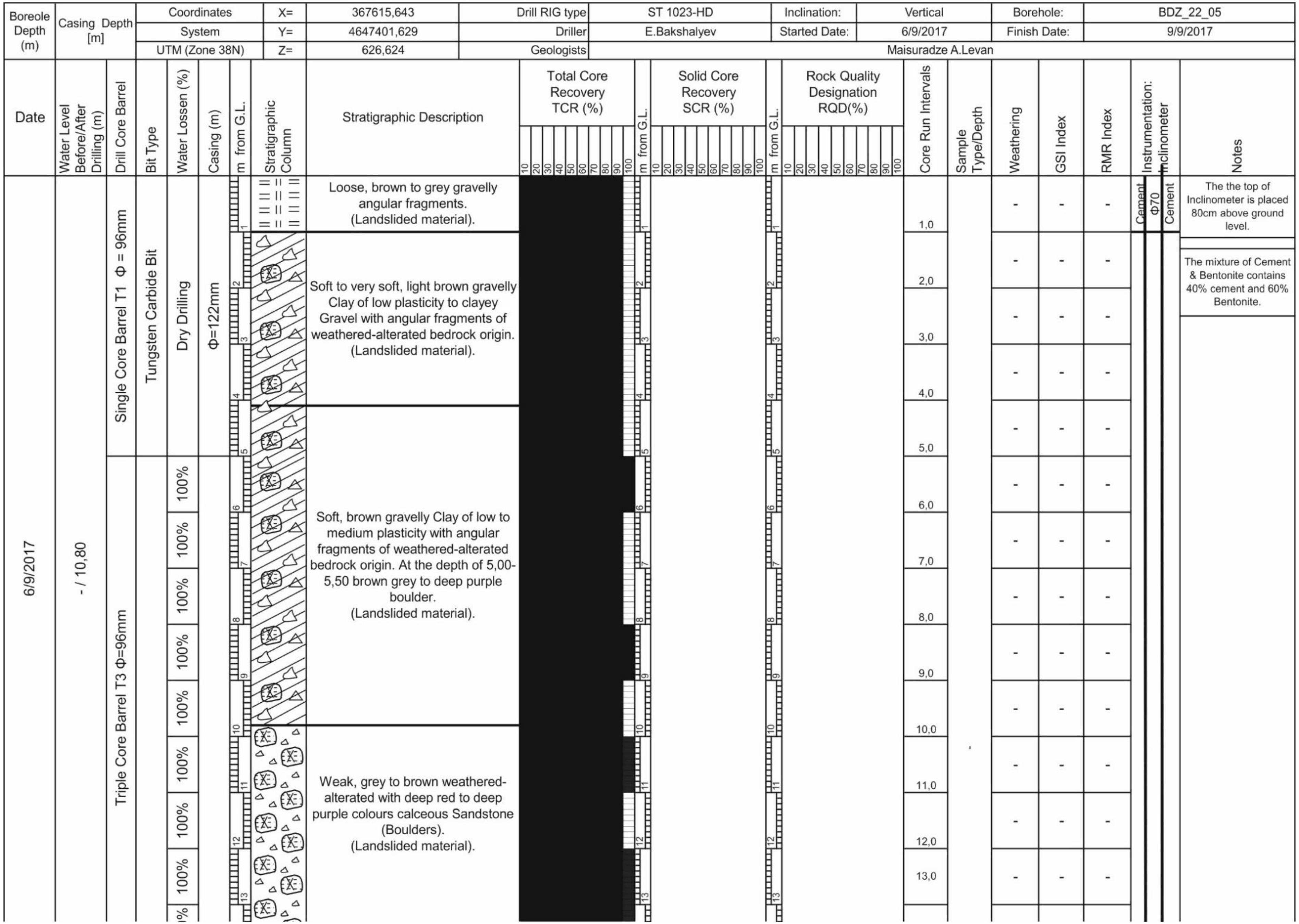

| Boreole Depth (m) | Casing Depth [m] | Coordinates | X= | 367615,643 | Drill RIG type | ST 1023-HD | Inclination: | Vertical | Borehole: | BDZ_22_05 |
|---|---|---|---|---|---|---|---|---|---|---|
| | | System | Y= | 4647401,629 | Driller | E.Bakshalyev | Started Date: | 6/9/2017 | Finish Date: | 9/9/2017 |
| | | UTM (Zone 38N) | Z= | 626,624 | Geologists | Maisuradze A.Levan | | | | |

| Date | Water Level Before/After Drilling (m) | Drill Core Barrel | Bit Type | Water Lossen (%) | Casing (m) | Stratigraphic Description | Core Run Intervals | Weathering | GSI Index | RMR Index | Instrumentation: Inclinometer | Notes |
|---|---|---|---|---|---|---|---|---|---|---|---|---|
| 6/9/2017 | - / 10,80 | Single Core Barrel T1 Φ = 96mm | Tungsten Carbide Bit | Dry Drilling | Φ=122mm | Loose, brown to grey gravelly angular fragments. (Landslided material). | 1,0 | - | - | - | Cement Φ70 Cement | The the top of Inclinometer is placed 80cm above ground level. |
| | | | | | | Soft to very soft, light brown gravelly Clay of low plasticity to clayey Gravel with angular fragments of weathered-alterated bedrock origin. (Landslided material). | 2,0<br>3,0<br>4,0 | - | - | - | | The mixture of Cement & Bentonite contains 40% cement and 60% Bentonite. |
| | | | | | | Soft, brown gravelly Clay of low to medium plasticity with angular fragments of weathered-alterated bedrock origin. At the depth of 5,00-5,50 brown grey to deep purple boulder. (Landslided material). | 5,0 | - | - | - | | |
| | | Triple Core Barrel T3 Φ=96mm | | 100%<br>100%<br>100%<br>100%<br>100% | | | 6,0<br>7,0<br>8,0<br>9,0<br>10,0 | - | - | - | | |
| | | | | 100%<br>100%<br>100% | | Weak, grey to brown weathered-alterated with deep red to deep purple colours calceous Sandstone (Boulders). (Landslided material). | 11,0<br>12,0<br>13,0 | - | - | - | | |

*Figure 132. Core Logging of borehole BDZ_22_05 (1/3)*

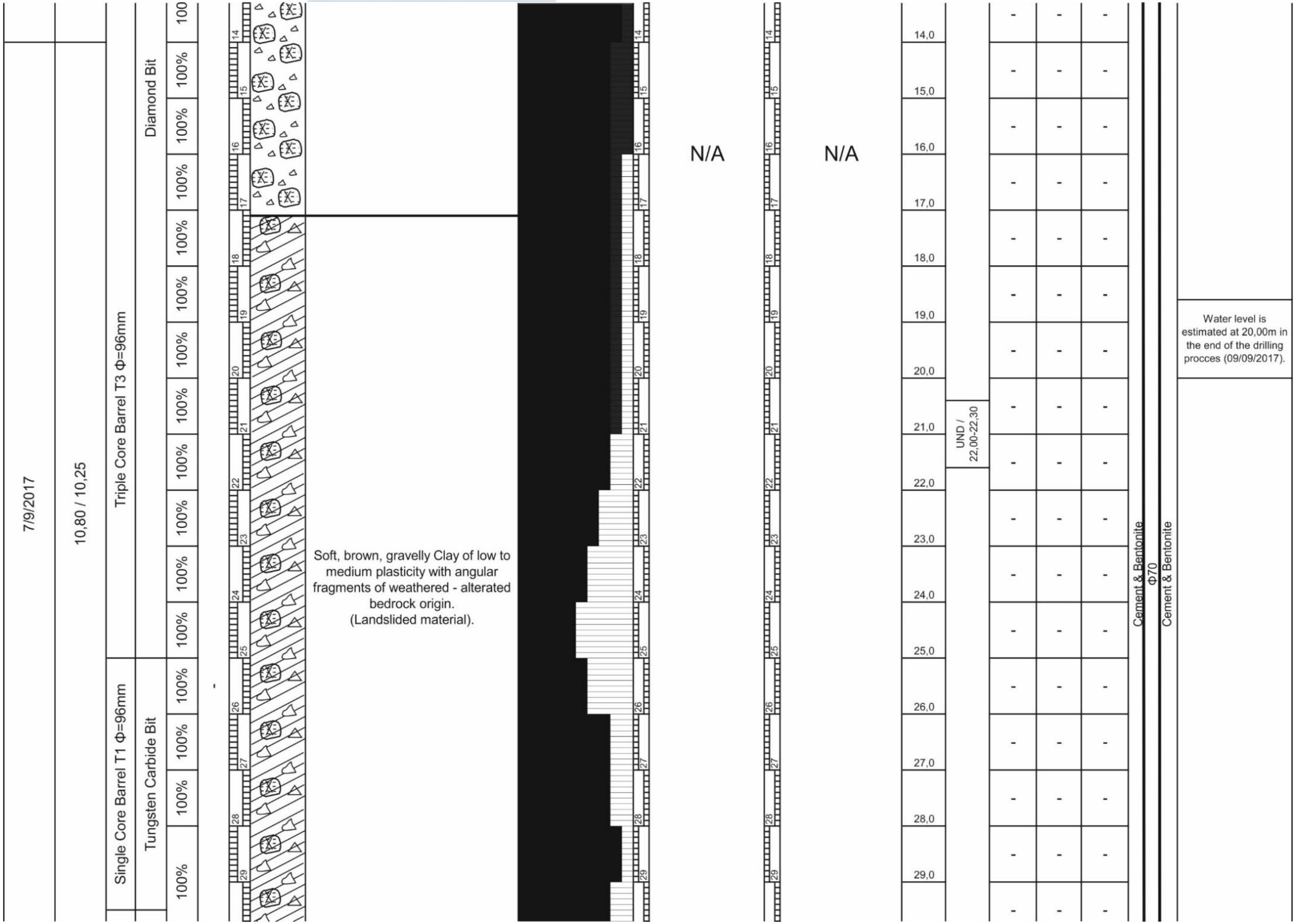

*Figure 133. Core Logging of borehole BDZ_22_05 (2/3)*

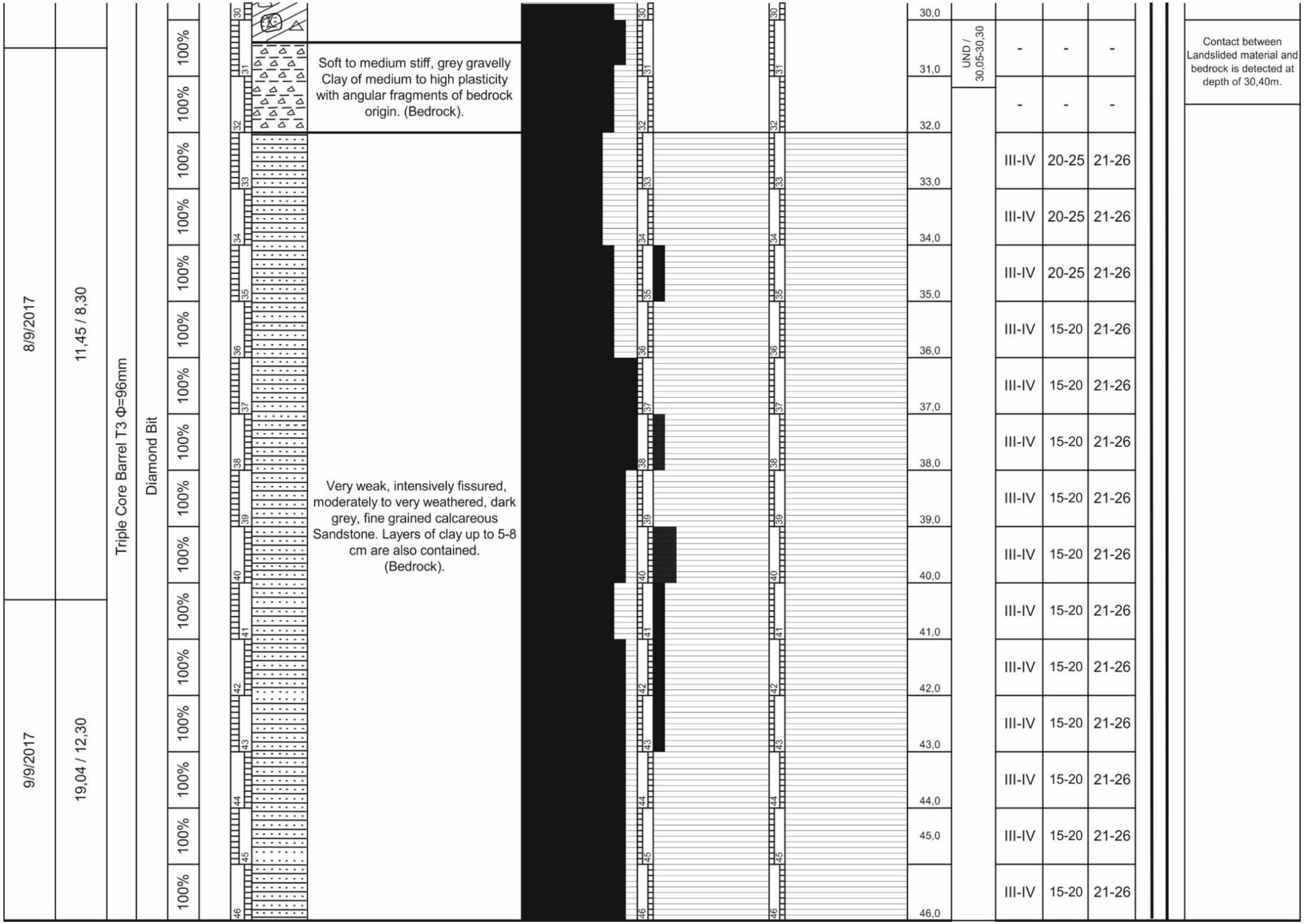

Soft to medium stiff, grey gravelly Clay of medium to high plasticity with angular fragments of bedrock origin. (Bedrock).

Very weak, intensively fissured, moderately to very weathered, dark grey, fine grained calcareous Sandstone. Layers of clay up to 5-8 cm are also contained. (Bedrock).

| | | | | |
|---|---|---|---|---|
| 31,0 | UND / 30,05-30,30 | - | - | - |
| 32,0 | | - | - | - |
| 33,0 | | III-IV | 20-25 | 21-26 |
| 34,0 | | III-IV | 20-25 | 21-26 |
| 35,0 | | III-IV | 20-25 | 21-26 |
| 36,0 | | III-IV | 15-20 | 21-26 |
| 37,0 | | III-IV | 15-20 | 21-26 |
| 38,0 | | III-IV | 15-20 | 21-26 |
| 39,0 | | III-IV | 15-20 | 21-26 |
| 40,0 | | III-IV | 15-20 | 21-26 |
| 41,0 | | III-IV | 15-20 | 21-26 |
| 42,0 | | III-IV | 15-20 | 21-26 |
| 43,0 | | III-IV | 15-20 | 21-26 |
| 44,0 | | III-IV | 15-20 | 21-26 |
| 45,0 | | III-IV | 15-20 | 21-26 |
| 46,0 | | III-IV | 15-20 | 21-26 |

Contact between Landslided material and bedrock is detected at depth of 30,40m.

*Figure 134. Core Logging of borehole BDZ_22_05 (3/3)*

| | | | | | | | | | | |
|---|---|---|---|---|---|---|---|---|---|---|
| Boreole Depth (m) | Casing Depth [m] | Coordinates | X= | 367603,921 | Drill RIG type | ST 1023-HD | Inclination: | Vertical | Borehole: | BDZ_22_06A |
| | | System | Y= | 4647324,87 | Driller | E.Bakshalyev | Started Date: | 13/8/2017 | Finish Date: | 19/8/2017 |
| | | UTM (Zone 38N) | Z= | 622,36 | Geologists | Maisuradze A. Levan | | | | |

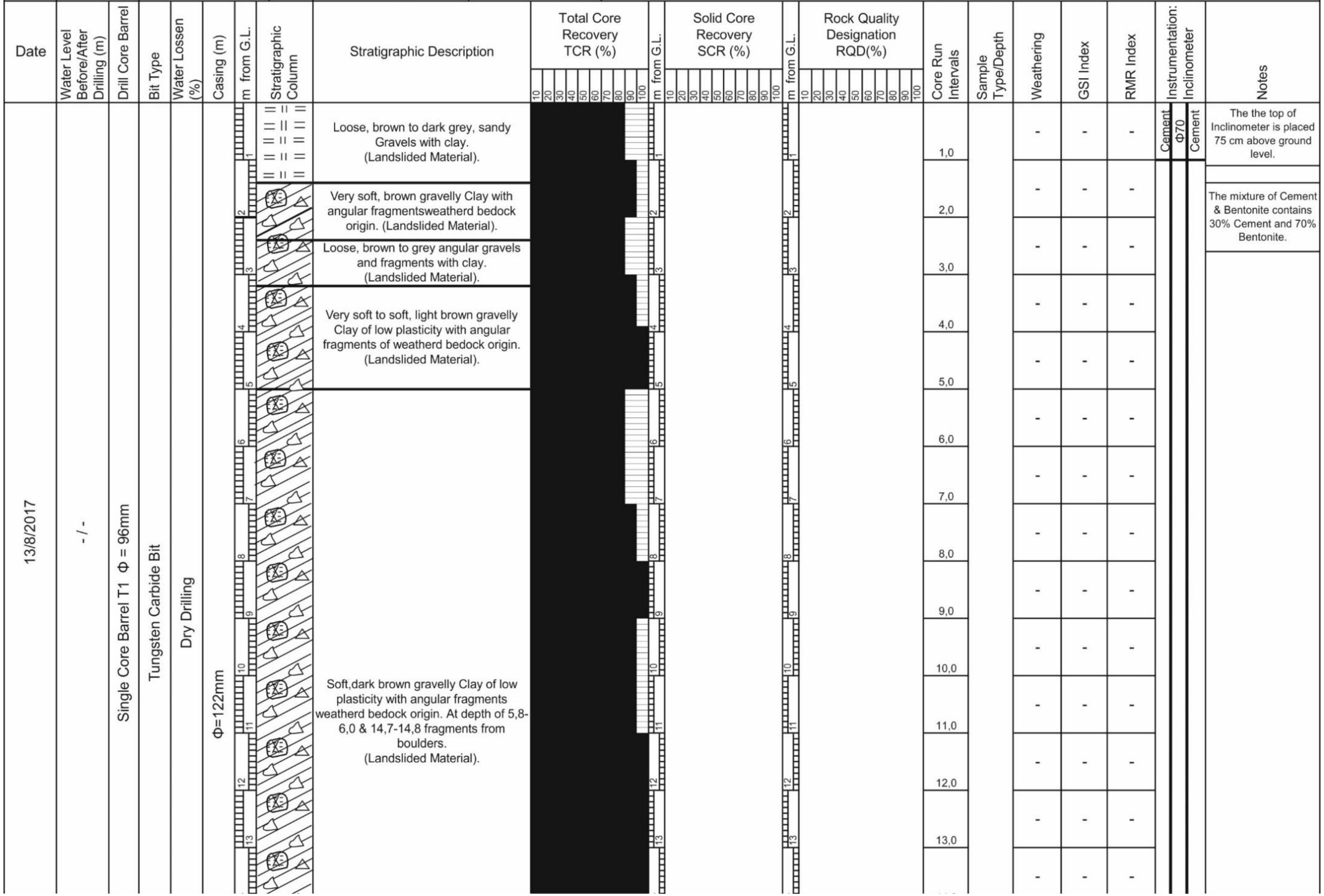

Loose, brown to dark grey, sandy Gravels with clay. (Landslided Material).

Very soft, brown gravelly Clay with angular fragmentsweatherd bedock origin. (Landslided Material).

Loose, brown to grey angular gravels and fragments with clay. (Landslided Material).

Very soft to soft, light brown gravelly Clay of low plasticity with angular fragments of weatherd bedock origin. (Landslided Material).

Soft,dark brown gravelly Clay of low plasticity with angular fragments weatherd bedock origin. At depth of 5,8-6,0 & 14,7-14,8 fragments from boulders. (Landslided Material).

The the top of Inclinometer is placed 75 cm above ground level.

The mixture of Cement & Bentonite contains 30% Cement and 70% Bentonite.

*Figure 135. Core Logging of borehole BDZ_22_06A (1/3)*

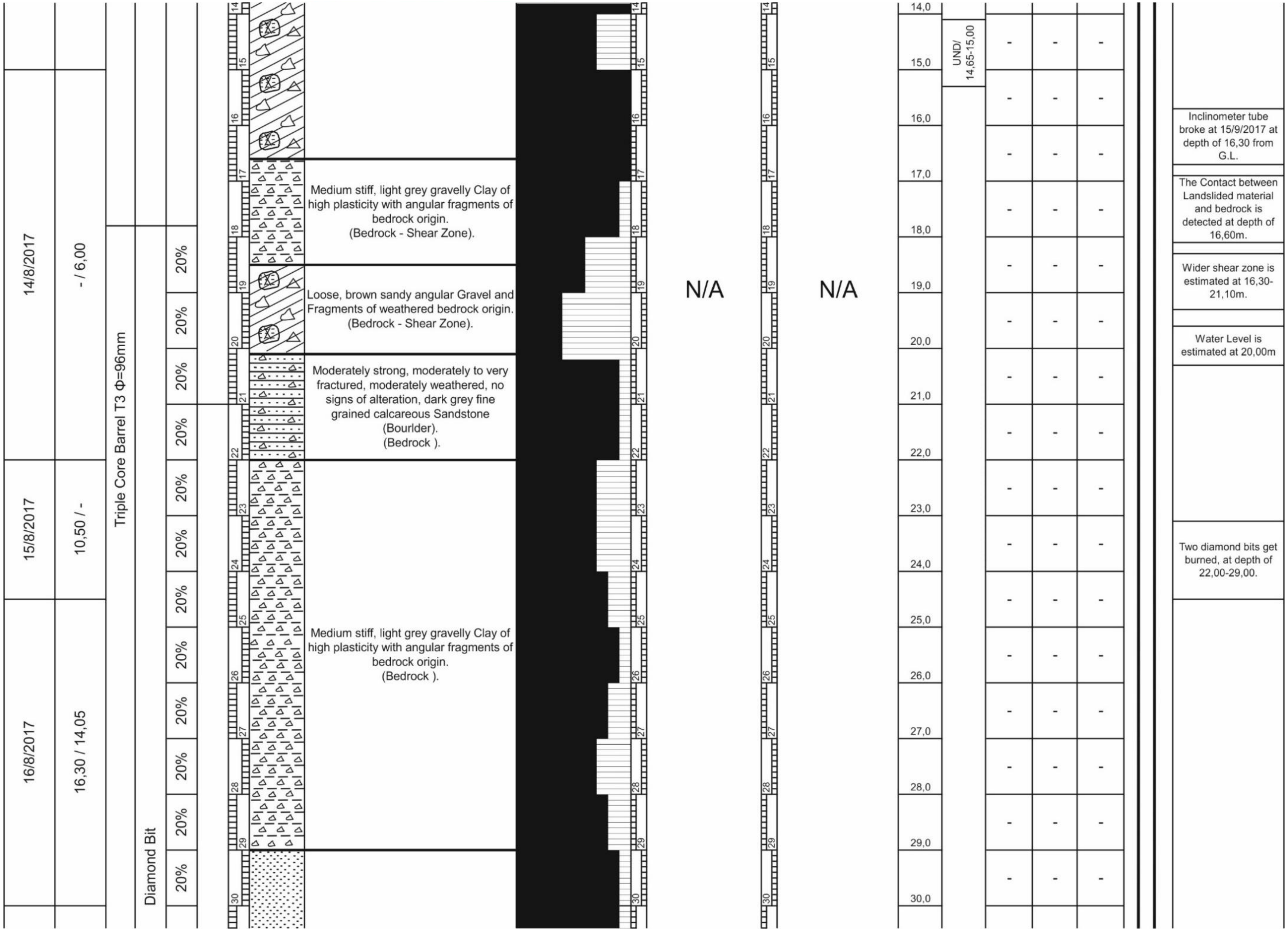

Medium stiff, light grey gravelly Clay of high plasticity with angular fragments of bedrock origin. (Bedrock - Shear Zone).

Loose, brown sandy angular Gravel and Fragments of weathered bedrock origin. (Bedrock - Shear Zone).

Moderately strong, moderately to very fractured, moderately weathered, no signs of alteration, dark grey fine grained calcareous Sandstone (Bourlder). (Bedrock ).

Medium stiff, light grey gravelly Clay of high plasticity with angular fragments of bedrock origin. (Bedrock ).

Inclinometer tube broke at 15/9/2017 at depth of 16,30 from G.L.

The Contact between Landslided material and bedrock is detected at depth of 16,60m.

Wider shear zone is estimated at 16,30-21,10m.

Water Level is estimated at 20,00m

Two diamond bits get burned, at depth of 22,00-29,00.

*Figure 136. Core Logging of borehole BDZ_22_06A (2/3)*

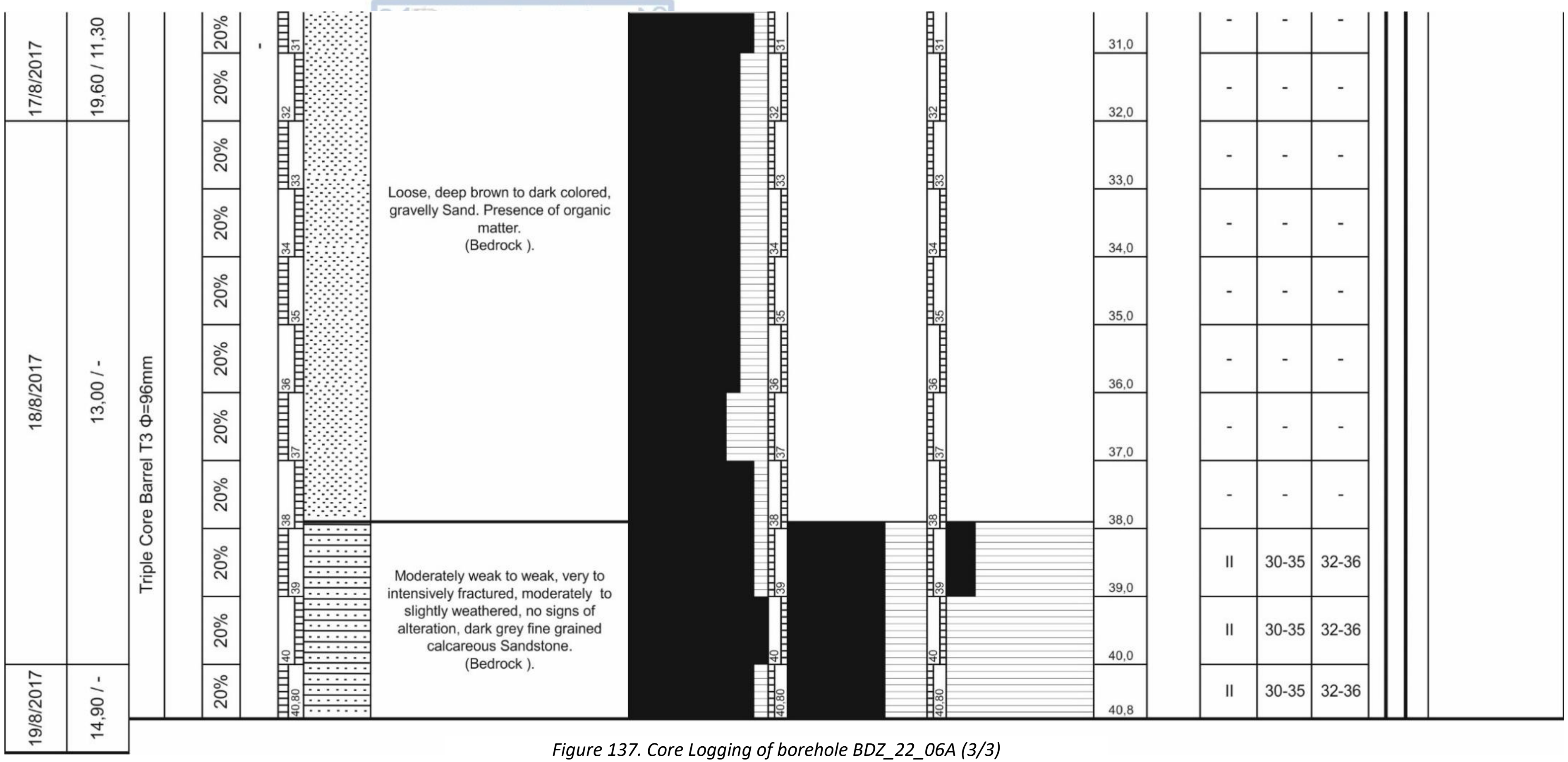

Loose, deep brown to dark colored, gravelly Sand. Presence of organic matter. (Bedrock ).

Moderately weak to weak, very to intensively fractured, moderately to slightly weathered, no signs of alteration, dark grey fine grained calcareous Sandstone. (Bedrock ).

*Figure 137. Core Logging of borehole BDZ_22_06A (3/3)*

| Boreole Depth (m) | Casing Depth [m] | Coordinates | X= | 367751,932 | Drill RIG type | ST 1023-HD | Inclination: | Vertical | | Borehole: | BDZ_22_07 |
|---|---|---|---|---|---|---|---|---|---|---|---|
| | | System | Y= | 4647356,323 | Driller | E.Bakshalyev | Started Date: | 29/8/2017 | | Finish Date: | 2/9/2017 |
| | | UTM (Zone 38N) | Z= | 641,302 | Geologists | Maisuradze A. Levan | | | | | |

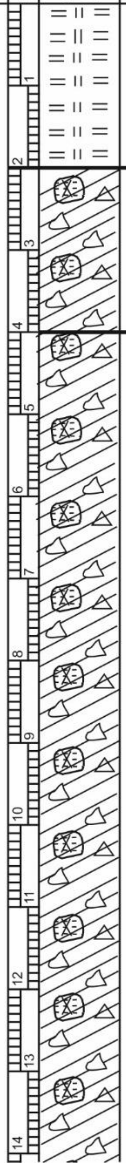

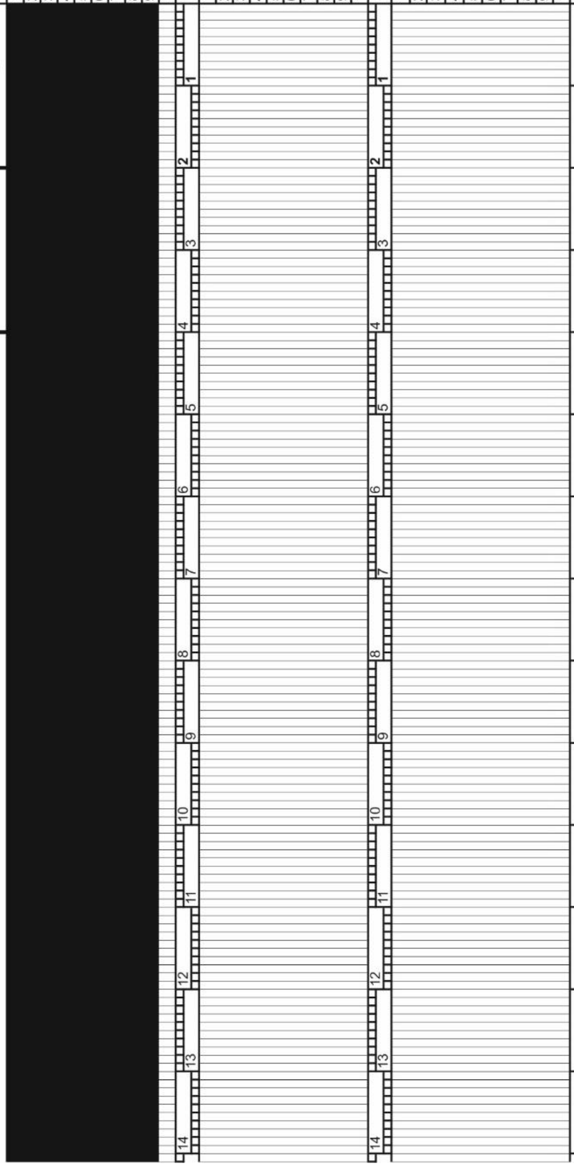

| Date | Water Level Before/After Drilling (m) | Drill Core Barrel | Bit Type | Water Lossen (%) | Casing (m) | m from G.L. | Stratigraphic Description | Core Run Intervals | Sample Type/Depth | Weathering | GSI Index | RMR Index | Instrumentation: Piezometer | Notes |
|---|---|---|---|---|---|---|---|---|---|---|---|---|---|---|
| 29/8/2017 | - | | | | | 1 | Very soft, dark brown to dark coloured gravelly organic Clay of low to medium plasticity with angular fragments of bedrock origin (Top Soil). (Landslided Material). | 1,0 | | - | - | - | Cement<br>Φ40<br>Cement | |
| | | | | | | 2 | | 2,0 | | - | - | - | Cement & Bentonite<br>Φ40<br>Cement & Bentonite | |
| | | | | | | 3 | Very soft, dark brown gravelly Clay of medium plasticity and angular fragments of bedrock origin. (Landslided Material). | 3,0 | | - | - | - | | |
| | | | | | | 4 | | 4,0 | | - | - | - | | |
| | | | | | | 5 | Very soft to soft, brown gravelly Clay of medium Plasticity to clayey Gravel with angular fragments of weathered bedrock origin. (Landslided Material). | 5,0 | | - | - | - | | |
| | | | | | | 6 | | 6,0 | | - | - | - | | |
| | | | | | | 7 | | 7,0 | | - | - | - | | |
| | | | | | | 8 | | 8,0 | | - | - | - | | |
| | | | | | | 9 | | 9,0 | | - | - | - | | |
| | | | | | | 10 | | 10,0 | | - | - | - | | |
| | | | | | | 11 | | 11,0 | | - | - | - | | |
| | | | | | | 12 | | 12,0 | | - | - | - | | |
| | | | | | | 13 | | 13,0 | | - | - | - | | |
| | | | | | | 14 | | 14,0 | | - | - | - | | |

*Figure 138. Core Logging of borehole BDZ_22_07 (1/3)*

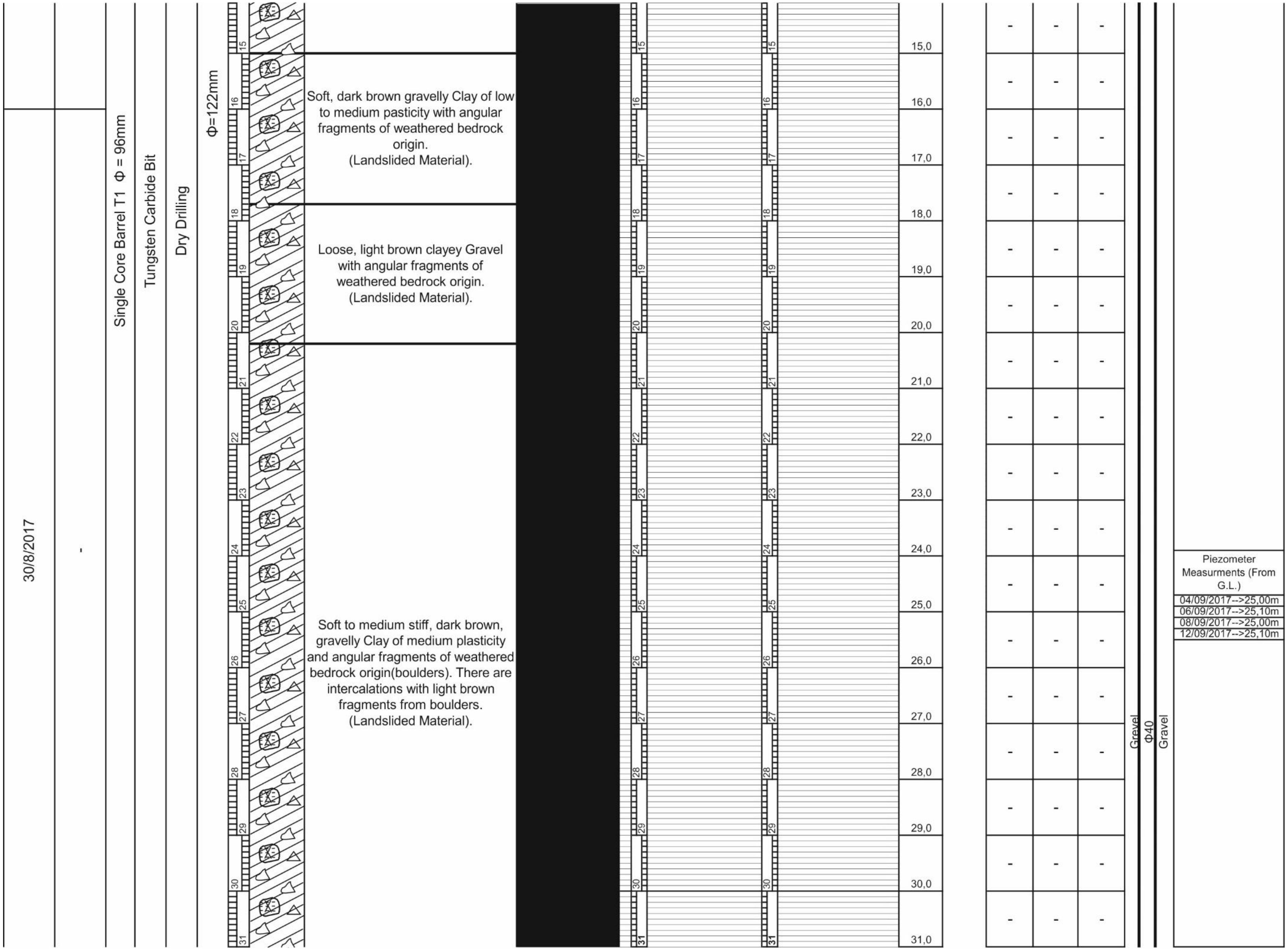

Soft, dark brown gravelly Clay of low to medium pasticity with angular fragments of weathered bedrock origin.
(Landslided Material).

Loose, light brown clayey Gravel with angular fragments of weathered bedrock origin.
(Landslided Material).

Soft to medium stiff, dark brown, gravelly Clay of medium plasticity and angular fragments of weathered bedrock origin(boulders). There are intercalations with light brown fragments from boulders.
(Landslided Material).

Piezometer Measurments (From G.L.)

04/09/2017-->25,00m
06/09/2017-->25,10m
08/09/2017-->25,00m
12/09/2017-->25,10m

Figure 139. Core Logging of borehole BDZ_22_07 (2/3)

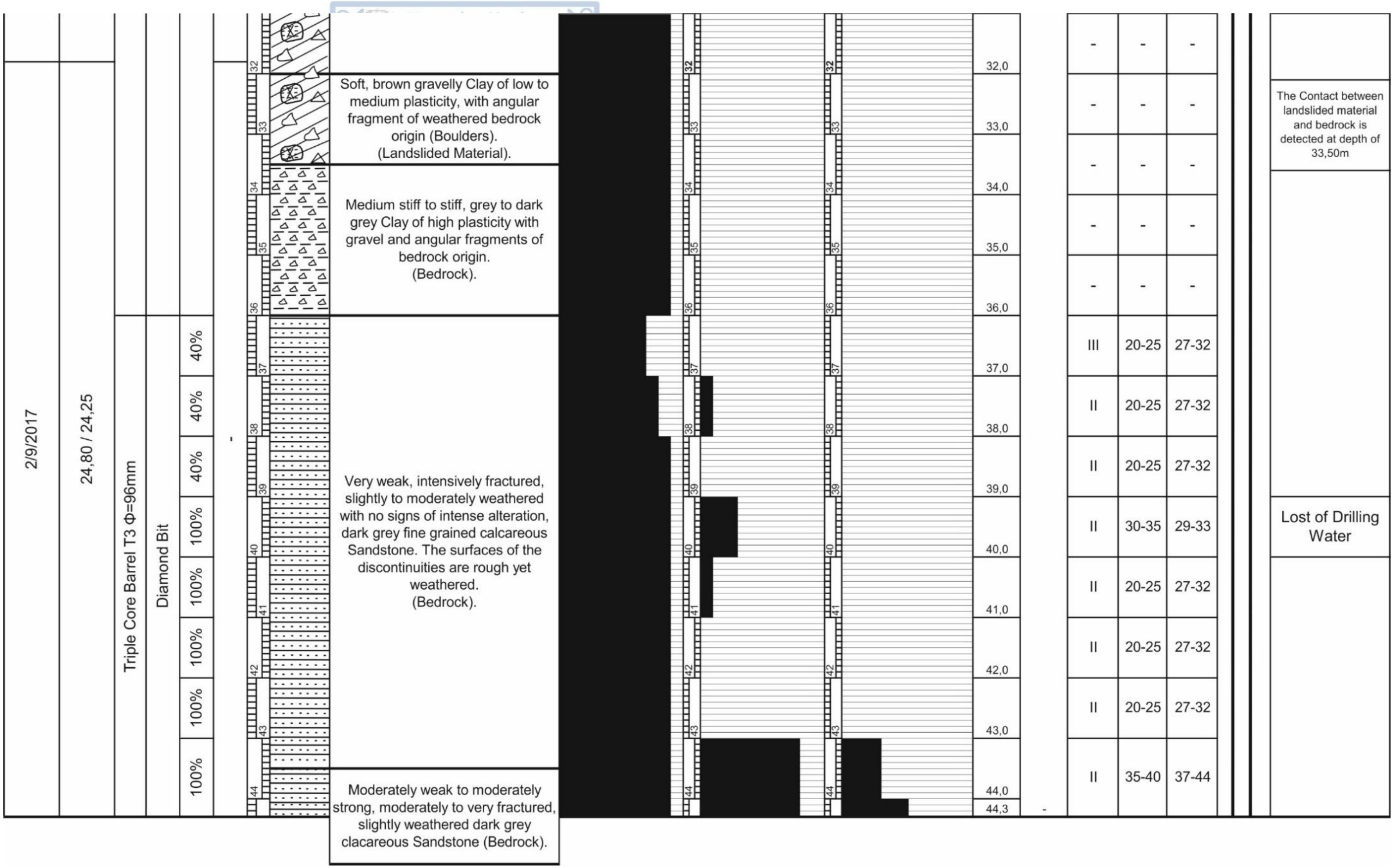

Soft, brown gravelly Clay of low to medium plasticity, with angular fragment of weathered bedrock origin (Boulders). (Landslided Material).

Medium stiff to stiff, grey to dark grey Clay of high plasticity with gravel and angular fragments of bedrock origin. (Bedrock).

Very weak, intensively fractured, slightly to moderately weathered with no signs of intense alteration, dark grey fine grained calcareous Sandstone. The surfaces of the discontinuities are rough yet weathered. (Bedrock).

Moderately weak to moderately strong, moderately to very fractured, slightly weathered dark grey clacareous Sandstone (Bedrock).

The Contact between landslided material and bedrock is detected at depth of 33,50m

*Figure 140. Core Logging of borehole BDZ_22_07 (3/3)*

| | | | | | | | | | | |
|---|---|---|---|---|---|---|---|---|---|---|
| Boreole Depth (m) | Casing Depth [m] | Coordinates | X= | 367695,718 | Drill RIG type | ST 1023-HD | Inclination: | Vertical | Borehole: | BDZ_22_08 |
| | | System | Y= | 4647277,019 | Driller | E.Bakshalyev | Started Date: | 10/9/2017 | Finish Date: | 13/9/2017 |
| | | UTM (Zone 38N) | Z= | 630,986 | Geologists | Maisuradze A.Levan | | | | |

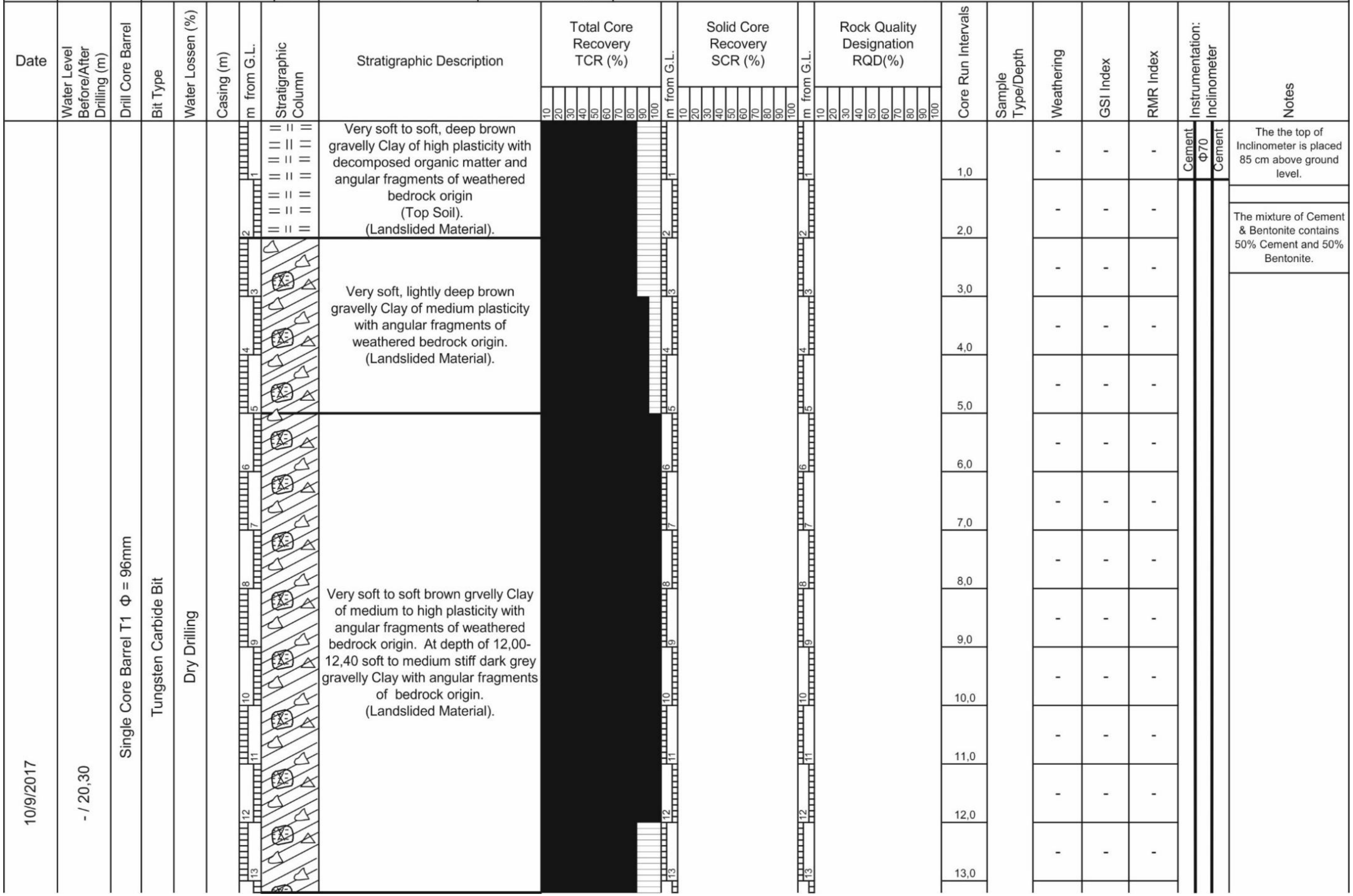

Very soft to soft, deep brown gravelly Clay of high plasticity with decomposed organic matter and angular fragments of weathered bedrock origin
(Top Soil).
(Landslided Material).

Very soft, lightly deep brown gravelly Clay of medium plasticity with angular fragments of weathered bedrock origin.
(Landslided Material).

Very soft to soft brown grvelly Clay of medium to high plasticity with angular fragments of weathered bedrock origin. At depth of 12,00-12,40 soft to medium stiff dark grey gravelly Clay with angular fragments of bedrock origin.
(Landslided Material).

The the top of Inclinometer is placed 85 cm above ground level.

The mixture of Cement & Bentonite contains 50% Cement and 50% Bentonite.

*Figure 141. Core Logging of borehole BDZ_22_08 (1/4)*

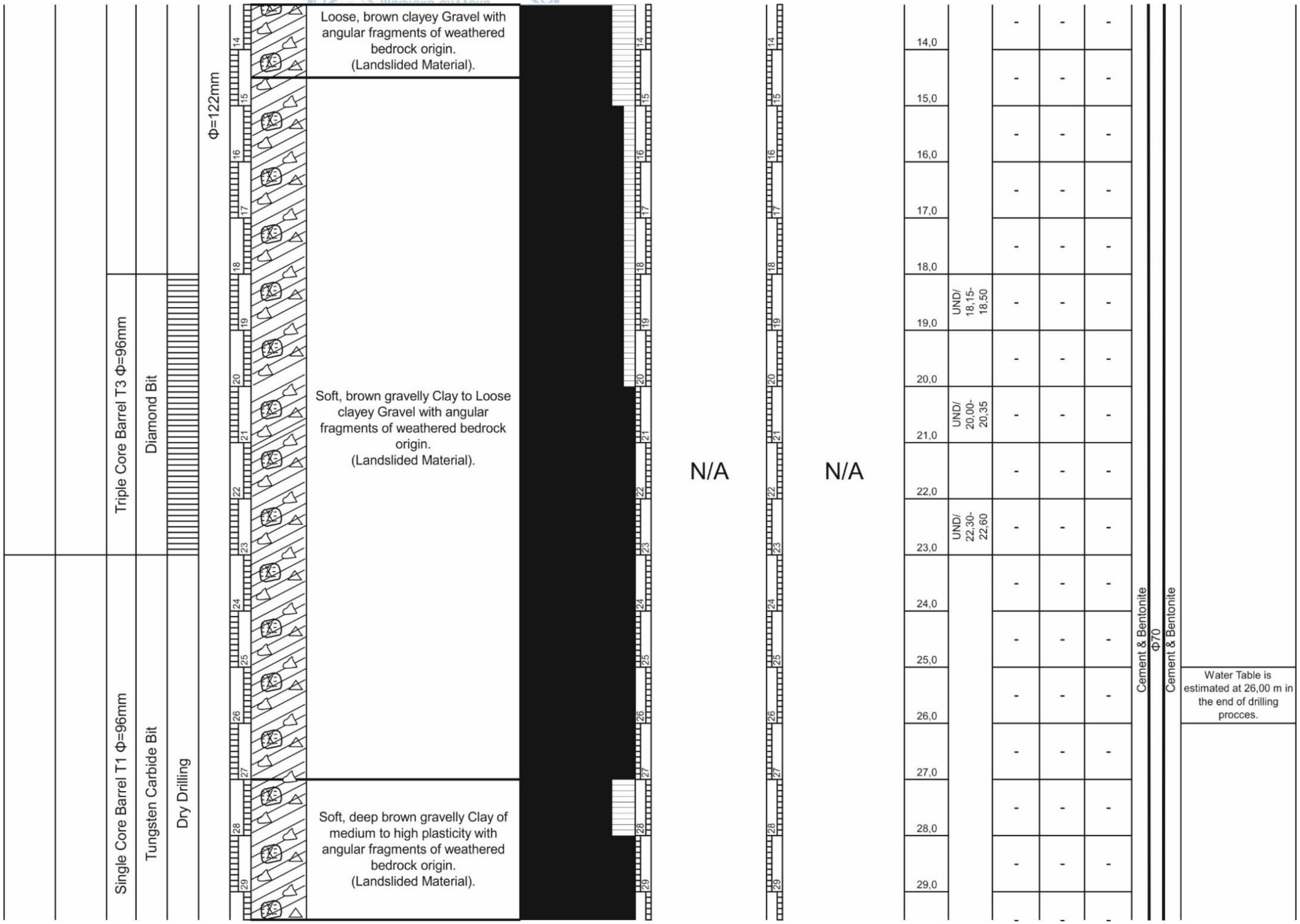

*Figure 142. Core Logging of borehole BDZ_22_08 (2/4)*

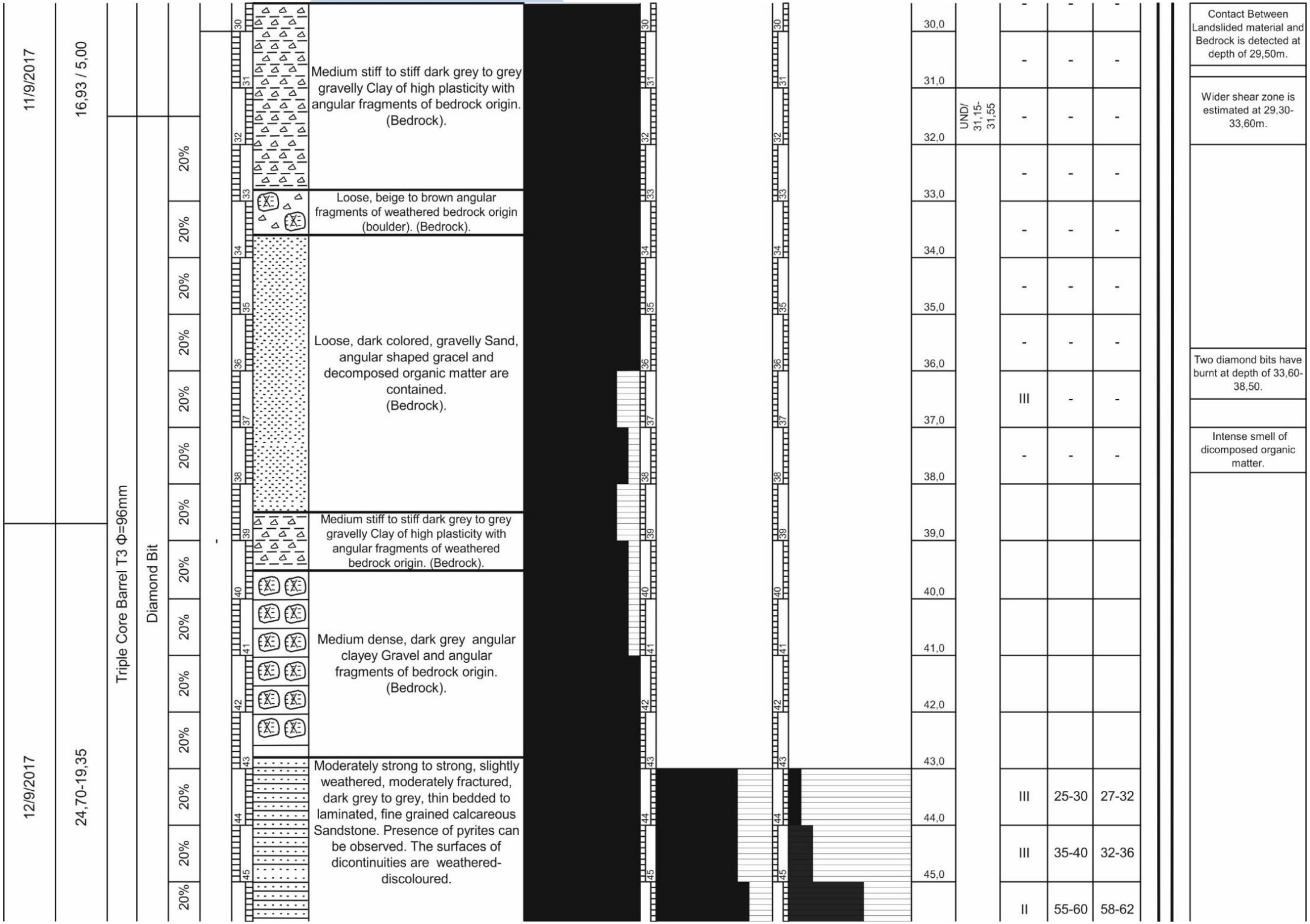

*Figure 143. Core Logging of borehole BDZ_22_08 (3/4)*

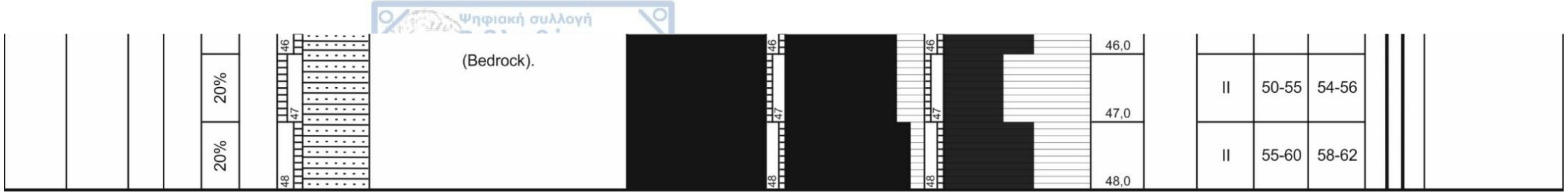

*Figure 144. Core Logging of borehole BDZ_22_08 (4/4)*

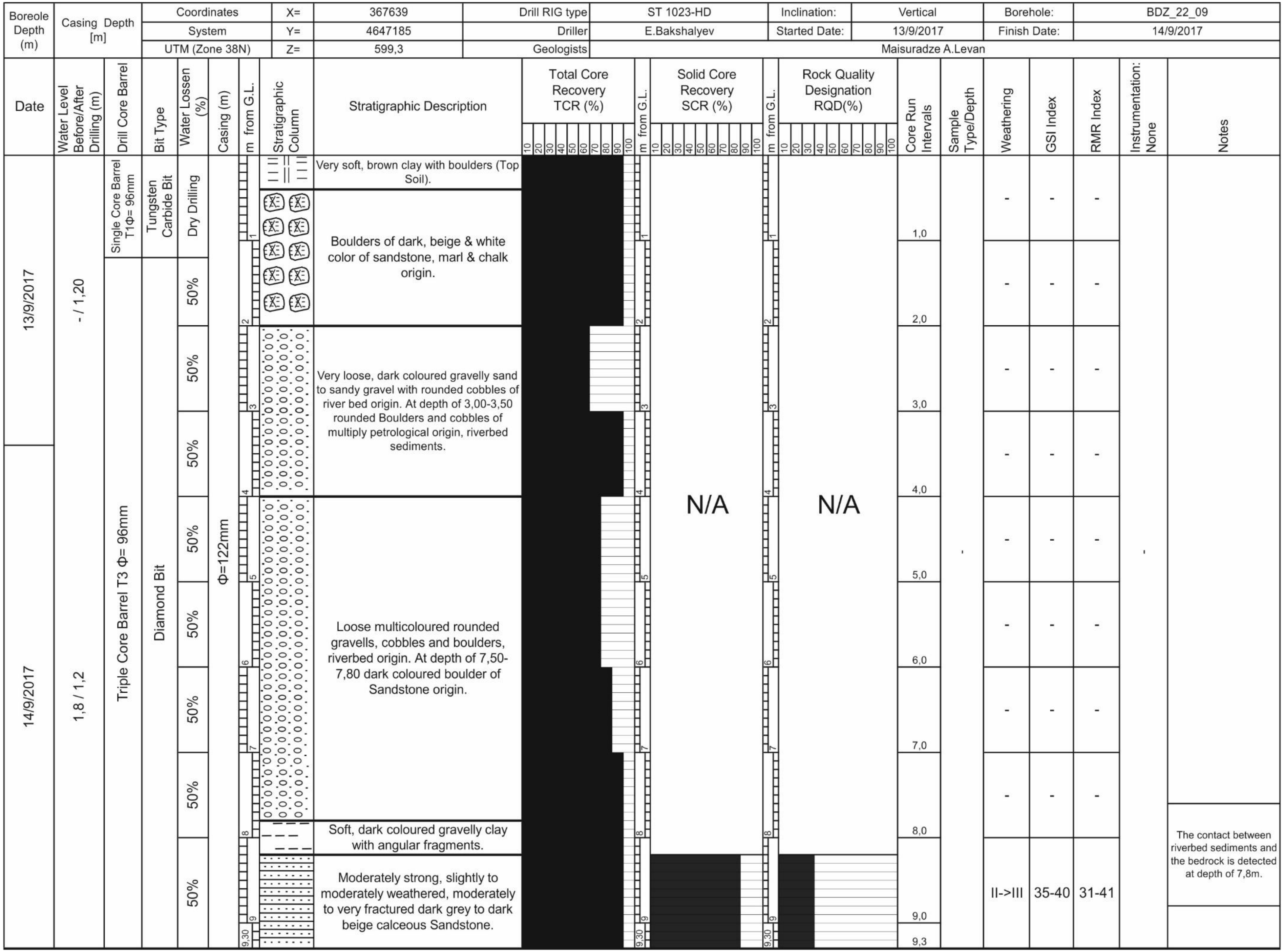

| Boreole Depth (m) | Casing Depth [m] | Coordinates | X= | 367639 | Drill RIG type | ST 1023-HD | Inclination: | Vertical | Borehole: | BDZ_22_09 |
|---|---|---|---|---|---|---|---|---|---|---|
| | | System | Y= | 4647185 | Driller | E.Bakshalyev | Started Date: | 13/9/2017 | Finish Date: | 14/9/2017 |
| | | UTM (Zone 38N) | Z= | 599,3 | Geologists | Maisuradze A.Levan | | | | |

| Date | Water Level Before/After Drilling (m) | Drill Core Barrel | Bit Type | Water Lossen (%) | Casing (m) | Stratigraphic Description | Solid Core Recovery SCR (%) | Rock Quality Designation RQD(%) | Core Run Intervals | Sample Type/Depth | Weathering | GSI Index | RMR Index | Instrumentation: None | Notes |
|---|---|---|---|---|---|---|---|---|---|---|---|---|---|---|---|
| 13/9/2017 | - / 1,20 | Single Core Barrel T1Φ= 96mm | Tungsten Carbide Bit | Dry Drilling | Φ=122mm | Very soft, brown clay with boulders (Top Soil).<br>Boulders of dark, beige & white color of sandstone, marl & chalk origin. | N/A | N/A | 1,0 | - | - | - | - | - | |
| | | Triple Core Barrel T3 Φ= 96mm | Diamond Bit | 50% | | | | | 2,0 | | - | - | - | | |
| | | | | 50% | | Very loose, dark coloured gravelly sand to sandy gravel with rounded cobbles of river bed origin. At depth of 3,00-3,50 rounded Boulders and cobbles of multiply petrological origin, riverbed sediments. | | | 3,0 | | - | - | - | | |
| 14/9/2017 | 1,8 / 1,2 | | | 50% | | | | | 4,0 | | - | - | - | | |
| | | | | 50% | | Loose multicoloured rounded gravells, cobbles and boulders, riverbed origin. At depth of 7,50-7,80 dark coloured boulder of Sandstone origin. | | | 5,0 | | - | - | - | | |
| | | | | 50% | | | | | 6,0 | | - | - | - | | |
| | | | | 50% | | | | | 7,0 | | - | - | - | | |
| | | | | 50% | | Soft, dark coloured gravelly clay with angular fragments. | | | 8,0 | | - | - | - | | |
| | | | | 50% | | Moderately strong, slightly to moderately weathered, moderately to very fractured dark grey to dark beige calceous Sandstone. | | | 9,0<br>9,3 | | II->III | 35-40 | 31-41 | | The contact between riverbed sediments and the bedrock is detected at depth of 7,8m. |

*Figure 145. Core Logging of borehole BDZ_22_09 (1/2)*

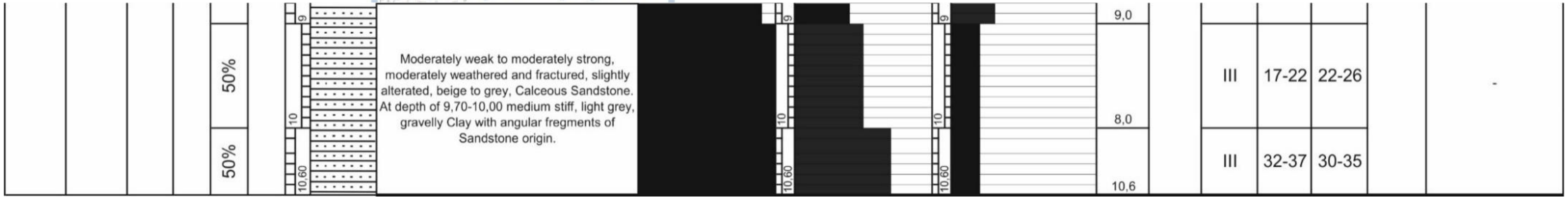

*Figure 146. Core Logging of borehole BDZ_22_09 (2/2)*

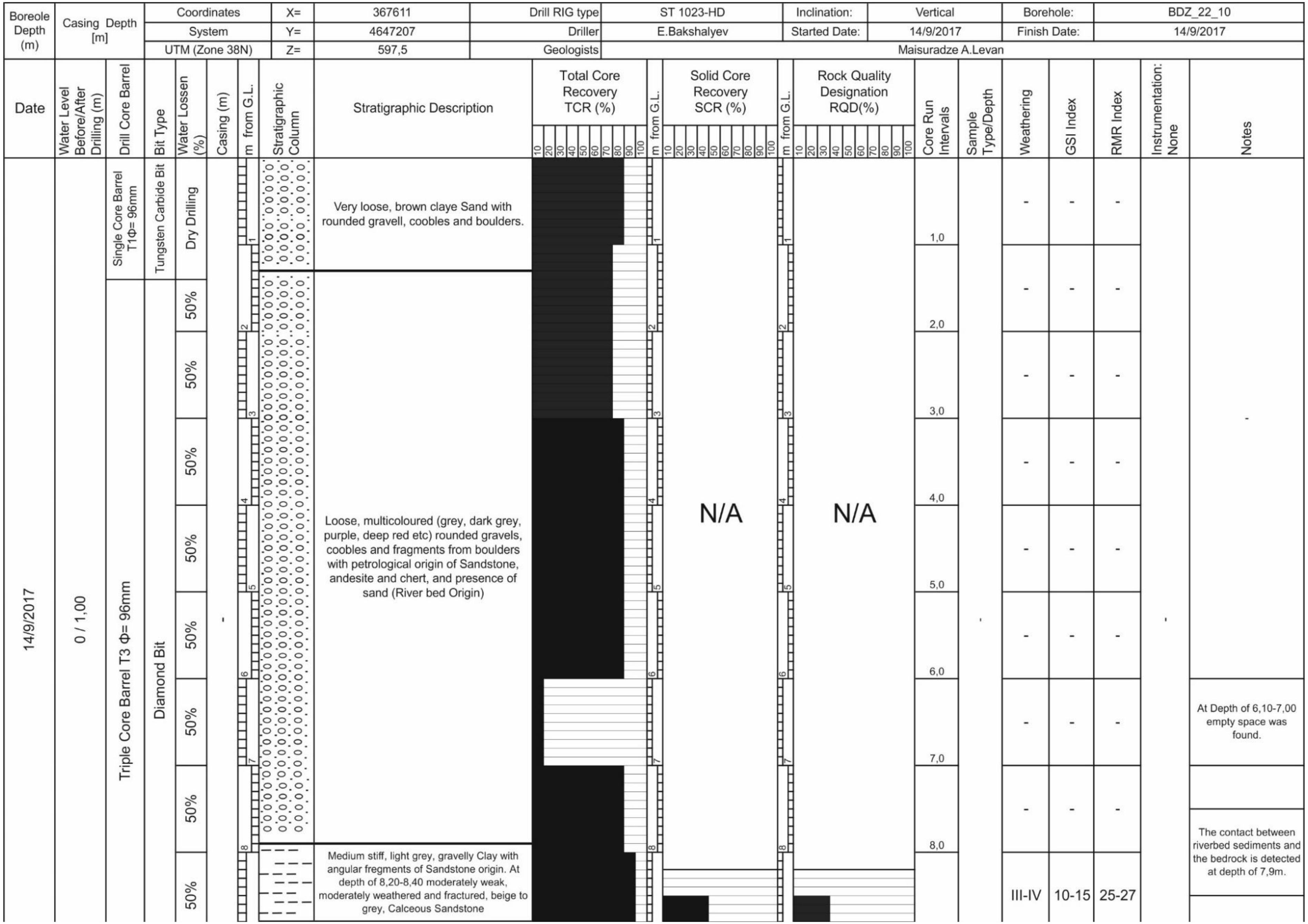

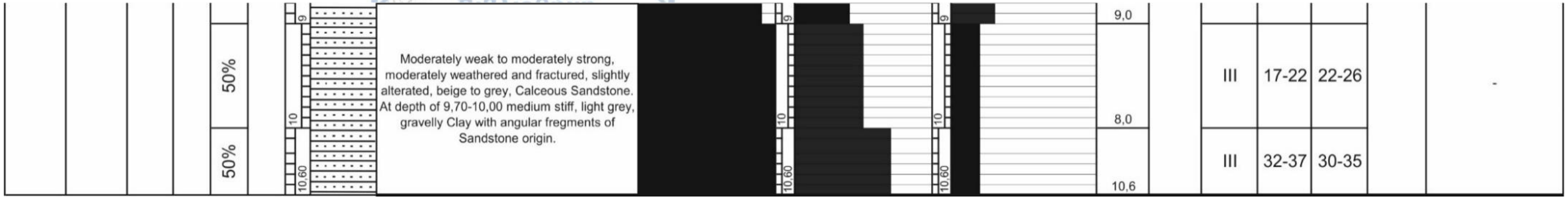

Moderately weak to moderately strong, moderately weathered and fractured, slightly altered, beige to grey, Calceous Sandstone. At depth of 9,70-10,00 medium stiff, light grey, gravelly Clay with angular fregments of Sandstone origin.

*Figure 148. Core Logging of borehole BDZ_22_10 (2/2).*

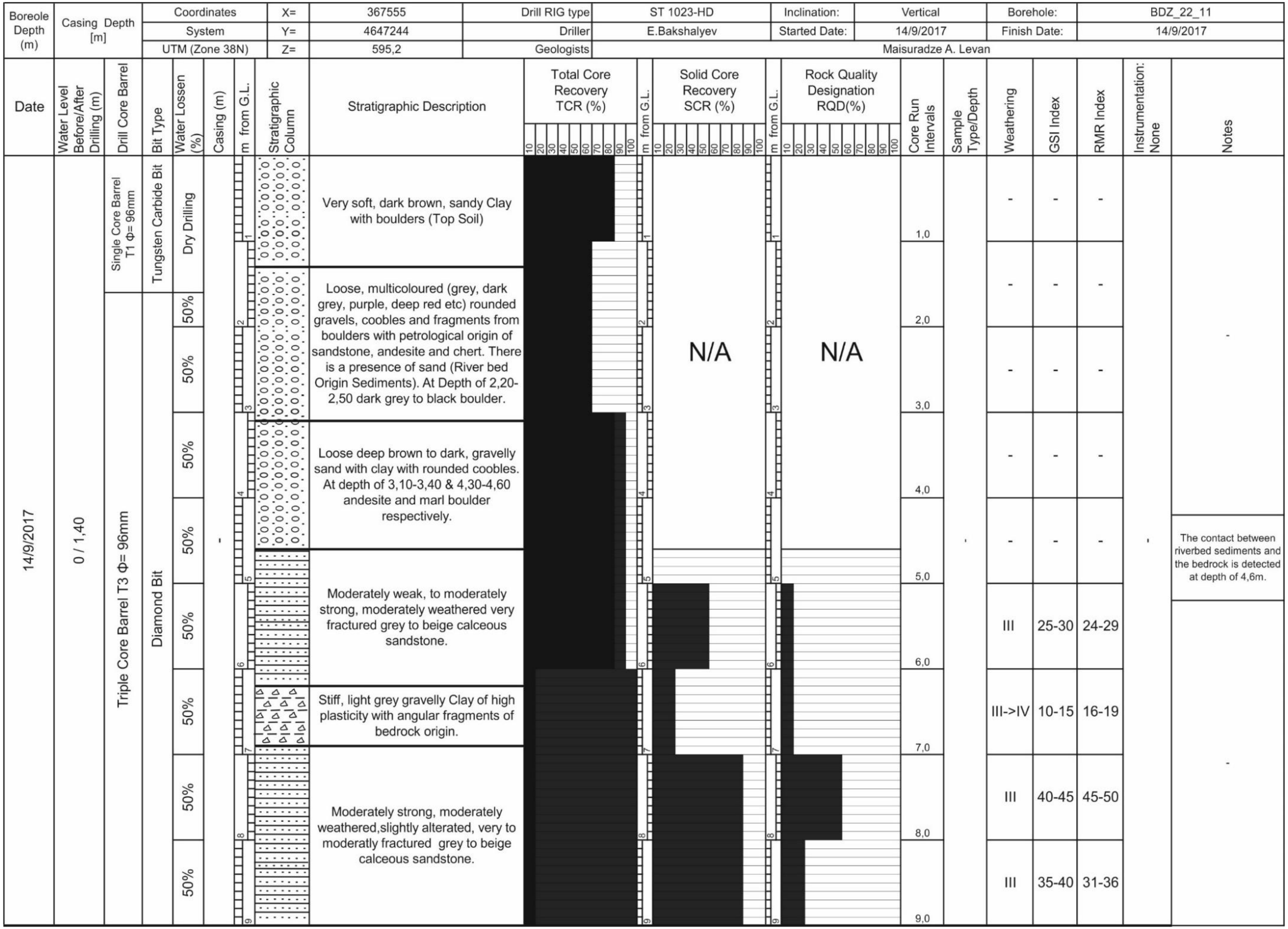

| | | | | | | | | | |
|---|---|---|---|---|---|---|---|---|---|
| Boreole Depth (m) | Casing Depth [m] | Coordinates System | X= | 367555 | Drill RIG type | ST 1023-HD | Inclination: Vertical | Borehole: | BDZ_22_11 |
| | | | Y= | 4647244 | Driller | E.Bakshalyev | Started Date: 14/9/2017 | Finish Date: | 14/9/2017 |
| | | UTM (Zone 38N) | Z= | 595,2 | Geologists | Maisuradze A. Levan | | | |

| Date | Water Level Before/After Drilling (m) | Drill Core Barrel | Bit Type | Water Lossen (%) | Casing (m) | m from G.L. | Stratigraphic Description | Total Core Recovery TCR (%) | Solid Core Recovery SCR (%) | Rock Quality Designation RQD(%) | Core Run Intervals | Sample Type/Depth | Weathering | GSI Index | RMR Index | Instrumentation: None | Notes |
|---|---|---|---|---|---|---|---|---|---|---|---|---|---|---|---|---|---|
| 14/9/2017 | 0 / 1,40 | Single Core Barrel T1 Φ= 96mm | Tungsten Carbide Bit | Dry Drilling | - | 1 | Very soft, dark brown, sandy Clay with boulders (Top Soil) | | N/A | N/A | 1,0 | - | - | - | - | - | - |
| | | Triple Core Barrel T3 Φ= 96mm | Diamond Bit | 50% | | 2 | Loose, multicoloured (grey, dark grey, purple, deep red etc) rounded gravels, coobles and fragments from boulders with petrological origin of sandstone, andesite and chert. There is a presence of sand (River bed Origin Sediments). At Depth of 2,20-2,50 dark grey to black boulder. | | | | 2,0 | | - | - | - | | |
| | | | | 50% | | 3 | | | | | 3,0 | | - | - | - | | |
| | | | | 50% | | 4 | Loose deep brown to dark, gravelly sand with clay with rounded coobles. At depth of 3,10-3,40 & 4,30-4,60 andesite and marl boulder respectively. | | | | 4,0 | | - | - | - | | |
| | | | | 50% | | 5 | | | | | 5,0 | | - | - | - | | The contact between riverbed sediments and the bedrock is detected at depth of 4,6m. |
| | | | | 50% | | 6 | Moderately weak, to moderately strong, moderately weathered very fractured grey to beige calceous sandstone. | | | | 6,0 | | III | 25-30 | 24-29 | | - |
| | | | | 50% | | 7 | Stiff, light grey gravelly Clay of high plasticity with angular fragments of bedrock origin. | | | | 7,0 | | III->IV | 10-15 | 16-19 | | |
| | | | | 50% | | 8 | Moderately strong, moderately weathered,slightly alterated, very to moderately fractured grey to beige calceous sandstone. | | | | 8,0 | | III | 40-45 | 45-50 | | |
| | | | | 50% | | 9 | | | | | 9,0 | | III | 35-40 | 31-36 | | |

*Figure 149. Core Logging of borehole BDZ_22_11*

*Figure 150. Coring samples photographs from borehole BDZ_22_01A (0-24m).*

Figure 151. Coring samples photographs from borehole BDZ_22_01A (24-47m).

Figure 152. Coring samples photographs from borehole BDZ_22_02 (0-24m).

*Figure 153. Coring samples photographs from borehole BDZ_22_02 (24-46m).*

Figure 154. Coring samples photographs from borehole BDZ_22_03A (0-24m).

*Figure 155. Coring samples photographs from borehole BDZ_22_03A (24-47m).*

Figure 156. Coring samples photographs from borehole BDZ_22_05 (0-24m).

*Figure 157. Coring samples photographs from borehole BDZ_22_05 (24-46m).*

Figure 158. Coring samples photographs from borehole BDZ_22_06A (0-24m).

*Figure 159. Coring samples photographs from borehole BDZ_22_06A (24-40.8m).*

*Figure 160. Coring samples photographs from borehole BDZ_22_07 (0-24m).*

Figure 161. Coring samples photographs from borehole BDZ_22_06A (24-44.30m).

*Figure 162. Coring samples photographs from borehole BDZ_22_08 (0-24m).*

Figure 163. Coring samples photographs from borehole BDZ_22_06A (24-48m).

*Figure 164. Coring samples photographs from boreholes BDZ_22_09, BDZ_22_10, BDZ_22_11.*

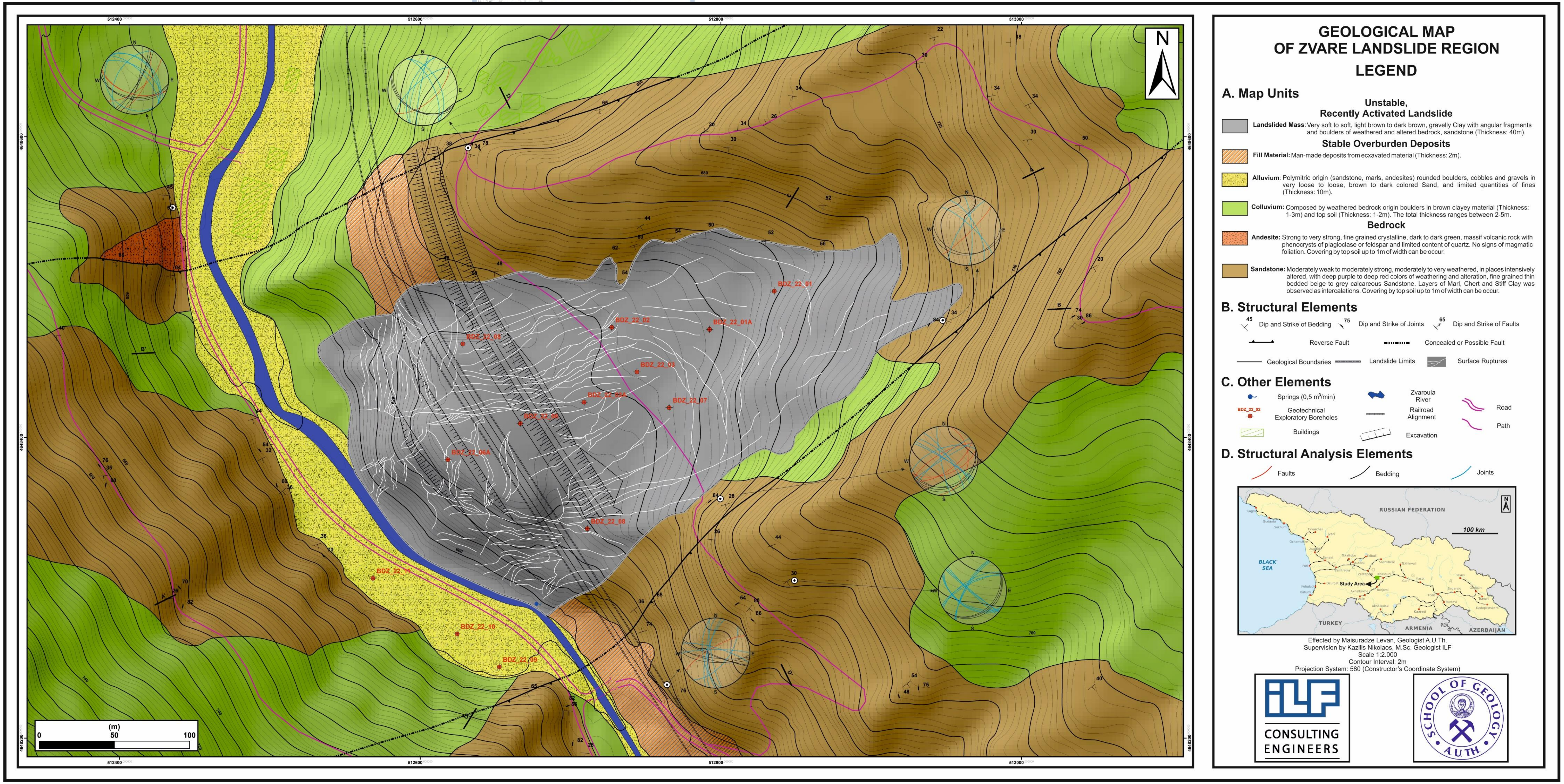

## GEOLOGICAL MAP
## OF ZVARE LANDSLIDE REGION
## LEGEND

### A. Map Units

**Unstable,
Recently Activated Landslide**

▨ **Landslided Mass**: Very soft to soft, light brown to dark brown, gravelly Clay with angular fragments and boulders of weathered and altered bedrock, sandstone (Thickness: 40m).

**Stable Overburden Deposits**

▨ **Fill Material:** Man-made deposits from ecxavated material (Thickness: 2m).

▨ **Alluvium**: Polymitric origin (sandstone, marls, andesites) rounded boulders, cobbles and gravels in very loose to loose, brown to dark colored Sand, and limited quantities of fines (Thickness: 10m).

🟩 **Colluvium:** Composed by weathered bedrock origin boulders in brown clayey material (Thickness: 1-3m) and top soil (Thickness: 1-2m). The total thickness ranges between 2-5m.

**Bedrock**

▨ **Andesite:** Strong to very strong, fine grained crystalline, dark to dark green, massif volcanic rock with phenocrysts of plagioclase or feldspar and limited content of quartz. No signs of magmatic foliation. Covering by top soil up to 1m of width can be occur.

▨ **Sandstone:** Moderately weak to moderately strong, moderately to very weathered, in places intensively altered, with deep purple to deep red colors of weathering and alteration, fine grained thin bedded beige to grey calcareous Sandstone. Layers of Marl, Chert and Stiff Clay was observed as intercalations. Covering by top soil up to 1m of width can be occur.

### B. Structural Elements

45 Dip and Strike of Bedding
75 Dip and Strike of Joints
65 Dip and Strike of Faults
Reverse Fault
Concealed or Possible Fault
Geological Boundaries
Landslide Limits
Surface Ruptures

### C. Other Elements

Springs (0,5 m$^3$/min)
Zvaroula River
BDZ_22_02 Geotechnical Exploratory Boreholes
Railroad Alignment
Road
Path
Buildings
Excavation

### D. Structural Analysis Elements

Faults
Bedding
Joints

Effected by Maisuradze Levan, Geologist A.U.Th.
Supervision by Kazilis Nikolaos, M.Sc. Geologist ILF
Scale 1:2.000
Contour Interval: 2m
Projection System: 580 (Constructor's Coordinate System)

*Figure 165. Geological & Engineering Geological Map of southern of village Zvare Region, Imereti, Central Georgia.*